

The author(s) shown below used Federal funds provided by the U.S. Department of Justice and prepared the following final report:

Document Title: Forensic Investigation Techniques for
Inspecting Electrical Conductors Involved in
Fire

Author: Richard J. Roby, Ph.D., Jamie McAllister, Ph.D.

Document No.: 239052

Date Received: July 2012

Award Number: 2010-DN-BX-K246

This report has not been published by the U.S. Department of Justice. To provide better customer service, NCJRS has made this Federally-funded grant final report available electronically in addition to traditional paper copies.

<p>Opinions or points of view expressed are those of the author(s) and do not necessarily reflect the official position or policies of the U.S. Department of Justice.</p>

Final Technical Report for Award No. 2010-DN-BX-K246

Forensic Investigation Techniques for Inspecting Electrical Conductors Involved in Fire

Combustion Science & Engineering, Inc.

8940 Old Annapolis Road, Suite L

Columbia, MD 21045

Point of Contact: Dr. Richard J. Roby, President and Technical Director
Phone: 410-884-3266
Fax: 410-884-3267
Email: rrobby@csefire.com

July 13, 2012

This project was supported by Award No. 2010-DN-BX-K246, awarded by National Institute of Justice, Office of Justice Programs, U. S. Department of Justice. The opinions, findings, and conclusions or recommendations expressed in this publication/program/exhibition are those of the author(s) and do not necessarily reflect those of the Department of Justice.

ABSTRACT

Many times, a fire investigator will conclude that a device was electrically energized at the time of a fire based on the presence of a bead on a wire. If an energized device is present in the area of origin, it is likely that it will be considered as a potential cause of a fire. Some training guides put forth that beads can only be formed from arcing on wires that were electrically energized when they were exposed to a fire or caused a fire. Therefore, the presence or absence of a bead on a wire can have a strong influence on the direction of a fire investigation. Hence, it is important to have a clear understanding of the various electrical and thermal conditions which can produce beads on electrical wires.

The main objective of this research was to determine, experimentally, if distinguishing characteristics exist between energized and non-energized wires subjected to various types of fire exposures. The large majority of research published in the literature has not tested energized and non-energized wires under the same conditions. A total of more than 190 wires were tested under various fire conditions. Wire types included 12-gauge and 14-gauge solid conductors and 16-gauge and 18-gauge stranded conductors. The tests were conducted using a bench-scale, premixed flame impingement apparatus, a bench-scale 125 kW/m² radiant tunnel apparatus, a 2/5-scale flashover compartment, and a full-scale flashover compartment. The use of various types of exposure conditions ensured that the characteristics on the wires (or lack thereof) were not caused by one specific type of thermal insult. Wires were tested in both an energized and non-energized state. Energized wires were tested under “load” and “no load” conditions. Under load conditions, the energized wires were plugged into a 110-120 volt power source with 9 to 13 amps of current. Under “no load” conditions, the wires were plugged into the power supply, but no current was flowing in the circuit.

Based on preliminary studies conducted by the authors, it was hypothesized that characteristic “arc-beads” could be formed on non-energized wires as well as energized wires. Additionally, it was hypothesized that the formation of a bead on a wire was not a function of its “energized state”, but a function of its “thermal state”. This hypothesis is based on the laws of physics, which states that liquids tend to form spherical structures due to cohesive surface forces. These hypotheses are in opposition of the current state-of-the-art in the field, which states that beads can only be formed on energized wires. Another review of all the test samples is still underway; however, these hypotheses are supported by the current research findings and sample analyses results. No trends or distinguishing visual or microscopic characteristics between energized and non-energized wires have been found in the samples reviewed to-date. Whether a wire was energized with load, energized without load, or non-energized had no significant effect on the visual or microscopic characteristics of the wire. Round copper globules with clear lines of demarcation, traditionally defined as “beads”, were produced on both energized and non-energized wires. Some energized wires that did arc failed to produce round copper globules with clear lines of demarcation, while some non-energized wires that did not arc did produce these characteristic beads. Under a microscope, beads from some of the energized wires were porous and contained a large quantity of internal void spaces, while other beads contained no void spaces. This same trend was true for non-energized wires. A study of selected samples under SEM/EDS also showed no trends in grain structure or chemical compositions.

A detailed metallurgical study of internal grain structures of the beads was also performed. The inner grain structures of the beads were studied for structure sizes, porosity, and general changes. None of the physical aspects of the beads studied showed any definitive, distinguishing traits between energized and non-energized wires. There was one trait, an internal

line of demarcation, which was found on forty percent (40%) of the energized beads but only found in one of the non-energized beads. The internal line of demarcation was marked by the abrupt change of the grain size between the bead and the adjoining wire. Of the beads that showed this characteristic, half of the samples had larger grain structures on the bead when compared to the wire, and the other half revealed the opposite condition. Since one of the non-energized beads did have an internal line of demarcation, it is not possible to conclude with 100% certainty that the presence of an internal line of demarcation indicates that a wire was energized at the time of bead formation. Additionally, since not all of the energized wires exhibited an internal line of demarcation, it is not possible to say that the absence of an internal line of demarcation indicates that a wire was non-energized.

NFPA 921, *Guide to Fire and Explosion Investigations* (2011 edition), defines a bead as a “round globule.....caused by arcing....characterized by a sharp line of demarcation.” NFPA 921 needs to be revised to reflect the findings of this research. The research findings clearly show that the sole use of visual characteristics to establish the energized state of a wire can lead to erroneous conclusions.

Table of Contents

ABSTRACT.....	2
List of Figures	7
List of Tables	9
NOMENCLATURE	10
EXECUTIVE SUMMARY	11
Introduction.....	11
Methods.....	15
Results.....	16
Discussion	17
TECHNICAL REPORT.....	19
I. INTRODUCTION.....	19
A. Statement of Problem.....	20
B. Literature Citation and Review	20
C. Hypothesis for the Research.....	26
II. METHODS.....	28
A. Current and Voltage Data Acquisition	29
B. Direct Flame Impingement Tests.....	30
C. 2/5-Scale Compartment Tests	33
D. Full Scale Compartment Tests.....	36
E. Sample Analysis.....	38
III. RESULTS.....	40
A. Summary of Results	40
B. Testing Data and Results.....	41
1. Direct Flame Impingement Tests.....	41
2. Radiant Tunnel Tests	46
3. 2/5-Scale Compartment Tests	51
4. Full Scale Compartment Tests	56
C. Stereo Microscope Results.....	61
D. Scanning Electron Microscope and EDS.....	65
E. Analysis with Metallurgical Microscope	68
F. Heat Transfer Analysis	74
IV. CONCLUSIONS.....	78
A. Discussion.....	78

1.	Direct Flame Impingement Tests.....	78
2.	Radiant Tunnel Tests	80
3.	2/5-Scaled Compartment Tests.....	81
4.	Full Scale Compartment Tests.....	83
5.	Comparisons between Various Exposures.....	85
6.	Analysis with Metallurgical Microscope	93
7.	Heat Transfer Analysis	96
B.	Summary.....	96
C.	Implications for Policy and Practice.....	99
D.	Implications for further research.....	100
V.	REFERENCES.....	102
VI.	DISSEMINATION OF RESEARCH FINDINGS	105

List of Figures

Figure 1: Data Acquisition Setup for Current and Voltage Measurements	30
Figure 2: Direct Flame Testing Setup	31
Figure 3: Radiation Testing Tunnel (Units in Inches)	32
Figure 4: Sketch of Compartment Testing Setup.....	35
Figure 5: Flashover Compartment	36
Figure 6: Wire Samples in the Ceiling with Thermocouple Tree	38
Figure 7: Average Time to Sever or Trip for All Wire Types (DF)	43
Figure 8: Average Time to Break or Trip for Energized and Loaded-Direct Flame Tests (DF) ..	43
Figure 9: Typical Amperage and Voltage Graph (Loaded Wire DF)	45
Figure 10: Arcing Through Char (DF).....	45
Figure 11: Average Break Time under Radiant Loading (R-All).....	48
Figure 12: Average Trip Time-Radiation Tunnel Tests (E and L-R)	49
Figure 13: Average Break Time and Trip Time under Radiant Loading (R)	50
Figure 14: Average Trip Time-Scaled Compartment Tests (SC)	53
Figure 15: Heat Flux at Circuit Trip Time-Scaled Compartment Tests (SC).....	54
Figure 16: Temperature at Circuit Trip Time-Scaled Compartment Tests (SC)	55
Figure 17: TEA at Trip Time for the Scaled Compartment Tests (SC).....	56
Figure 18: Circuit Trip Time for Full-Scale Compartment Tests (FSC)	59
Figure 19: Average Temperature at Trip Time for Full-Scale Compartment Tests (FSC)	59
Figure 20: Average Heat Flux at Trip Time for Full-Scale Tests (FSC)	60
Figure 21: TEA for Full-Scale Compartment Tests (FSC).....	60
Figure 22: Beads Produced with Direct Flame Exposure (12-gauge: NE, E (center), and L).....	62
Figure 23: Beads Produced with Radiant Tunnel Exposure (16-gauge: NE, 12-gauge: E (center) and L)	62
Figure 24: Beads Produced with Scaled Compartment Exposure (12-gauge: NE, E (center), and L).....	62
Figure 25: Beads Produced with Full-Scale Compartment Exposure (16-gauge: E, 18-gauge: L)	62
Figure 26: Mounted Samples (Cut and Etched).....	63
Figure 27: SM Images of Loaded Wires under Direct Flame Exposure (12-gauge: L-DF)	63
Figure 28: SM Images Loaded Wire under Scaled Compartment Exposure (12-gauge: L-SC) ..	63
Figure 29: SM Images of Loaded Wires under Radiant Tunnel Exposure (12-gauge: L-R).....	63
Figure 30: SM Images of Non-energized wires under direct flame Exposure (18-gauge: NE-DF)	64
Figure 31: SM Images of Non-energized Wires under Scaled Compartment Exposure (18-gauge: NE-SC).....	64
Figure 32: SM Images of Non-energized Wires under Radiant Tunnel Exposure (18-gauge: NE-R).....	64
Figure 33: SM and SEM Images of MS Wires under different Electrical Conditions.	66
Figure 34: EDS Graph for a Bead Surface formed on an Energized Wire (DF)	66
Figure 35: EDS Graph for a Bead Surface formed on a Non-energized Wire (DF).....	67
Figure 36: Grain Structures of Wire Control Samples (Unexposed Wires: Solid (Top) and Stranded (Bottom))	70

Figure 37: Metallurgical Microscope Images of Beads formed under Direct Flame Exposure (All Loaded 12-R Wires).....	71
Figure 38: Metallurgical Microscope Images of Beads formed under Scaled Compartment Exposure (All Loaded 18-MS Wires).....	72
Figure 39: Metallurgical Microscope Images of Beads formed under Direct Flame Exposure (12-R NE (A) and 12-R L (B))	73
Figure 40: Metallurgical Microscope Images of Beads formed under Scaled Compartment (12-R L (A)) and Radiation (14-R NE (B)).....	74
Figure 41: Metallurgical Microscope Images of Beads formed under Scaled Compartment (18-MS NE (A) and 18-MS L (B)).....	74
Figure 42: Copper Wire Sample Setup for Heat Transfer Simulation.....	75
Figure 43: Heat Transfer Simulation Results-Temperature change with Time.....	76
Figure 44: Axial Temperature Change along Wire Length (Dc similar to 12-R conductors).	77
Figure 45: Maximum Heat Flux (averaged for each wire type) measured during Testing. (FSC v SC)	86
Figure 46: Maximum Temperature (averaged for each wire type) measured during Testing. (FSC v SC)	87
Figure 47: Average Trip Times for Compartment Fires (FSC v SC)	88
Figure 48: Full-Scale Compartment Trip Time Analysis (FSC)	89
Figure 49: Scaled Compartment Trip Time Analysis (SC)	89
Figure 50: Total Energy per Area Comparison (SC and FSC)	90
Figure 51: Comparison of Loaded and Non-energized Beads for various Exposures (SM Images) (Letters denote type of exposure)	92
Figure 52: Internal Pattern Comparison of Loaded and Non-energized Beads for various Exposures (SM Images).....	93
Figure 53: Line of Demarcation (Direct Flame (A and B) and Radiation (C))	95
Figure 54: Line of Demarcation (Scaled Compartment-All).....	96

List of Tables

Table 1: Wire Specifications.....	28
Table 2: Direct Flame Testing Results (DF).....	42
Table 3: Radiation Testing Results (R).....	47
Table 4: Scaled Compartment Testing Results (SC)	52
Table 5: Full-Scale Compartment Testing Results (FSC)	57
Table 6: Average Failure Time-All Exposures for Non-loaded Wires and Loaded Wires.	85
Table 7: Percentage of Samples with Bead Formation.....	90
Table 8: Average Bead Diameter.....	92

NOMENCLATURE

12R	12 AWG Romex Wire
14R	14 AWG Romex Wire
16MS	16 AWG Multi-stranded Wire
18MS	18 AWG Multi-stranded Wire
A	Amperage (AC)
ARAI	Accident Reconstruction Analysis, Inc.
CFM	Cubic Feet per Minute
CSE	Combustion Science & Engineering, Inc.
Dc	Diameter of Copper Conductor or Strand in Wire
DF	Direct Flame Exposure
E	Electrical Wire with Potential only
E-SC	Energized Wire tested in Scaled Compartment
EDS	Energy Dispersive X-ray Spectrometry
FEMA	Federal Emergency Management Agency
FSR	Full-Scale Compartment Exposure
h	Convective Heat Transfer Coefficient
IR	Infrared (Bulbs)
L	Wire with Load
L-SC	Loaded Wire tested in Scaled Compartment
L-R	Loaded Wire tested in Radiation Tunnel
MS	Multi-Stranded Wire
NE	Non-Energized Electrical Wire
q_c	Convective Heat Flux
q_f	Flame Heat Flux
R	Radiation Exposure
SC	Scaled Compartment Exposure
SEM	Scanning Electron Microscope
SIMS	Secondary Ion Mass Spectroscopy
SM	Stereo Microscope
TEA	Total Energy per Unit Area (Area under the Curve)
V	Voltage (AC)

EXECUTIVE SUMMARY

Introduction

There are an estimated 28,300 residential building electrical fires annually in the United States according to a Federal Emergency Management Agency's (FEMA) report issued in 2008. These fires, on average, cause 360 deaths, 1000 injuries, and nearly a billion dollars in direct loss. Almost half of these electrical fires were linked to building wiring.

Fire investigators often rely on the appearance of electrical wires and the perceived presence of electrical activity (e.g. arc-beads) on wires to assess the potential involvement of the wires or attached appliances in the initiation of a fire. In fact, some training guides suggest that the presence of a bead on a wire is evidence that a device was electrically energized at the time of a fire, and therefore, should be evaluated as a potential cause of the fire. Since the presence or absence of a bead on a wire can have a strong influence on the direction of a fire investigation, it is important to have a clear understanding of the various electrical and thermal conditions which can produce beads on electrical wires. Although many researchers have attempted to define the conditions under which particular characteristics occur on electrical wires, many, if not all, of these studies did not test a control. For example, if it is believed that a bead can only be formed in an energized wire, then a control must also be tested to ensure that the same characteristic bead cannot be formed on a non-energized wire.

Several studies have attempted to establish distinguishing characteristics between beads formed before the fire (cause) and beads formed during the fire (effect). In almost every case, wire failures were produced by passing overcurrent through the wire or by subjecting an energized wire to a thermal insult.

A. Statement of Problem

There have been many studies that focused on role of energized electrical wires in starting fires where researchers studied ‘cause’ and ‘effect’ beads. The central focus of most of these studies was the role of energized wires in igniting a fire; researchers assumed that beads could only form on energized wires. None of the previous studies have focused on non-energized wires and the potential for bead formation on these wires due to melting.

The main objective of this research was to determine, experimentally, if distinguishing characteristics exist between energized and non-energized wires subjected to various types of fire exposures. Four methods for generating the thermal environment were used: bench-scale direct flame impingement, bench-scale radiant heating, and 2/5-scale and full-scale radiant/convective heating in a flashover compartment. Additionally, energized wires were tested under “load” and “no load” conditions. Under load conditions, the energized wire had current flow and under “no load” conditions, the energized wires were plugged into a power source but no current was flowing through the wires (e.g. electrical potential only).

B. Literature Review

Gray et al. (1983) exposed electrical conductors to overload conditions and flame impingement. Tiny holes were present on beads produced during overload, but this was not seen on the beads produced with the flame exposure. Gray proposed that the internal heating in copper lead to melting and expulsion of small copper pellets from the surface. Anderson (1989 and 1994) tried to identify the cause and effect beads with Auger Electron Spectroscopy (AES). He studied the presence of combustion products trapped in the bead by removing micrometer size layers off the bead’s surface and analyzing the surface with AES.

Anderson's claims were disputed by Henderson and Manning (1998) who concluded that the concentration of combustion products is not significantly different below the surface in beads formed from overload versus those formed from flame exposure. Beland (1994) further refuted Anderson's work concluding that beads formed on insulated wires, whether from cause or effect, contained the same combustion products. Furthermore, Howitt (1997) showed that the solubility of combustion products in copper is much lower than the detectable limits of AES, so, the method proposed by Anderson was not precise enough to distinguish between cause and effect beads.

Lee et al (2002) and Chen et al (2003) tried different approaches to identify "cause and effect" beads. Lee and his group produced beads with overcurrent and flame and studied these beads for presence of amorphous and graphitized carbon. Both types of carbon were found in cause beads while only amorphous carbon was found in effect beads. However, only 26% of the cause beads showed both graphitized and amorphous carbon, so the method was not 100% effective in identifying cause beads. Chen used Secondary Ion Mass Spectrometry (SIMS) to measure the amount of chlorine present below the surface of cause and effect beads. It was shown that effect beads had thicker layers of chlorine from 0-3 micrometers below the surface of the beads as compared to cause beads. This trend was only observed in two samples.

There have been attempts by many researchers to identify signatures in cause and effect beads. Every study observed energized wires based on wide spread belief that beads can only be produced while electrical wires are energized. No researcher has looked at non-energized wires to determine if the characteristic "bead" can be produced under the right thermal conditions. Additionally, no one had microscopically compared beads formed on non-energized wires with those formed on energized wires.

C. Hypothesis for Research

As discussed above, there are thousands of building fires in the United States every year that are started by electrical fires; these fires cause deaths, injuries, and billions of dollars in property damage. There have been many studies to date that have tried to distinguish between cause and effect beads based on the analysis of damage to wiring, particularly wires with evidence of beading.

Many studies have used different analysis methods to evaluate electrical wires, but there is no single method developed thus far that is endorsed by the fire investigation community. Also, it is widely believed that beads can only form when wires are energized, but preliminary studies done by the authors show that if copper wires are exposed to the right thermal conditions, beads will form on the conductor regardless of its electrical state (i.e. energized versus non-energized). The beads produced on non-energized wires had similar physical appearance to those created on energized wires with and without load.

The main goal for the present research was to address whether distinguishing characteristics exist between the beads produced on non-energized and energized wires after they are subjected to fire exposures. Based on preliminary findings, it is hypothesized that the formation of a bead on a wire is not inherently related to the energized state of the wire, but rather is a function of the thermal kinetics of the copper. This is contrary to the belief that beads can only be formed on energized electrical wires; however, the theory that beads can only be formed on energized wires is contrary to the phenomenon of surface tension. The basic laws of physics show that the same theories that apply to water droplets can be applied to other liquids; surface tension is the true cause of the “bead” shape that forms when copper melts. According to White (1948) liquids form their spherical shape due to cohesive surface forces, and the necessity

to minimize “wall tension”. All liquids would be “perfectly spherical” if no other forces existed, e.g. gravity. Therefore, it is the liquidification (melting) of the metal that results in the formation of a bead. Whether this melting occurs as a result of fire exposure or arcing is irrelevant, since the outcome is independent of the melting conditions. Hence, it is hypothesized that the characteristic “bead”, typically defined as a round globule with a clear line of demarcation, can form on both non-energized and energized wires. Furthermore, it is hypothesized that the porosity and chemical composition of the beads will vary based on the conditions under which the beads are formed.

Methods

Four methods for testing were developed to encompass various real fire scenarios that may arise. One testing method involved direct flame exposure to the wire. This was accomplished by subjecting the wires to direct flame impingement from a propylene torch. All four wires were tested under three electrical conditions of non-energized, energized with potential only, and energized with load. Each test scenario was repeated six times for a total of 72 samples.

The second testing method utilized a radiant tunnel designed and built by CSE. The tunnel was constructed with 1200 watt infrared bulbs that produced temperatures and heat flux sufficient to melt copper, e.g. 125 kW/m² and 1050-1100 °C. Each wire was tested under all three electrical conditions and each testing scenario was repeated three times for a total of 36 wire samples.

The third thermal exposure was performed in a 2/5-scale flashover compartment. The compartment was furnished with carpet, and a standard wood crib was used as the fuel source to

generate flashover conditions. The fire was extinguished after post-flashover conditions were reached. Each testing scenario was repeated 6 times for a total of 70 samples.

The final test method utilized a full-scale flashover compartment. These tests were performed at the National Fire Academy. Similar to the scaled compartment, wires were exposed to a combined convective and radiative heating. Each testing scenario was repeated three times for a total on 36 samples.

After the tests were completed, each wire sample was inspected for thermal damage and bead formation. Each bead was photographed with a stereomicroscope. Some selected samples were analyzed with SEM/EDS. Other select samples were analyzed under a metallurgical microscope.

Results

After thermal testing, the wires were analyzed with a high resolution stereomicroscope. Some wires were also analyzed using a Scanning Electron Microscope (SEM) and Electron Dispersive Spectrometry (EDS), as well as, a metallurgical microscope to define visual and elemental characteristics and patterns in and on the wires. Whether a wire was energized with load, energized without load, or non-energized had no significant effect on the visual or microscopic characteristics of the wire. Round copper globules with clear lines of demarcation, traditionally defined as “beads”, were produced on both energized and non-energized wires. Some energized wires that did arc failed to produce round copper globules with clear lines of demarcation, while some non-energized wires that did not arc did produce these characteristic beads. Under microscope, beads from some of the energized wires were porous and contained a large quantity of internal void spaces, while other beads contained no void spaces. This same

trend was true for non-energized wires. A study of the selected samples under SEM/EDS also showed no trends in grain structure or chemical compositions.

None of the physical aspects of the beads studied using a metallurgical microscope showed any definitive, distinguishing grain structure traits that were present in 100% of the cases. There was one trait, an internal line of demarcation, which was found on forty percent (40%) of the energized beads but only found in one of the non-energized beads. The internal line of demarcation was marked by the abrupt change of the grain size between the bead and the adjoining wire. Of the beads that showed this characteristic, half of the samples had larger grain structures on the bead when compared to the wire, and the other half revealed the opposite condition.

Discussion

Based on the findings of this research to-date, there is no evidence to support the statement that a bead on a wire can only be “caused by arcing.” The findings of this research show that a bead is not inherently related to an arcing event. While it may be common for a bead to form from arcing, it is also common for no bead to be formed during arcing, or for a bead to be formed in the absence of an arcing event. The findings of this research show that investigators should use caution when developing hypotheses regarding the energized state of a wire based solely on the presence of a bead; the information provided in NFPA 921 regarding the identification of arc beads is incorrect; NFPA 921 (2011 edition) defines a bead as “a rounded globule of re-solidified metal at the end of the remains of an electrical conductor that was caused by arcing and is characterized by a sharp line of demarcation between the melted and unmelted conductor surfaces.” Hence, NFPA 921 states that beads can only be formed from an arcing event and that the presence of a bead can be used to distinguish between energized and non-

energized wires. The research findings clearly show that the use of visual characteristics to establish the energized state of a wire can lead to erroneous conclusions. Analysis with SEM/EDS does not provide any common trends within wires tested at similar electrical conditions. Also, there were no common or distinguishing characteristics observed between energized and non-energized wires.

A detailed metallurgical study of internal grain structures of beads by ARAI did not reveal any distinguishing characteristics between beads formed on energized and non-energized wires. The inner grain structures of the beads were studied for structure sizes, porosity, and changes in grain structures. None of the physical aspects of the beads studied showed any definitive, distinguishing traits between energized and non-energized wires. There was one trait, an internal line of demarcation, which was found on forty percent (40%) of the energized beads but only found in one of the non-energized beads. The internal line of demarcation was marked by the abrupt change of the size of the grain between the bead and the adjoining wire. Of the beads that showed this characteristic, half of the samples had larger grain structures on the bead when compared to the wire, and the other half revealed the opposite condition. Since one of the non-energized beads did have an internal line of demarcation, it is not possible to conclude with 100% certainty that the presence of an internal line of demarcation indicates that a wire was energized at the time of bead formation. Additionally, since not all of the energized wires exhibited an internal line of demarcation, it is not possible to say that the absence of an internal line of demarcation indicates that a wire was non-energized. However, it is recommended that further research be conducted in this area to produce larger data sets which may yield higher degrees of confidence.

TECHNICAL REPORT

I. INTRODUCTION

According to an NFPA report (Hall Jr., 2012) on home electrical fires, in 2009 about 44,800 home structure fires reported to fire departments included some type of electrical failure as the cause. The result of these fires included 472 deaths, 1500 civilian injuries, and approximately \$1.6 billion in property damage. Electricity and fire is perhaps one of the most controversial couplings in the fire investigation field. The electrical fire cause classification is often misused, unused, and overused due to the lack of resources and information available to the investigation community. NFPA 921, *Guide for Fire and Explosion Investigations* (NFPA, 2011), devotes an entire chapter to electrically initiated fires; this chapter includes descriptions of various modes of wire failure. Several images of damaged wires and the causes of that damage are presented as examples for investigators to use in their analysis of electrical wires. Specifically, these images focus on the production of arc beads on different types of electrical cords. Fire investigators, often, rely on the appearance of electrical wires and the presence of arc-beads to assess the potential involvement of the wires or attached appliances in the initiation of a fire. Many times, a fire investigator will conclude that a device was electrically energized at the time of a fire, and therefore, could have potentially caused the fire, based on the presence of an arc bead on a wire. Unfortunately, there are many limitations in the current state-of-the-art for electrical wire analysis. Although many researchers have attempted to define the conditions under which particular characteristics occur on electrical wires, many, if not all, of these studies did not test a control. For example, if it is believed that arc beads are only formed in energized wires, then a control study must be performed to ensure that the same characteristic “bead” cannot be formed on non-energized wires.

The main objective of this research was to determine, experimentally, if distinguishing characteristics exist between energized and non-energized wires subjected to various types of fire exposures; direct flame impingement, radiant heating, and radiant/convective heating. Electrical copper conductors were tested under three electrical conditions that included non-energized, energized with potential only, and energized with load. After fire exposure testing was completed, the wires were analyzed with a stereomicroscope and metallurgical microscope, as well as, a Scanning Electron Microscope (SEM) and Electron Dispersive Spectrometry (EDS) to define visual and elemental characteristics and patterns in and on the beads and adjoining wires.

A. Statement of Problem

There have been many studies that focused on the role of energized electrical wires in the initiation of fires; many researchers have studied the causes of beads on electrical wires. However, most of this research has focused on distinguishing between beads formed due to a failure condition which resulted in a fire (cause) versus beads formed from exposure to a fire (effect). All these studies have focused on energized wires with the apparent assumption that beads only form on energized wires. Limited research has been performed to establish the ability of a “bead” to form on a non-energized wire. Therefore, the inherency of the formation of “beads” on energized wires and the relevance of these beads in the context of the fire cause is unknown. The overriding purpose of this research was to address whether any distinguishing characteristics exist between beads found on energized wires versus those found on non-energized wires.

B. Literature Citation and Review

Gray et al. [1983] performed a series of experiments to distinguish between beads formed from overloading the wire with current versus beads formed from flame exposure. In both cases,

the wires were energized. In the first test, an overload (7-10 times the amperage rating) was passed through the wires until heat caused the insulation to melt and the wires to short circuit. Flaming was only observed when 5-amp rated wires were exposed to currents above 30 amps. In the second test, wires were subjected to normal or slightly elevated current conditions and exposed to a flame. Once the wire insulation burned off, arcing occurred and typically resulted in the formation of a bead.

A Scanning Electron Microscope (SEM) was used to study the difference between the beads. Beads produced under overload conditions clearly showed small holes on the bead surface; this characteristic was not present on the wires exposed to a flame under normal load conditions. Gray et al. hypothesized that the holes found in the overloaded wire samples were caused by resistive heating of the copper above 260°C during the overload event. The heating, then caused the expulsion of minute crystals from the bead surface. Furthermore, Gray et al. hypothesized that the crystallization did not happen on the wires exposed to flame, because the wire insulation provided “some degree of thermal insulation” which prevented the wires from overheating prior to failure. Gray et al. also hypothesized that the holes were due to the copper being heated throughout its entire length during overload, as opposed to localized surface heating which occurred during the flame exposure. The total number of experiments performed was not discussed; therefore, the level of certainty in the analysis is unknown.

Anderson (1989 and 1996) used Auger Electron Spectroscopy (AES) to study wires damaged in fire. AES is used to outline elements found below the residue in an arc bead. AES works by scanning the surface of the bead using a focused electron beam and measuring the kinetic energy produced by collision between the element and the impacting electron. In Anderson’s study, the bead was examined for the presence of different chemicals to better

understand the environmental conditions under which the bead was formed. Anderson focused on the presence of common combustion products in fires such as carbon, sulfur, chlorine, and calcium.

Anderson hypothesized that beads formed prior to a fire (cause) would have a different chemical composition when compared to beads formed after the fire initiation (effect). Specifically, Anderson stated that combustion products would not be present in “cause” beads but would be present in “effect” beads. Three case studies were conducted on copper beads from actual fires. In the first case, a refrigerator cord was involved, which was assumed to have started the fire. AES analysis showed high levels of carbon, calcium, and chlorine, and low levels of oxygen. Anderson concluded that the bead was not the cause but an effect of fire exposure because it contained elements of combustion products.

In the second case, arcing was found in the copper coils of a heater fan. In this case, bead analysis showed low levels of carbon, calcium, and chlorine, and high levels of oxygen. Anderson concluded that the fire must have started in the fan based on the lack of high levels of combustion products. In the final case, a crock-pot power cord was involved in a restaurant fire. AES analysis was used to indicate that the bead was created from fire exposure and was not the cause of the fire due to the presence of combustion products. Anderson did not set any quantitative standards on the presence of elements in beads for concluding that a bead was the cause of or an effect of fire.

Beland (1994) discussed the difficulties of analyzing an arc bead due to its varying composition and was critical of Anderson’s work, stating that the AES method was not effective in distinguishing between cause and effect beads. Beland’s opinion of Anderson’s AES method was based on the fact that the same elements (calcium, chloride, carbon, oxygen, etc.) would be

present regardless of whether the bead was formed from cause or effect; these elements are produced from the melting and burning of the wire insulation, which would occur during a failure condition prior to arcing or would occur during fire exposure. Beland tested several similarly prepared wire samples for chlorine, carbon and oxygen. Beads were created by subjecting energized wires to flame or by creating a short-circuiting in the wires. The elemental composition of the beads formed under these conditions did not show consistent concentration of elements trapped in beads. This was true for different beads as well as different locations in a given bead. No significant patterns were observed to indicate that a bead was the cause or effect of a fire. Beland stated that Anderson's method might be effective for bare wires but not for insulated wires.

Howitt (1997) reviewed the literature on the solubility of gases in liquid copper. He determined that there was no scientific justification for the hypothesis that atmospheric gases will become trapped in a bead as it solidifies. Howitt was able to conclude that the solubility of oxygen in copper is much lower than the detectable level of AES analysis, and oxygen is more soluble in copper in the solid state than in the liquid state where beads are formed. Howitt concluded that AES spectra of arc beads contain no relevant information to conclude whether a bead was the cause or effect of a fire.

Hoffman (2002) tested more than 700 electrical appliance power cords under various thermal conditions to assess their performance in fires and to evaluate the type of material damage sustained by the power cords. Power cords were exposed to radiant heating and direct flame impingement. Hoffman concluded that energized wires do not always produce evidence of electrical faults when exposed to radiant heating, that appearance of tested samples does not

depend on the type of exposure, and that electrically caused damage to wire conductors produced in laboratories does not differ from that found in actual fires.

Chen et al (2002) used SEM to analyze beads formed on energized wires. They evaluated the beads for graphitized and amorphous carbon. Chen et al. concluded that the beads produced from exposure to fire only had amorphous carbon, whereas beads produced from an electrical fault had both graphitized and amorphous carbon. However, only 26% of the beads produced from electrical activity showed both types of carbons, hence, this trend is not consistent through all the samples. The study did not test or analyze non-energized wires.

As stated above, many other researchers have disagreed with Anderson's analysis. According to Babrauskas (2003), Satoh et al. showed that AES analysis is not as good as Secondary Ion Mass Spectrometry [SIMS] in measuring the concentration of impurities found in beads. Babrauskas (2003) strongly disagreed with Anderson based on the fact that wires have insulation that is made of carbon containing polymers. According to Babrauskas, the insulation would vaporize on a wire heated to the point of shorting due to over-current, and a bead produced under these pre-fire conditions could contain carbon from the vaporizing insulation. Babrauskas also pointed out that calcium carbonate is a common filler in wire insulations and that PVC insulation consists of chloride, which could result in the presence of calcium and chlorine in both cause and effect beads.

Levinson (1977) studied micro and macro structures of copper conductors. According to Levinson, untested copper only contains elongated copper structures and is considered single phase. The untested copper is highly pure and oxygen free and is also known as OFHC (oxygen-free high conductivity) copper wire. The second type of copper wire is known as ETP (Electrolytic tough-pitch). According to Levinson, this copper has similar microstructures to the

untested copper, except it also contains copper oxide which is visible as small gray microstructures within the copper.

Levinson found that copper wires start to recrystallize if they are heated above 260°C. The recrystallization time decreases from hours at 260°C to seconds at 540°C or above. According to Levinson, if enough oxygen is absorbed, Cu₂O dendrites can form in the microstructure. Microstructures will be porous if the wire was heated or arced in the presence of insulation or any carbonaceous materials. This characteristic cannot be attributed to heating or arcing of the wire. Levinson stated that the melting of the wires with heat or arcing will lead to the formation of droplets (beads) at the broken ends, and the presence of droplets on wire ends is not proof that the wire was under load and arced when it broke.

As discussed above, there have been many studies that focused on the role of energized electrical wires in the initiation of fires. Many researchers have, specifically, studied the causes of arc beads in energized electrical wires. The main areas of research has focused on distinguishing between cause and effect, e.g. an arc bead which is formed due to a failure condition which causes a fire versus an arc bead that is formed from exposure to a fire (effect). Based on the literature review, there is apparent disagreement between researchers in placing a value on the analysis of arc beads. Additionally, limited research has been performed on non-energized conductors, so no one has yet provided a comparison between energized and non-energized wire damage on a microscope level. The present research will address the limitations of the current methods available to fire investigators to evaluate electrical wires, and thereby, enhance the accuracy of fire origin and cause determinations.

C. Hypothesis for the Research

As shown in the previous section, there have been many studies that focused on the role of energized electrical wires in the initiation of fires; however, most of this research has focused on distinguishing between beads formed due to a failure condition which resulted in a fire (cause) versus beads formed from exposure to a fire (effect). Even with an extensive volume of research, there is still little agreement on an appropriate methodology for evaluating beads. Furthermore, there is little agreement on the usefulness and validity of the information gathered from the analysis of a wire bead in the context of fire origin and cause investigation. Additionally, one of the largest potential flaws in the research is the assumption that beads only form on energized wires. Only limited research has been performed to establish the ability of a “bead” to form on a non-energized wire. Therefore, the ability of “beads” to only form on energized wires and the relevance of these beads in the context of the fire cause is unknown.

The main goal of this research was to address whether any distinguishing characteristics exist between beads found on energized wires versus those found on non-energized wires. Based on preliminary findings, it is hypothesized that the formation of a bead on a wire is not inherently related to the energized state of the wire, but rather is a function of the thermal kinetics of the copper. This is contrary to the belief that beads can only be formed on energized electrical wires; however, the theory that beads can only be formed on energized wires is contrary to the phenomenon of surface tension. The basic laws of physics show that the same theories that apply to water droplets can be applied to other liquids; surface tension is the true cause of the “bead” shape that forms when copper melts. According to White (1948), liquids form their spherical shape due to cohesive surface forces, and the necessity to minimize “wall tension”. All liquids would be “perfectly spherical” if no other forces existed, e.g. gravity. Therefore, it is the

liquidification (melting) of the metal that results in the formation of a bead. Whether this melting occurs as a result of fire exposure or arcing is irrelevant, since the outcome is independent of the melting conditions. Hence, it is hypothesized that the characteristic “bead”, typically defined as a round globule with a clear line of demarcation, can form on both non-energized and energized wires. Furthermore, it is hypothesized that the porosity and chemical composition of the beads will vary based on the conditions under which the beads are formed.

II. METHODS

Both energized and non-energized wires of different sizes were exposed to a variety of different fire conditions. The use of various types of exposure conditions ensured that the characteristics on the wires (or lack thereof) were not caused by one specific thermal exposure. Energized wires were tested under “load” and “no load” conditions. Under load conditions, the energized wires were plugged into a 110-120 volt power source with 9-13 amps of load. Under “no load” conditions, the wires were plugged into the power supply but no load (i.e. current flow) was placed on the circuit.

Four types of electrical wires with copper conductors were chosen in order to represent most of wires commonly found in households. The wires chosen included two multi-stranded (MS) and two single stranded Romex wires. The specific wire details are provided in Table 1.

Manufacturer	UL Listing	Size (AWG)	Conductors	Strands	Type	Temperature (C)	Voltage (V)	Ampacity (A)	Flame Rating	Insulation Thickness (mm)	Material	Insulation Color
Southwire	E18679	12	2	1	NM-B	90	600	20	N/A	0.483 C 0.762 J	PVC/ Nylon	Yellow
Southwire	E18679	14	2	1	NM-B	90	600	15	N/A	0.483 C 0.762 J	PVC/ Nylon	White
Southwire	E46194	16	2	65	SPT-2	105	300	13	VW-1	1.14	PVC	Black
Southwire	E46194	16	2	65	SPT-2	105	300	13	VW-1	1.14	PVC	Brown
I-Sheng	E315167	18	2	41	SPT-2	60	300	10	VW-1	1.14	PVC	Black
Weber	E157652	18	2	41	SPT-2	105	300	10	VW-1	Unknown	PVC	Green

Table 1: Wire Specifications

Multi-stranded wires were chosen based on an at-home survey of power cords including all lights and small appliances. It was discovered that most of the power cords were made of 18-gauge or 16-gauge, two-conductor, multi-stranded copper wires. Also, the most common branch

circuit wiring was 2-conductor, 14-gauge and 12-gauge Romex. The same Romex wiring brand was utilized for all tests; however, this was not the case for the stranded wires. The 16-gauge Southwire brand (black) and 18-gauge I-Sheng brand wires were utilized for direct flame testing. The 16-gauge Southwire brand (brown) and 18-gauge Weber brand wires were utilized for all other testing. Due to availability, the Southwire and Weber brands were utilized for the later tests.

A. Current and Voltage Data Acquisition

Various combinations of Labview and Pdaq View software and hardware were used to acquire and record data during each testing session. The voltage on the energized wires ranged from 110-120 volts, and the amperage on the loaded wires ranged from 9-13 amps. An Avtron Model K490 load bank was used to generate current on the wire to be tested under loaded condition. Electrical activity and time to failure were monitored in the energized wires using a Ohio Semitronics, model VT-120E, voltage transducer and a CR Magnetics, model CR-4320-20, current transmitter. Continuous data was recorded with the acquisition system for the entire duration of each test. A schematic of this data acquisition system and current and voltage setup are shown in Figure 1 below. In this schematic, the Test Cell represents the method of exposure: a torch, a radiation tunnel, or a compartment (scaled and full). Energized with load, energized with no-load, and non-energized wires were tested simultaneously in both full and scaled compartment tests (Sections II-D and II-E). In direct flame (Section II-B) and in radiation testing (Section II-C) wires were tested individually.

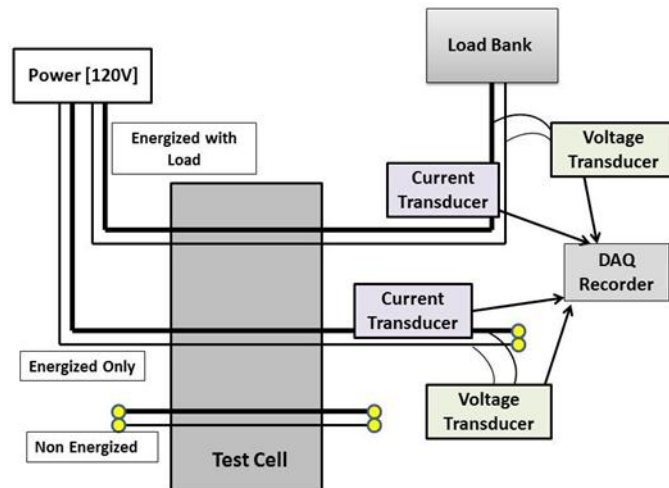


Figure 1: Data Acquisition Setup for Current and Voltage Measurements

B. Direct Flame Impingement Tests

A Benzomatic Max Power Propylene torch was used to expose all four wire types (12-gauge solid, 14-gauge solid, 16-gauge stranded, and 18-gauge stranded) to direct flame impingement. Wires were tested under three electrical scenarios: energized with load, energized with no load, and non-energized. The voltage on the energized wires ranged from 110-120 volts (V), and the amperage on the loaded wires ranged from 9-13 amps (A). Continuous data was recorded with an acquisition system utilizing Labview software. Currents and voltages were measured using the set-up described in Section II-A.

A wooden holder, shown in Figure 1, was utilized to ensure consistent wire placement relative to the torch. The wire was held about $\frac{3}{4}$ of an inch away from the tip of the torch. The adiabatic temperature for a propylene torch is approximately 1982°C (3600°F). A flame temperature of approximately 1300°C was measured with a thermal probe in the location of the wire. The mass loss rate of the fuel from the canister was 0.00426 kg/s. The heat of combustion of propylene is about 48,820 kJ/kg, therefore, the heat release rate of the torch was approximately 208 kW.



Figure 2: Direct Flame Testing Setup

The wire was held in the flame, tension free, by clamps until it broke due to melting, arcing, or shorting. Each test variation was repeated six times resulting in a total of 72 tests.

C. Radiant Tunnel Tests

A radiant tunnel apparatus, designed for this study, was utilized to expose all four wire types (12-gauge solid, 14-gauge solid, 16-gauge stranded, and 18-gauge stranded) to approximately 125 kW/m^2 and $1050\text{-}1100^\circ\text{C}$ until melting or electrical failure. Wires were tested under three electrical scenarios: energized with load, energized with no load, and non-energized. The voltage on the energized wires ranged from 110-120 V, and the amperage on the loaded wires ranged from 9-13 A. Data was recorded with an acquisition system utilizing Labview software. Currents and voltages were measured using the set-up described in Section II-A. Time to failure was documented on the non-energized wires using a stopwatch. The radiant tunnel apparatus is shown in Figure 2.

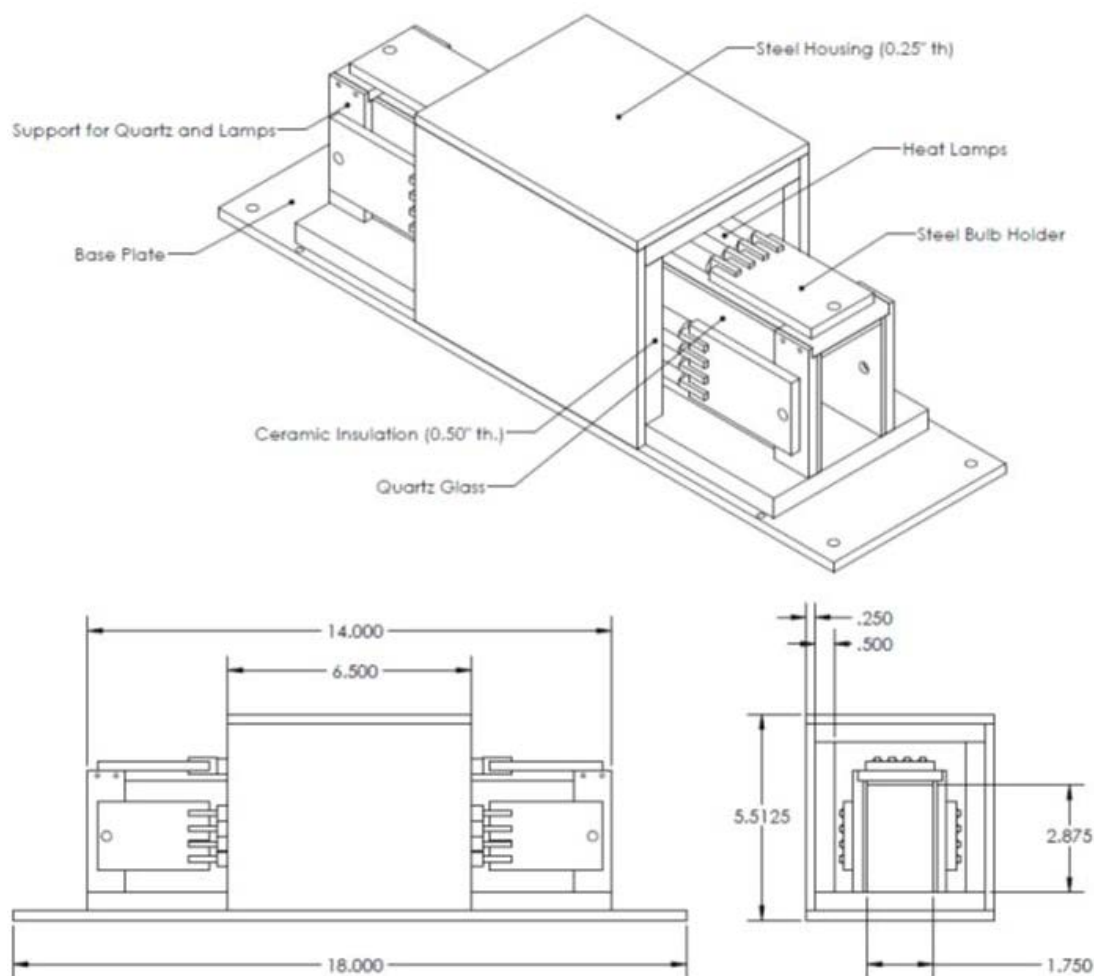


Figure 3: Radiation Testing Tunnel (Units in Inches)

The apparatus contained twelve (12), 120 volt, 1200 watt bulbs inside a 14-inch long tunnel. Four bulbs were installed on the ceiling and each of the two vertical walls. Wires were run horizontally through the tunnel and supported on each end with clamps. The exterior of the tunnel was constructed of 1/4 inch steel, and the interior of the tunnel was lined with marinite. The bulbs were mounted on the marinite and a protective quartz glass shield was used around the bulbs to prevent breakage due to arc spatter. Voltage and amperage to the bulbs was adjusted using a Model 18D Solid State Power Supply manufactured by Payne Engineering. The tunnel was calibrated before the start of each test to ensure that the heat flux and temperature output

was consistent. A Vatell Corporation circular foil heat flux transducer (Model TG1000-30, maximum flux: 150 kW/m²) was used for the calibration.

In order to avoid pre-heating of the samples during placement inside the tunnel, a heavily insulated, fiberglass sample holder was utilized. The wire was placed in the sample holder and clamped at one end of the tunnel. The sample holder was removed from the wire when the test was ready to begin. Once the sample holder was removed, the wire was clamped on the other end of the tunnel. No tension was placed on the wire. The wire was exposed to radiation until it broke due to heat and/or electrical activity.

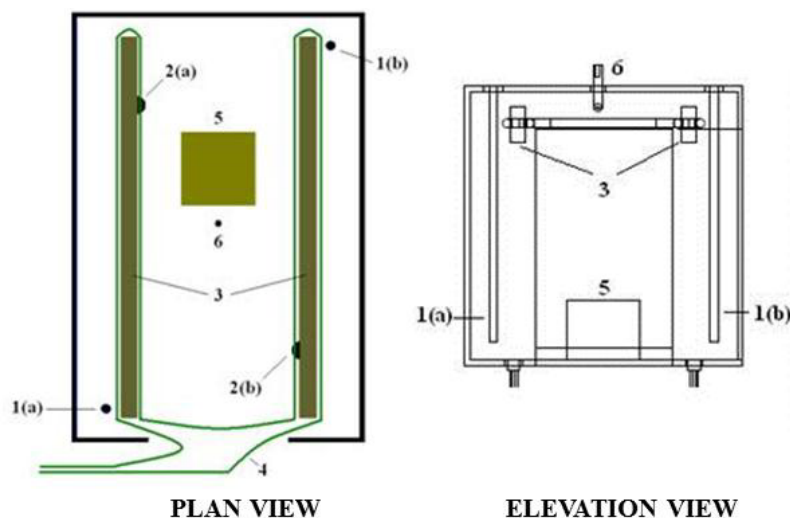
The design of the radiant tunnel apparatus was improved throughout the testing process as issues arose; however, there were still some challenges that were faced when running this piece of equipment. In particular, some of the IR bulbs intermittently or completely stopped working between tests. The failures appeared to be caused by the premature aging of the bulbs and their connections due to the dramatic thermal cycling of the apparatus. The bulbs were replaced several times in order to continue testing. Finally, it was decided that the tunnel would be run continuously for one day to eliminate the thermal cycling. By running the tunnel continuously, a large number of tests were completed and no bulb replacement was necessary due to the elimination of the heating and cooling cycle. Each test variation was repeated three times resulting in a total of 36 tests.

D. 2/5-Scale Compartment Tests

A 2/5-scaled compartment was utilized to expose all four wire types (12-gauge solid, 14-gauge solid, 16-gauge stranded, and 18-gauge stranded) to a fire from incipient stage to fully-developed stage. Wires were tested under three electrical scenarios: energized with load, energized with no load, and non-energized. The voltage on the energized wires ranged from

110-120 V, and the amperage on the loaded wires ranged from 9-13 A. An Avtron (Model K490) load bank was used to generate current. Electrical activity and time to failure were monitored in the energized wires using the setup described in Section II-A. Temperatures within the compartment were monitored with two thermocouples trees located in the front left and middle of the compartment. Each tree contained eight (8), Type K thermocouples spaced approximately 6 inches apart from ceiling to floor. Heat flux within the compartment was monitored with two Medtherm Corporation, heat flux transducers (Model 64-10-20, 100 kW/m²) located at floor level in the front right and back left corners. Temperature, heat flux, and electrical data were recorded with an acquisition system utilizing Labview software.

The 2/5-scale compartment was modeled after the ASTM E1822 full-scale compartment. The interior dimensions of the compartment measured 38.5 inches wide by 58 inches long by 38.5 inches high. The ventilation opening at the front of the compartment measured 18 inches wide by 32 inches high as shown in Figure 3. The interior walls were constructed of ½ inch gypsum wallboard covered with a ½ inch layer of marinite. The exterior walls of the compartment were built with ¾ inch plywood on (2x4)-inch wood studs. The compartment was constructed to withstand temperatures in excess of 900 °C which are typically found during room flashover conditions. Wire samples were mounted on (2x4)-inch wood studs and hung from the ceiling of the compartment as seen in the plan view in Figure 3. The wiring was secured to the wood with metal staples. The staples were loosely secured into the wood in order to prevent any excessive pressure on the cable insulation and to minimize the potential for localized electrical activity between the wires and the staples. Each tested wire was about 40 feet long, which provided a sufficient length of wire to be routed through the ceiling of the compartment and out to the data acquisition system.



- 1(a) – TC Tree (4 inches from front and left wall)
- 1(b) – TC Tree (4 inches from back and right wall)
- 2(a) – Radiometer (12 inches from front wall, 8 inches from left wall)
- 2(b) – Radiometer (12 inches from back, 8 inches from right wall)
- 3 – 2x4 Wood Beams (6 inches from sides, 3 inches below ceiling)
- 4 – Wire (attached to wood beams via metal staples)
- 5 – Wood Crib ((10X10X9) inches on top of 12-inch diameter dish)

Figure 4: Sketch of Compartment Testing Setup

After preliminary tests were conducted in the compartment, it was determined that the compartment only reached a maximum temperature of 930°C during post-flashover conditions. This was due to limited ventilation within the compartment, and the greater surface-to-volume ratio when compared to a full-scale compartment. This temperature was not sufficient to melt the non-energized copper wires. In order to increase the temperature within the compartment, the amount of ventilation available for combustion was increased using a forced air blower. The blower fan was ducted to the bottom portion of the doorway of the compartment. The ducting was 8 inches in diameter and was fitted with a 4 inch by 18 inch adapter at the compartment doorway. Figure 4 shows the general layout of the compartment and ducting using in a prior study by Goodman et al (2010). The original adapter size was modified for the purposes of this study to run the entire doorway width.



Figure 5: Flashover Compartment

Because test samples were placed near the ceiling, the ventilation ducting was positioned at the bottom of the doorway to minimize disruption of the upper thermal layer development within the compartment. The blower produced an air flow velocity of approximately 6 m/s measured at the 8-inch diameter duct opening, so the flow rate was slightly higher than 400 CFM. Each test variation was repeated six times resulting in a total of 72 tests.

E. Full Scale Compartment Tests

Full scale compartment fire tests were performed at the National Fire Academy (NFA) in Emmitsburg, Maryland in conjunction with the Academy's fire origin and cause investigations course. NFA utilizes up to eight (8) test cells to simulate various types of fire scenes that investigators may encounter in the field. Most of the test cells are furnished with carpeting, couches, armchairs, coffee tables, televisions, lamps, and various other household items. Each compartment measured 156 inches (13 feet) long by 108 inches (9 feet) wide by 96 inches (8 feet) high with a 23 inch wide by 35 inch high window and a 32 inch wide by 82 inch high doorway. In some cases, the window was partially open during the test, in other cases; it was opened at some point during the test. In all cases, the position of the doorway was varied

throughout the test to control the ventilation; if the fire growth slowed down, the door was opened and if the fire growth was too fast, the door was closed. This was done until flashover conditions were reached in the test room. In most cases, the fire was extinguished by the fire fighters immediately after flashover conditions were observed.

The compartments were utilized to expose all four wire types (12-gauge solid, 14-gauge solid, 16-gauge stranded, and 18-gauge stranded) to a fire from incipient stage to fully-developed stage. Wires were tested under three electrical scenarios: energized with load, energized with no load, and non-energized. The voltage on the energized wires ranged from 110-120 V, and the amperage on the loaded wires ranged from 9-13 A. A load bank (Avtron Model K490) was used to generate current. Electrical activity and time to failure were monitored in the energized wires using the setup described in Section II-A. Temperatures within the compartment were monitored with a thermocouple tree located in the center of the room. The tree contained eight (8), Type K thermocouples spaced approximately 12 inches apart from ceiling to floor. The heat flux within the compartment was monitored with a Medtherm Corporation heat flux transducers (Model 64-5-20, 50 kW/m²) located at floor level in the center of the room. Temperature, heat flux, and electrical data were recorded with an acquisition system utilizing Labview software.

The electrical wire samples were hung from the ceiling in a manner similar to the 2/5-scale compartment testing. The orientation of the wires is shown Figure 5.



Figure 6: Wire Samples in the Ceiling with Thermocouple Tree

As was encountered with the small-scale tests, it was difficult to achieve temperatures in the compartment that exceeded 900 °C. This was partly because of ventilation conditions within the compartments, and partly because of the need to leave the cells in suitable condition for post-fire investigation. Since the test cells were being utilized for investigation training, it was important to have some remains for the student to evaluate. Therefore, the test fires were not allowed to remain in a fully-developed stage for a long period of time. In a few instances, the temperature did exceed the melting point of copper, and effects were seen on the non-energized copper wires; however, this was not the case for every test. Each test variation was repeated three times resulting in a total of 36 tests.

F. Sample Analysis

After each set of four thermal exposures was completed, damage on each wire sample was photographed using a Nikon SMZ800 stereomicroscope with 40x magnification. Some samples were analyzed with an SEM at University of Maryland (College Park, MD) or at Unified Engineering (Aurora, IL). Samples analyzed at University of Maryland were not mounted, cut, polished, or etched; only the exterior surface was analyzed. Samples analyzed at Unified

Engineering, Inc. were mounted in Buehler epomet epoxy, rough sanded with 100 grit paper until the features were exposed, and then progressively sanded to a final polish of 3 μm . After polishing, the samples were etched for 20 -30 seconds with a solution of 1 gram FeNO_3 , 15 mL H_2O and 5 MI HCl . These samples were also photographed with stereo microscope at CSE.

Some of the samples were also sent to Accident Reconstruction Analysis, Inc. (ARAI) to evaluate the internal bead structure with a metallurgical microscope. The ARAI staff, particularly Dr. Charles Manning, has vast experience in the metallurgical analysis of copper wires. Samples were mounted and etched with an Ammonium Hydroxide-Hydrogen Peroxide solution.

Lastly, a one dimensional (1-D) heat transfer analysis was performed to determine the axial heat transfer within the copper conductor away from the section being heated by the flame. A simple conduction model was used to perform the simulation.

III. RESULTS

A. Summary of Results

A total of 190 wire samples were tested. Wire types included 12-gauge and 14-gauge solid and 16-gauge and 18-gauge stranded conductors. The tests were conducted using a bench-scale, premixed flame impingement apparatus, a bench-scale 125 kW/m² radiant tunnel apparatus, and 2/5-scale and full-scale flashover compartments.

Temperature, heat flux, current, voltage, trip time, and break time were recorded for each test. All of the collected data was analyzed for commonalities and trends. All of the wire samples were photographed, and the location and number of failure points was documented. Additionally, some of the wire samples were mounted, cut, polished, etched, and analyzed using a combination of stereomicroscopic, metallurgical, and SEM/EDS techniques.

Based on preliminary studies, it was hypothesized that characteristic “arc-beads” could be formed on energized wires as well as non-energized wires. Additionally, it was hypothesized that the formation of a bead on a wire was not a function of its “energized state”, but a function of its “thermal state”. These hypotheses have been further validated by the research results discussed below. No trends or distinguishing visual or microscopic characteristics that definitively differentiate between beads formed on energized and non-energized wires have been found in the samples reviewed to-date.

Whether a wire was energized with load, energized without load, or non-energized had no significant effect on the visual or microscopic characteristics of the wire. Round copper globules with clear lines of demarcation, traditionally defined as “beads”, were produced on both energized and non-energized wires. Some energized wires that did arc failed to produce round copper globules with clear lines of demarcation, while some non-energized wires that did not arc

did produce these characteristic beads. Under the microscope, beads from some of the energized wires were porous and contained a large quantity of internal void spaces, while other beads contained no void spaces. This same trend was true for non-energized wires. A preliminary view of the samples under SEM/EDS also showed no trends in grain structure or chemical compositions. A detailed study by ARAI of the inner grain structures of the beads did reveal some significant distinguishing trends between energized and non-energized wires but not in all samples.

B. Testing Data and Results

Data and results are presented in four subsections and separated according to thermal exposure type: direct flame impingement, radiant tunnel, 2/5 scale compartment, and full-scale compartment.

1. Direct Flame Impingement Tests

A Bernzomatic Max Power Propylene torch was utilized to exposure wires to direct flame impingement. The wire samples were held near the center of the premixed flame until they severed due to melting and/or electrical activity. Testing was discontinued after a break in the wire occurred or the circuit breaker tripped due to short-circuiting or arcing. Table 2 shows the breakage time or trip time for each wire type under all three electrical conditions.

Test No.	Romex 12/2			Romex 14/2		
	NE	E	L	NE	E	L
	Time to Break or Trip (Minutes)					
1	2.92	1.04	0.75 (T)	3.50	0.79	0.77
2	2.25	0.73 (T)	0.64 (T)	3.50	0.57	0.65
3	1.68	0.63	0.50 (T)	3.38	0.48	0.82
4	2.67	0.76 (T)	0.56 (T)	3.20	0.83	0.75
5	2.33	0.86 (T)	0.63 (T)	3.40	0.51	0.58
6	2.48	0.68 (T)	0.67 (T)	5.43	0.84	0.75
Average	2.39	0.78	0.62	3.74	0.67	0.72
Test No.	Multi-Strand 16/2			Multi-Strand 18/2		
	NE	E	L	NE	E	L
1	1.13	0.42	0.37 (T)	2.00	0.42	0.30
2	0.49	0.32	0.30	1.72	0.25	0.27 (T)
3	0.49	0.33	0.38 (T)	1.18	0.25	0.23 (T)
4	0.61	0.33	0.26 (T)	0.73	0.25	0.24 (T)
5	0.49	0.29	0.30	1.52	0.25 (T)	0.26 (T)
6	0.69	0.28	0.34	2.67	0.25	0.39
Average	0.65	0.33	0.33	1.64	0.28	0.28
NE = Non-Energized, E = Energized, No Load and L = Energized, Loaded (T) Circuit tripped but wire did not break						

Table 2: Direct Flame Testing Results (DF)

The test was discontinued when the circuit tripped or the wire broke. In the 12-gauge solid wire tests, trip time occurred before breakage time in 4 out of 6 tests for energized, no load conditions, and 6 out of 6 tests for energized, loaded conditions. No circuit breaker trips occurred in any of the 14-gauge solid wire tests. The stranded wires were variable, with circuit tripping occurring in 3 out of 6 tests of 16-gauge, energized, loaded wires. In the stranded, 18-gauge wires, circuit tripping occurred in 1 out of 6 tests of energized, non-loaded wires, and 4 out of 6 tests of energized, loaded wires. Overall, between all wire types, however, the difference between trip times and breakage times was not significant. Hence, trip time did not seem to occur any earlier or later than breakage time. The data from Table 2 was plotted for each wire type under all three electrical conditions as shown in Figure 6. The results for the

energized wires were plotted again, in Figure 7, to provide easier visual comparison. The remaining plots for the direct flame testing are presented in Appendix A.

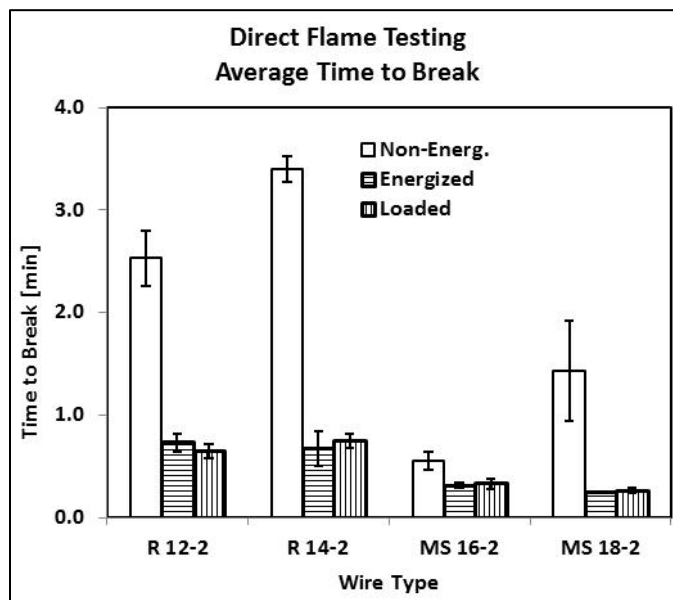


Figure 7: Average Time to Sever or Trip for All Wire Types (DF)

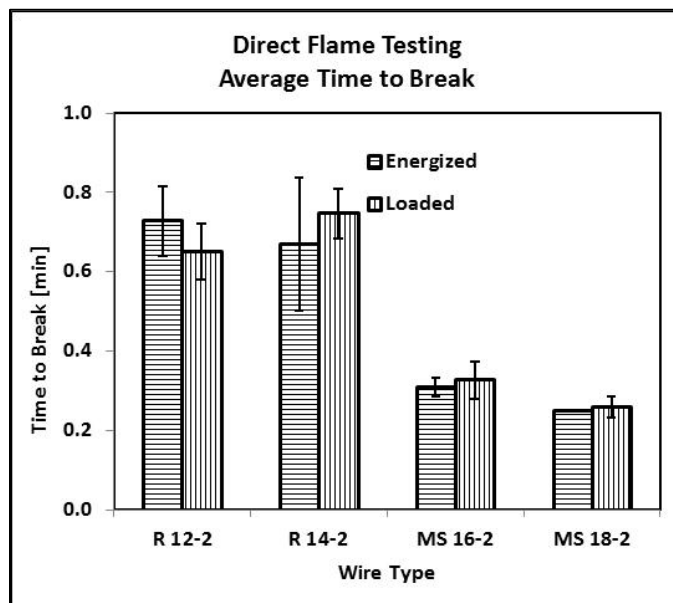


Figure 8: Average Time to Break or Trip for Energized and Loaded-Direct Flame Tests (DF)

A significant difference was present between the breakage times under the non-energized conditions when compared to the energized condition. However, no significant difference was

present between the breakage times in the energized, loaded and energized, non-loaded wires. When comparing different wire types, the breakage times were longer for the solid (14 and 12) gauge, energized wires (loaded and non-loaded) then for the stranded (16 and 18) gauge, energized wires; the same was true for the non-energized wires. Hence, overall, it took a longer period of time, regardless of energized state, for the solid wires to break when compared to the stranded wires. When evaluating within the solid, non-energized wire group, however, longer breakage times were not associated with larger wire gauges; the same was true for the stranded wire group. The 14-gauge solid wires (smaller) had a significantly longer breakage times then the 12-gauge solid wires (larger), as did the 18-gauge stranded wires when compared to the 16-gauge stranded wires. Hence, the dissipation of heat in the wires does not appear to be solely based on wire diameter, but is also dependent on wire geometry (stranded versus solid).

For the loaded and energized wires, current and voltage data was recorded to monitor any electrical activity in the wire before failure. A representative graph of this data is shown in Figure 8 and Figure 9. In most cases, as shown in Figure 8, the wire broke and the current went to zero without any registered change in the current or voltage before failure.

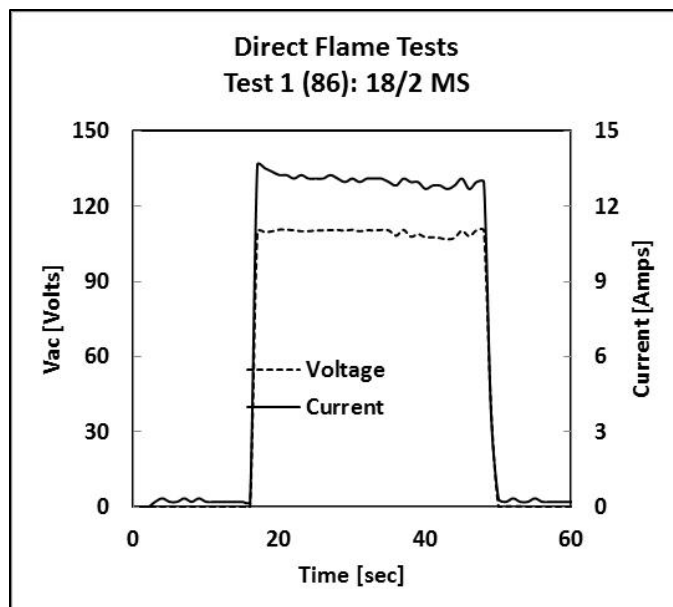


Figure 9: Typical Amperage and Voltage Graph (Loaded Wire DF)

In some cases, however, large spikes in the current occurred before the wire was severed. The spikes, as shown in Figure 9, appear to be consistent with arcing through the conductive char formed between the hot, neutral, and ground conductors from the burning insulation.

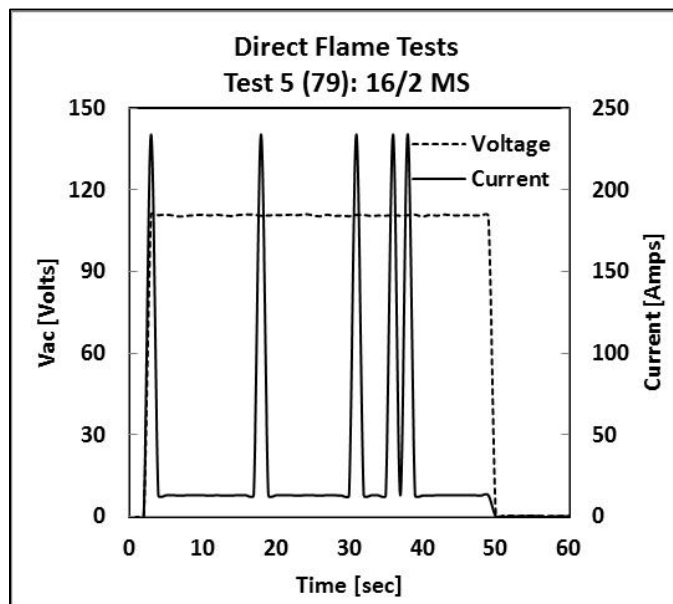


Figure 10: Arcing Through Char (DF)

Current spikes were observed in 9 of the 24 tests that were conducted with loaded wires. All six tests utilizing the 16-gauge, multi-stranded wires exhibited arcing through char; however,

none of the 18-gauge, multi-stranded wires exhibited this effect. Only 25% (3 of 12) of the solid gauge wires exhibited arcing through char (two 14-gauge wires and one 12-gauge wire). The tendency of some wires to exhibit arcing through char is believed to be linked to the wire insulation type. Hence, the ability of the wire insulation to support charring is a significant factor in the breakage times; the 16-gauge wire exhibited the highest predominance of arcing through char which produced the shortest breakage time.

It should be noted that the maximum current output of the transmitter is approximately 240 amps; there were no recorded spikes above this value. Hence, the true current spike may have been greater than the recorded value. The measured currents in this study are consistent with those found by other researchers; Hagimoto et al. (1999) measured currents up to 250 amps produced during arcing conditions through carbonized pathways in PVC-covered electrical cords.

2. Radiant Tunnel Tests

Table 3 shows the breakage times and trip times for each wire type under all three electrical conditions: energized, loaded, and non-energized for radiant tunnel testing. In some cases, the circuit tripped due to arcing prior to a breakage in the wire. In some cases, the wire broke when the circuit tripped. Under the direct flame condition, the test was discontinued when the circuit tripped or the wire broke. In the radiant tunnel condition, the tests were run until a complete severing of the wire occurred regardless of the trip time. Hence, some breakage (severing) times are longer than the trip times, and some breakage in energized wires occurred after circuit tripping when the wire was de-energized.

Test No.	Romex 12-2				
	NE	E		L	
	Break	Trip	Break	Trip	Break
	[min]	[min]	[min]	[min]	[min]
1		0.67	0.67	0.45	0.45
2	1.03	0.45	1.15	0.47	1.12
3	0.95	0.47	0.50	0.42	0.42
Averages	1.00	0.53	0.77	0.44	0.66
Test No.	Romex 14-2				
1	1.07	0.58	0.67	0.37	0.75
2	1.03	0.45	0.50	0.42	0.78
3	0.92	0.32	0.45	0.47	0.47
Averages	1.01	0.45	0.54	0.42	0.67
Test No.	Multi-Stranded 16-2				
1	1.05	0.25	0.48	0.22	0.22
2	0.70	0.23	0.82	0.32	0.50
3	0.97	0.30	0.92	0.28	0.28
Averages	0.91	0.26	0.74	0.27	0.33
Test No.	Multi-Stranded 18-2				
1	0.53	0.20	0.20	0.20	0.20
2	0.58	0.18	0.58	0.22	0.22
3	0.55	0.18	0.18	0.20	0.20
Averages	0.56	0.19	0.32	0.21	0.21

Table 3: Radiation Testing Results (R)

Out of the 24 energized wires tested (12 with load and 12 with potential only), 11 had the same breakage and trip times. Of the 11 that did have the same trip times, 8 were under load conditions. Therefore, approximately half of the energized wires that broke did so due to an arcing or shorting event that was significant enough to cause the circuit to trip. Additionally, there was a slightly higher tendency for this to occur in loaded wires as opposed to energized wires with potential only.

The charts below represent the average break time and trip time for each wire under different electrical conditions. Figure 10 includes the average break times for all three electrical

conditions separated by wire type, while Figure 11 includes average trip times for the energized wires separated by wire type.

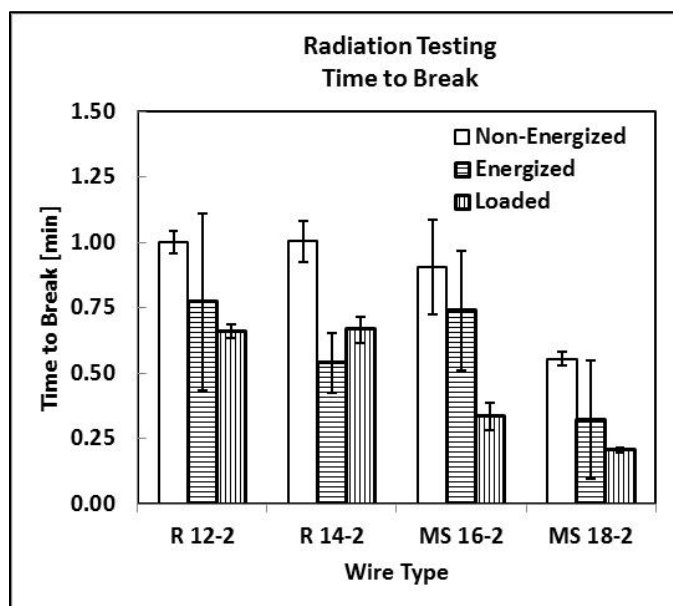


Figure 11: Average Break Time under Radiant Loading (R-All)

A significant difference in the breakage times was present between the non-energized and energized, loaded wires. The loaded wires had quicker breakage times than the non-energized wires. This is related to the tendency of the energized, loaded wires to break and trip the circuit at the same time. Hence, arcing of the wires played a large role in the shorter breakage times for the energized wires. This trend was also seen in the direct flame tests.

There was no significant difference in the breakage times for the energized, loaded and energized, non-loaded wires with the exception of the 16-gauge stranded wires. Wire gauge did play some role in the breakage times for energized, loaded wires; the smaller the wire gauge the faster the breakage times with the exception of the 12-gauge and 14-gauge wires which had approximately the same breakage times. Additionally, the stranded wires had quicker breakage times than the solid gauge wires. This trend was also similar to that found in the direct flame studies.

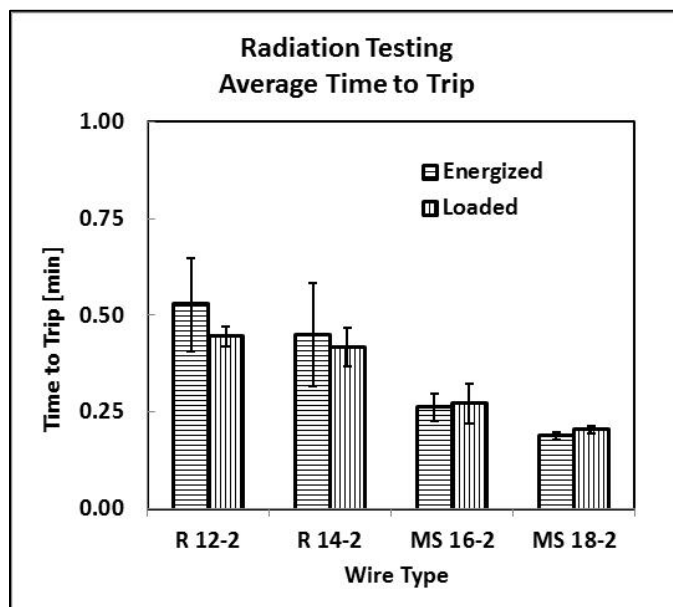


Figure 12: Average Trip Time-Radiation Tunnel Tests (E and L-R)

The trip times for the energized and loaded wires did not vary significantly within wire types; however, the trip times did trend downward with decreasing wire gauge. Therefore, the trip time does show some dependence on wire size. The average trip times for the radiation testing is slightly lower than for the direct flame testing. In the direct flame tests, the wire insulation melted, charred, and then arcing resulted in breakage or tripping. In the tunnel tests, the wire insulation was vaporized almost instantaneously due to the substantial heat flux present in the tunnel. In the tunnel tests, the copper wires were de-insulated very early in the exposure period, and a char did not form on the insulation. Without the protective insulation, it is likely that the wires would arc or short more quickly in the tunnel tests, which is consistent with the test results. Figure 12 provides a comparison of the various wire types grouped by average break times and trip times for energized, loaded and energized, non-loaded wires.

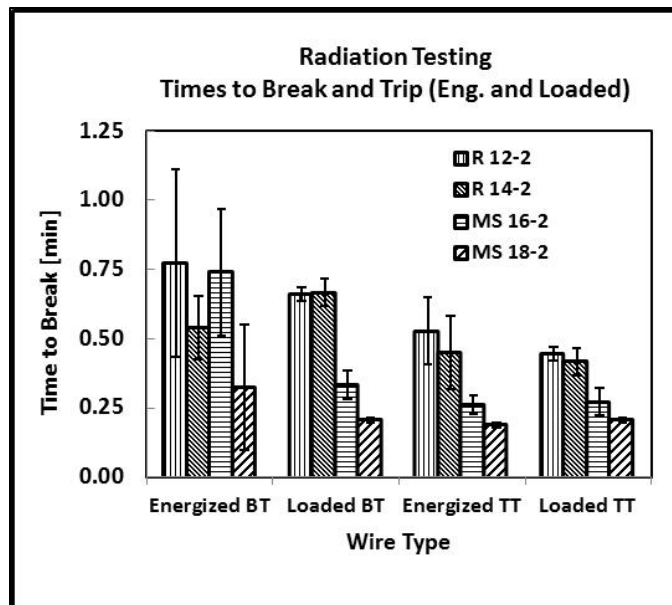


Figure 13: Average Break Time and Trip Time under Radiant Loading (R)

The break times for the non-loaded wires (Energized breakage times) were quite variable when compared to the other three conditions (Loaded breakage times, Energized trip times, and Loaded trip times). If a break occurred in the non-loaded wires, it happened under two possible scenarios: 1) at the same time as the circuit tripped, or 2) after the breaker tripped. If the break occurred after the circuit tripped, then the wire was de-energized and the break occurred solely due to melting as opposed to arcing. Hence, the large variation in the breakage times is likely due to the fact that some wires had to melt in order to break (resulting in a longer breakage times) while others arced and broke (resulting in a shorter breakage times). The presence of load on the circuit did appear to support wire failure more quickly when compared to those wires that had electric potential only. This result could be due to the added heat generation from the presence of power (I^2R) in the wire or due to the ability of arcing to be more easily established between wires because of the presence of an electric field.

3. 2/5-Scale Compartment Tests

The maximum temperatures and heat fluxes measured in the compartment throughout the duration of the tests is shown in Table 4. The trip times, as well as, the maximum temperatures and heat fluxes at the time of tripping are also presented in the table. The total heat flux per unit area (TEA) between $t=0$ and $t=\text{trip}$ was calculated to establish the total energy output from the fire in the compartment. The trapezoidal method was used to derive the area under the curve to calculate the TEA.

The average maximum temperatures in the compartment ranged from 996 °C to 1149 °C. The average maximum heat fluxes in the compartment ranged from 91 kW/m² to 255 kW/m². In the 14-gauge wire studied, the rear heat flux meter appeared to be measuring above normal heat fluxes typically given as 90-150 kW/m². The meter was re-calibrated and measurements taken after re-calibration were within expected ranges based on the temperature profiles inside the compartment.

Test	T Max		HF Max		Trip Time		T Max _{Trip}		HF Max _{Trip}		TEA	
	Front	Back	Front	Back	E	L	E	L	E	L	E	L
	[°C]		[kW/m²]		[min]		[°C]		[kW/m²]		[kJ/m²]	
	Romex 12-2											
1	1108	1026	89.5	98.7	3.48	3.48	705	705	5.25	5.25	295	295
2	1123	1078	93.2	116	3.39	3.77	738	690	7.06	7.01	432	281
3	1119	1017	98.4	138.2	3.77	3.77	672	672	5.31	5.31	394	394
4	1190	1125	147	145.8	4.77	4.77	494	494	4.35	4.35	243	243
5	1034	1047	64.3	133.3	4.38	4.38	407	407	10.32	10.32	321	321
6	1206	1007	87.5	NA	NA	NA	605	605	3.01	3.01	208	208
7	879	675	161	97.7	3.13	3.13	611	611	4.69	4.69	448	448
Ave	1094	996	105.8	121.6	3.82	3.88	604	598	5.71	5.7	334	313
Test	Romex 14-2											
1	1117	1098	75.1	273.4	3.92	3.92	466	466	5.15	5.15	455	455
2	1150	1020	89.3	241	4.42	4.42	472	472	3.81	3.81	311	311
3	1154	1071	89.4	245.4	4.9	4.9	329	329	2.66	2.66	262	262
4	1173	1020	110.2	260.3	3.81	3.81	336	336	2.43	2.43	172	172
Ave	1149	1052	91	255	4.26	4.26	401	401	3.51	3.51	300	300
Test	Multi-Stranded 16-2											
1	1039	1150	229.9	145.9	4.24	3.34	397	261	5.33	3.28	524	282
2	1163	1047	162.3	134.1	3.61	3.51	597	592	6.08	4.72	436	400
3	1041	1148	86.4	197	No Trip	3.71	No Trip	462	No Trip	1.9	464	305
4	1050	1158	109.1	211	3.41	2.99	709	620	8.75	4.72	314	256
5	1059	1139	211.3	150.2	4.38	4.03	482	482	3.13	3.13	178	168
6	1077	1143	132.7	161	2.64	2.54	781	754	10.04	9.38	518	282
Ave	1072	1131	155.3	166.5	3.66	3.35	593	528	6.66	4.52	405	282
Test	Multi-Stranded 18-2											
1	967	1256	176.6	135.8	5.31	4.31	638	536	5.85	2.69	931	300
2	1033	1047	155.6	151.8	No Trip	3.96	715	501	12.8	4.2	No Trip	NA
3	1051	1085	147.4	133.9	5.53	5.38	613	579	5.97	4.65	484	434
4	1042	1081	155.1	119.4	5.28	4.48	449	405	5.04	3.01	438	251
5	1001	1179	NA	NA	3.31	2.66	704	569	12.8	5.81	786	346
Ave	1019	1130	158.7	135.2	4.86	4.16	624	518	8.49	4.07	660	333

Table 4: Scaled Compartment Testing Results (SC)

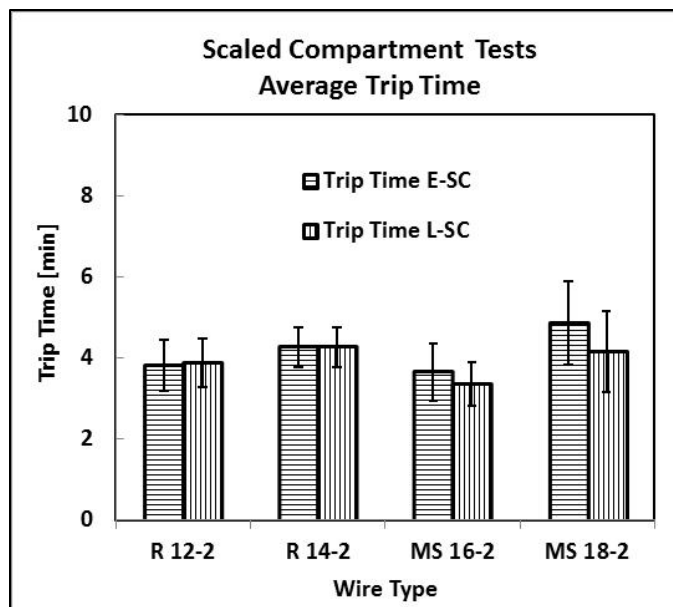


Figure 14: Average Trip Time-Scaled Compartment Tests (SC)

The average trip time ranged from 3.4 minutes to 4.9 minutes, as shown in Figure 14. When comparing wire types, there was no significant difference in trip times. It should be noted that the testing performed on the solid gauge, energized wires with load and without load was done at the same time in the test compartment, and both wires (loaded or un-loaded) were plugged into the same power source. Hence, when a trip occurred and the circuit was de-energized, it was not possible to identify which wire (loaded or unloaded) caused the trip. Therefore, the temperatures and heat fluxes at the time of tripping are the same for the wires energized with load and without load. In order to avoid this same issue with the stranded wire tests, separate circuits were utilized for the loaded and unloaded energized wires. There was no significant difference between the times to trip for the energized with load versus those energized without load.

Also, Table 4 lists the maximum heat fluxes and temperatures in the compartment at the time of circuit tripping. The heat fluxes ranged from 3.5 kW/m² to 8.5 kW/m², and the

temperatures ranged from 401 °C to 624 °C. The average maximum heat fluxes and temperatures at time of tripping are shown in Figure 15 and Figure 16, respectively.

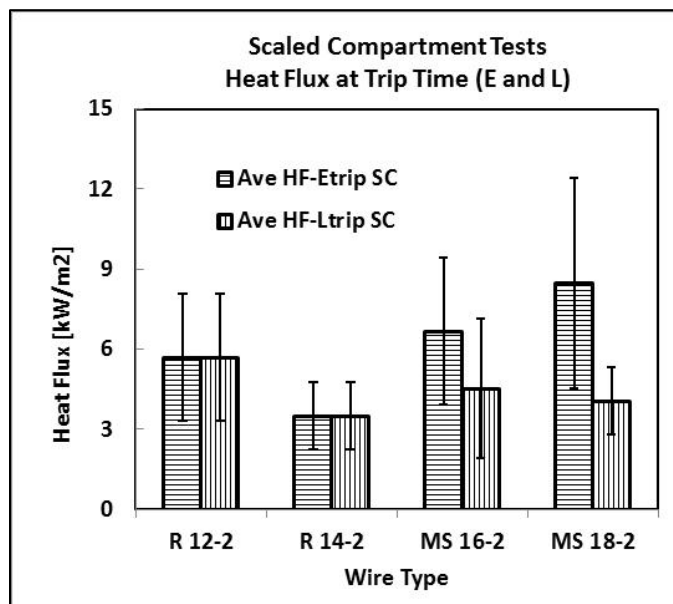


Figure 15: Heat Flux at Circuit Trip Time-Scaled Compartment Tests (SC)

When comparing wire types, there were no significant difference between the heat fluxes and temperatures at circuit trip time. The 14-gauge wires had lower average temperatures and heat fluxes at trip times. The loaded, stranded wires also had trip times at lower temperatures and heat fluxes. However, these differences were not highly significant based on the standard deviation in the measurement.

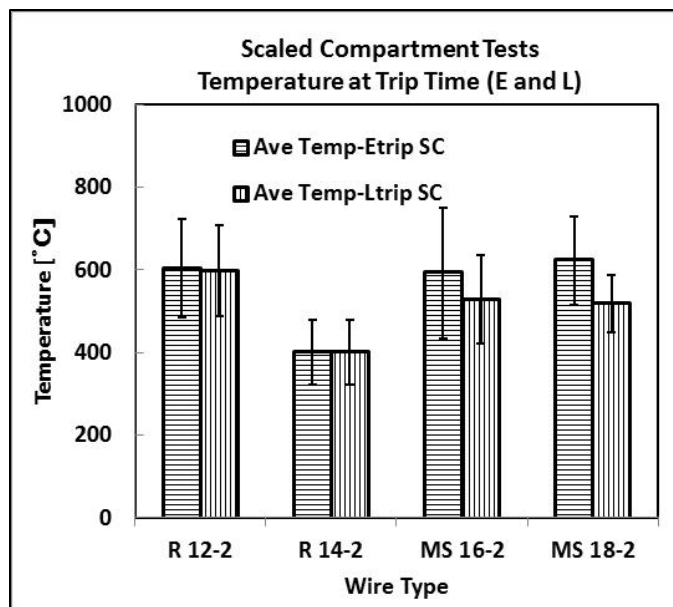


Figure 16: Temperature at Circuit Trip Time-Scaled Compartment Tests (SC)

Another method for comparison of the failure times for different wires was through examination of the total energy per unit area (TEA) that the wire was exposed to at the time of failure. The total energy per unit area was calculated by integrating the heat flux data as a function of time. The average TEA ranged of 282 kJ/m² to 660 kJ/m². The TEA for the energized, non-loaded wires had a larger range of 300 kJ/m² to 660 kJ/m² when compared to the TEA for the energized, loaded wires which had a range of 282 kJ/m² to 333 kJ/m². This finding is consistent with the direct flame and radiant tunnel tests, which shows that loaded wires tripped sooner than non-loaded wires.

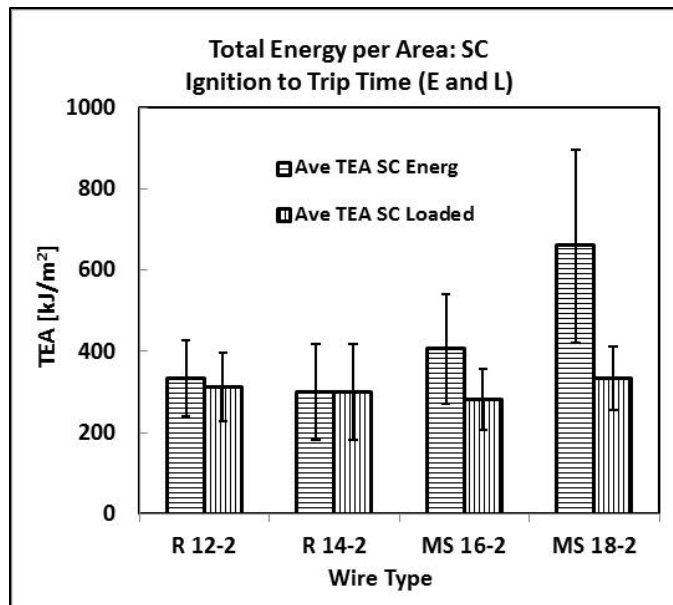


Figure 17: TEA at Trip Time for the Scaled Compartment Tests (SC)

Additionally, in some cases, the higher TEA values were due to the fact that the circuit breaker did not trip at the first sign of breakage. This condition occurred for a number of the 18-gauge wire tests, where the first breakage of the wire did not trip the circuit. Additionally, in one case the circuit breaker did not trip at all during the test. Figure 17 provides a graphical representation of the TEA data. Like the temperature and heat flux data, the TEA values are also consistent throughout all wire types. The TEA for the stranded wires was less for the loaded conditions than for the non-loaded conditions, as discussed above.

4. Full Scale Compartment Tests

The maximum temperatures and heat fluxes measured in the full-scale compartment throughout the duration of each test are shown in Table 5. The trip times, as well as, the maximum temperatures and heat fluxes at the time of tripping are also presented in the table. The total heat flux per unit area (TEA) between $t = 0$ and $t = \text{trip}$ was also calculated to establish the total energy output from the fire in the compartment. The trapezoidal method was used to

derive the area under the curve to calculate the TEA. Due to gaps in data logging at the beginning of the 18-gauge wire tests, maximum heat flux and temperature values were recorded, but the total heat flux profile needed for TEA calculations was not recoverable.

Test No	T Max	HF Max	Trip Time	T Max _{Trip}	HF Max _{Trip}	Load	TEA
	[°C]	[kW/m ²]	[min]	[°C]	[kW/m ²]	[amps]	[kJ/m ²]
Romex 12-2							
1	1178	111.0	4.85	278	5.7	9.2	945
2	841	134.7	2.66	821	45.4	9.3	621
3	917	134.6	2.63	751	38.5	13.0	342
Averages	979	126.8	3.38	617	29.9	10.5	636
Romex 14-2							
1	910	138.5	3.05	831	42.5	13.0	270
2	848	94.7	3.02	713	15.4	9.1	624
3	1001	107.6	2.88	760	20.1	12.7	273
Averages	920	113.6	2.98	768	26.0	11.6	389
Multi-Stranded 16-2							
1	776	67.0	3.80	479	14.0	12.4	476
2	1000	128.0	1.55	759	23.8	12.4	103
3	930	83.8	2.79	775	65.0	12.7	270
Averages	902	92.9	2.71	671	34.3	12.5	283
Multi-Stranded 18-2							
1	933	115.3	3.27	342	6.7	11.7	No Data
2	846	63.9	4.88	314	14.7	12.0	No Data
3	907	109.4	3.81	209	19.5	11.6	No Data
Averages	895	96.2	3.99	288	13.6	11.8	No Data

Table 5: Full-Scale Compartment Testing Results (FSC)

The average maximum temperature in the compartment ranged from 895 °C to 979 °C. The average maximum heat flux ranged from 93 kW/m² to 127 kW/m². The range of maximum temperatures and heat fluxes achieved in the full-scale studies was slightly lower than in the scaled compartment. Since these tests were conducted in conjunction with tests at NFA which were being used for an investigations training course, there was no ability to artificially raise the temperatures within the compartment through the use of forced ventilation. Additionally, the

fires were extinguished quickly after the compartment reached flashover conditions to leave some remains for the investigations class to evaluate. This quick extinguishment also limited the maximum temperatures and fluxes in the compartment.

The average trip times ranged from 2.7 minutes to 4.0 minutes, which were within the range found in the scaled compartment tests. The maximum temperatures and heat fluxes at the time of circuit tripping ranged from 288 °C to 768 °C and 14 kW/m² to 34 kW/m², respectively. The variability in the temperature range was greater than in the scaled compartment tests; however, the scaled compartment temperature values did fall within the full-scale compartment range. The heat flux range in the full-scale compartment was approximately four (4) times higher than that found in the scaled compartment. The heat flux gauges were placed closer to the corners in the scaled compartment, whereas the heat flux gauge in the full-scale compartment was placed in the middle of the compartment but in-line with the compartment doorway. The higher heat fluxes measured in the full-scale tests are believed to be the result of better ventilation which occurred in-line with the compartment doorway.

The average trip times for four different wire types are plotted in Figure 18 below. The average maximum temperatures and heat fluxes at the time of tripping are shown in Figure 19 and Figure 20, respectively. Figure 21 provides a graphical representation of the TEA data.

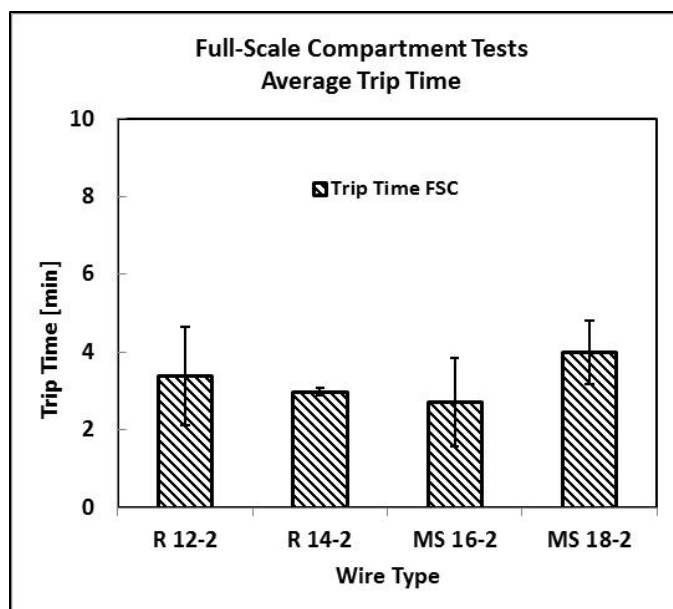


Figure 18: Circuit Trip Time for Full-Scale Compartment Tests (FSC)

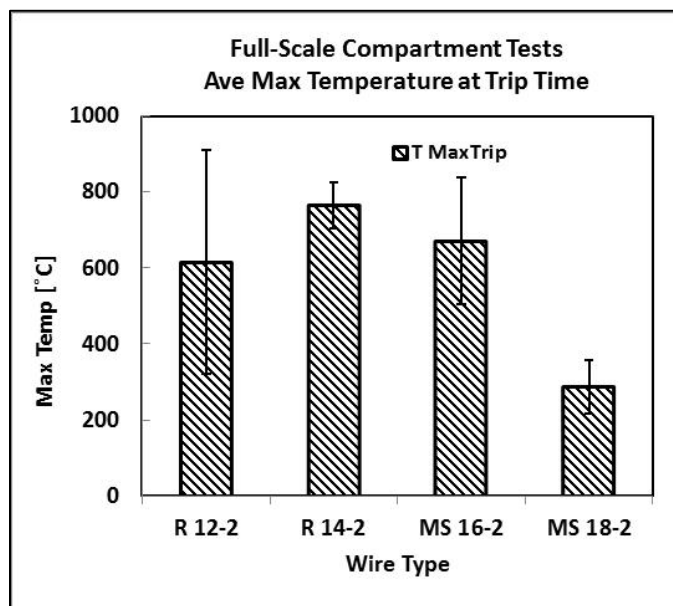


Figure 19: Average Temperature at Trip Time for Full-Scale Compartment Tests (FSC)

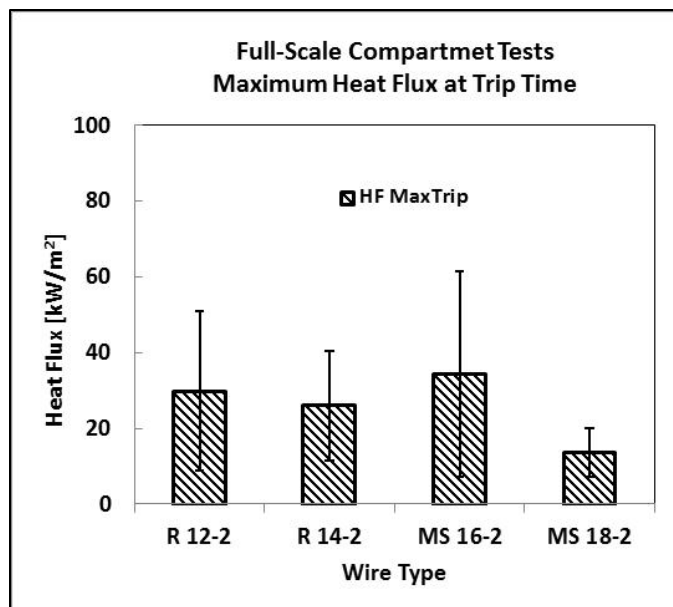


Figure 20: Average Heat Flux at Trip Time for Full-Scale Tests (FSC)

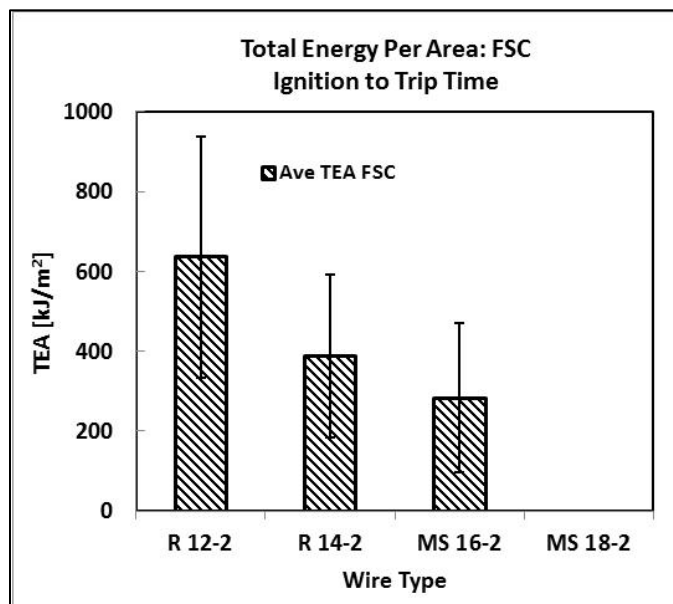


Figure 21: TEA for Full-Scale Compartment Tests (FSC)

The average trip times between all wire types were consistent. It should be noted that testing performed on the solid and stranded gauge, energized wires with load and without load were done at the same time in the test compartment, and both energized wires (with and without load) were plugged into the same power source. Hence, when a trip occurred and the circuit was

de-energized, it was not possible to identify which wire (loaded or unloaded) caused the circuit to trip. Therefore, the temperatures and heat fluxes at the time of tripping are the same for the energized wires with load and without load.

The maximum temperatures at the time of tripping were significantly lower for the 18-gauge wires than for any of the other three wire types. The maximum heat fluxes at trip times for the 18-gauge wires, while not significantly lower, were also less than the other three wire types. The cause of these differences may be related to the wire insulation type or particular dynamics of the fire. The TEA values for the wire types trended downward, according to the size of wire gauge, from larger to smaller. Hence, the amount of energy required for circuit trip time decreased as the wire diameter became smaller. While this trend was not significant based on the standard deviation in the measurement, it is logical: less energy should be required for heating of a smaller wire than a bigger wire. This same trend, however, was not seen in the scaled compartment tests.

C. Stereo Microscope Results

All test wires with thermal or electrical damage were photographed with a stereomicroscope. Specifically, each sample was analyzed for the presence of beads and the bead diameter was measured. All of the bead pictures were organized according to test number and type of damage. These pictures are presented in Appendix B. Figures 22 through 25 are representative images of beads formed under various thermal and electrical conditions.



Figure 22: Beads Produced with Direct Flame Exposure (12-gauge: NE, E (center), and L)



Figure 23: Beads Produced with Radiant Tunnel Exposure (16-gauge: NE, 12-gauge: E (center) and L)

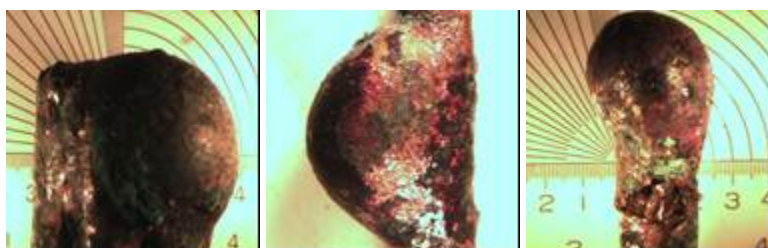


Figure 24: Beads Produced with Scaled Compartment Exposure (12-gauge: NE, E (center), and L)

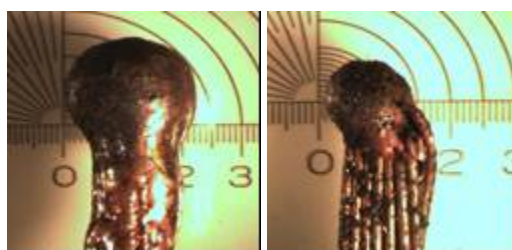


Figure 25: Beads Produced with Full-Scale Compartment Exposure (16-gauge: E, 18-gauge: L)

A total of 32 wire samples were mounted, cut, polished, and etched with FeNO_3 solution to allow for microscopic surface analysis. Figure 26 shows two of the mounted samples.



Figure 26: Mounted Samples (Cut and Etched)

The mounted samples were photographed with a high resolution microscope at various magnifications. Figures 27 through 29 are representative images of selected loaded wires tested under different thermal exposures.

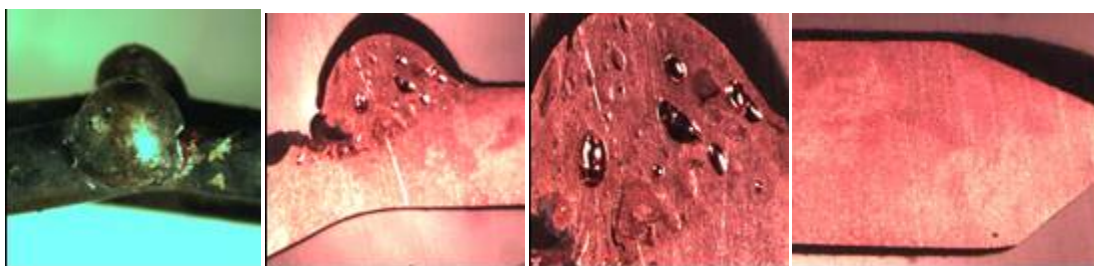


Figure 27: SM Images of Loaded Wires under Direct Flame Exposure (12-gauge: L-DF)

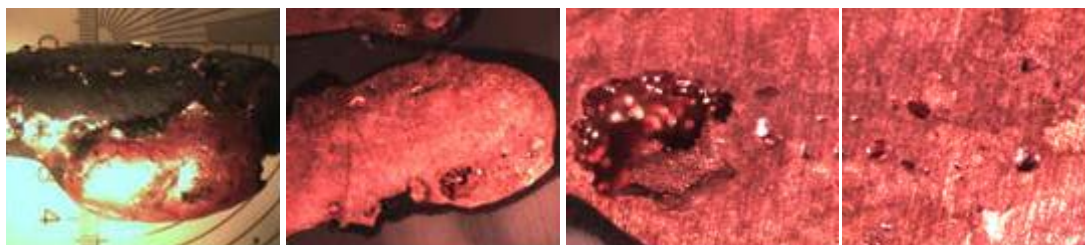


Figure 28: SM Images Loaded Wire under Scaled Compartment Exposure (12-gauge: L-SC)

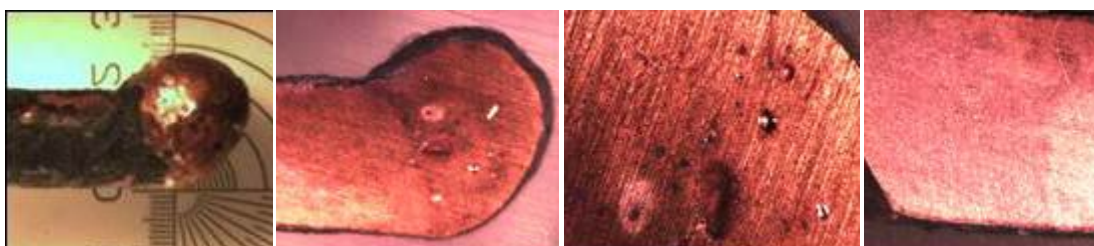


Figure 29: SM Images of Loaded Wires under Radiant Tunnel Exposure (12-gauge: L-R)

Figures 30 through 32 are representative images of selected non-energized wires tested under different thermal exposures. A full catalog of all the stereomicroscopic images is provided in Appendix C.

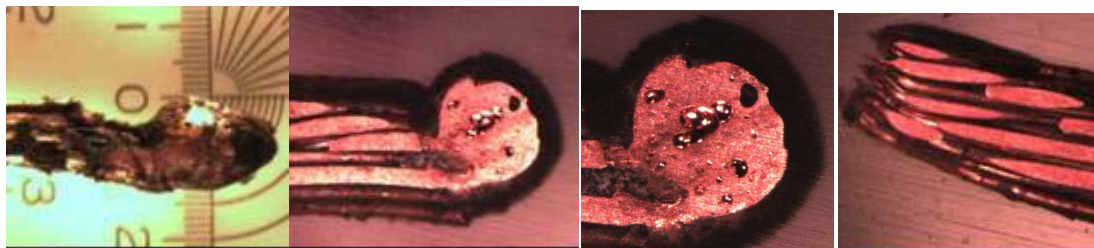


Figure 30: SM Images of Non-energized wires under direct flame Exposure (18-gauge: NE-DF).

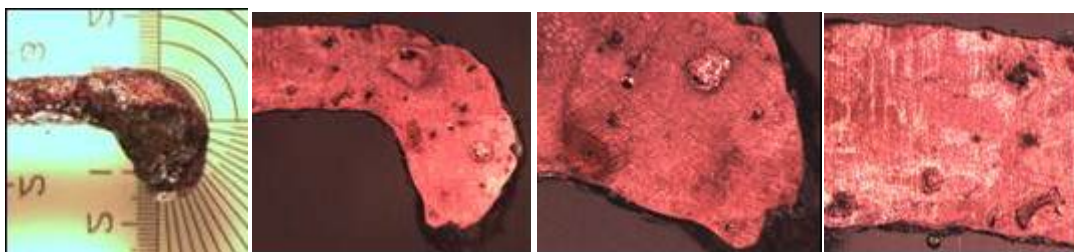


Figure 31: SM Images of Non-energized Wires under Scaled Compartment Exposure (18-gauge: NE-SC).

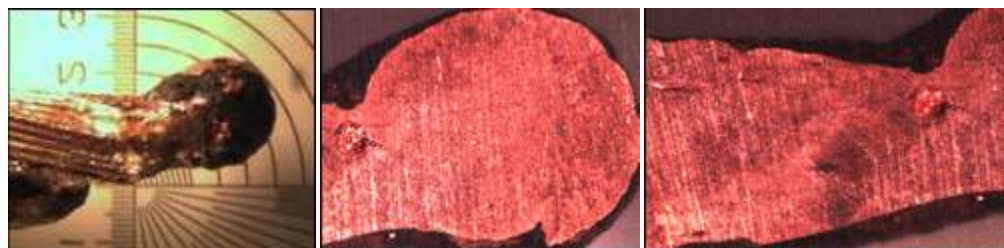


Figure 32: SM Images of Non-energized Wires under Radiant Tunnel Exposure (18-gauge: NE-R)

The mounted samples were evaluated for bead porosity, and any other characteristic trends that could be identified. In the images shown, direct flame impingement appeared to result in a more porous bead structure regardless of the energized state of the wire. However, this trend was not present in all the samples evaluated, and no consistent trends could be identified within exposure types, wire types, or energized states using a stereomicroscope. A discussion of the SEM/EDS results is given below.

D. Scanning Electron Microscope and EDS

Some samples were analyzed using SEM/EDS to determine if any differences existed between beads formed from melting versus beads formed from electrical activity. This analysis was performed by CSE staff at the University of Maryland and by Dr. Elizabeth Buc at the Fire and Materials Research Lab in Livonia Michigan. Some analyses were also performed by Dr. Lori Streit at Unified Engineering, Inc. and on-going analysis is being performed by Dr. Charles Manning of Accident Reconstruction Analysis, Inc. The main component found on the bead surface was copper, as would be expected. There was no significant difference in the chemical composition of beads from non-energized wires or energized wires or under different thermal exposures.

The stereomicroscope and SEM images from Dr. Buc's analysis are shown in Figure 33 where the left column shows a non-energized wire exposed to radiation, and the right column shows a loaded wire exposed to direct flame.

Dr. Buc did observe differences in the porosity of the beads formed on non-energized, multi-stranded wires when compared to the porosity of beads formed on energized, multi-stranded wires. These observations, however, were based on the analysis of four samples. Further analysis of the remaining bead samples has not supported the same trends.

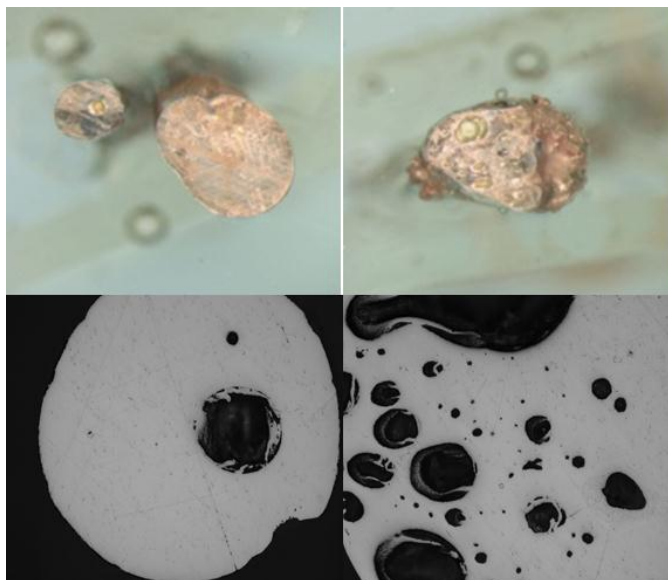


Figure 33: SM and SEM Images of MS Wires under different Electrical Conditions.

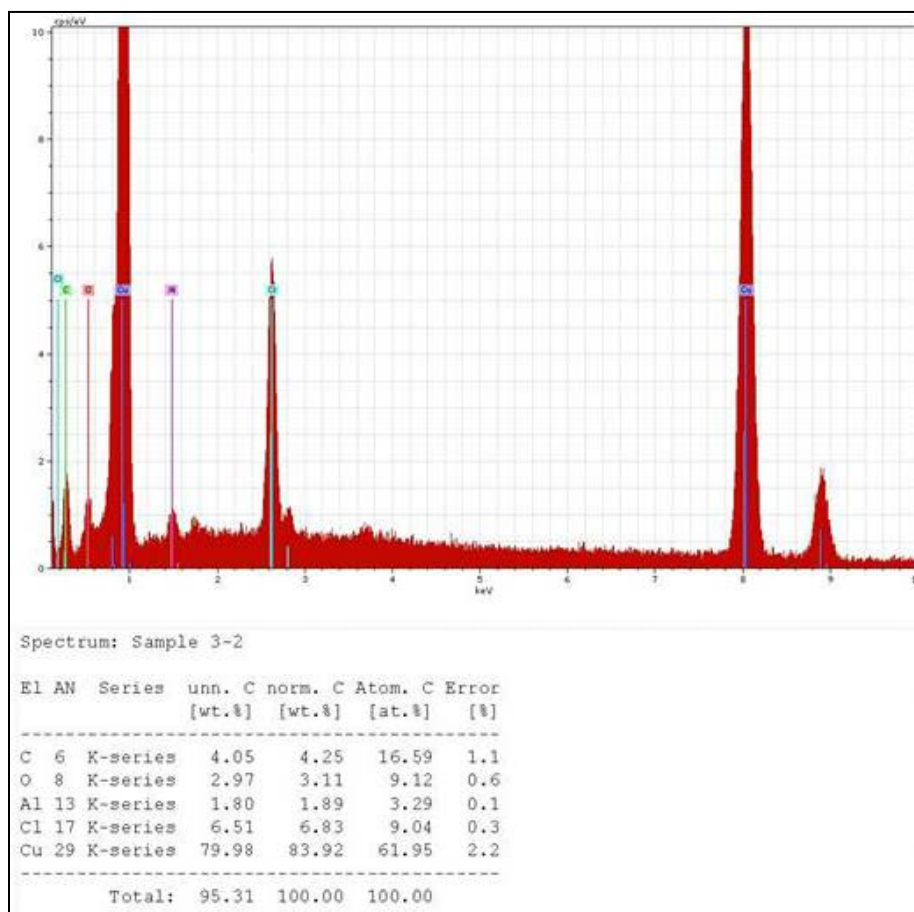


Figure 34: EDS Graph for a Bead Surface formed on an Energized Wire (DF)

Figure 34 and Figure 35 show the EDS graphs from energized and non-energized wires analyzed with the SEM at the University of Maryland. The table below each chart shows the elemental composition of the bead. Six wire samples were analyzed, and no specific trends were identified in the elemental composition of the beads formed after thermal exposure under different electrical conditions. The wires contained various elements including: carbon, oxygen, chloride, aluminum, calcium, and copper. The content of the beads was not related to their exposure condition, size, energized state, etc.

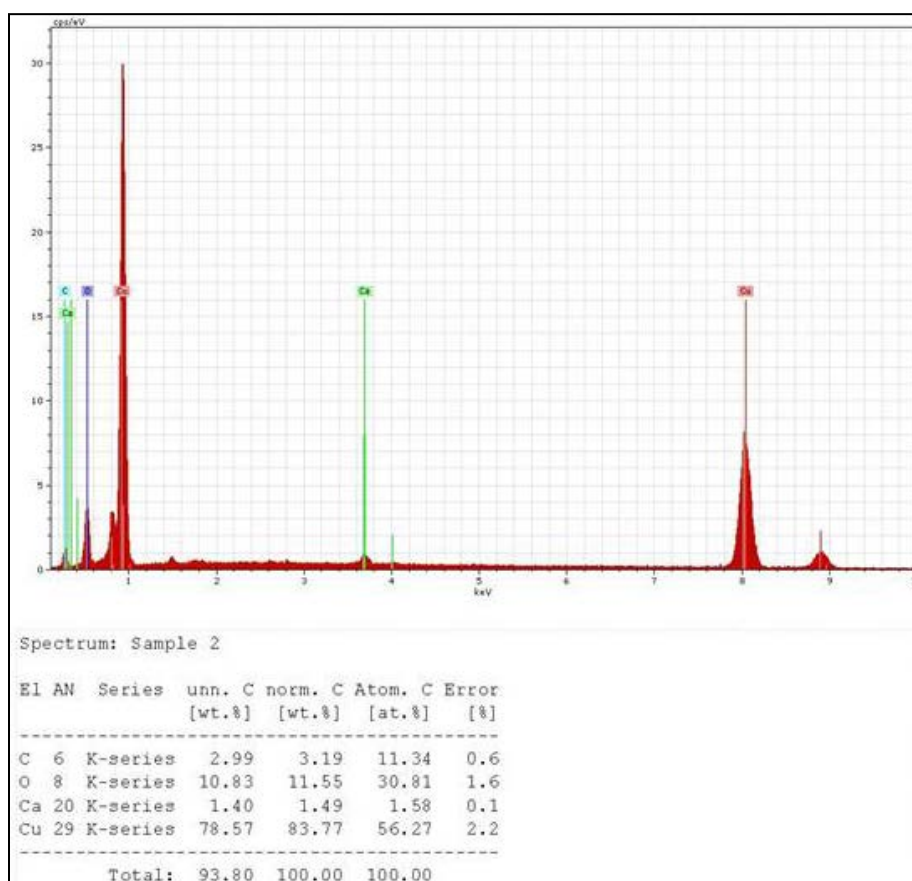


Figure 35: EDS Graph for a Bead Surface formed on a Non-energized Wire (DF)

Dr. Lori Streit performed further SEM/EDS analysis on the interior structure of the beads. Based on Dr. Streit's preliminary review of the beads, she found high concentrations of copper in both non-energized and energized beads. Dr. Streit was of the opinion that further

SEM/EDS analysis would not provide useful information. Additionally, Dr. Streit felt that SEM analysis of the beads provided no more information on porosity than what could be seen utilizing a stereomicroscope, so it was decided to discontinue SEM analysis and focus on stereomicroscopic analysis. Based on these recommendations, stereomicroscopic analysis was conducted on all of the mounted samples. Based on the limited outcomes of the SM and SEM/EDS results a further analysis of the inner grain structure of copper beads was done by ARAI as discussed in the next section.

E. Analysis with Metallurgical Microscope

Samples mounted and etched at Unified Engineering were re-mounted and re-etched at ARAI to be studied with an Olympus 1X70 metallurgical microscope. The etchant, known as Ammonium Hydroxide-Hydrogen Peroxide or AP etch, consisted of 5 parts ammonium hydroxide (NH_4OH), 5 parts water (H_2O), and 4 parts hydrogen peroxide (H_2O_2) [30, 33]. After etching, samples were analyzed and photographed with a Nikon DS-Fi1 digital camera mounted to an Olympus 1X70 metallographic microscope. Samples were photographed at a magnification range of 60X-110X. A program in Adobe Photoshop called Photomerge was utilized to combine localized, sectional images of the beads into one comprehensive image.

Metallography is useful in evaluating the differences between non-energized and energized beads, because copper undergoes grain structure changes when heated, and in some cases, these changes can be related to thermal exposure conditions [34, 39]. The grain structure begins to enlarge when temperatures reach or exceed 260°C [34]. Therefore, based on the size of the grain structures, it may be possible to distinguish between wires that had signs of arcing versus wires that were non-energized and only thermally heated. In some cases, the conditions

of arcing are masked by continued heating of the bead. In these cases, the beads formed from arcing may look similar to beads formed from melting.

ARAI analyzed 29 beads of which 14 were produced while the wires were energized with load and 15 while the wires were non-energized. These samples were selected from wires exposed to direct flame, radiation, and scaled compartment fires. After examining the wire images taken with metallurgical microscope, ARAI concluded that there were several structural features present in the copper beads, but none of the features were present 100% of the time within the two groups analyzed (non-energized versus energized). ARAI did note that the inner structure of six of fourteen energized beads showed clear lines of demarcation, as seen in Figure 37 (Images A and B) and Figure 38 (Image C). This trend was only observed in one out of 15 non-energized samples. In the energized wire samples that did not exhibit internal clear lines of demarcation, ARAI concluded that further heating of the sample after arcing likely masked the demarcation. Hence, on a microscopic level, clear lines of demarcation are more prevalent in beads formed under energized conditions where post-event heating is limited.

Another prevailing trend found in both energized and non-energized wires was voids of varying sizes. Voids were present in 19 of 29 samples evaluated. Levinson [34] concluded that voids result in the copper structure due to the trapping of gaseous combustion products while the copper is molten. As is consistent with ARAI's findings, Levinson also concluded that the presence of voids was not a function of the electrical condition of the wire which is different from the conclusion of Gray et al [18].

The full report from ARAI, as well as, images of the beads is included as part of Appendix D. Some representative images are discussed below.

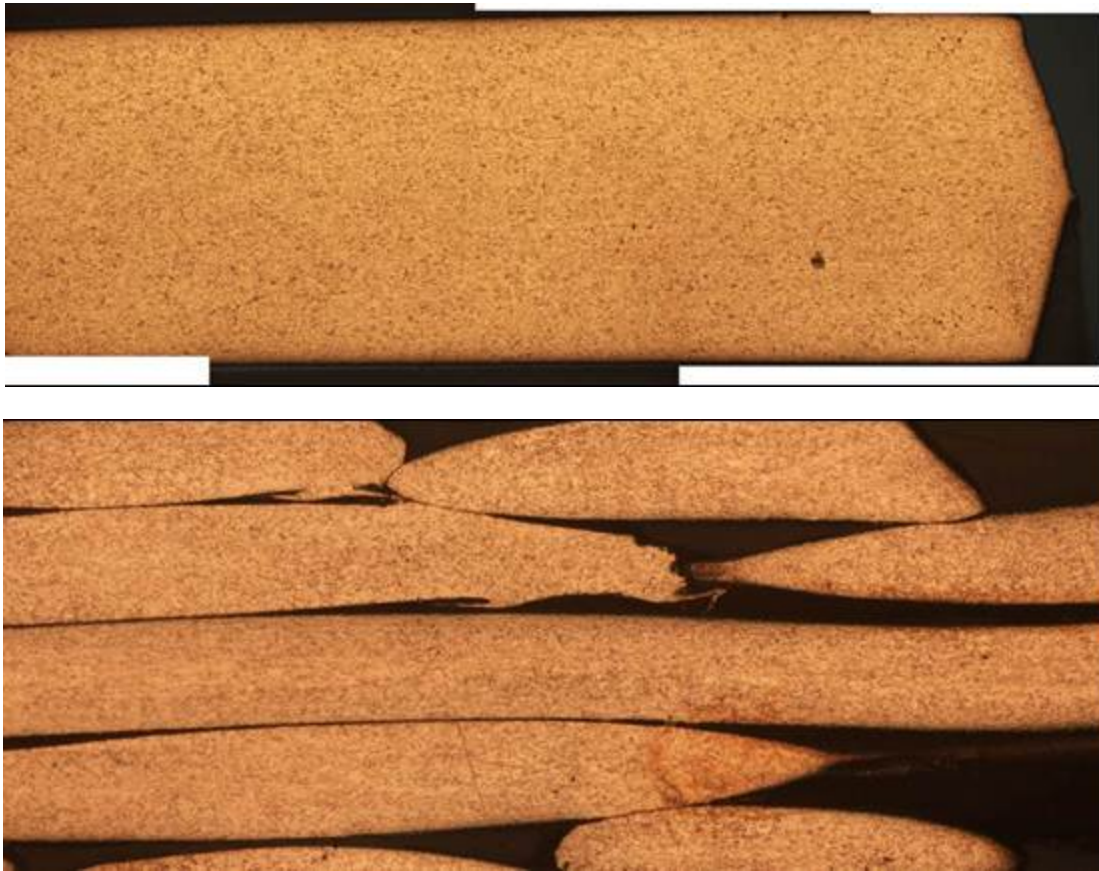


Figure 36: Grain Structures of Wire Control Samples (Unexposed Wires: Solid (Top) and Stranded (Bottom))

Figure 36 shows images of control samples (unexposed wires) for both solid and stranded wires. These samples were used to obtain the grain structures of the wire prior to thermal exposure and served as the baseline or control samples. When copper conductors were analyzed without thermal exposure, they showed very small grain structures. As seen in Figure 37, these grain structures grow as the copper is heated [34 and 39]. The images displayed are 12-gauge, solid, energized wires tested under direct flame exposure. All images show signs of arcing, as evident by the beads, but only the top two (A and B) show internal lines of demarcation and voids in the bead structures. Image C does not show any difference in grain structure when comparing the bead section to the longitudinal wire section.

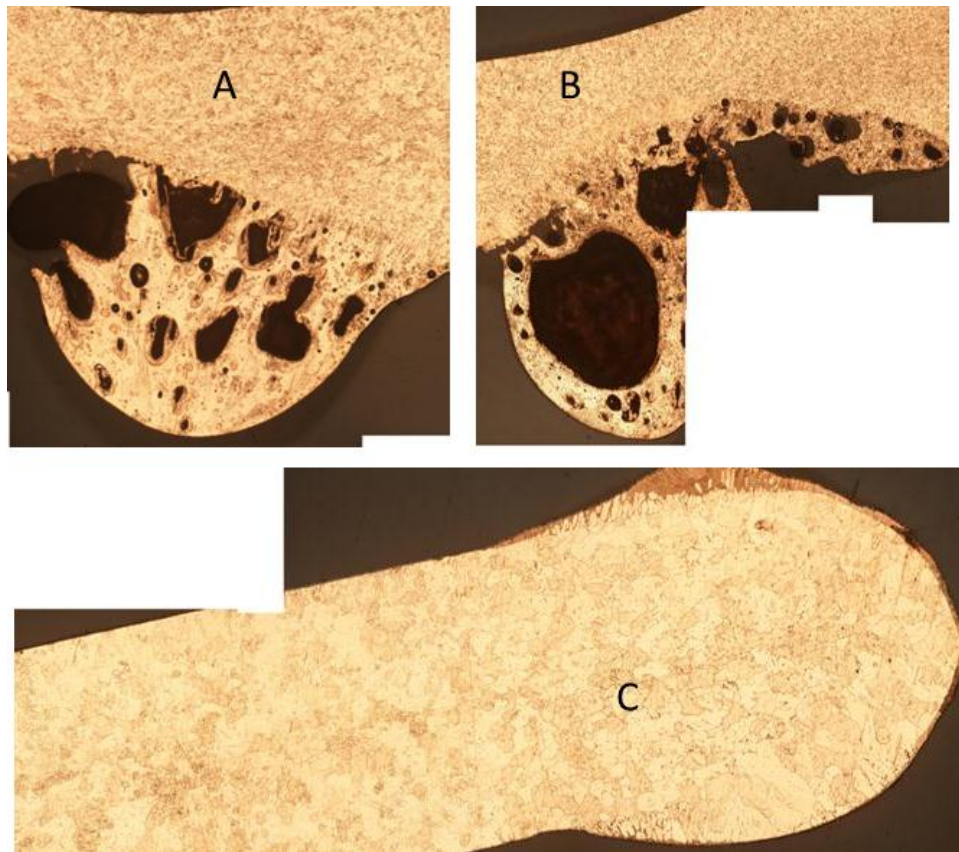


Figure 37: Metallurgical Microscope Images of Beads formed under Direct Flame Exposure (All Loaded 12-R Wires)

Figure 38 below shows images of 18-gauge, stranded energized wires tested in the scaled flashover compartment. Images B and C have large voids, and image A has no voids. Images A and B show no lines of demarcation and enlarged grain structures, whereas Image C shows a clear line of demarcation. Image C also shows a smaller grain structures on the bead and a larger grain structures on the wire.

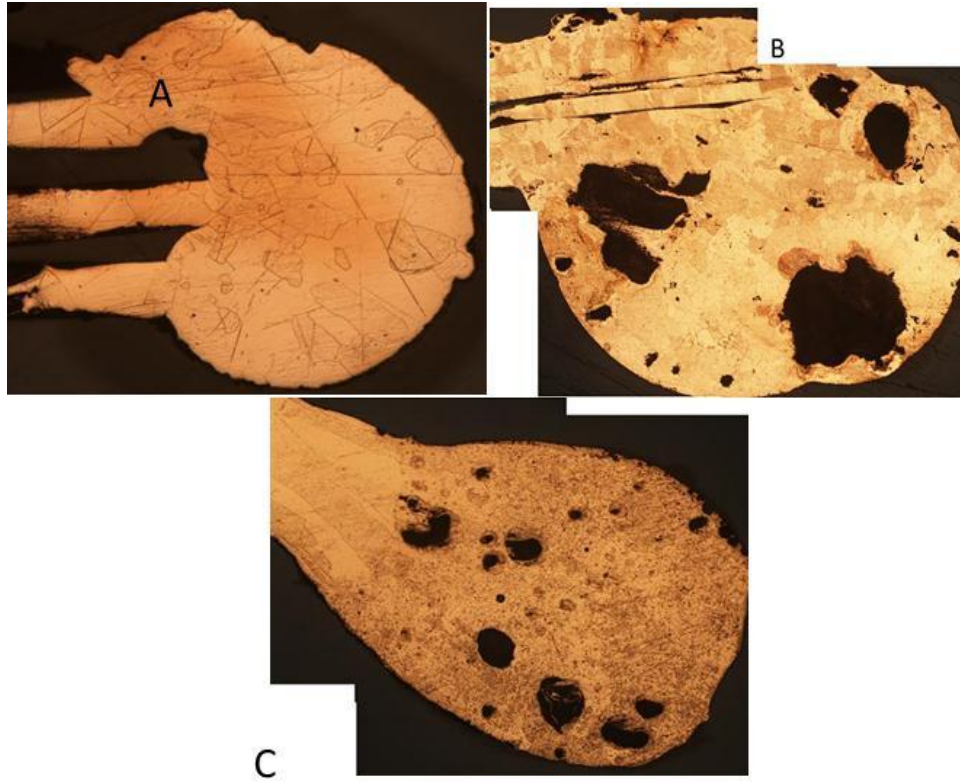


Figure 38: Metallurgical Microscope Images of Beads formed under Scaled Compartment Exposure (All Loaded 18-MS Wires)

Figure 39 shows beads formed on 12-gauge, solid, energized and non-energized wires exposed to direct flame impingement. The images show very similar grain structures but both wires were not held under the same electrical condition: sample A was non-energized while sample B was energized with load.

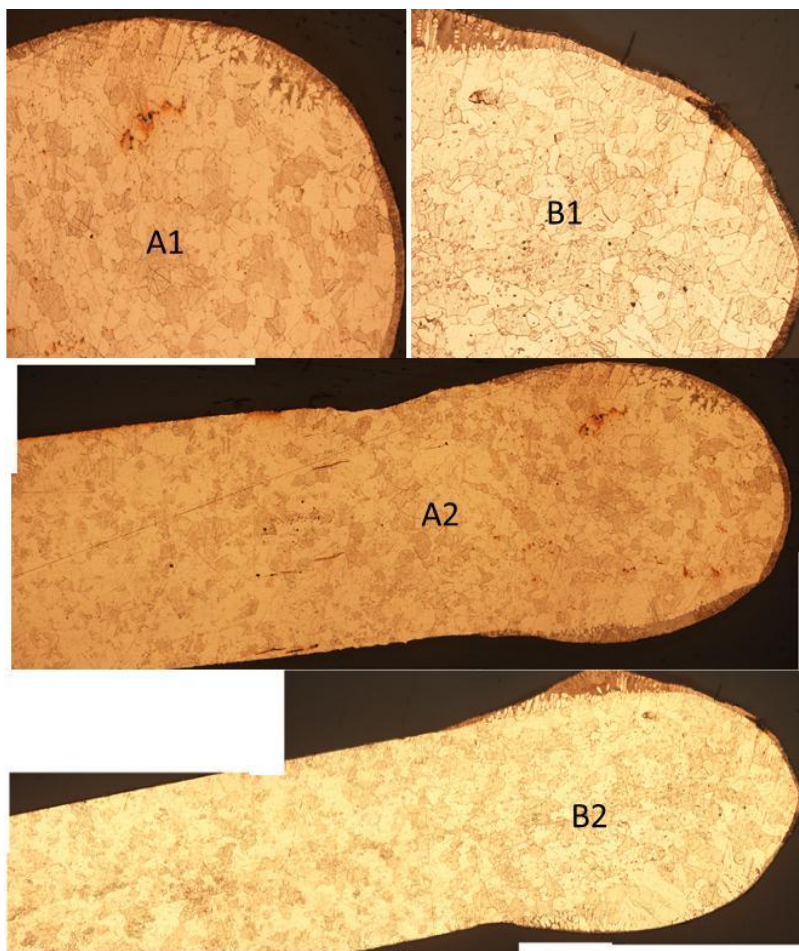


Figure 39: Metallurgical Microscope Images of Beads formed under Direct Flame Exposure (12-R NE (A) and 12-R L (B))

Figure 40 and Figure 41 also show images of grain structures that look very similar, but the wires were tested under different electrical conditions. This may have been caused by continued heating of the wire after arcing, which typically occurred minutes prior to flashover. Figure 40 shows dendrite structures. These structures are believed to be produced when melted copper interacts with oxygen to produce Cu_2O [34]

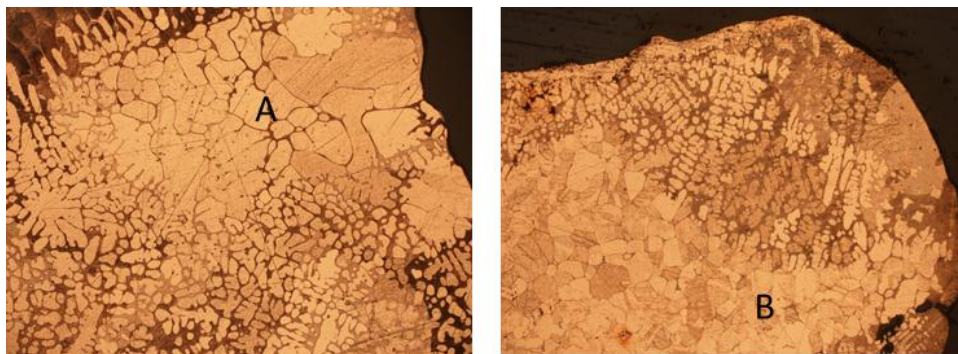


Figure 40: Metallurgical Microscope Images of Beads formed under Scaled Compartment (12-R L (A)) and Radiation (14-R NE (B))

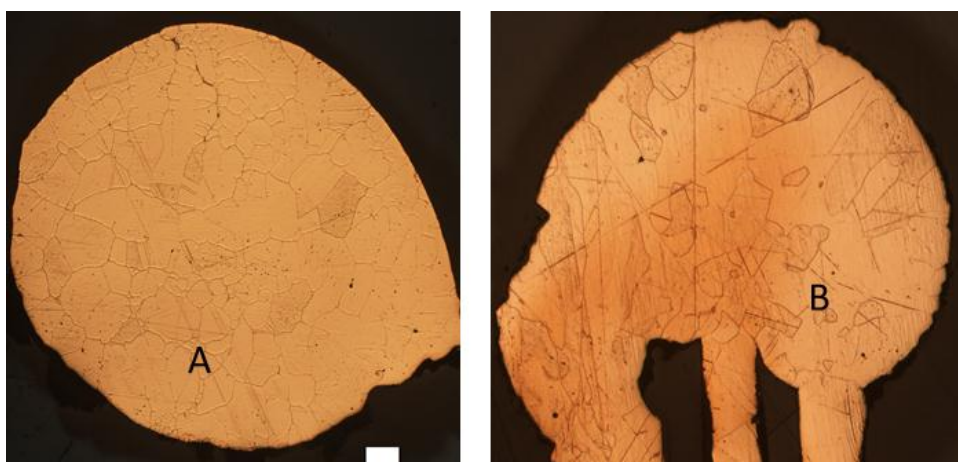


Figure 41: Metallurgical Microscope Images of Beads formed under Scaled Compartment (18-MS NE (A)) and 18-MS L (B))

F. Heat Transfer Analysis

A numerical heat transfer simulation was run to better understand the results produced during testing. A one dimensional (1-D) conduction heat transfer model was developed to evaluate the axial temperature change within the heated section of the wire. Figure 42 shows a schematic of the simplified problem. A copper cable of diameter D_c and length $2L$ has its axis aligned in the x direction. Only the $x > 0$ portion of the cable is considered due to symmetry at the $x = 0$ plane. Hence, property gradients are zero at $x = 0$. The cable is exposed to heat from a flame q_f (W/m²) in the region $0 < x < l$ and loses heat due to free convection q_c (W/m²) in the region

$l < x < L$. Blue dashed lines represent a control volume where conservation of energy was applied to run the 1-D conduction model.

Because of the high conductivity of copper and the small diameter of the cable, heat conduction is assumed to occur only along the axis of the cable. Therefore, the conduction problem is transient and one-dimensional. It is also assumed that there is no plastic insulation in the region $0 < x < l$ where the flame impinges on the cable. This assumption is justified, because the time it takes for the insulation to melt (about 75°C) is much less than the time it takes for the copper to reach its melting temperature (about 1083°C). Ambient conditions are defined as 1 atm and 25°C . The theoretically derived time to reach the melting temperature of copper (1083°C) was compared against the experimental break/trip times.

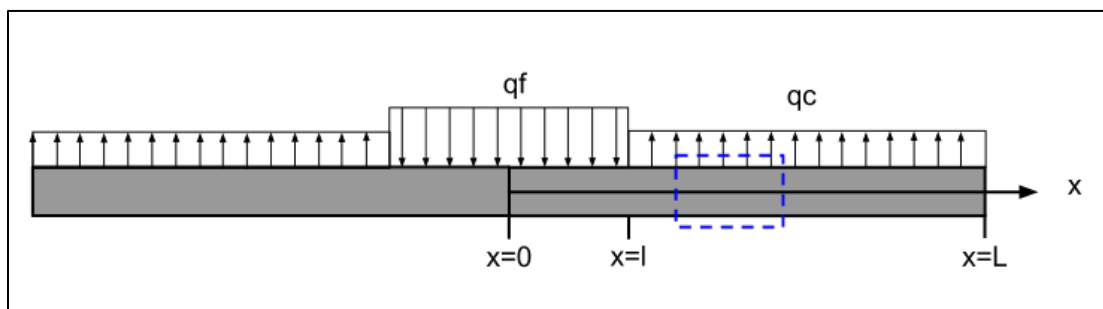


Figure 42: Copper Wire Sample Setup for Heat Transfer Simulation

The results of the numerical simulation demonstrating the effects of the cable diameter for a one meter long wire are shown in Figure 43. The horizontal line denotes the melting temperature of copper (1358 K or 1083°C). It should be noted in Figure 43B that the curves collapse when the time is scaled with the diameter of the wire squared (D_c^2). Thus a cable with twice the diameter of another cable will take 4 times longer to reach the melting temperature. The melting time for the 2 mm wire is about 300 seconds and for 1 mm wire it is about 75 seconds as seen in Figure 43A.

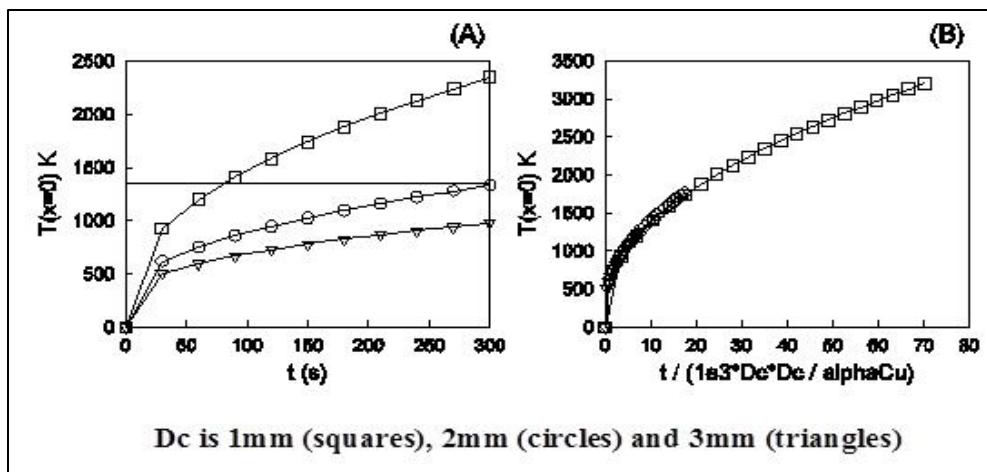


Figure 43: Heat Transfer Simulation Results-Temperature change with Time

The simulation results for the axial temperature variations while the wire is being heated at the center are seen in Figure 44. The plot represents one axial side away from the heated section. The horizontal line on the plot is the approximate melting temperature of PVC, the insulation component on the wire. The model predicts that in most cases the wire temperature is less than the melting temperature of PVC at about 25 cm away from the section exposed to flame, so the wire remains insulated in this area. This shows that most of the heat input is utilized to heat the section of the wire in the flame which eventually melts and breaks. This simulation was modeled for a non-energized direct flame testing condition. An energized wire that arcs experiences temperatures in excess of 5000 K [5]. There will be even less heat transferred axially away from the arcing section due to the rapid nature of the arcing event. Also a short duration event, such as an arc, will not lead to big changes in the grain structure of copper.

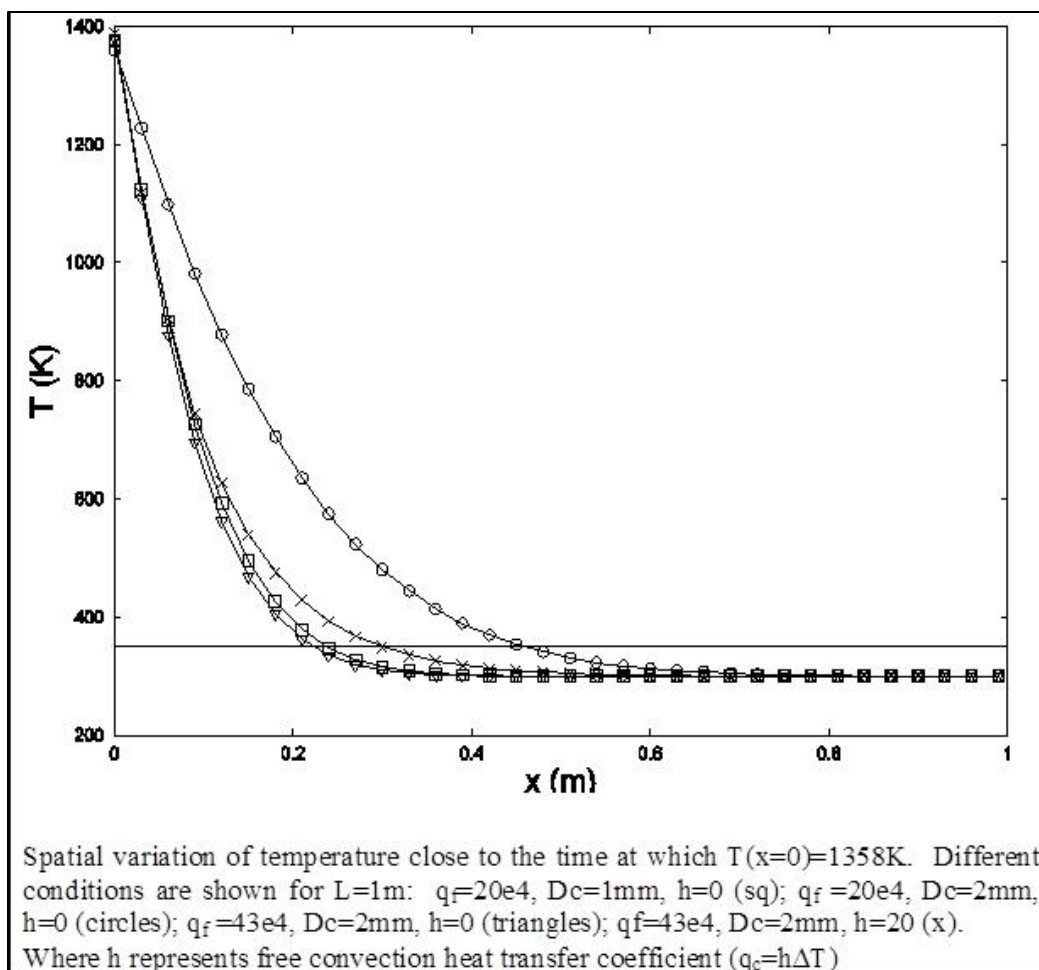


Figure 44: Axial Temperature Change along Wire Length (D_c similar to 12-R conductors).

IV. CONCLUSIONS

A. Discussion

The above section detailed the outcomes of each of the four exposure scenarios (e.g. direct flame, radiant tunnel, scaled compartment, full-scale compartment). The outcomes of these exposures are summarized below. Additionally, the discussion section provides a comparison of results from different exposures to establish if certain trends were only seen under specific exposure conditions.

1. Direct Flame Impingement Tests

A larger portion of the energized, loaded wires tripped the circuit than did the energized, non-loaded wires with the exception of the 14-gauge wire tests where no circuits tripped. This result could be due to the presence of the electrical field in the loaded wires more easily supporting the development of an arc across the carbonized insulation. Current spikes were observed in 9 of the 24 tests that were conducted with loaded wires; hence, arcing through char was documented in the loaded wires. The greater propensity for circuit tripping may also be related to the fact that the wire is already under load. Hence, when additional load is placed on the wire due to short-circuiting or another low-resistance event, less additional current is required to overload the circuit.

When comparing the non-energized wires to the energized (loaded and non-loaded) wires, a significant difference was present between the break times and the trip times. This is a logical outcome for two reasons. Firstly, the carbonization of the insulation in the energized wires supports arcing through char which can result in early failure. Secondly, the energized wires are at a higher internal temperature due to the resistance generated by the current traveling through the wire, hence, a smaller ΔT is required to reach the melting temperature of the copper.

Another interesting finding was that the breakage times for the solid (14 and 12) gauge energized wires was longer than for the stranded (16 and 18) gauge energized wires; the same was true for the non-energized wires. Hence, overall, it took a longer period of time, regardless of the energized state, for the solid wires to break when compared to the stranded wires. One reason for this difference could be the slightly thicker insulation that is present on the solid gauge wires, which are double insulated (conductor and jacket). Additionally, since the solid wires are a larger mass of copper (12 and 14-gauge) compared to the, thermally thin stranded wires (16 and 18-gauge), it could be concluded that the longer breakage times was related to the difference in mass, rather than the wire geometry (stranded vs. solid).

However, when evaluating within the solid, non-energized wire group, a longer breakage time was not associated with the larger wire gauge; the same was true for the stranded wire group. The 14-gauge solid wires (smaller) had a significantly longer breakage times then the 12-gauge solid wires (larger), as did the 18-gauge stranded wires when compared to the 16-gauge stranded wires. Hence, the dissipation of heat in the wires does not appear to be solely based on wire diameter, but is also dependent on wire geometry (stranded versus solid). The higher surface area of the stranded wires when compared to the solid wires may play a role in the longer break times. Since one single strand is thermally thin, heat can be transferred through the strands more quickly. Hence, heat is transferred more quickly to the surrounding copper strands, allowing for faster heat transfer radially through the diameter of the wire, as opposed to axially down the length of the wire. On the other hand, in the solid gauge wires, heat may be transferred more quickly in the radial direction resulting in longer times to melt through the conductor or arc between conductors.

Based on these findings, the fire investigator should expect to see a tripped circuit more often than not if the involved conductors on the circuit were under load or energized. Additionally, the time to failure of a non-energized wire subjected to direct flame impingement is on the order of minutes when compared to energized wires, which typically fail in less than one minute. Whether the wire is stranded or solid will dictate its placement on the failure timeline, with solid wires having a longer time to failure than stranded wires. As one example, these findings could be useful in the investigation of a potential product failure. Many products on the market are designed with flame resistant or fire retardant materials; some of these materials do not support flame spread or sustained flaming. In some cases, the flaming duration is less than one minute. Hence, the presence or absence of damage on internal electrical wires in the product may reveal information about the energized state of the product and potential exposure scenarios.

2. Radiant Tunnel Tests

Out of the 24 energized wires tested (12 with load and 12 with potential only), 11 had the same breakage and trip times. Of the 11 that did have the same trip times, 8 were under load conditions. Therefore, approximately half of the energized wires that broke did so due to an arcing or shorting event that was significant enough to cause the circuit to trip. Additionally, there was a slightly higher tendency for this to occur in loaded wires as opposed to energized wires with potential only. These findings are consistent with the direct flame test results, which showed that loaded wires had a higher tendency to trip circuits than did non-loaded wires.

A significant difference in the breakage times was present between the non-energized wires and the energized, loaded wires. The loaded wires had quicker breakage times than the non-energized wires. The stranded wires had shorter breakage times than the solid wires. These

findings are consistent with the direct flame tests; therefore, these outcomes are not greatly affected by the exposure condition.

The average trip times for the radiation testing is slightly lower than for the direct flame testing. In the direct flame tests, the wire insulation melted, charred, and then arced, resulting in breakage or circuit tripping. In the tunnel tests, the wire insulation was vaporized almost instantaneously due to the substantial heat flux present in the tunnel. In the tunnel tests, the copper wires were de-insulated very early in the exposure period, and a char did not form on the insulation. Without the protective insulation, it is likely that the wires would arc or short more quickly in the tunnel tests, which is consistent with the test results.

Based on these findings, the fire investigator should expect to see a tripped circuit more often than not if the involved conductors on the circuit were under load. While the time to failure of the non-energized wires was longer than the energized wires in the tunnel exposure, the overall difference in failure times was not as large as in the direct flame testing. In all cases, regardless of the wire type or energized state, failure occurred in one minute or less. When energized, more (but not all) solid wires failed between 0.50 to 1 minute, and more (but not all) stranded wires failed in less than 0.50 minute; however, it is likely that these failure times are too close to be resolvable for field applications.

3. 2/5-Scaled Compartment Tests

The average trip time in the scaled compartment tests ranged from 3 to 5 minutes. This range was higher than in the direct flame and radiant tunnel tests. This is an expected outcome, since the heat source in the compartment tests was a wood crib which required time to reach a maximum burning rate. The direct flame and radiant tunnel tests utilized a constant heat source from beginning to end, so there was no lag in wire heating.

When comparing wire types, there was no significant difference in trip times in the stranded wires. It should be noted that testing performed on the solid gauge, energized wires with load and without load was done at the same time in the test compartment, and both wires (with and without load) were powered using the same source. Hence, when a trip occurred and the circuit was de-energized, it was not possible to identify which wire (loaded or unloaded) caused the circuit to trip. Therefore, the temperatures and heat fluxes at the time of tripping are the same for the energized wires with load and without load. In order to avoid this same issue with the stranded wire tests, separate circuits were utilized for the loaded and unloaded wires. For the stranded wires, there was no significant difference between the time to trip for the energized with load wires versus the energized without load. At the time the circuit tripped, the average heat fluxes and temperatures ranged from 3 to 9 kW/m² and 400°C to 600°C, respectively. The temperature was measured close to ceiling level. The melting temperature of PVC is between 180°C -260°C, and the melting temperature of copper is approximately 1083°C. Since failure occurs in the energized wires prior to the compartment reaching the melting temperature of copper, it is clear that insulation deformation and charring played a role in the wire failure, e.g. arcing and short-circuiting. When comparing wire types, there was no significant difference between the heat fluxes and temperatures at trip times. There was no way to establish the breakage times of the non-energized wires during the fire; therefore, a comparison of non-energized to energized failure times could not be made.

The average total amount of energy required per unit area to achieve failure was 300 kJ/m² to 700 kJ/m². The TEA for the energized, non-loaded wires had a larger range 300 kJ/m² to 660 kJ/m² when compared to the TEA for the energized, loaded wires which had a range of

282 kJ/m² to 333 kJ/m². This finding is consistent with the direct flame and radiant tunnel tests, which shows that loaded wires tripped sooner than non-loaded wires.

These findings are relevant to fire investigation, because they provide a temperature and heat flux range under which the investigator would not expect to see wire damage regardless of energized state. The results also provide a failure timeline, however, it should be noted that these failure times would not be applicable for wires installed in concealed spaces, such as behind walls and ceilings, until wall or ceiling failure. Additionally, it should be noted that not all compartments that undergo flashover will reach temperatures in excess of the melting point of copper (1083°C). The thermal conditions within the compartment will be highly dependent on the available fuel and ventilation. Even in the presence of ample fuel, ventilation will be the limiting factor in the ability of a compartment to reach temperatures capable of melting non-energized copper wires. In cases where electrical damage to wiring is present, and the electrical state of the wire is in question, the investigator may utilize various tools, such as fire modeling, to evaluate the maximum temperatures achieved in the compartment based on fuel loading and ventilation conditions.

4. Full Scale Compartment Tests

The average trip time in the full-scale compartment tests ranged from 3 to 4 minutes. This is an expected outcome, since the average trip time in the 2/5-scale compartment tests ranged from 3 to 5 minutes, and the heat source in both tests had a similar t^2 growth curve. The agreement between the 2/5-scale and full-scale compartment trip times further validates the application of the 2/5-scale compartment test results to full-scale scenarios.

The average heat fluxes and temperatures ranged from 13 kW/m² to 35 kW/m² and 300°C to 770°C, respectively. This temperature range is consistent with those measured in the 2/5-

scaled compartment at the time of failure. The heat fluxes, however, are higher than those measured in the scaled compartment. The difference in measurements is believed to be due to the placement of the heat flux meter in the compartment and was previously discussed in the Results Section in Chapter 4 of this report. When comparing wire types, there was no significant difference between the heat fluxes and temperatures at trip times. There was no way to establish the breakage times of the non-energized wires during the fire, therefore, a comparison of non-energized to energized failure times could not be made. Additionally, since most tests did not reach temperatures in excess of the melting point of copper, there were very few non-energized wires that melted.

Since the fire source (wood crib) in the scaled compartment was different from the fire sources (variable room layouts with fires starting on couches, chairs, etc.) in the full-scale compartments, the TEA is useful in comparing the two compartment types. The average total amount of energy required per unit area to achieve failure was 300 kJ/m^2 to 640 kJ/m^2 . This amount is consistent with the 2/5-scaled compartment TEA of 300 kJ/m^2 to 700 kJ/m^2 , and again, supports the use of the scaled compartment data in full-scale scenarios.

These findings are relevant to fire investigation, because they provide a temperature and heat flux range under which the investigator would not expect to see wire damage regardless of energized state. The results also provide a failure timeline; however, it should be noted that these failure times would not be applicable for wires installed in concealed spaces, such as behind walls and ceilings, until wall or ceiling failure. Additionally, it should be noted that not all compartments that undergo flashover will reach temperatures in excess of the melting point of copper (1083°C). The thermal conditions within the compartment will be highly dependent on available fuel and ventilation. Even in the presence of ample fuel, ventilation will be the limiting

factor in the ability of a compartment to reach temperatures capable of melting non-energized copper wires. In cases where electrical damage to wiring is present, and the electrical state of the wire is in question, the investigator may utilize various tools, such as fire modeling, to evaluate the maximum temperatures achieved in the compartment based on fuel loading and ventilation conditions.

5. Comparisons between Various Exposures

a. Average Failure Times

The average failure time (by wire breaking or circuit tripping) for energized wires under all thermal exposures is shown in Table 6 where “E” represents non-loaded wires and “L” represents loaded wires.

	12R		14R		16MS		18MS	
	E	L	E	L	E	L	E	L
Exposure	Wire Failure Time (Trip and/or Break)							
DF	0.78	0.62	0.67	0.72	0.33	0.33	0.28	0.28
R	0.53	0.44	0.45	0.42	0.26	0.29	0.19	0.21
C	3.82	3.88	4.26	4.26	3.66	3.35	4.86	4.16
FR	3.38	3.38	2.98	2.98	2.71	2.71	3.99	3.99

Table 6: Average Failure Time-All Exposures for Non-loaded Wires and Loaded Wires.

The direct flame and radiant tunnel exposures produced similar failure times. The 2/5-scale and full-scale compartment fires also produced similar failure times. These findings are expected, since the direct flame impingement and radiant tunnel tests are bench-scale, localized, and highly controlled methods, whereas, the compartment fire tests (both 2/5-scale and full-scale) have a t^2 growth rate. It should be additionally noted that there is good agreement between the 2/5-scale and full-scale test results. Hence, the scaled-compartment results can be applied to full-scale scenarios.

b. 2/5-Scale versus Full-Scale Compartment Comparison

Figure 45 and Figure 46 provide a comparison of the temperatures and heat fluxes in the 2/5-scale and full-scale compartments.

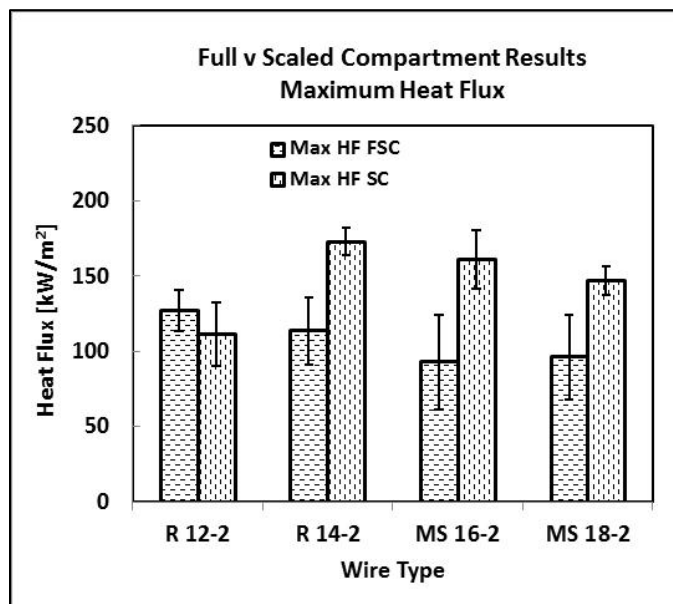


Figure 45: Maximum Heat Flux (averaged for each wire type) measured during Testing. (FSC v SC)

The maximum temperatures achieved in the 2/5-scaled compartment were slightly higher than those achieved in the full-scale compartment. The same was true for the heat fluxes, with the exception of the 12-gauge Romex tests. The higher temperatures and heat fluxes are consistent with the use of forced ventilation in the scaled compartment tests. Prior to the introduction of forced air, the temperatures and fluxes within the 2/5-scale compartment were more consistent with those in the full-scale compartment.

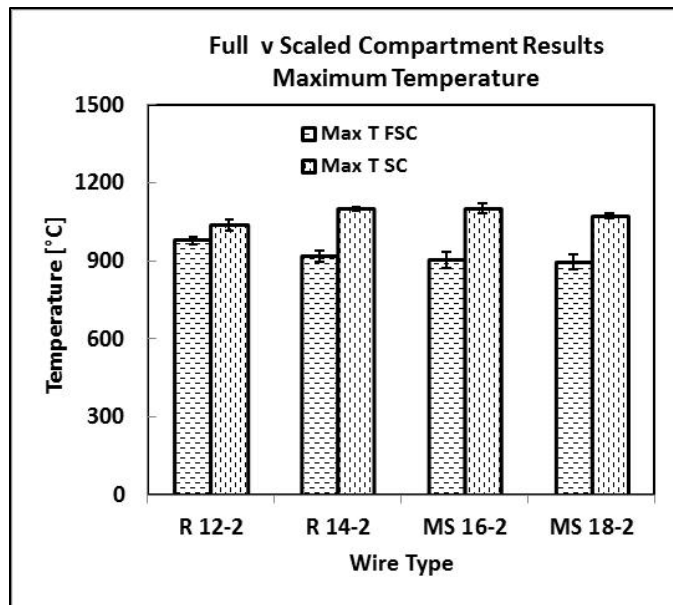


Figure 46: Maximum Temperature (averaged for each wire type) measured during Testing. (FSC v SC)

Regardless of the higher overall temperatures and fluxes in the 2/5-scaled compartment, the energized wires still appeared to react in a similar fashion in both compartments. Figure 47 shows that the wires in both the 2/5-scale compartment and the full-scale compartments had similar average trip times.

The consistency in results between the 2/5-scale compartment and the full-scale compartment are expected, since the trip time is not related to the maximum temperature or heat flux achieved in the compartment. The trip times occurred well before the maximum temperatures were achieved in the compartment.

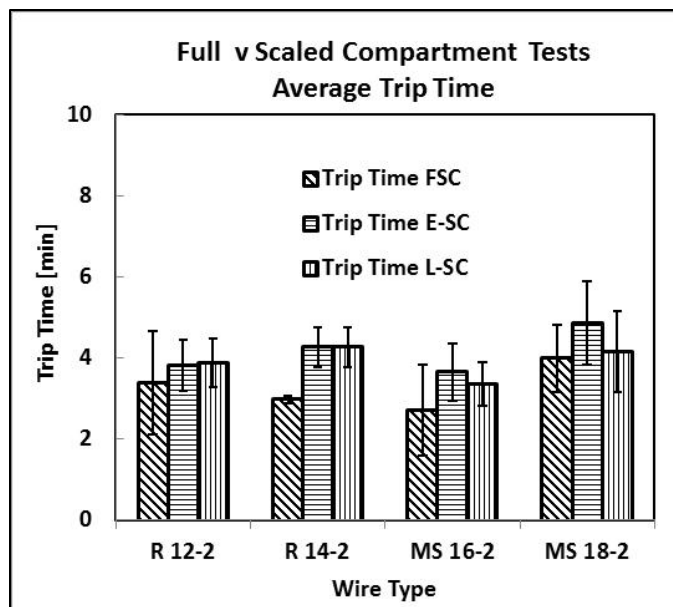


Figure 47: Average Trip Times for Compartment Fires (FSC v SC)

The trip times for both compartments were plotted against the maximum temperatures and heat fluxes at the time of tripping and are shown in Figure 48 and Figure 49. Both of the graphs show similar trends; the trip time decreases with increasing heat flux and temperature. Additionally, the slopes and intercepts of the lines for the temperatures and heat fluxes in both compartments are similar, showing good agreement between the 2/5-scale and full-scale compartments.

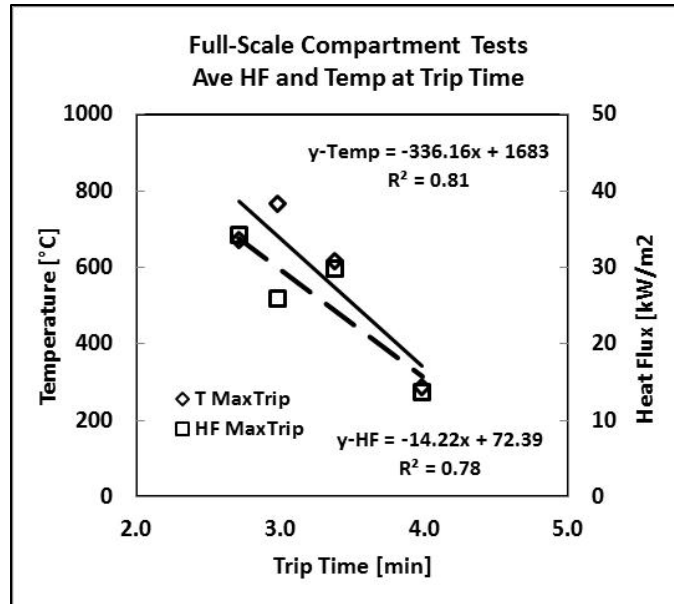


Figure 48: Full-Scale Compartment Trip Time Analysis (FSC)

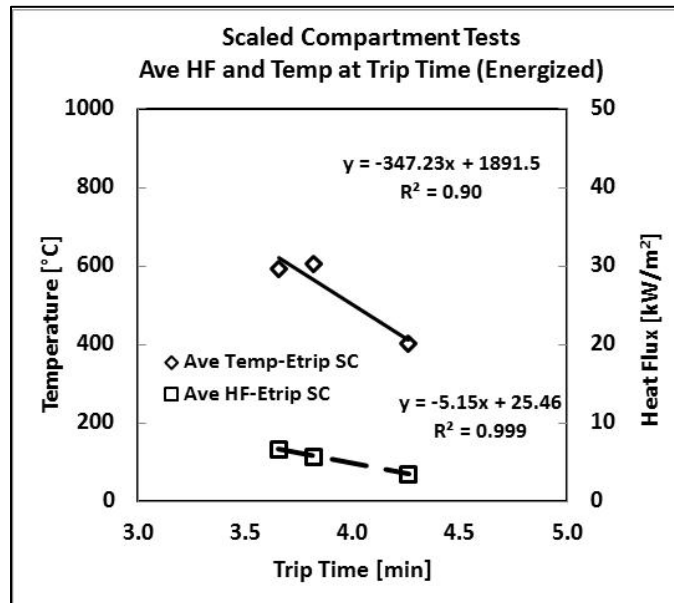


Figure 49: Scaled Compartment Trip Time Analysis (SC)

The TEA for the 2/5-scale and full-scale compartments was also compared. The average results are shown in Figure 50. In all cases, the average TEAs in both compartments was within the same range.

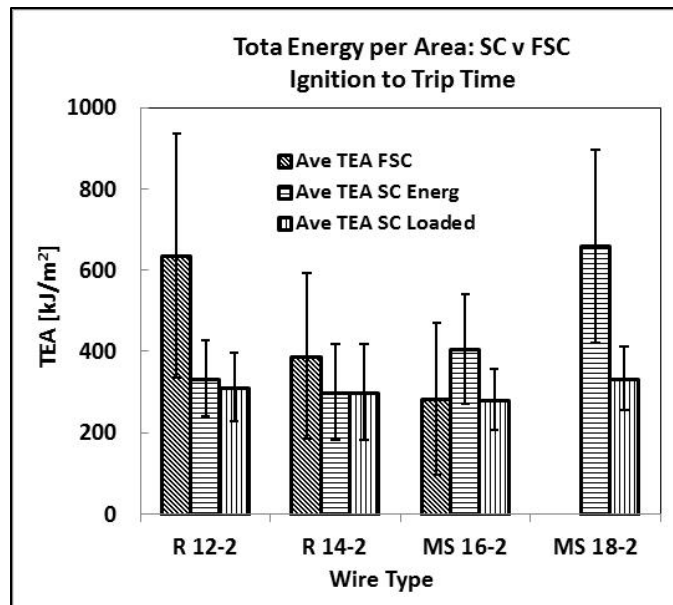


Figure 50: Total Energy per Area Comparison (SC and FSC)

This outcome is expected, since the total energy required to produce a failure in the wires should be the same regardless of the compartment geometry or specific fire type.

c. Bead Characteristics

Below, Table 7 shows the percentage of beads that were produced on wires based on their exposure condition, wire type, and energized state.

	12R			14R			16MS			18MS		
	NE	E	L	NE	E	L	NE	E	L	NE	E	L
Exposure	Percentage of Samples with Bead Formation											
DF	67	17	83	83	83	100	67	67	67	17	83	50
R	0	33	67	67	100	67	66	100	33	33	66	100
C	80	25	50	50	50	100	100	66	66	100	71	33
FR	0	33	33	0	0	0	0	33	33	0	33	33

Table 7: Percentage of Samples with Bead Formation

The production of beads on non-energized wires in the full-scale compartment was minimal. The lack of bead production occurred because on average, the compartment did not exceed 950°C. Beads were formed on non-energized wires in all scenarios except the full-scale

testing and 12-gauge radiant tunnel testing. The average of the percentage of beads formed under all three exposure conditions (full-scale not included) for non-energized, energized with no load, and energized with load wire are 61%, 63%, and 68%, respectively. Therefore, when conditions are sufficient to produce temperatures within the melting range of copper, the likelihood that a bead will form on a non-energized wire (61%) is approximately the same as the likelihood that it will form on an energized wire (63%-68%).

The beads which formed on the conductors were also measured for their diameters. The average diameters are shown in Table 8. The diameters are averaged for each wire type under each electrical condition. The average bead diameter increases with increasing wire gauge, as would be expected.

An evaluation of the visual characteristics of the beads is discussed below. Both non-energized and energized wires showed similar damage as seen in Figure 51. NFPA 921 outlines methods to distinguish between the beads formed on energized and non-energized wires, namely the presence of a clear line of demarcation on beads which formed from arcing (e.g. beads formed on energized wires). As seen below, both energized and non-energized wires show beads that have clear lines of demarcation. Additionally, in some cases, beads formed on energized wires do not show clear lines of demarcation.

	12R			14R			16MS			18MS		
	NE	E	L	NE	E	L	NE	E	L	NE	E	L
Exposure	Average Bead Size [mm]											
DF	4.0	4.0	3.1	2.7	2.2	2.6	2.7	2.7	1.3	1.5	1.8	1.5
R	0	3.5	3.4	2.5	2.5	3.7	2.0	1.1	2.4		0.9	1.5
C	4.8	5.6	4.5	4.5	0	4.6	2.6	2.3	2.4	2.8	3.1	3.1
FR								2.5	2.1		2.0	1.0
Wire D =>	2.16			1.65			0.76			0.64		
Wire D given is Diameter for Single Conductor before Exposure												

Table 8: Average Bead Diameter

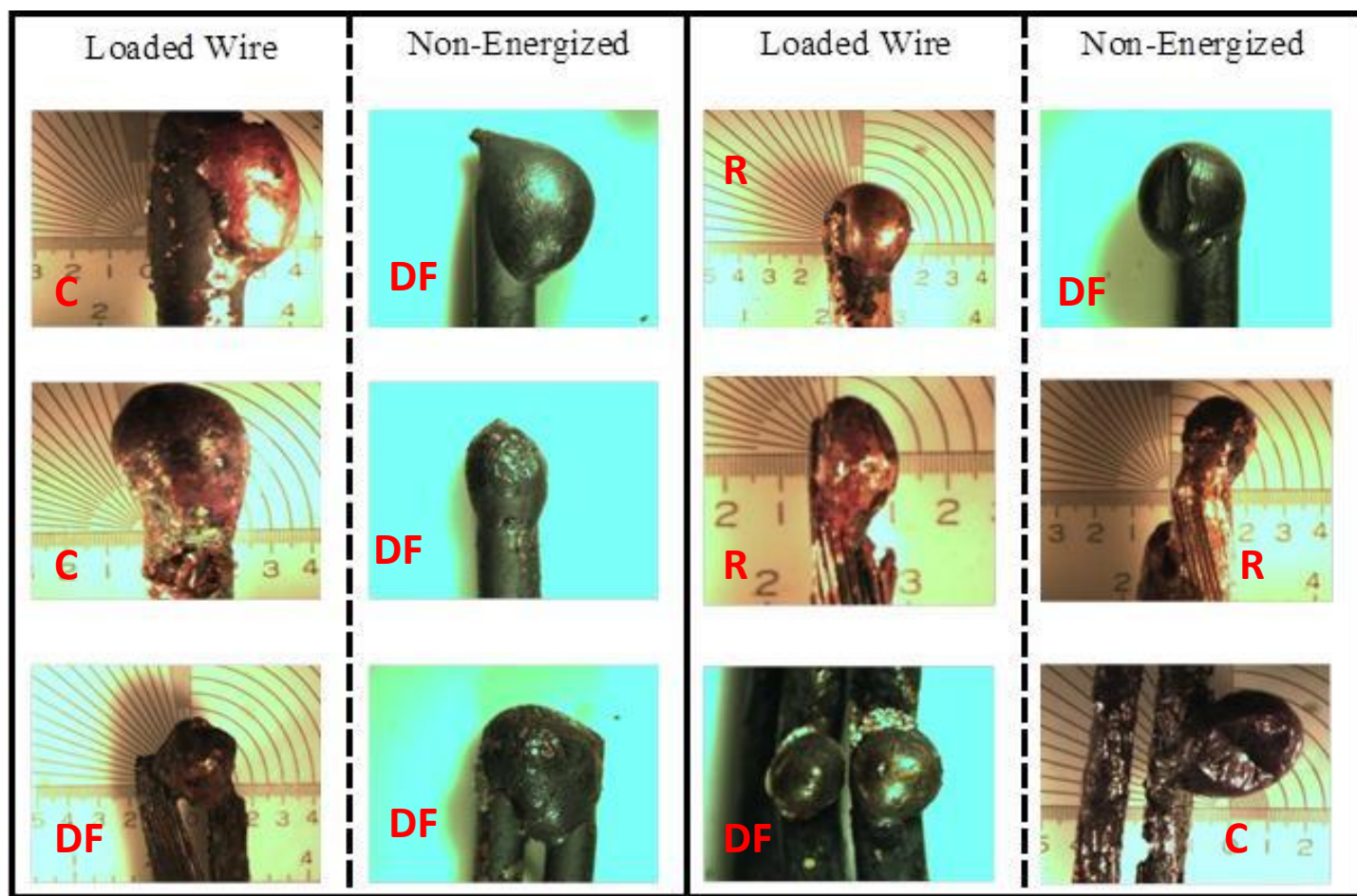


Figure 51: Comparison of Loaded and Non-energized Beads for various Exposures (SM Images) (Letters denote type of exposure)

Based on a preliminary evaluation of the exterior bead structure, there is no indication that the unloaded, energized bead was characteristically different from the loaded, energized bead. Most of the selected wires were 12-gauge solid and 18-gauge multi-stranded.

A side-by-side comparison of some of the patterns observed under the stereomicroscope is shown in Figure 52. Images were paired together based on similarities in the internal bead structure. It is evident from Figure 52 that there are no consistent, visible patterns (at a maximum of 44 x magnification) in beads formed on loaded and non-energized samples.

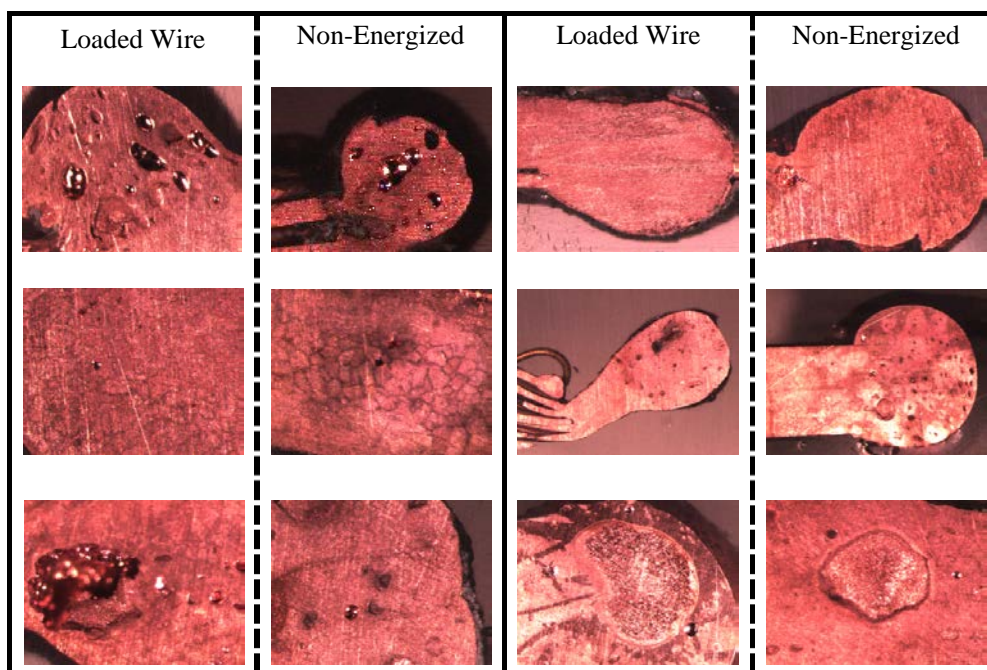


Figure 52: Internal Pattern Comparison of Loaded and Non-energized Beads for various Exposures (SM Images)

6. Analysis with Metallurgical Microscope

To further evaluate the grain structure of the samples, they were sent to a metallurgist, Dr. Charles Manning of ARAI in South Carolina. According to ARAI and the literature [34 and 39], copper wires will experience grain structure enlargement when exposed to elevated thermal conditions, due to the known metallurgical characteristics of copper. Therefore, copper wires that experience arcing may be identifiable based upon changes in grain structure, if further

heating of the beads, post-arcing, is limited. Post-arcing, heating can result in continued enlargement of the grain structure, making it similar to the grain structures of a bead produced under non-energized conditions.

Some of the energized wires showed clear lines of demarcation; however, some did not (see Figure 37 and Figure 38). An internal line of demarcation was found on forty percent (40%) of the energized beads but only found in one of the non-energized beads. Since one of the non-energized beads did have an internal line of demarcation, it is not possible to conclude with 100% certainty that the presence of an internal line of demarcation indicates that a wire was energized at the time of bead formation. Additionally, since not all of the energized wires exhibited an internal line of demarcation, it is not possible to say that the absence of an internal line of demarcation indicates that a wire was non-energized.

The six beads that displayed clear lines of demarcation are shown in Figure 53 and Figure 54.

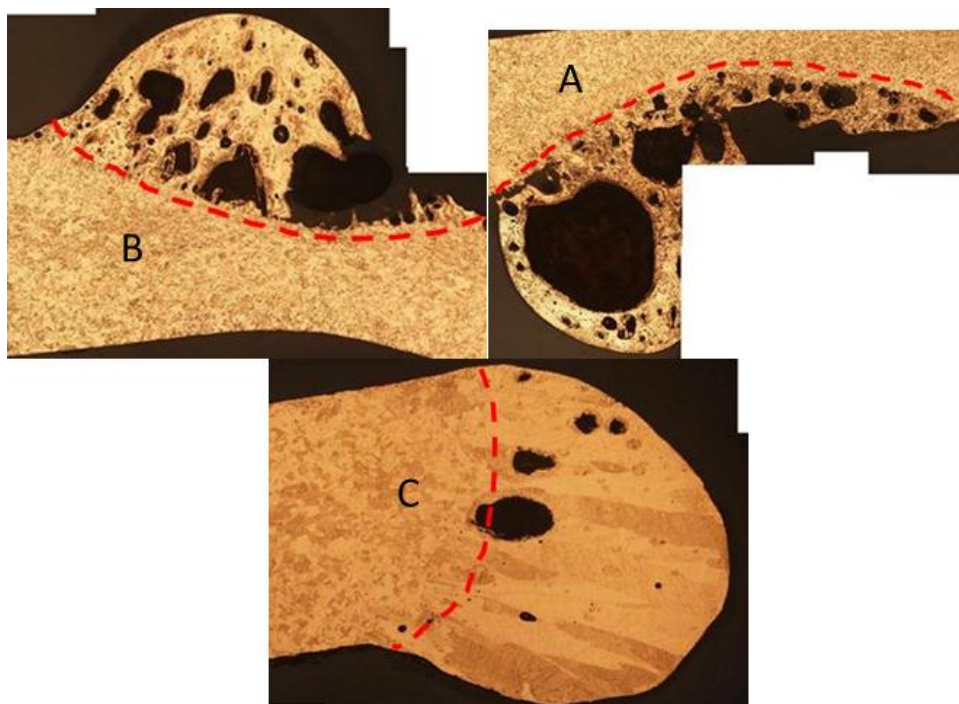


Figure 53: Line of Demarcation (Direct Flame (A and B) and Radiation (C))

There were two trends observed in the grain structure of the beads with visible lines of demarcation. The beads in Figure 53 showed an enlargement of the grain structure on the bead when compared to the longitudinal wire section. These beads were formed under energized, direct flame (Image A and B) and radiation (Image C) testing conditions. The images shown in Figure 54 show the beads formed during energized compartment testing. The grain structure in these images is opposite; the beads show small grain structures as compared to the longitudinal section of the wire.

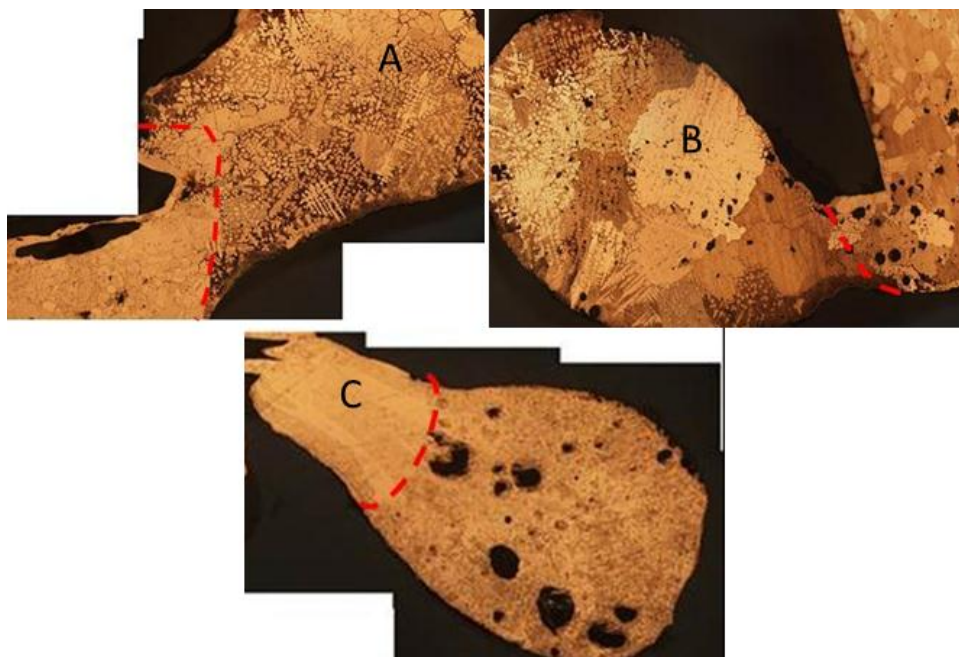


Figure 54: Line of Demarcation (Scaled Compartment-All)

7. Heat Transfer Analysis

A one dimensional conduction simulation of the direct flame scenario showed that most of the heat from the flame is absorbed by the small section of the wire being heated. The axial heat transfer is small compared to the heated region as seen in Figure 44 in Section F of Results Chapter.

B. Summary

There are about 400,000 household fires reported per year in the United States, and the cause of more than ten percent (10%) of these fires is electrical in nature. These fires result in hundreds of injuries per year, as well as, losses of life and property. When beads are found on electrical wires during a fire scene investigation, investigators often conclude that the wire was energized at the time of bead formation. In some cases, this causes the investigator to more heavily focus on the potential for the fire to be electrical in nature. Current training suggests

that beads are only produced on energized electrical wires, however, the findings of this research prove otherwise; characteristic “beads” can form on energized and non-energized wires.

The purpose of this research was to identify patterns on or inside beads that can be used to distinguish between the beads formed on non-energized wires (due to melting) and on energized wires (due to electrical activity). In order to encompass various thermal conditions found in fires, wires were tested in four different settings. These test methods covered convective, radiative, and a combination of convective/radiative exposures.

Some of the wire beads were analyzed with SEM/EDS. SEM/EDS analysis was done at the University of Maryland (College Park) by CSE, at the Unified Engineering (Aurora, IL), and at the Fire and Materials Research Laboratory (Livonia, MI). Analysis with SEM did not show any trends that could be used to distinguish between the beads formed on non-energized and energized wires. It was additionally concluded that SEM/EDS analysis of samples did not show any useful trends in the elemental composition of the beads or in structural patterns.

Another round of analysis was done with a stereo microscope to study the internal structures of the beads. The images of non-energized and energized beads showed several common patterns on the beads including voids. These patterns were present in both non-energized and energized wire beads. It was concluded that although several patterns were present within the bead structures, no distinguishing patterns were found between energized and non-energized beads.

In final analysis method, beads were photographed with a high resolution Nikon camera attached to the metallurgical microscope. This imaging revealed the grain structures of the copper beads. Six out of 14 (40%) beads formed on the energized wires showed a clear line of demarcation between the bead grain structures on the wire and only one of the 15 non-energized

beads also showed a line of demarcation. Some of the energized beads had grain structures similar to those found on the non-energized beads.

Two important conclusions that disprove previous beliefs about beads present or absent on copper wiring exposed to fire can be derived. First, the presence or absence of a bead on a wire exposed to fire does not provide a reliable indication whether the wire was energized or non-energized at the time of the fire. Furthermore, the presence of a bead cannot be used to determine whether the electrical wire failure was a cause or effect of the fire. Second, all of the bead analysis methods used during this research indicate that it is not possible to differentiate between the beads formed on energized and non-energized wires exposed to fire with a high degree of certainty. These conclusions show that fire investigators cannot rely on the presence or absence of beads alone to understand the role copper wiring may have played in a fire. The fire investigators must look at other scene information, like extent of the fire, duration of the fire, and nature of the fire to reach valid conclusions about the performance of copper wiring in the fire. Finally, it was hypothesized at the beginning of this research that beads will form on both energized and non-energized wires. It was also hypothesized that macroscopic and/or microscopic analysis of these beads would lead to indicators that could be used to differentiate between beads formed on energized and non-energized wires. Based on this work, it can be concluded that beads can form on wires regardless of electrical condition, and that it is not possible to differentiate between the beads formed on energized and non-energized wires to a high degree of certainty using the macroscopic and microscopic analysis techniques used in this research.

One promising result of the research was related to the grain structure analysis. Since one of the non-energized beads did have an internal line of demarcation, it is not possible to

conclude with 100% certainty that the presence of an internal line of demarcation indicates that a wire was energized at the time of bead formation. Additionally, since not all of the energized wires exhibited an internal line of demarcation, it is not possible to say that the absence of an internal line of demarcation indicates that a wire was non-energized. However, it is recommended that further research be conducted in this area to produce larger data sets which may yield higher degrees of confidence.

C. Implications for Policy and Practice

Faults in electrical equipment or systems are cited as a major cause of fires. Electrical failures led to over 50,000 reported household fires in 2006 (Hall, 2009). Fires attributed to electrical failure and malfunction accounted for 13% of all household fires. This also resulted in 13% of all fire deaths and 21% of all property damage due to electrical fires. The cost of these losses surpassed one billion dollars (\$1B). Hence, electrical failures are thought to be a leading cause of fire and fire damage in the United States.

However, there is still tremendous inconsistency and lack of knowledge within the forensic community when identifying electrical conductors involved in the ignition of the fire versus those damaged by the fire. Several studies have focused on distinguishing between post-fire and pre-fire arc beads on copper wire as discussed in the Literature Review Section above. Babrauskas (2003) concluded that there is not much promise with any of the proposed methods for distinguishing between post-fire and pre-fire beads because “most of the studies have been put forth as qualitative and subjective without means of quantification.” This study aimed to close the knowledge gap and provide quantitative guidance to the forensic and investigative communities.

NFPA 921: *Guide to Fire and Explosion Investigations* is the *de facto* standard of care in the fire investigation community. The guide is utilized by many training academies and private and public sector training organizations throughout the country. The current edition of NFPA 921 (2010) defines a bead as “a rounded globule of re-solidified metal at the end of the remains of an electrical conductor that was caused by arcing and is characterized by a sharp line of demarcation between the melted and unmelted conductor surfaces.” Hence, by definition, this characteristic bead can occur due to arcing. Based on the findings of this research, the long standing assumption that beads on wires can only be formed from arcing is provably false as seen in Figure 39 above. The findings of this research clearly show that non-energized electrical wires subjected to fire can form characteristic rounded globules with clear lines of demarcation. Additionally, energized wires subjected to arcing may not have these characteristic beads.

Hence, the findings of this study will impact the investigative community by requiring that investigators analyze damage on electrical wires based on more than physical characteristics. While there may be some conditions under which an investigator may be able to distinguish between an “cause bead” and an “artifact bead”, investigator must use caution in putting forth generalized relationships between wire damage and the electrical state (non-energized, energized with load, energized without load) of the wire at the time of damage.

D. Implications for further research

There is a general lack of reproducible, consistent techniques available for the analysis of beads formed on electrical wires. When this research proposal was first developed, it was assumed that the material science and metallurgical communities had some type of established, uniform techniques to analyze copper beads developed under fire conditions. Additionally, it was assumed that these established techniques would not only allow for the analysis of individual

beads but for the comparison of beads from various exposures. While the material science and metallurgical communities have available techniques for analysis of copper beads, there appears to be a general disagreement as to which technique is valid and appropriate.

The three main issues in bead analysis which require further research are establishing the appropriate etch and preparation techniques, the appropriate analysis technique (SM, SEM, EDS, Auger, etc.), and the appropriate location on the bead. Since different etches reveal different grain structures, the first issue is establishing which grain structure is most important for the specific condition of interest. Since fire is a dynamic thermal process, it is probably necessary to select multiple etches and re-etch and re-evaluate the samples accordingly. Additionally, various researchers have discussed the utility of difference kinds of analysis equipment. Some researchers suggest that stereomicroscopic analysis is sufficient, while others suggest that SEM/EDS, or various other combinations of metallurgical and material analysis should be used. Furthermore, when analyzing a bead using EDS, the following questions arise: 1) Should the surface of the bead be analyzed, and if so, should it be cleaned first and how should it be cleaned? 2) What location on the surface of the bead should be analyzed, and if multiple locations are recommended for analysis, how many is enough? 3) If the interior of the bead should be analyzed, what depth is appropriate, what surface area is appropriate, and how many locations are appropriate? 4) Can a technique developed based on the size and shape of one bead be equally applied to another bead of a different size or shape, and if so, will the result truly be comparable? A full study could be employed to address all of these questions, which are outside of the scope of this research. CSE, however, feels that this is an exceptionally important area that needs further research. Samples from this research project can be utilized for future efforts in this area.

V. REFERENCES

Anderson, R. N. (1989). Surface Analysis of Electrical Arc Residues in Fire Investigation. *Journal of Fire Sciences*, 34 (3), 633-637.

Anderson, R. N. (1996). Which Came First? Arcing or the Fire: A Review of Auger Analysis of Electrical Arc Residues. *Fire and Arson Investigator*, 46 (3), 38-40.

Andersson, P. and Van Hees, P. (2005). Performance of Cables Subjected to Elevated Temperatures. *Fire Safety Science—Proceedings of the Eighth International Symposium*, pp. 1121-1132.

Armstrong, W. R. (1999). Thermally Induced Failure of Low-Voltage Electrical Nonmetallic-sheathed Cable Insulation. *Fire Technology*, 35(3).

Babrauskas, V. (2003). How do Electrical Wiring Faults Lead to Structure Ignitions? *Fire and Materials*, 189-201.

Babrauskas, V. (2004). Arc Beads from Fire: Can ‘Cause’ Beads be Distinguished from ‘Victim’ Beads by Physical or Chemical Testing?. *Journal of Fire Protection Engineering*, 14.

Beland, B. (1980). Examination of Electrical Conductors Following a Fire. *Fire Technology*, 16, 252-258.

Beland, B. (1981). Arcing Phenomenon as Related to Fire Investigations. *Fire Technology*, 17 (3), 180-210.

Beland, B. (1982). Considerations on Arcing as a Fire Cause. *Fire Technology*, 18, 188-202.

Beland, B. (1994). Examination of Arc Beads. *Fire and Arson Investigator*, 44 (4), 20-22.

Chen, C.Y. et al. SIMS Depth Profiling Analysis of Electrical Arc Residues in Fire Investigation. *Applied Surface Science*, 203-204, 779-784, 2003.

Churchward, D. L. and Cox, R. M. (2010). The ‘Benefits’ of Arcing. *International Symposium on Fire Investigation Science and Technology*. University of Maryland, College Park.

Delplace, M. and Vos, E., (1983). Electric Short Circuits Help the Investigator Determine Where the Fire Started. *Fire Technology*, 19 (3), 185-191.

Ettling, B. (1978). Electrical Wire in Building Fires. *Fire Technology*, 14, 317-325.

FEMA (2008). Residential Building Electrical Fires. 8 (2).

Ferrino-McAllister, J., Roby, R.J., Milke, J. (2006). Heating of Electrical Contacts: Characterizing the Effects of Torque, Contact Area, and Movement on the Temperature of Residential Receptacles. *Fire Technology*, 42(1), pp. 49-74.

Ferrino-McAllister, J.L., Roby, R.J., Klassen, M.S., Milke, J. (2005). Heating of Electrical Conductors: Characterizing the Deformation of Cable Exposed to External Radiant Heating and Internal Overload. *Fire and Arson Investigator*, 56(2).

Gray, D. and Lewis, F.A. (1983). Identification of Electrical Sources of Ignition in Fires. *Fire Safety Journal*, 6, 147-150.

Goodman, A., Schooler, C. and McAllister, J.L. (2010). Physical Characteristics of Non-energized and Energized Cables in Scaled Compartment Fires. *International on Fire Investigation Science and Technology*.

Hall Jr, J. (2012), NFPA, 'Home electrical fires'

Hall, J. (2009). Home Fires Involving Electrical Failure or Malfunction.

Henderson, R., Manning, C., and Barnhill, C. (1998). Questions Concerning the Use of Carbon Content to Identify "CAUSE" vs. "RESULT" Beads in Fire Investigation. *Fire and Arson Investigator*, Volume 48, Number 3.

Hirschler, M. M. (1997). Analysis of an Potential Correlations Between Fire Tests for Electrical Cables, and How to Use This Information for Fire Hazard Assessment. *Fire Technology*, 33(4).

Hoffman, D. J. (2002). Electrical Power Cord Damage from Radiant Heat and Fire Exposure and Full Scale Burn Tests of Television Sets and Electronic Appliances. DRI Fire and Casualty Seminar, (p. 223). New Orleans.

Hagimoto, Y., Watanabe, N. and Okamoto. (1999). Arcing Faults on PVC-covered Electrical Cords, *Proc. 1st Conf. of the Assn. of Korean-Japanese Safety Engineering Society*, Kyongju, Korea, p. 221-224.

Howitt, D. G. (1997). The Surface Analysis of Copper Arc Beads-A Critical Review. *Journal of Forensic Sciences*, 42 (4), 608-609.

Jacobs, J. J. and Dinman, D. J. (2004). Systematic Analysis of Bicistronic Reporter Assay Data. *Nucleic Acid Research*, 32(20).

Karlsson, B., and Quintiere, J. (2000). *Enclosure Fire Dynamics*, Chapter 2, page 18.

Lee, E-P., Ohtani, H., Matsubara, Y., Seki, T., Hasegawa, H., Imada, S., and Yashiro, I. (2002). Study on Discrimination between Primary and Secondary Molten Marks using Carbonized Residue. *Fire Safety Journal*, 37, 353-368, 2002.

Lennard, C. Fire-Determination of Cause: A Review 1995-1998.

Levinson, D.W. (1977). Copper Metallurgy as a Diagnostic Tool for Analysis of the Origin of Building Fires. *Fire Technology*, 13 (3), 211-222, 1977.

NFPA. (2011). *Guide for Fire and Explosion Investigation*, Chapter 8: Electricity and Fires.

Singh, R.P. (1987). Scanning Electron Microscopy of Burnt Electric Wires. *Scanning Microscopy*, 1(4), 1539-1544, 1987.

Slenski, G. and Galler, D. (2004). Wire and Cables. *Electronic Failure Analysis Handbook*, Chapter 15.

White, H.E. (1948). *Modern College Physics*. Van Nostrand Reinhold Company, New York, NY.

VI. DISSEMINATION OF RESEARCH FINDINGS

The main objective of this research was to better understand the effects of thermal insult on copper electrical conductors under conditions that are representative to those commonly found in compartment fires. The ability to accurately distinguish if a beaded wire was energized or non-energized during fire is critical, especially in scenarios where electricity is presumed to be the culprit. A long standing assumption in the field of fire investigation is that beads can only be formed on energized wires; based on the findings of this research, this assumption is provably false. The findings of this research have shown that investigators should use extreme caution when putting forth opinions regarding the electrical state of a conductor solely based on evidence of a beaded wire, since beads can form on both energized and non-energized wires.

The findings of the preliminary study, which were the basis for this research proposal, were presented at the 2010 International Symposium on Fire Investigation Science and Technology in College Park, MD. Preliminary findings of this research were presented in poster form at the 2011 International Association for Fire Safety Science Conference in College Park, MD. After completion of this research, CSE intends to submit a publication to *Fire Technology* and *Fire and Arson Investigator Magazine*. CSE also intends to present the findings of this research to the NFPA 921 committee and submit proposals for changes to the *Electricity and Fire* chapter in the NFPA 921 guide.

Additionally, this research was conducted as part of a Master of Science thesis in the Fire Protection Engineering Department at the University of Maryland. Therefore, the research was presented to the University faculty for approval, and the final results of this research were memorialized in a written thesis document.

Note:

NE – Non Energized

EN – Energized

L – Loaded

COMPARTMENT TEST; 16-2 MULTISTRAND WIRE

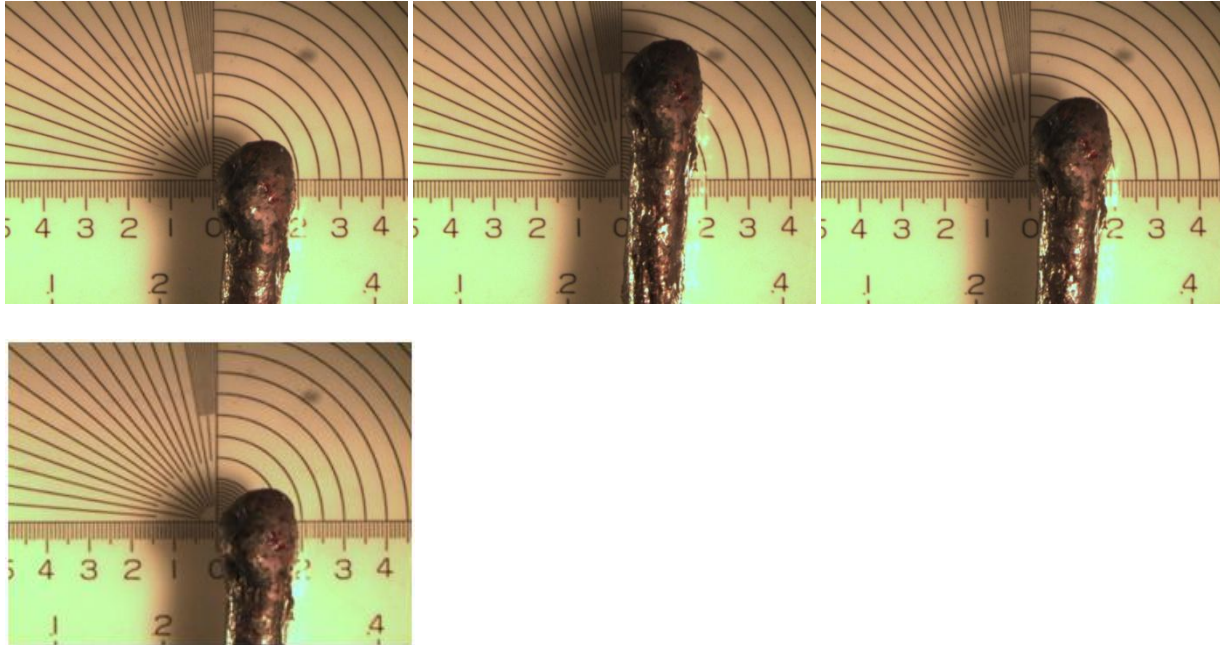


Figure A1: Compartment Tests, MS 16-2, Energized (Test No. 30)

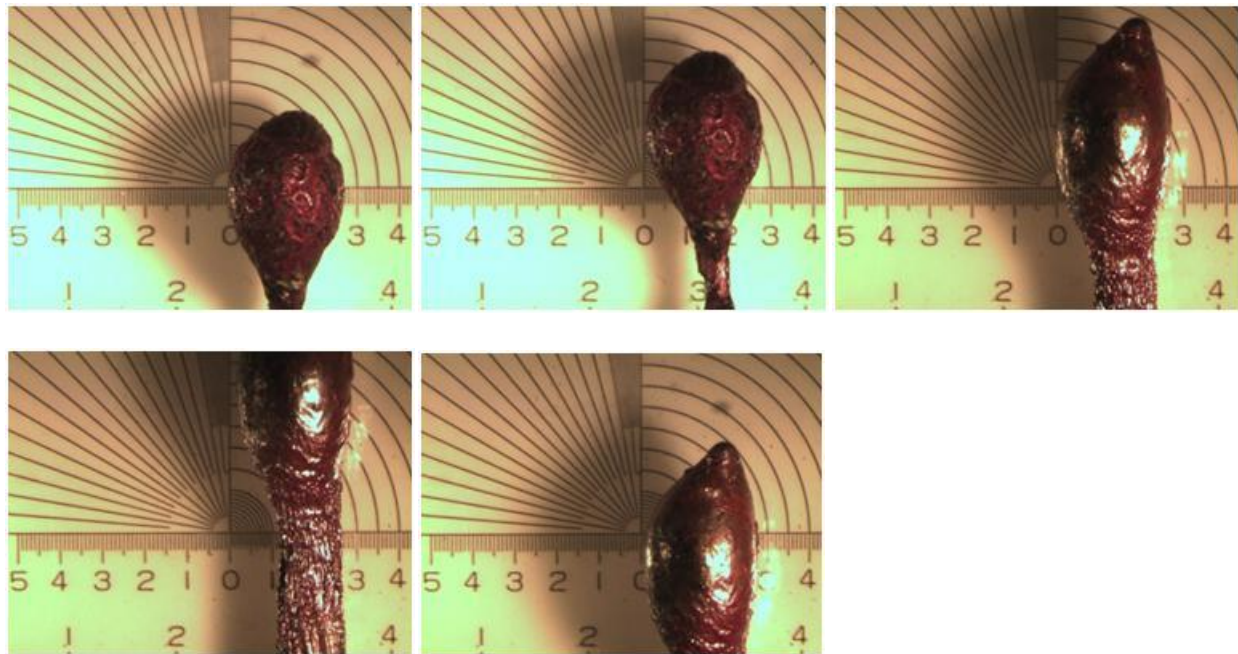


Figure A2: Compartment Tests, MS 16-2, Non Energized (Test No. 36)

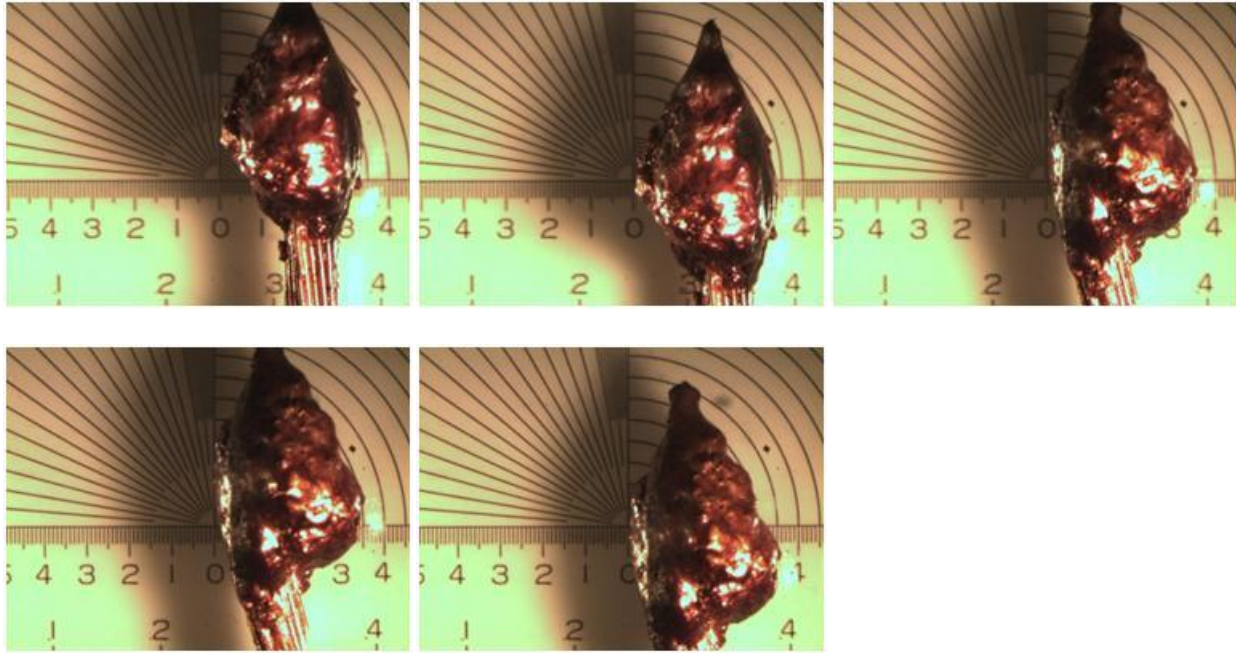


Figure A3: Compartment Tests, MS 16-2, Energized (Test No. 37)

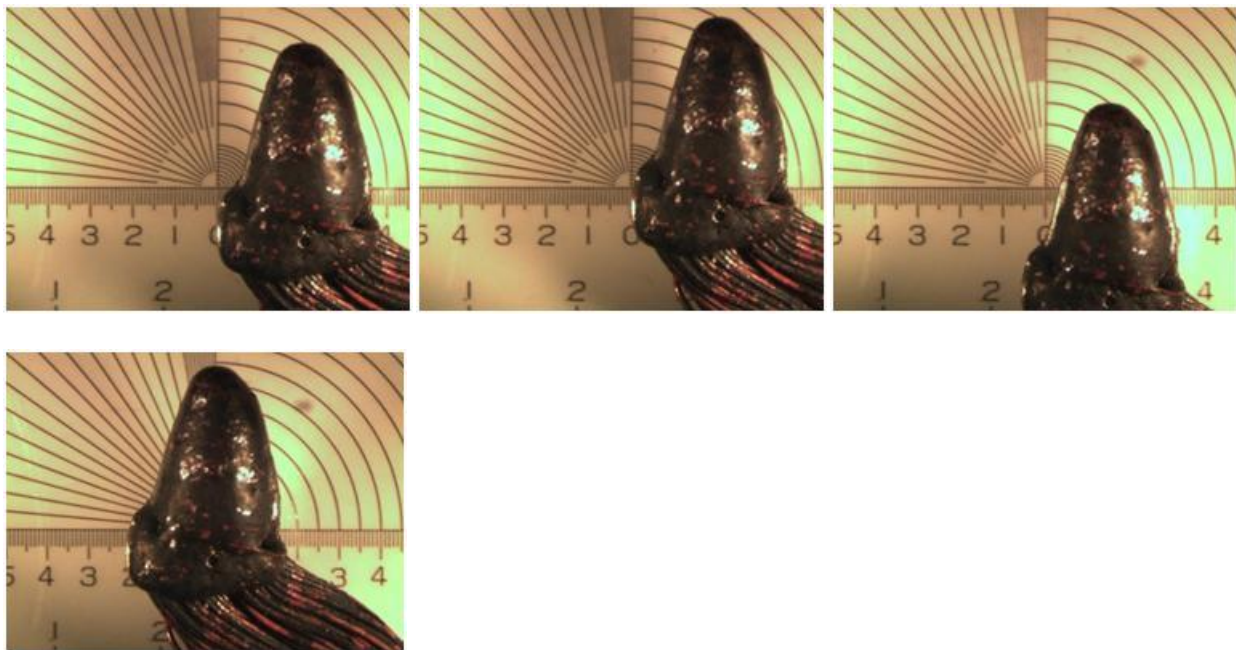


Figure A4: Compartment Tests, MS 16-2, Loaded (Test No. 37)

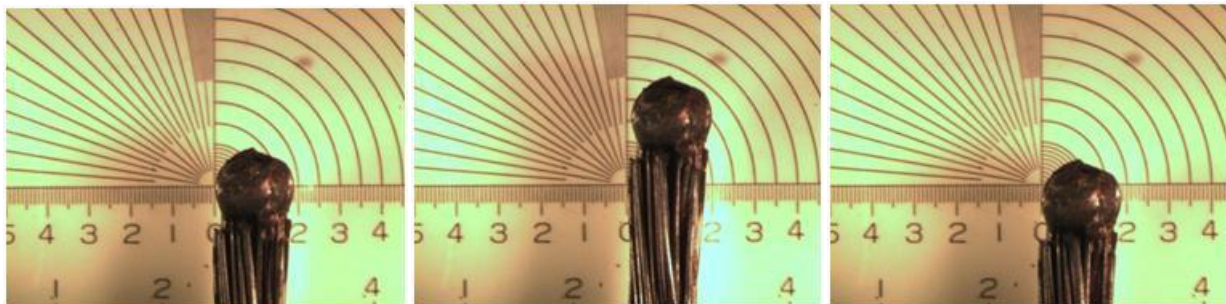


Figure A5: Compartment Tests, MS 16-2, Energized (Test No. 38)

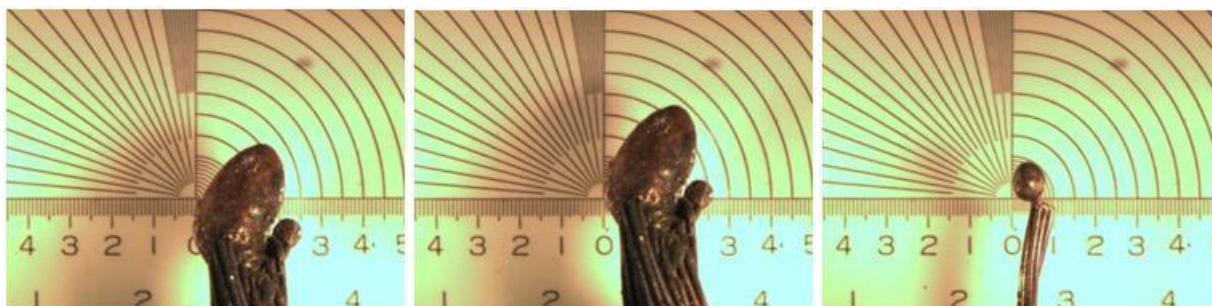
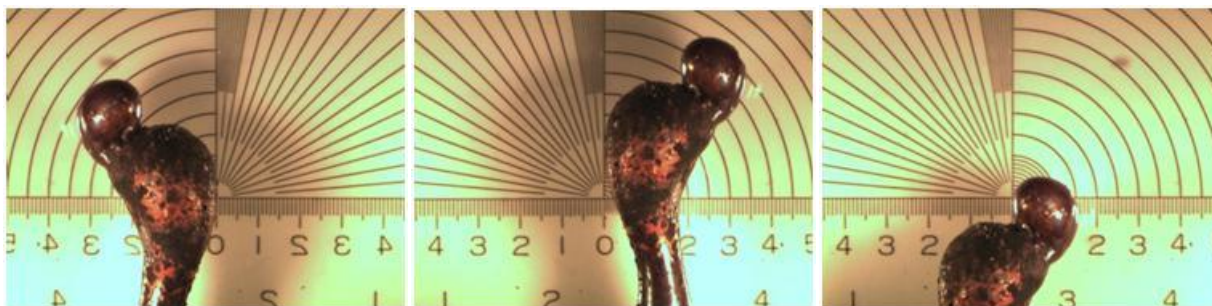


Figure A6: Compartment Tests, MS 16-2, Energized (Test No. 39)



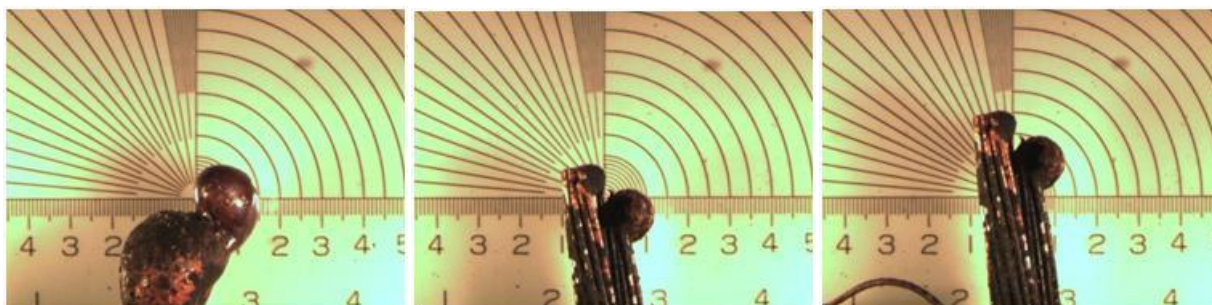


Figure A7: Compartment Tests, MS 16-2, Loaded (Test No. 39)

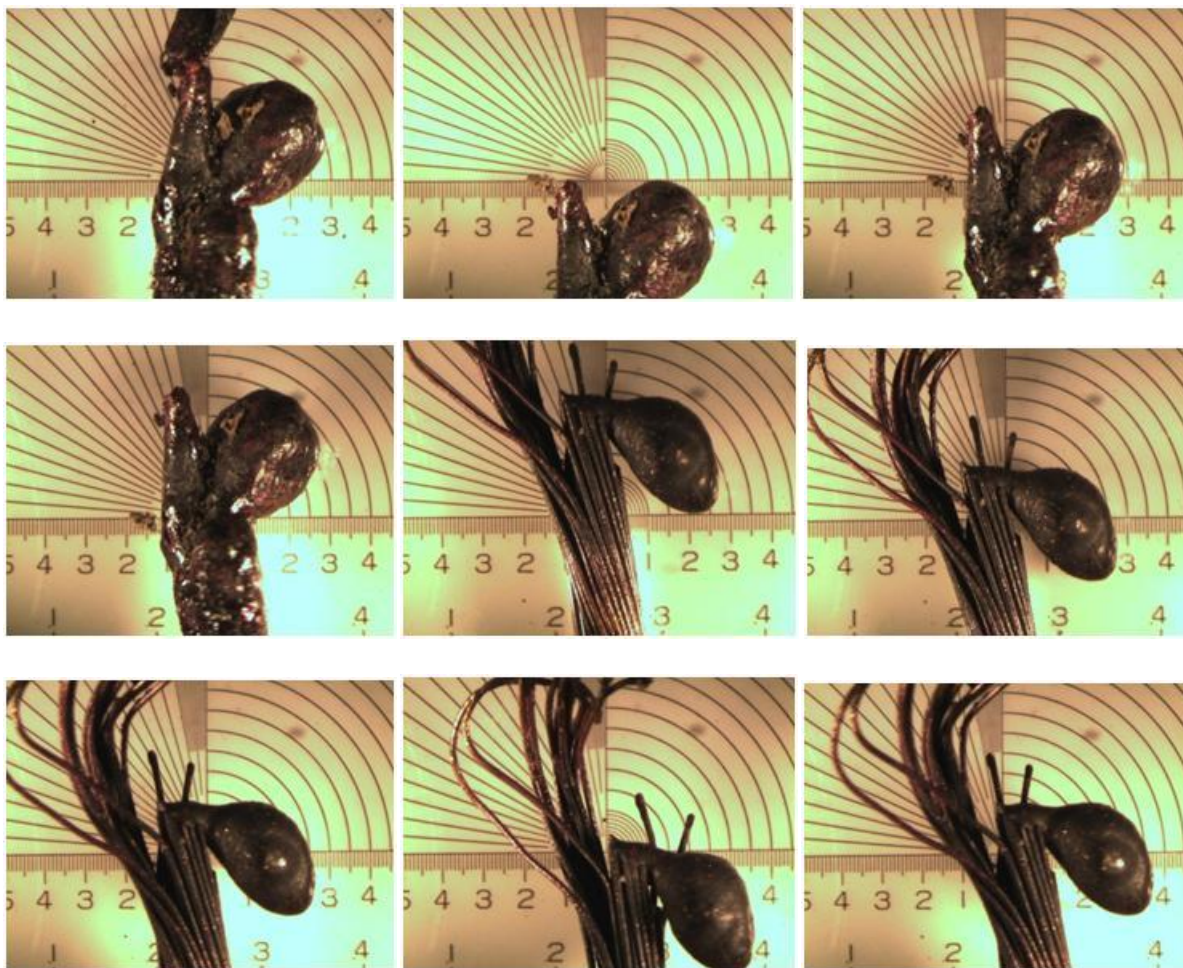
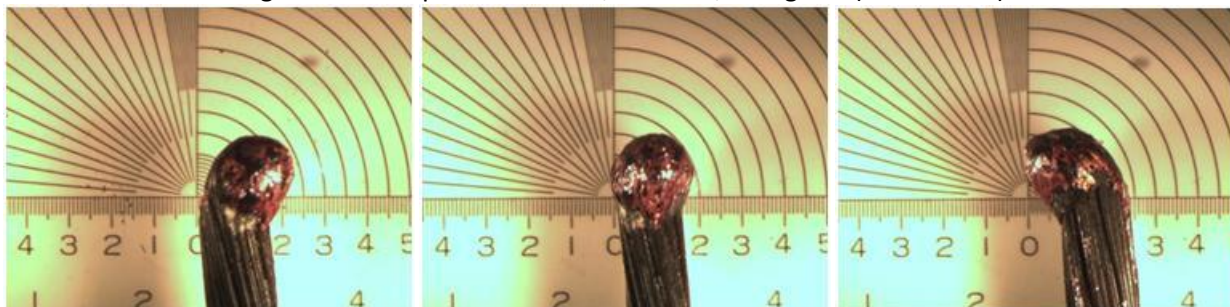


Figure A8: Compartment Tests, MS 16-2, Energized (Test No. 40)



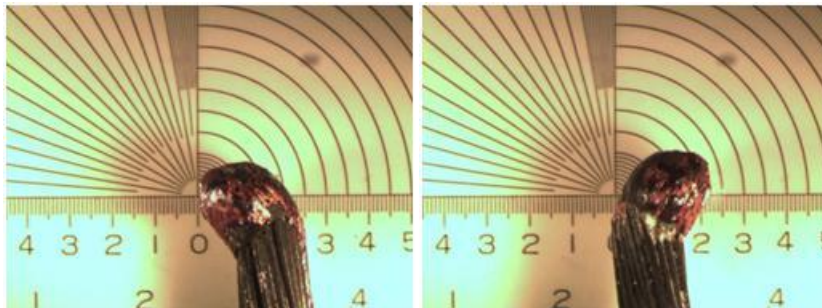


Figure A9: Compartment Tests, MS 16-2, Loaded (Test No. 41)

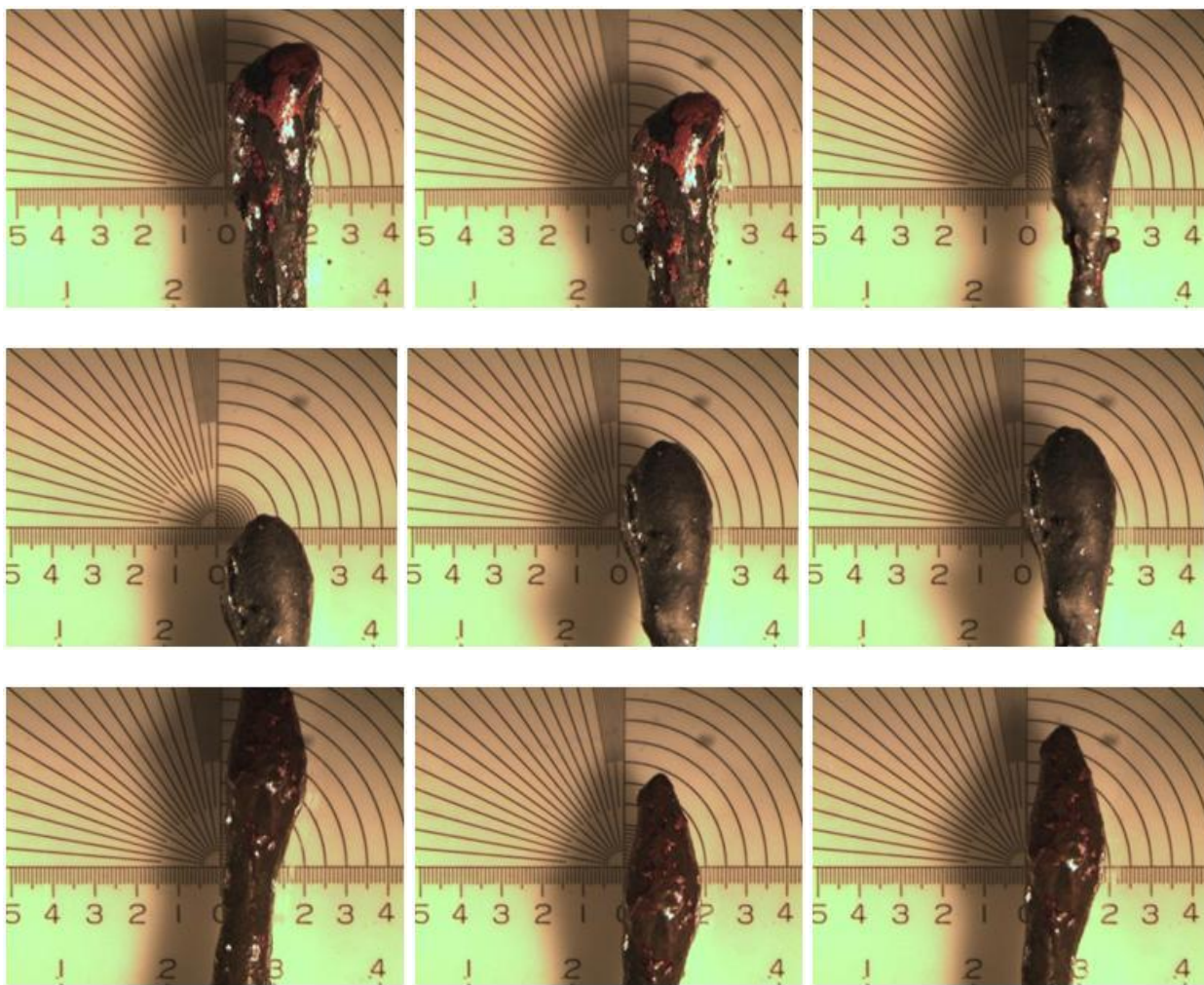


Figure A10: Compartment Tests, MS 16-2, Non Energized (Test No. 42)

This document is a research report submitted to the U.S. Department of Justice. This report has not been published by the Department. Opinions or points of view expressed are those of the author(s) and do not necessarily reflect the official position or policies of the U.S. Department of Justice.

COMPARTMENT TEST; 18-2 MULTISTRAND WIRE

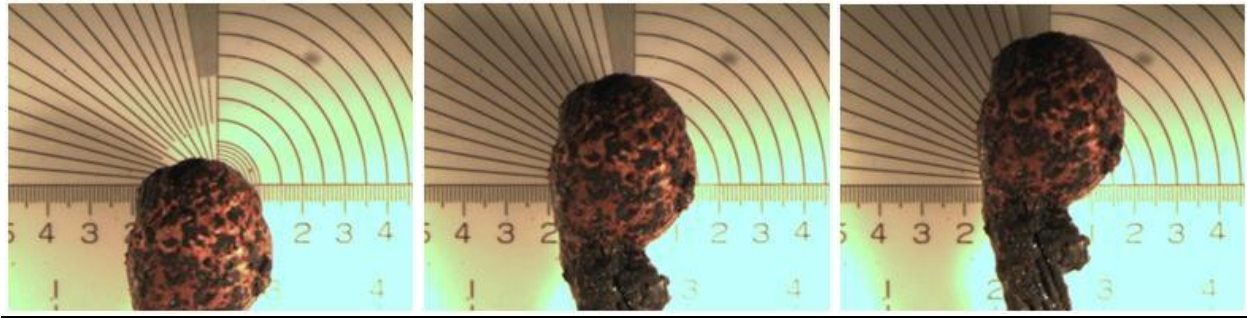


Figure A11: Compartment Tests, MS 18-2, Non Energized (Test No. 27)

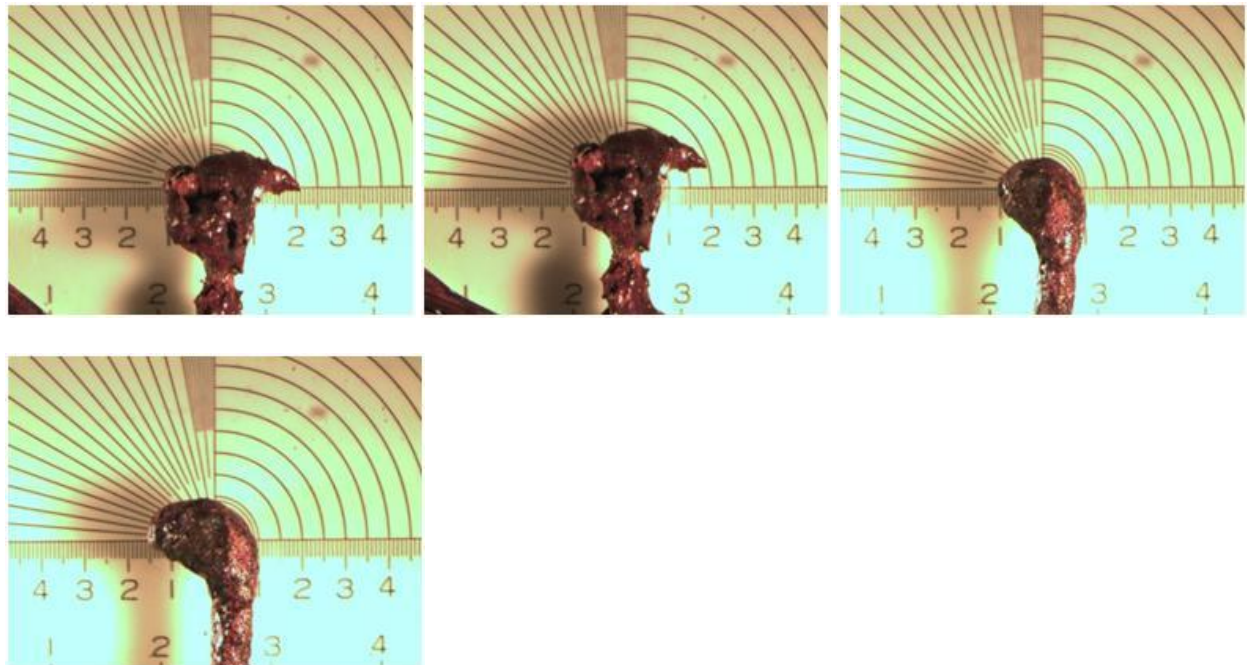
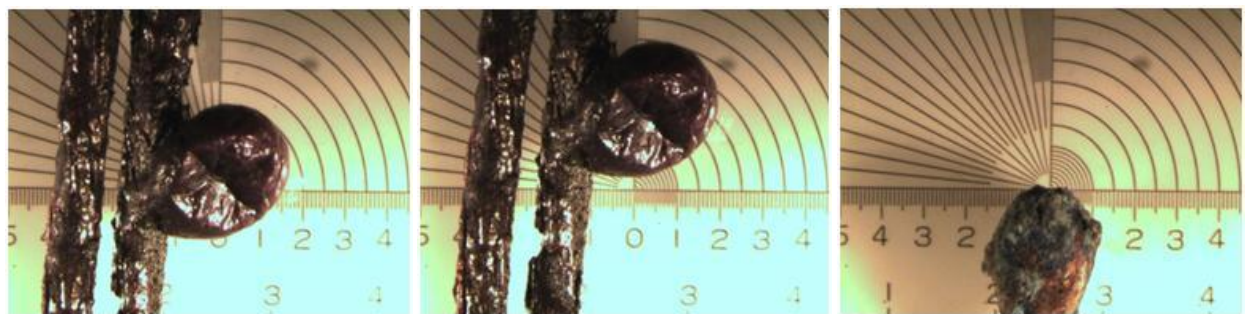


Figure A12: Compartment Tests, MS 18-2, Loaded (Test No. 27)



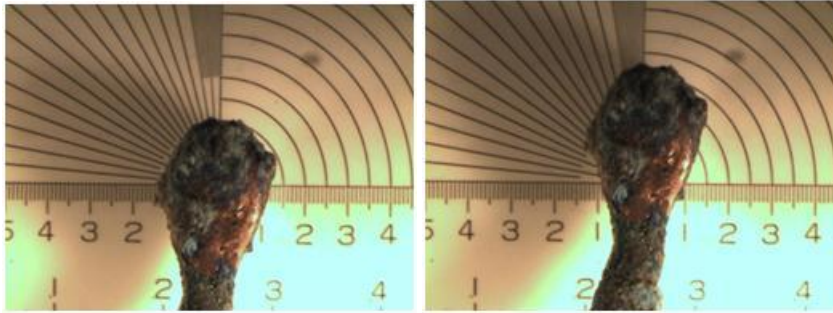


Figure A13: Compartment Tests, MS 18-2, Non Energized (Test No. 28)

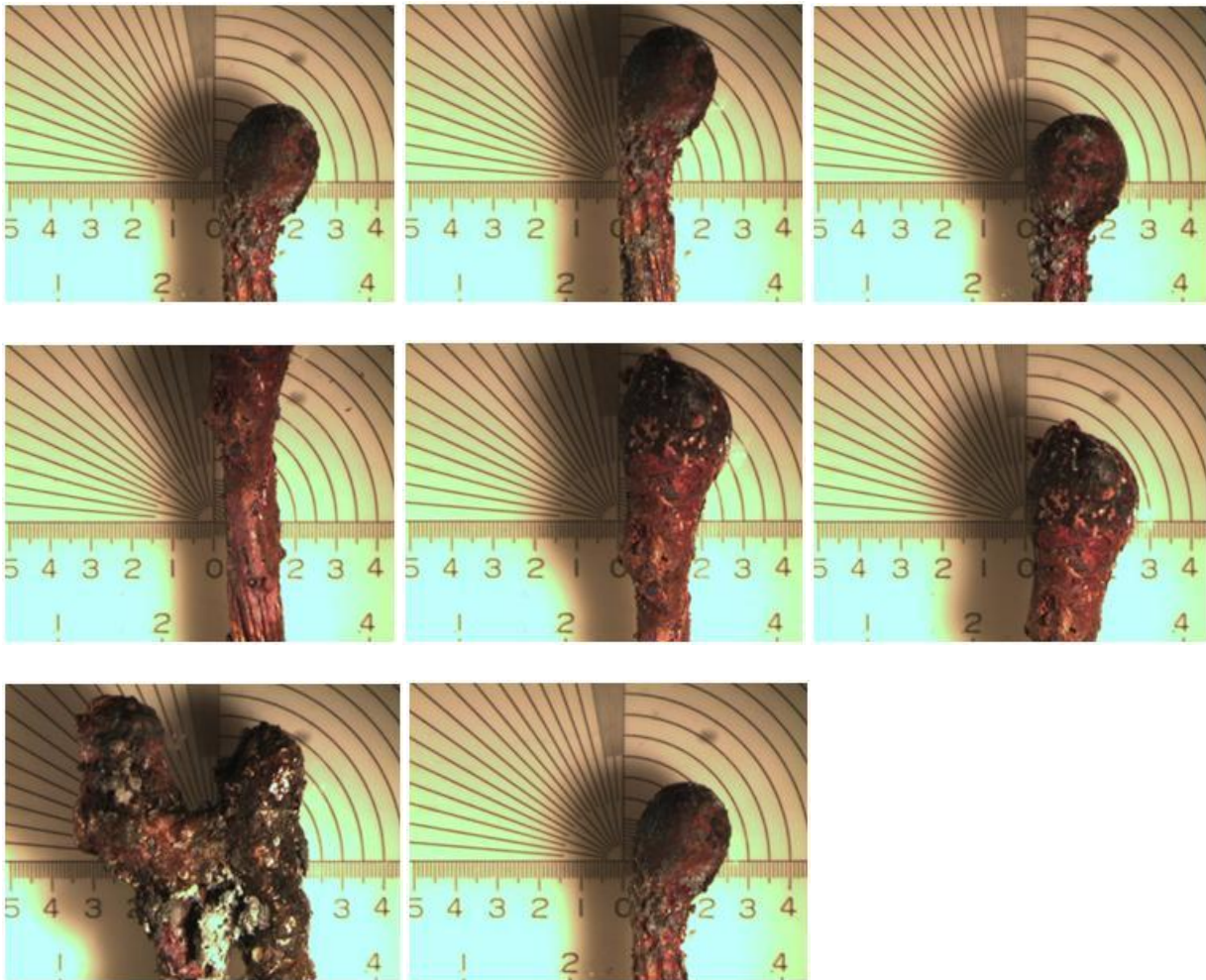


Figure A14: Compartment Tests, MS 18-2, Energized (Test No. 31)

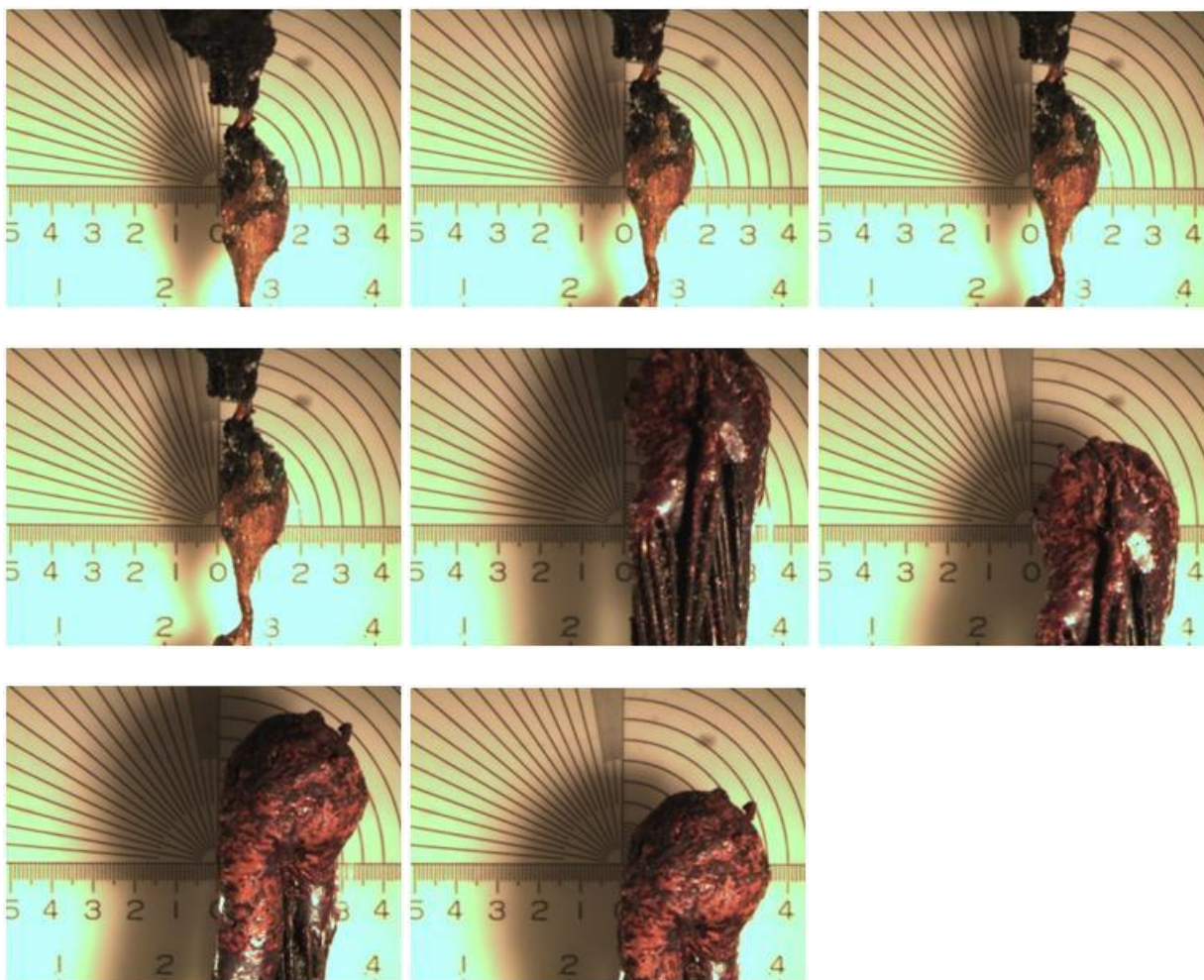


Figure A15: Compartment Tests, MS 18-2, Loaded (Test No. 31)

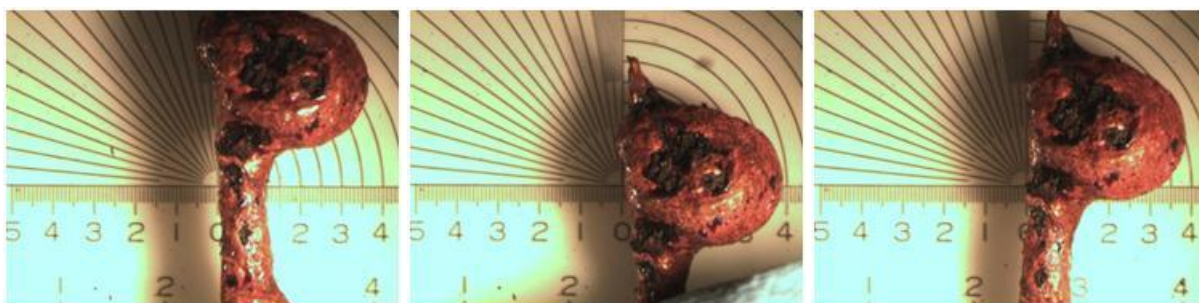


Figure A16: Compartment Tests, MS 18-2, Energized (Test No. 32)

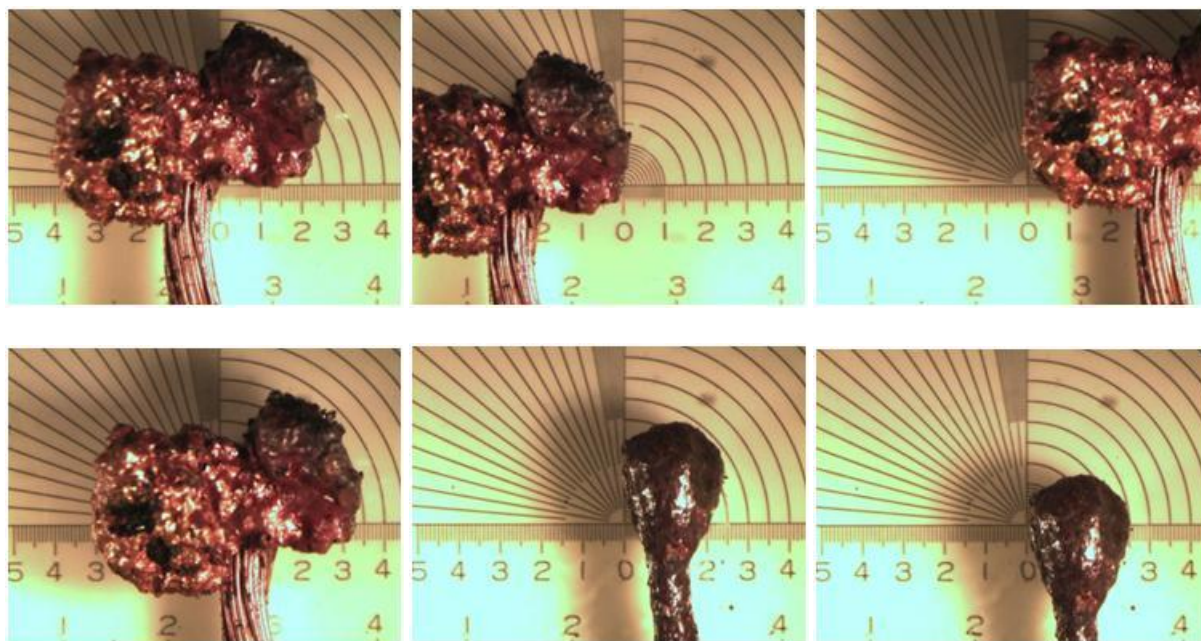


Figure A17: Compartment Tests, MS 18-2, Loaded (Test No. 32)

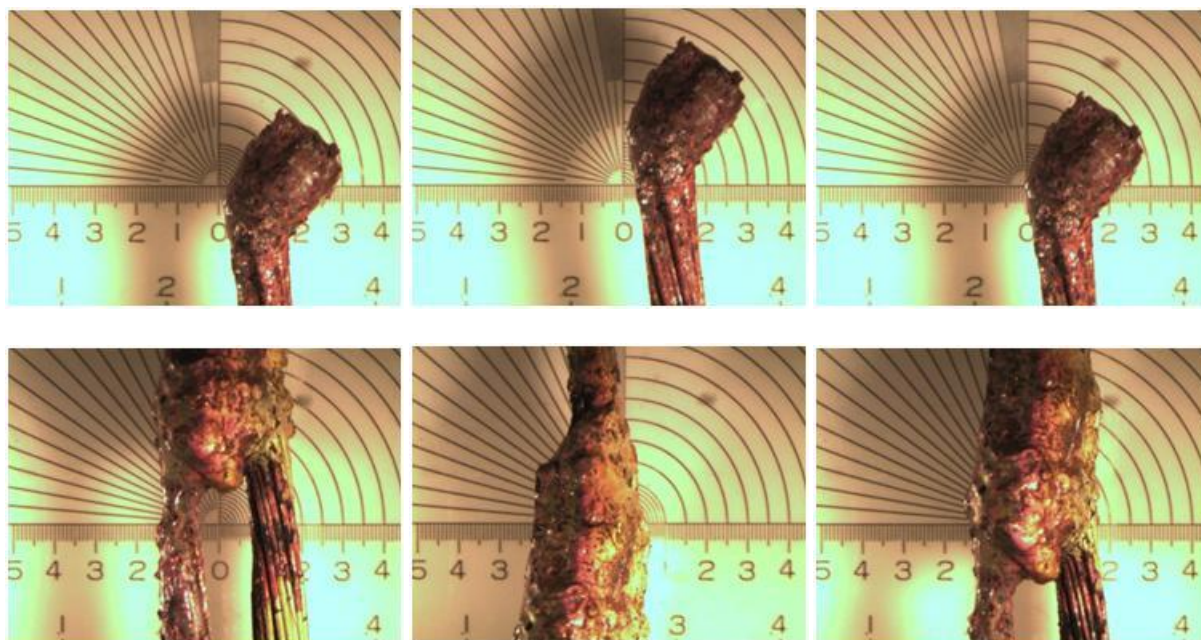


Figure A18: Compartment Tests, MS 18-2, Energized (Test No. 33)

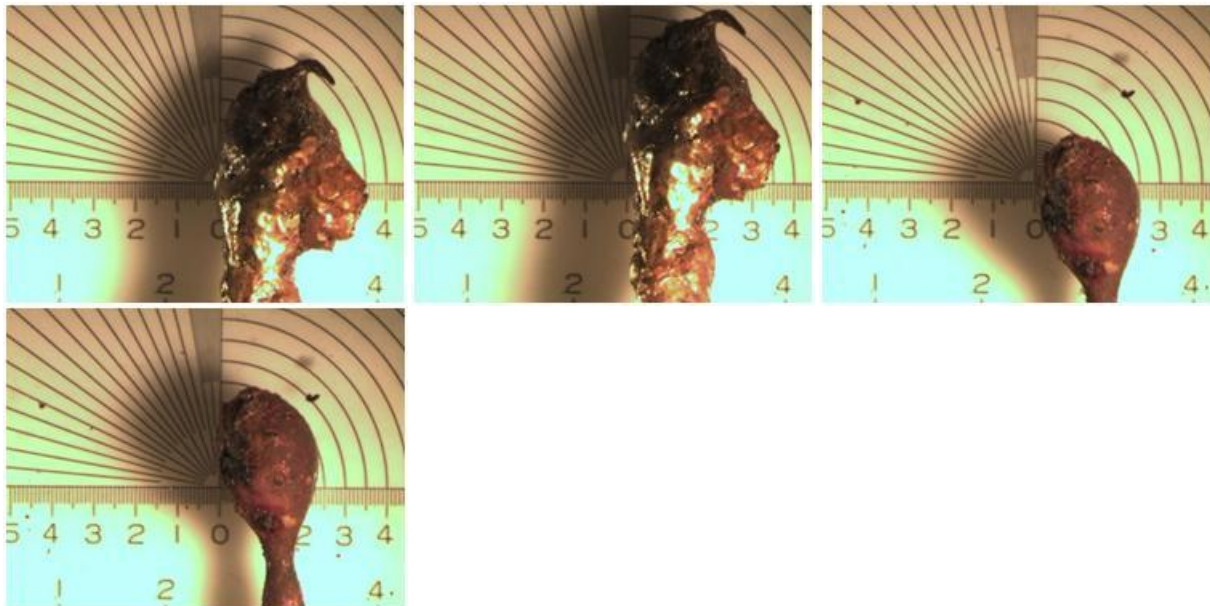


Figure A19: Compartment Tests, MS 18-2, Energized (Test No. 34)

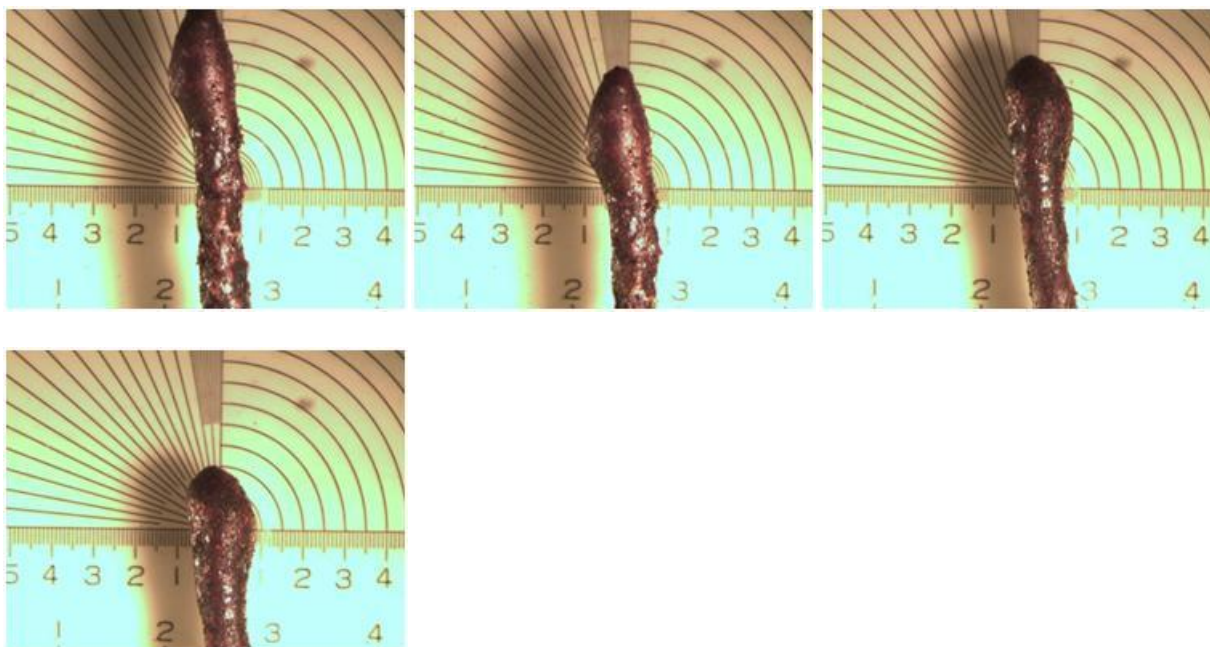


Figure A20: Compartment Tests, MS 18-2, Loaded (Test No. 34)

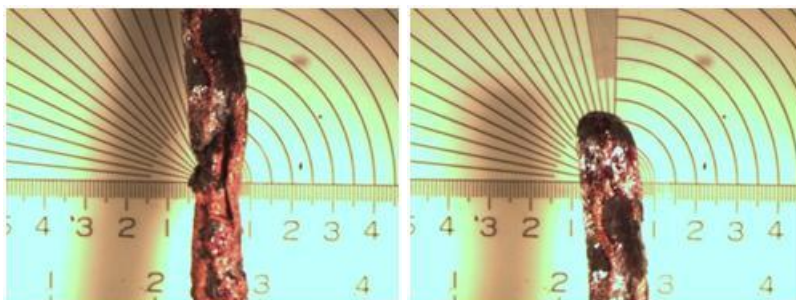


Figure A21: Compartment Tests, MS 18-2, Energized (Test No. 35)

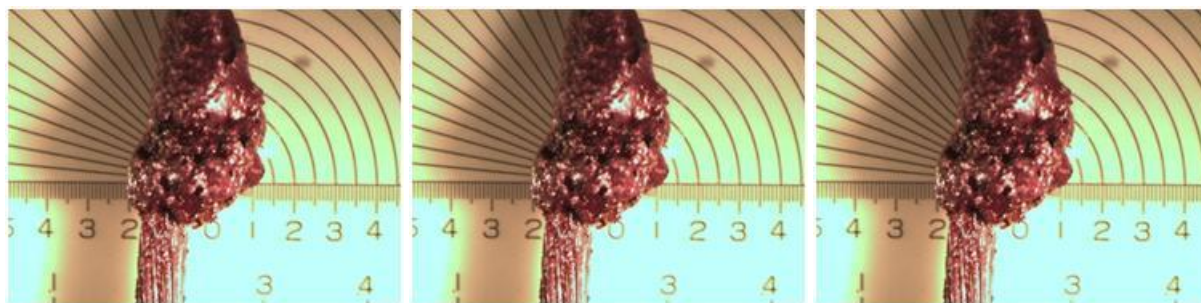


Figure A22: Compartment Tests, MS 18-2, Loaded (Test No. 35)

COMPARTMENT TEST; 12-2 ROMEX WIRE

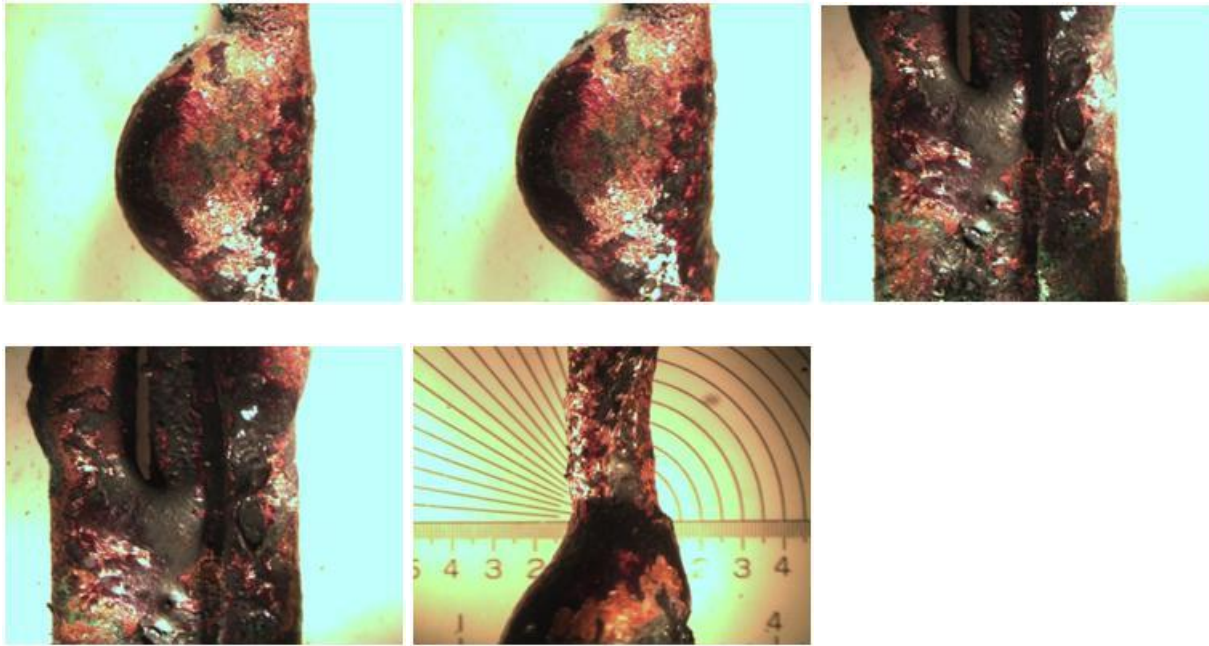


Figure A23: Compartment Tests, ROMEX 12-2, Energized (Test No. 12)

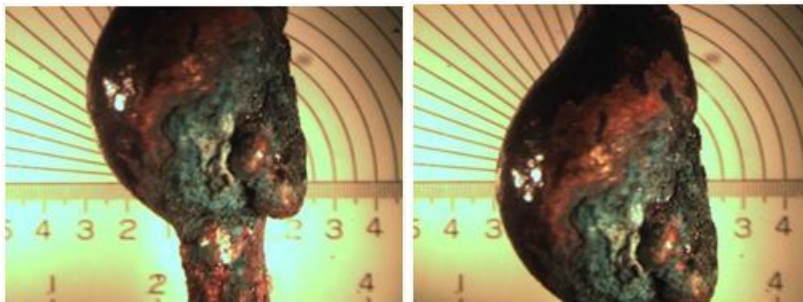


Figure A24: Compartment Tests, ROMEX 12-2, Loaded (Test No. 12)

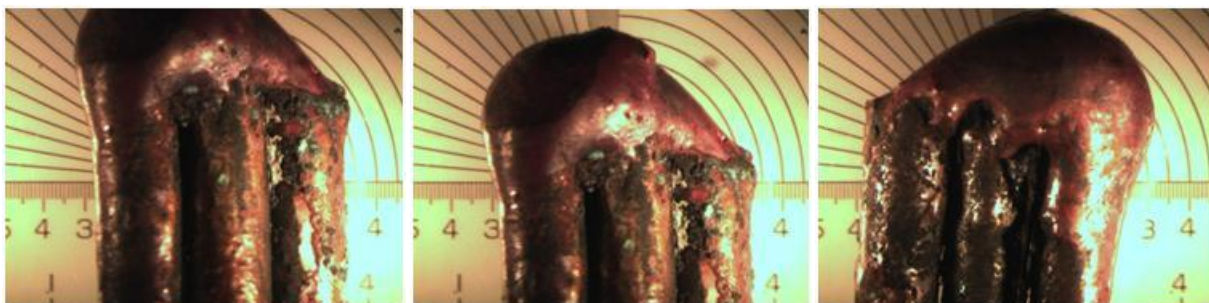


Figure A23: Compartment Tests, ROMEX 12-2, Energized (Test No. 14)

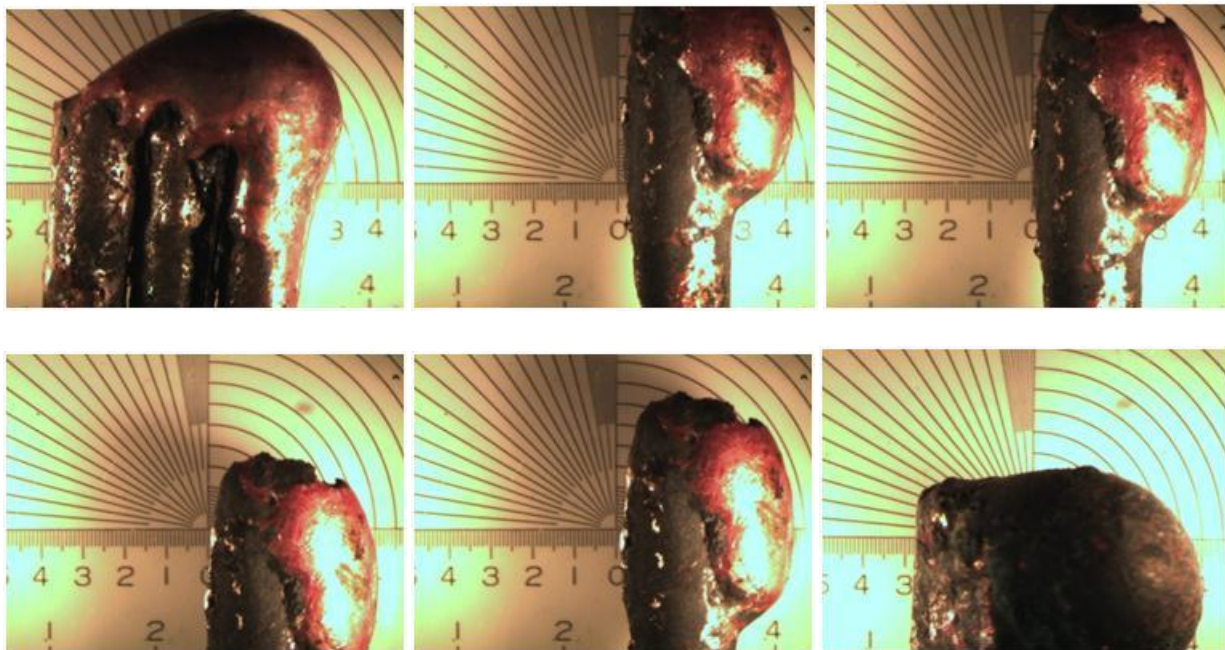


Figure A24: Compartment Tests, ROMEX 12-2, Loaded (Test No. 15)

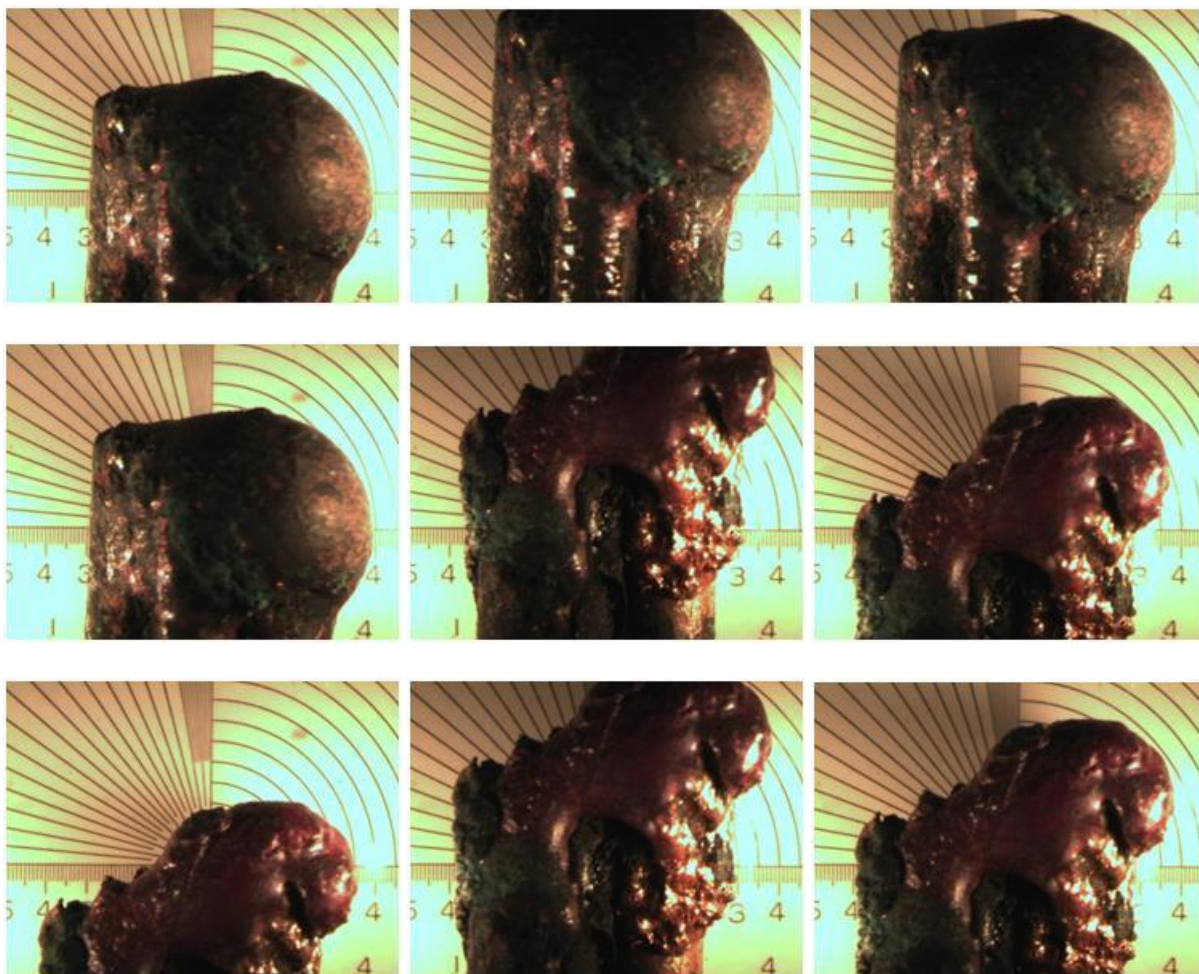


Figure A25: Compartment Tests, ROMEX 12-2, Non Energized (Test No. 14)

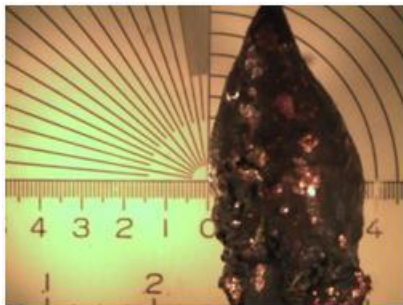
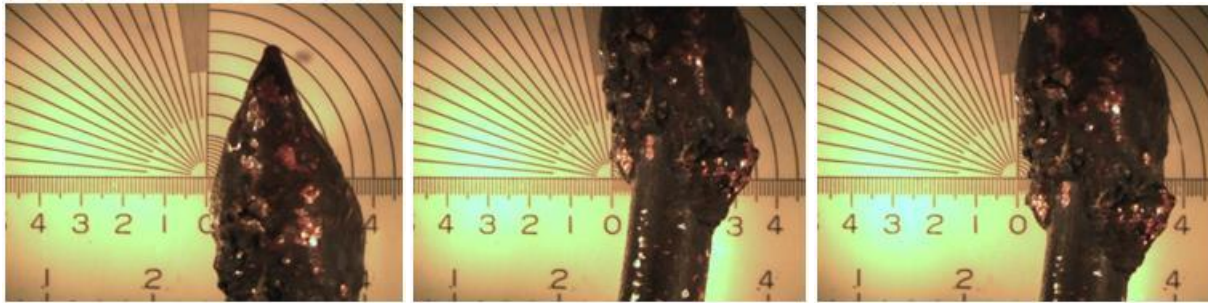


Figure A26: Compartment Tests, ROMEX 12-2, Loaded (Test No. 15)

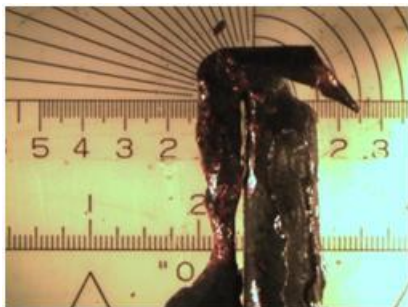
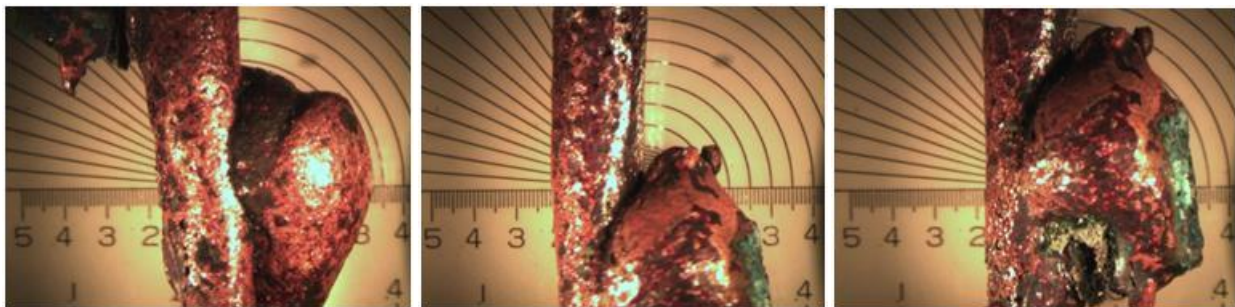


Figure A27: Compartment Tests, ROMEX 12-2, Non Energized (Test No. 15)



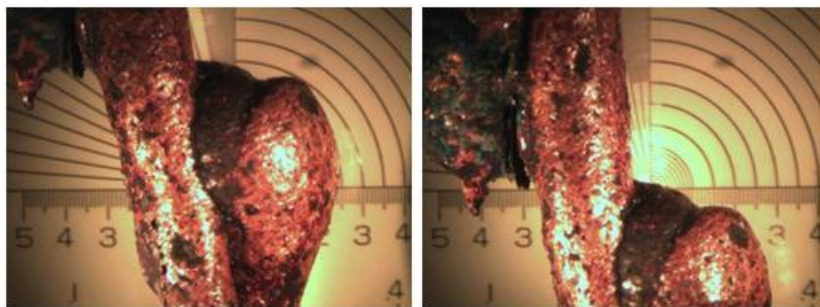


Figure A28: Compartment Tests, ROMEX 12-2, Energized (Test No. 21)

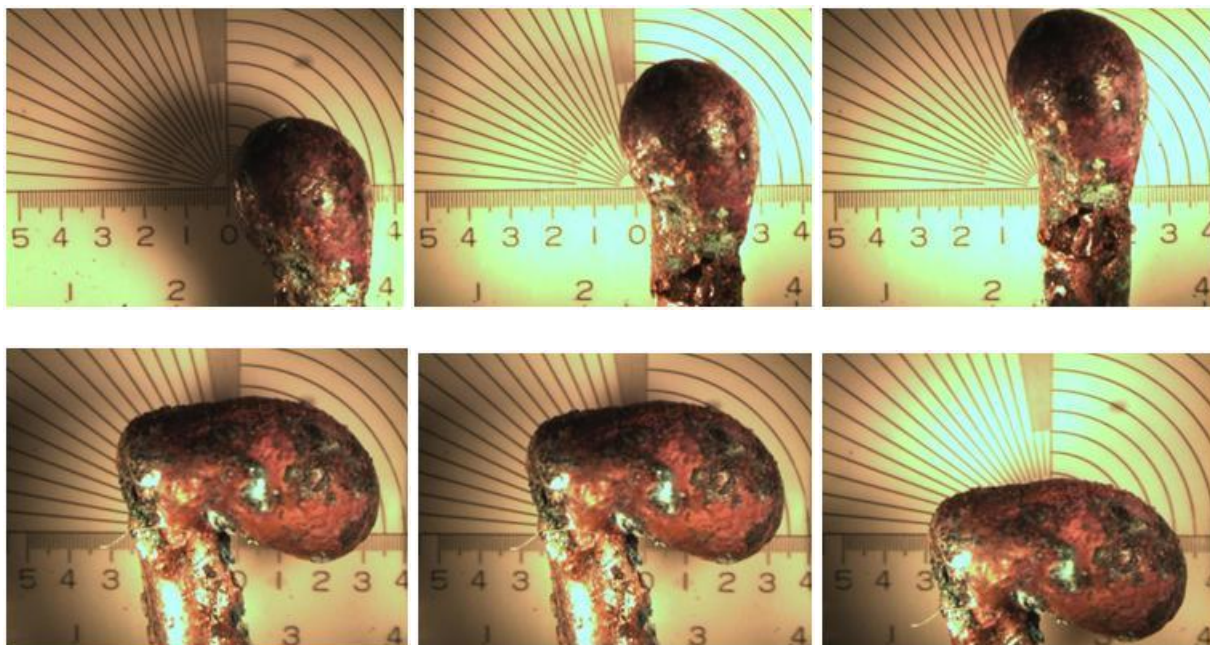


Figure A29: Compartment Tests, ROMEX 12-2, Loaded (Test No. 21)

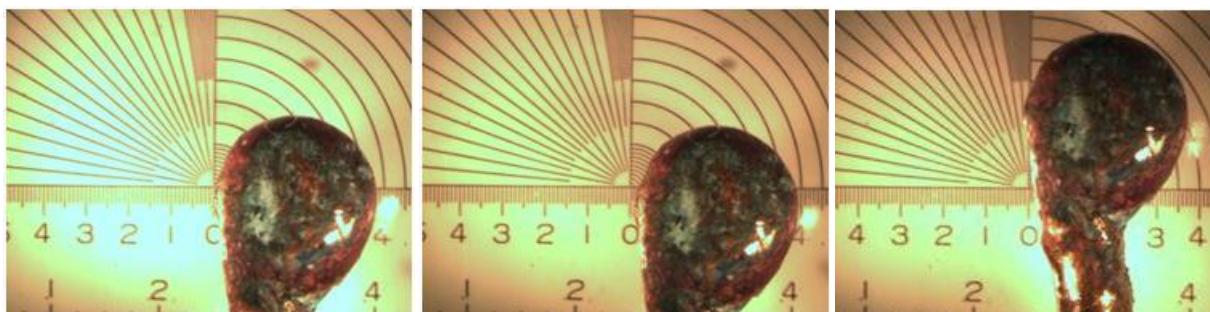


Figure A30: Compartment Tests, ROMEX 12-2, Non Energized (Test No. 25)

COMPARTMENT TEST; 14-2 ROMEX WIRE

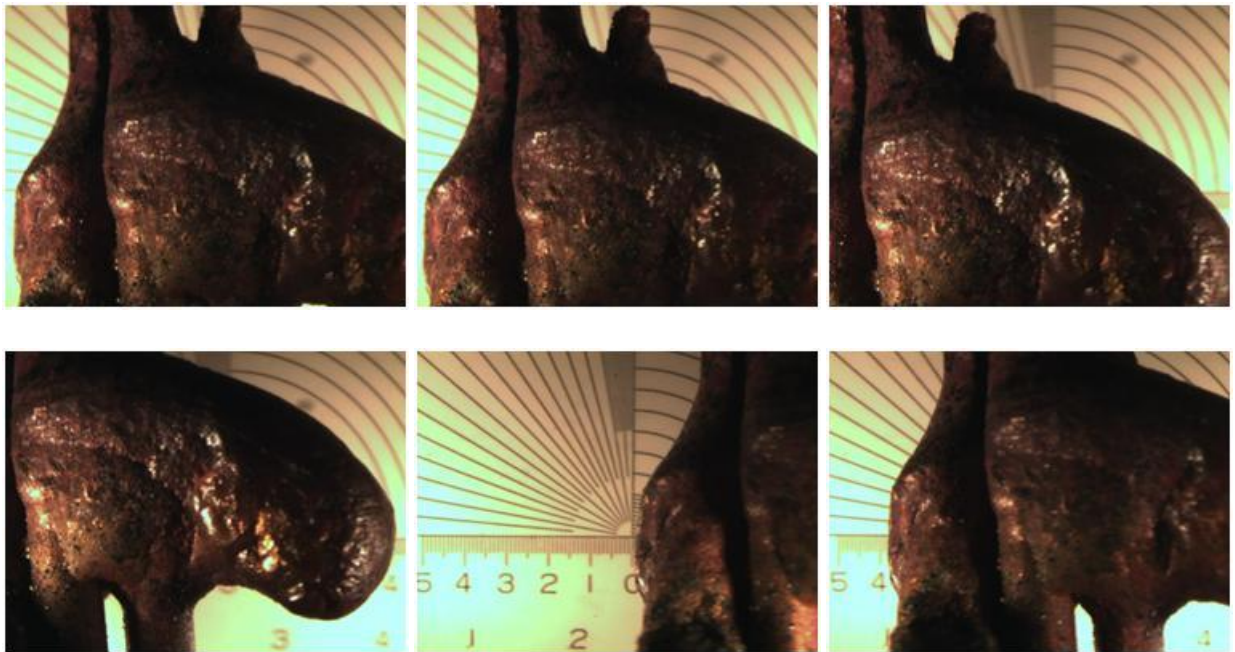
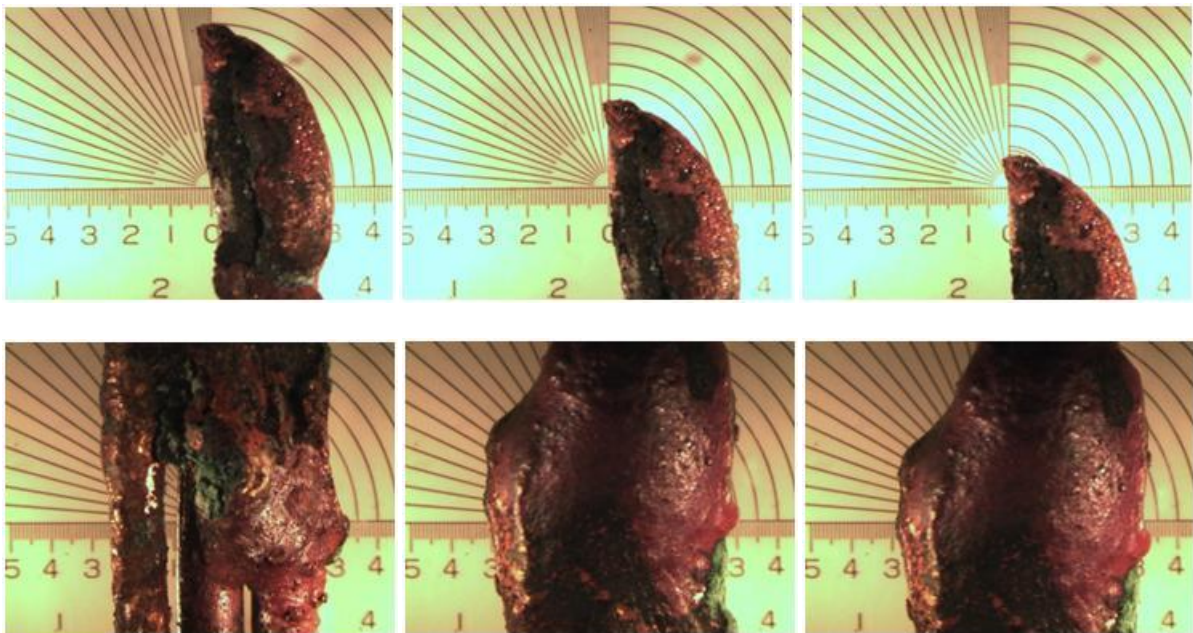


Figure A31: Compartment Tests, ROMEX 14-2, Energized (Test No. 16)



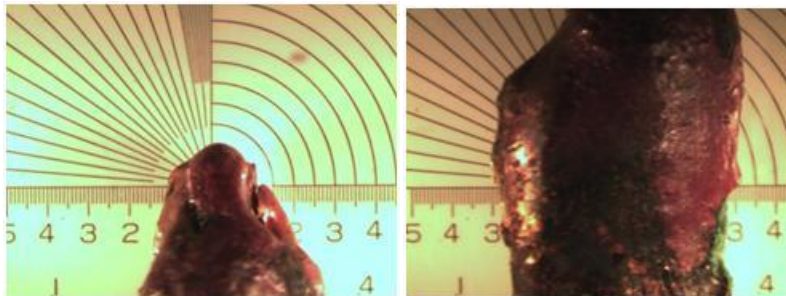


Figure A32: Compartment Tests, ROMEX 14-2, Energized (Test No. 16)

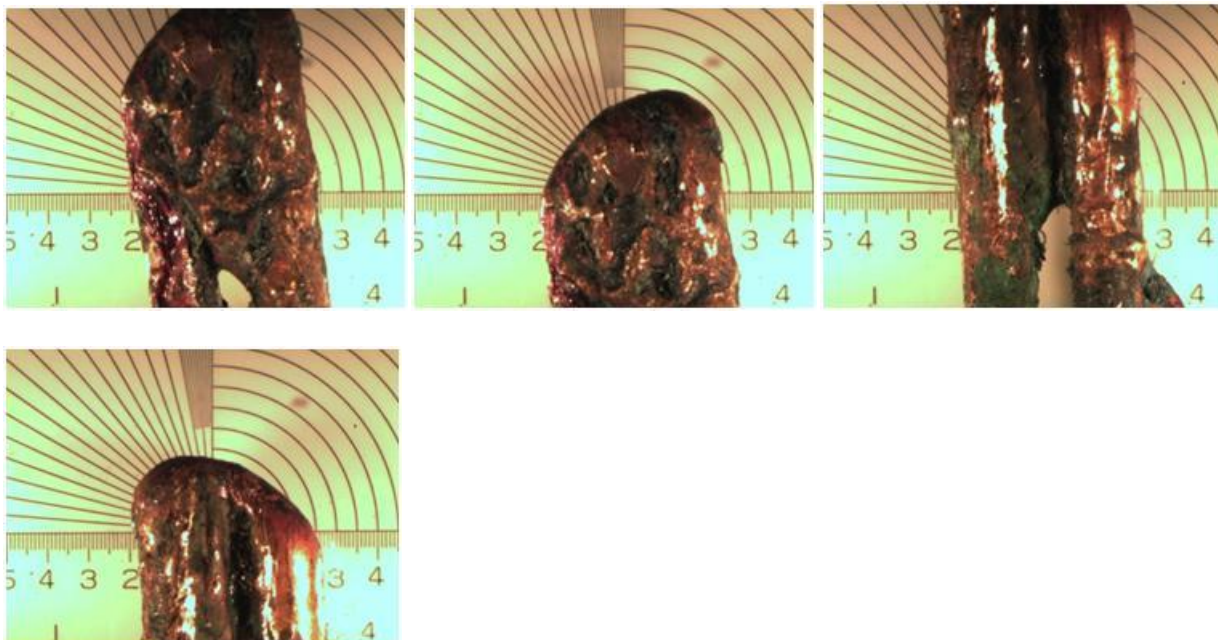


Figure A33: Compartment Tests, ROMEX 14-2, Non Energized (Test No. 16)

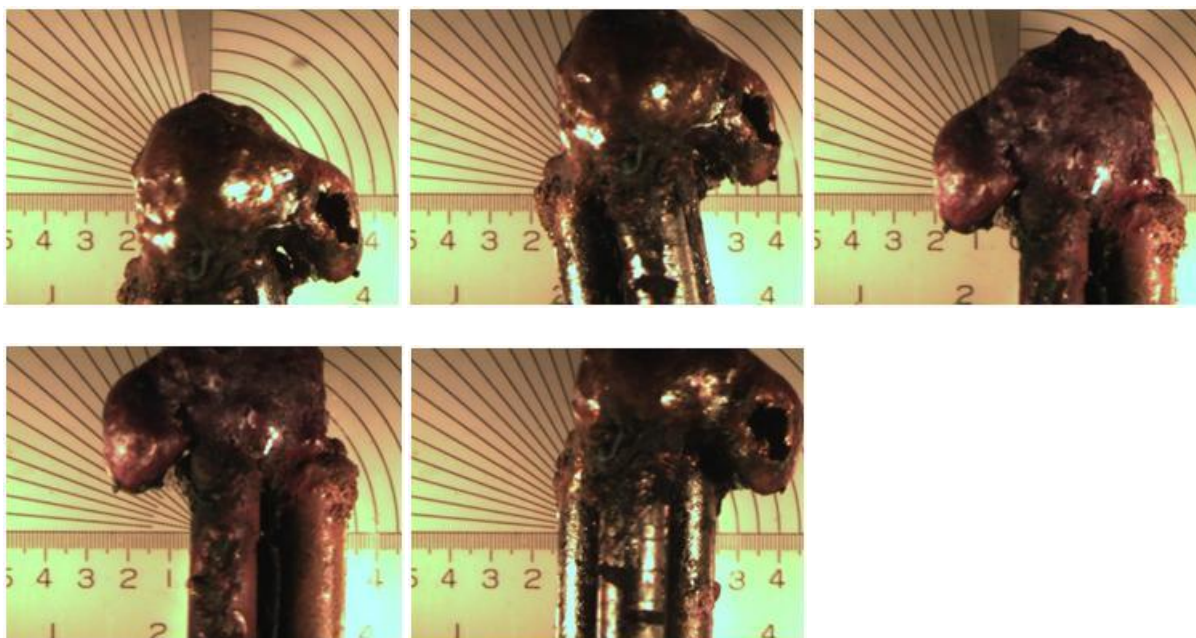


Figure A34: Compartment Tests, ROMEX 14-2, Energized (Test No. 17)

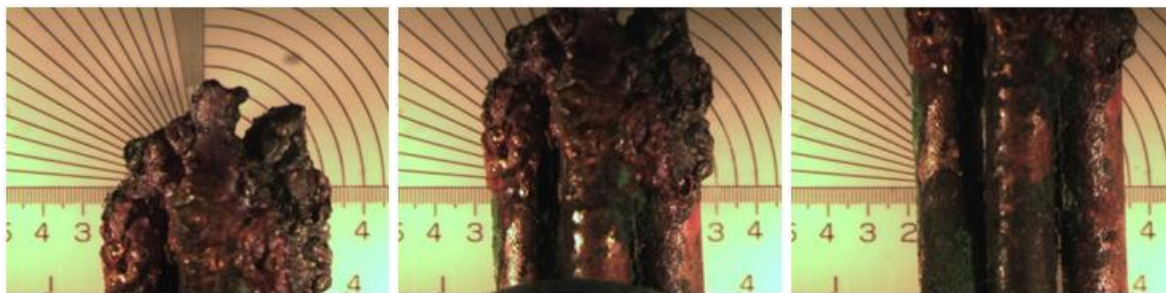
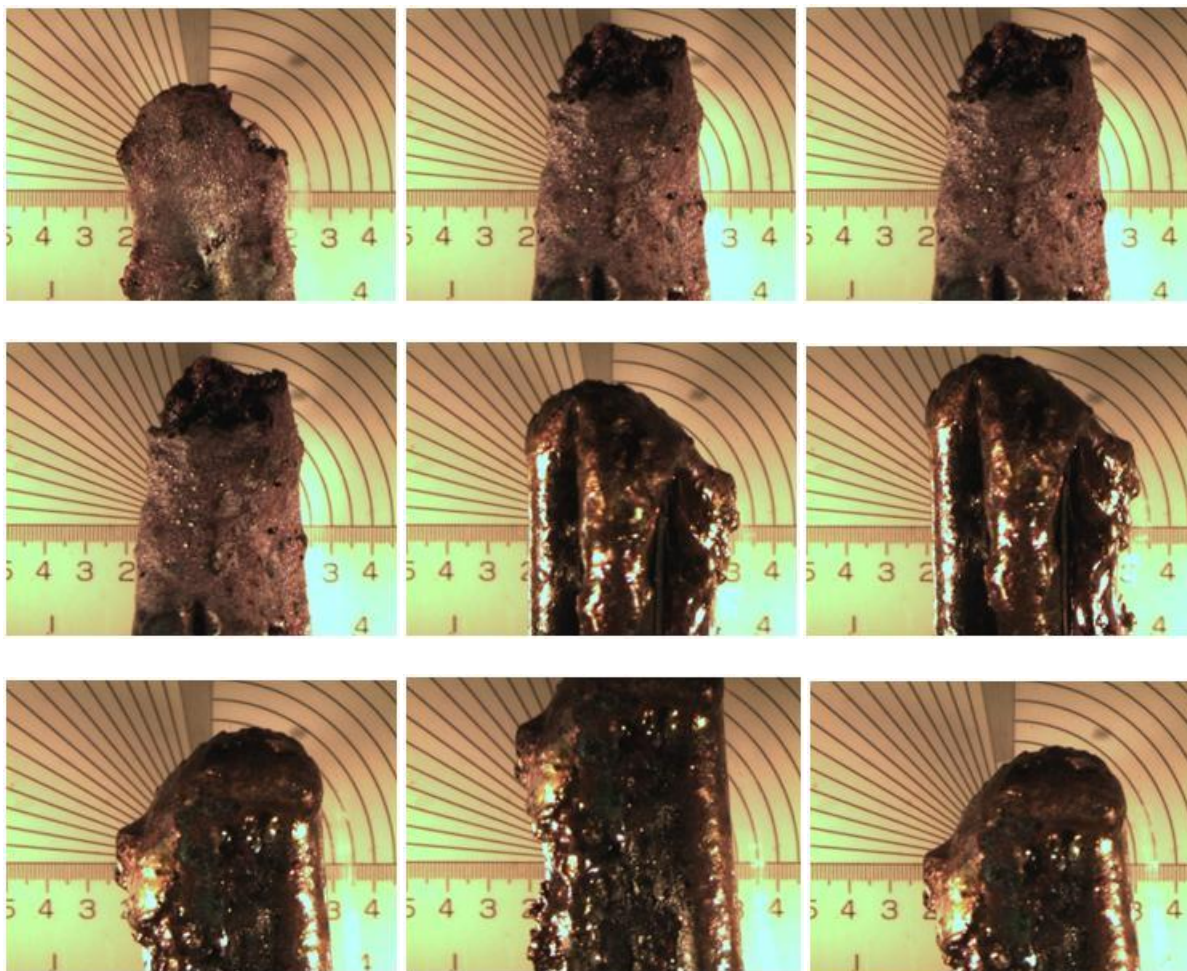


Figure A35: Compartment Tests, ROMEX 14-2, Energized (Test No. 18)



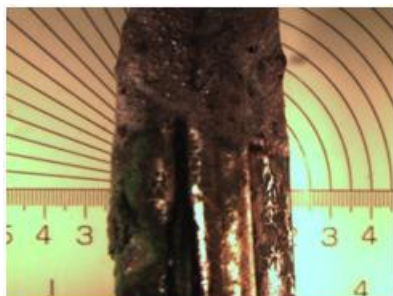


Figure A36: Compartment Tests, ROMEX 14-2, Loaded (Test No. 18)

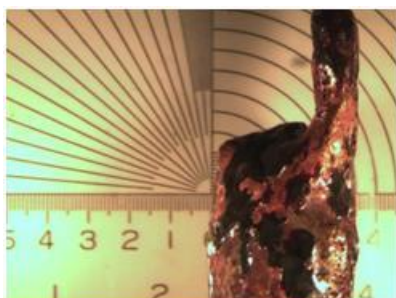
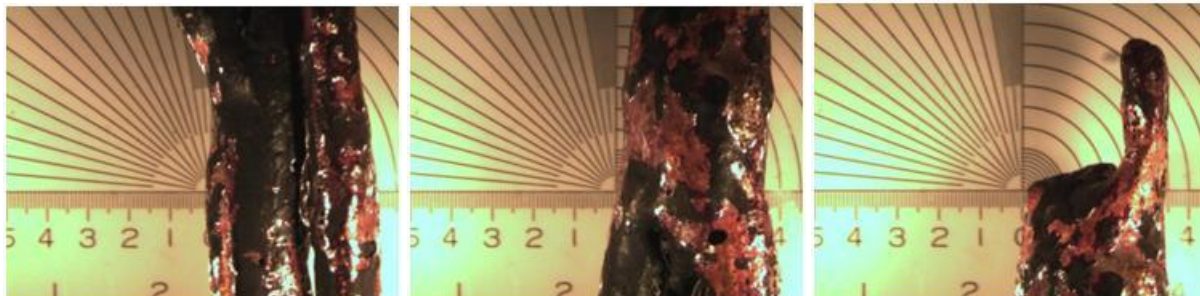


Figure A37: Compartment Tests, ROMEX 14-2, Energized (Test No. 19)



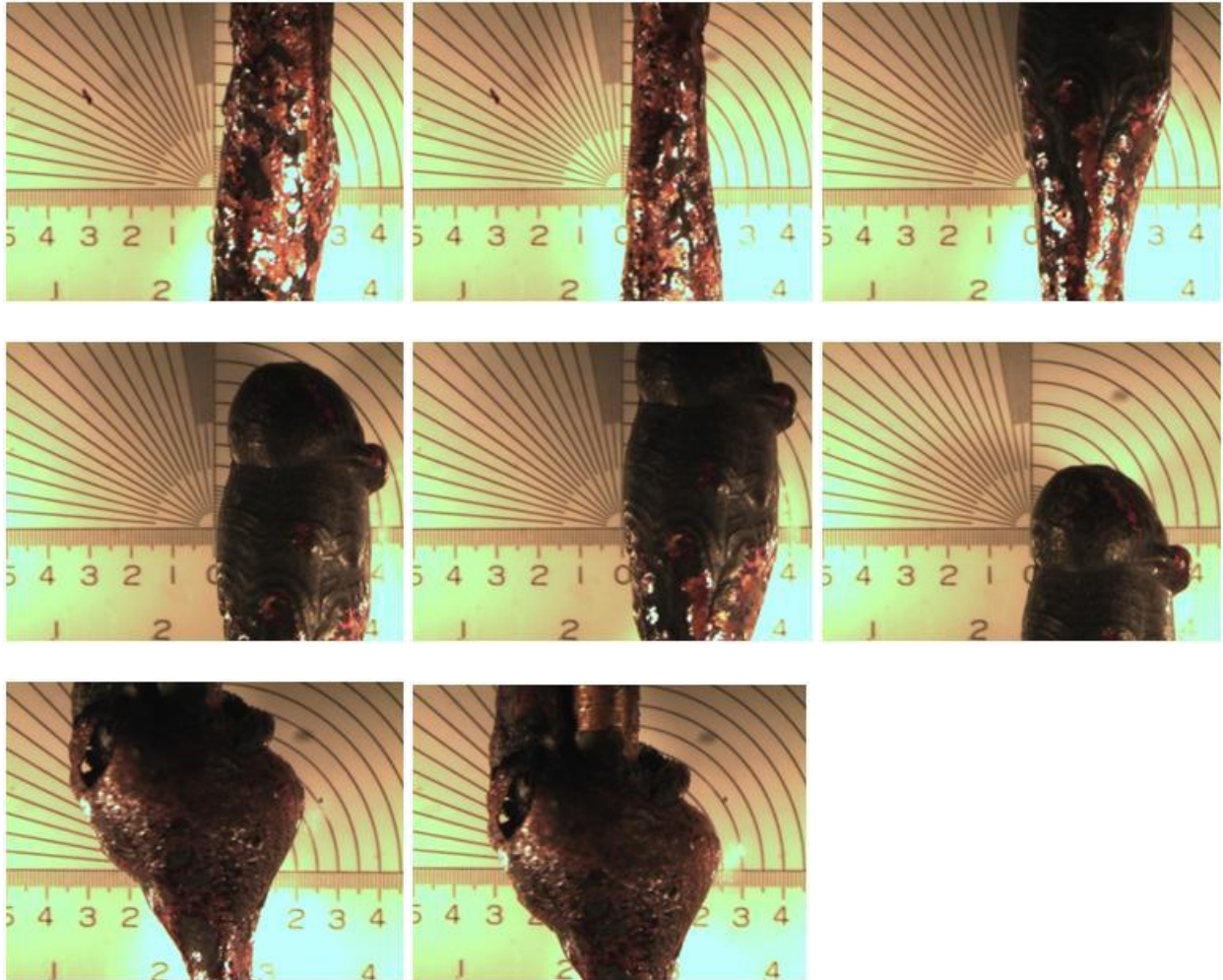


Figure A38: Compartment Tests, ROMEX 14-2, Loaded (Test No. 19)

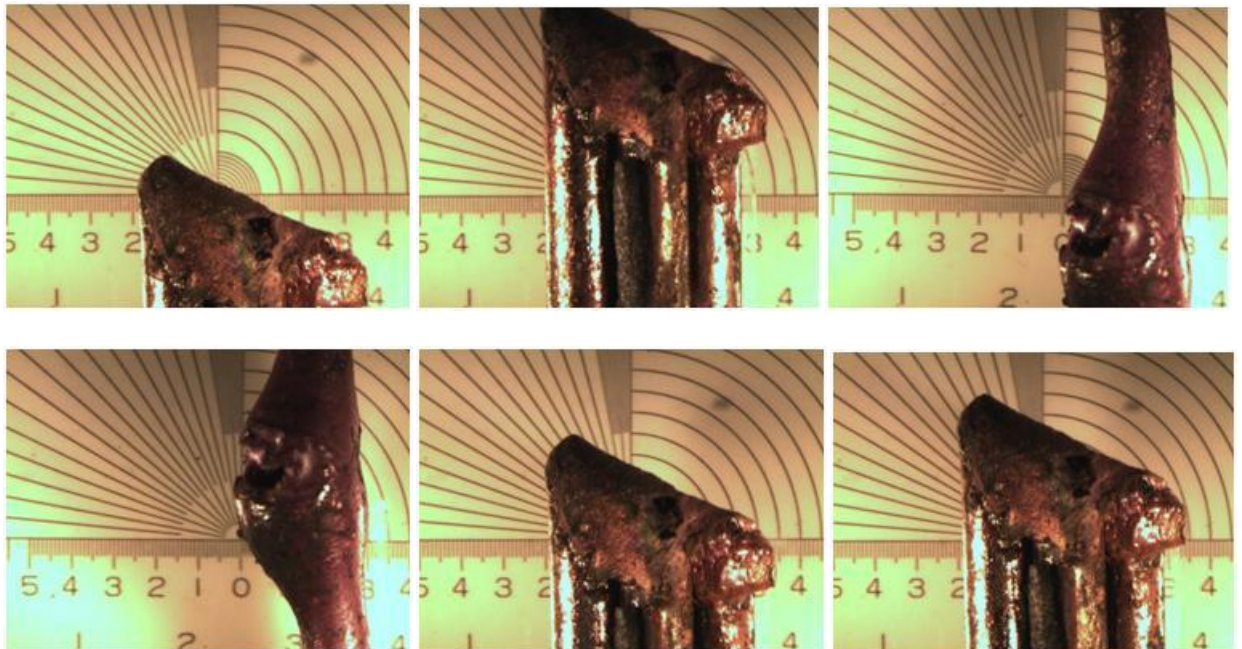


Figure A39: Compartment Tests, ROMEX 14-2, Non Energized (Test No. 19)

DIRECT FLAME TEST; 12-2 ROMEX WIRE

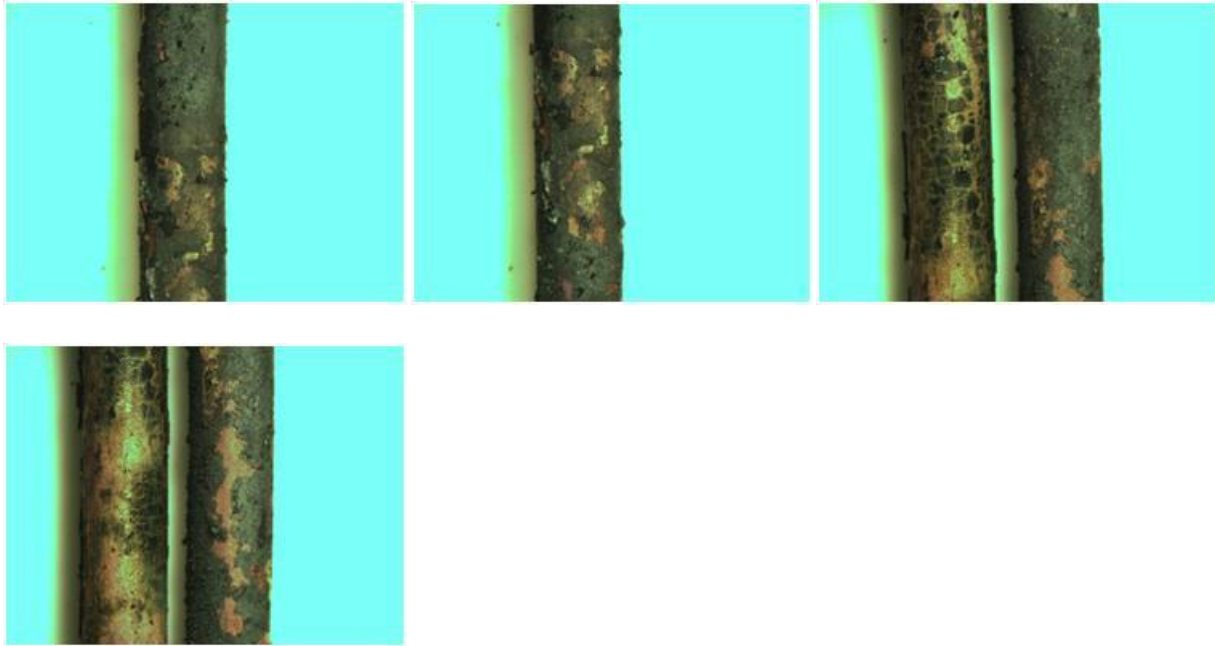


Figure A40: Direct Flame, ROMEX 12-2, Non Energized (Test No. 1)

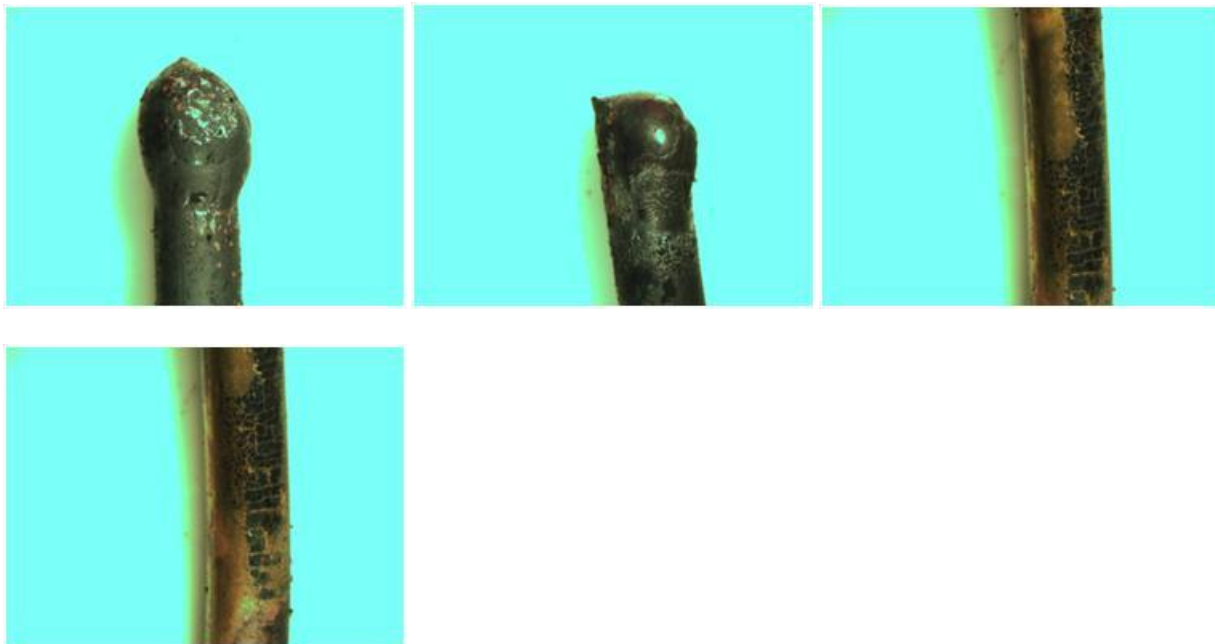


Figure A41: Direct Flame, ROMEX 12-2, Non Energized (Test No. 2)

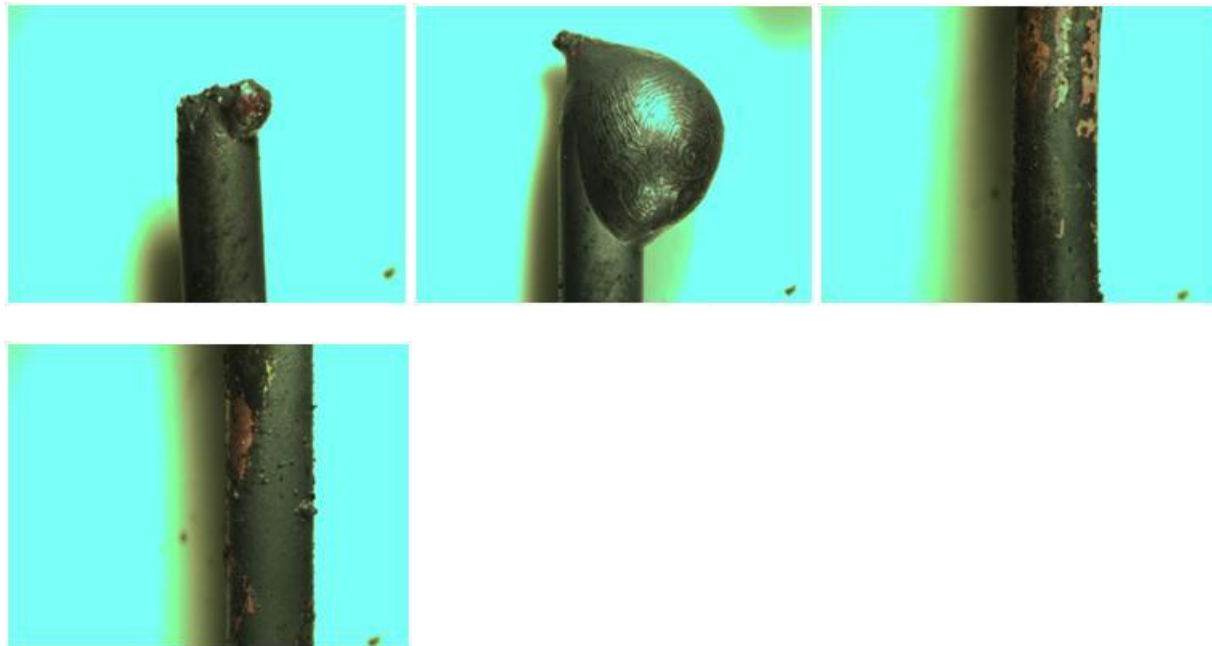


Figure A42: Direct Flame, ROMEX 12-2, Non Energized (Test No. 3)

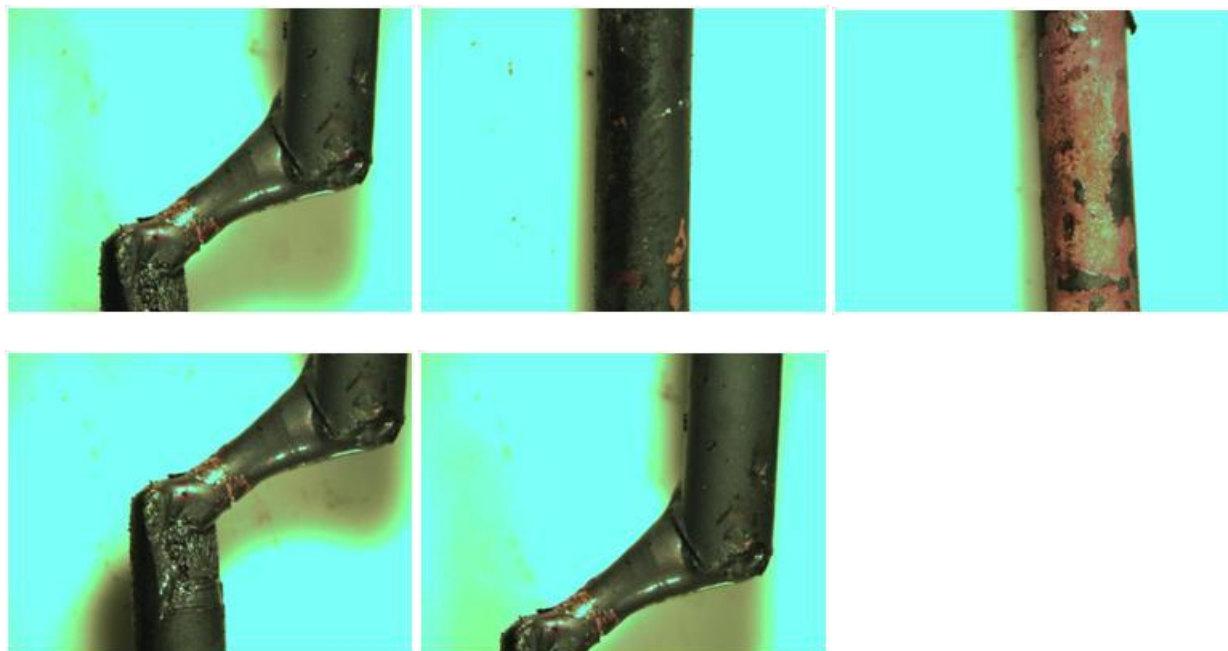


Figure A43: Direct Flame, ROMEX 12-2, Non Energized (Test No. 4)

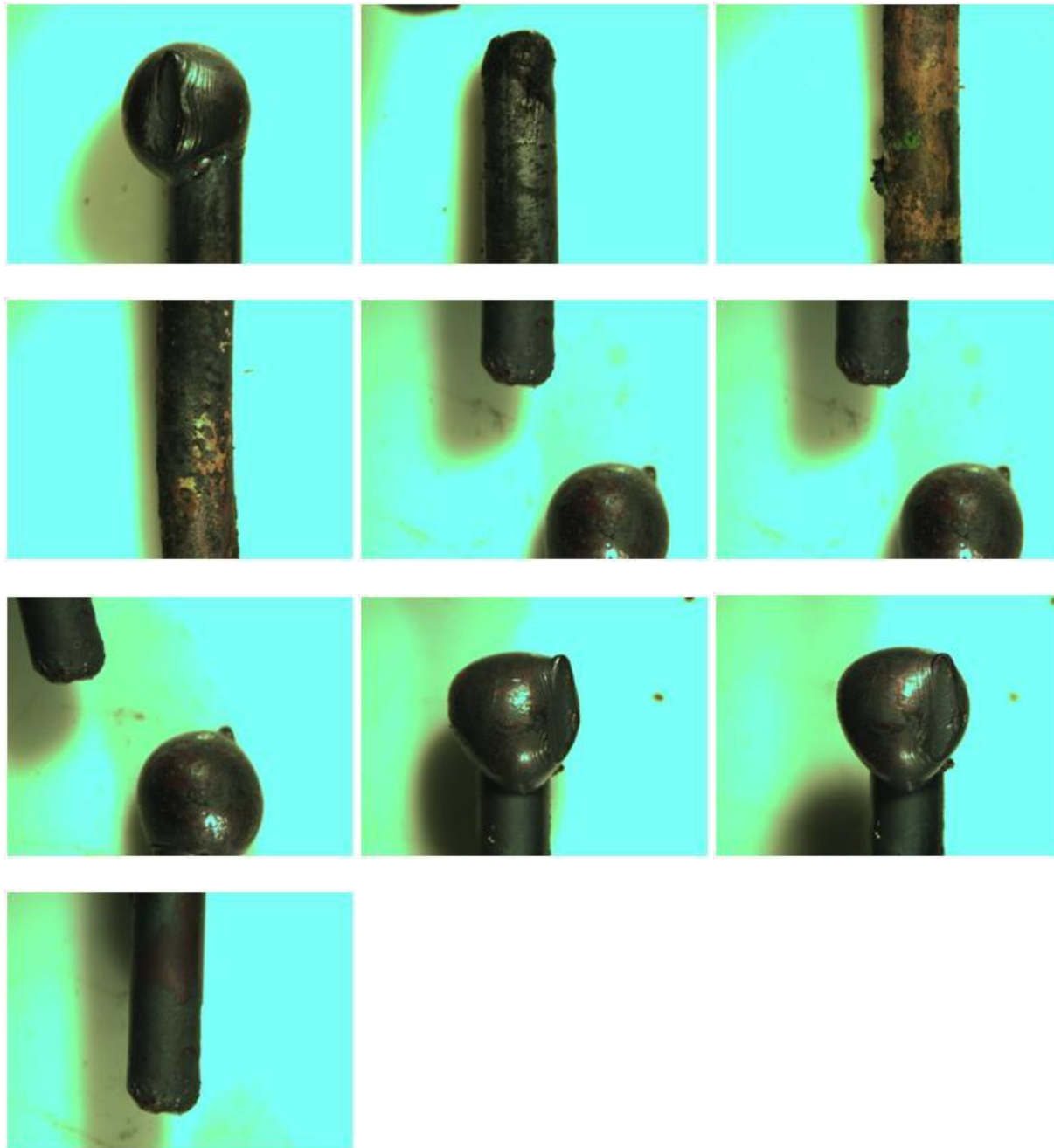


Figure A44: Direct Flame, ROMEX 12-2, Non Energized (Test No. 5)



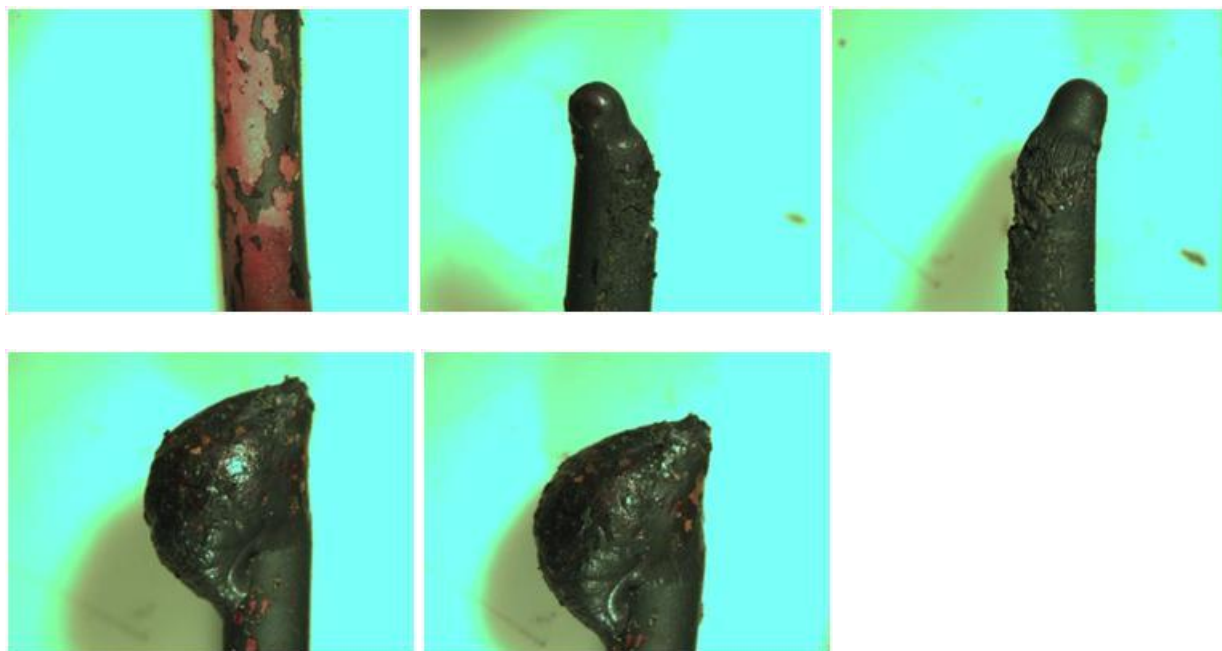
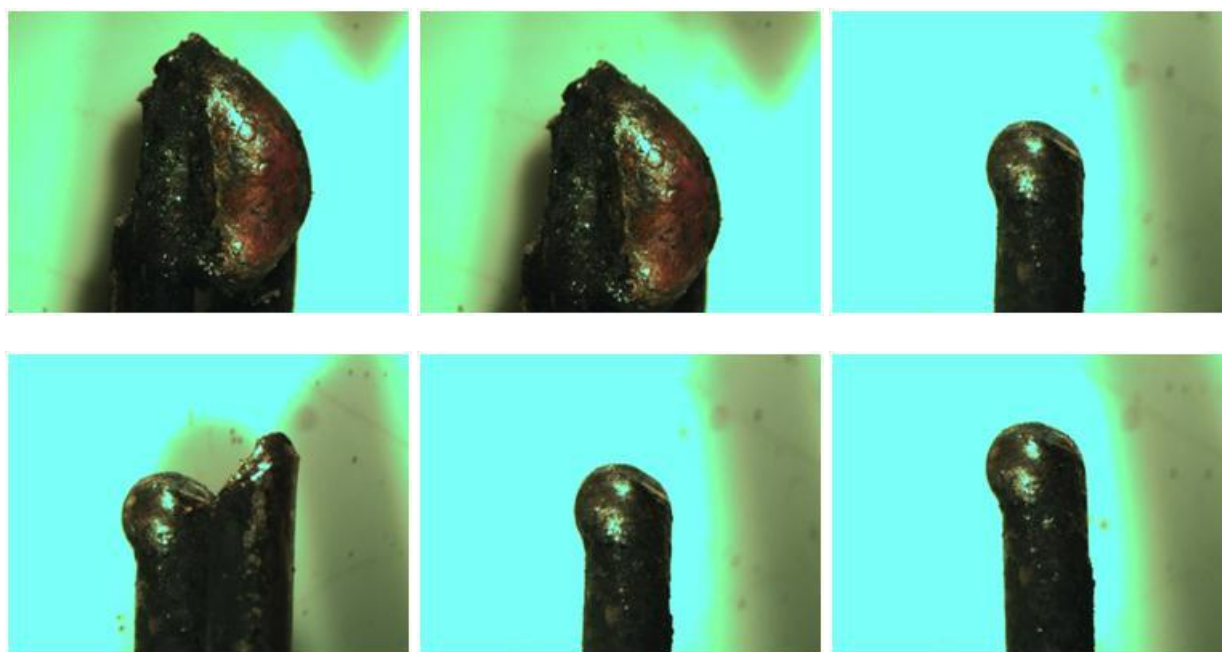


Figure A45: Direct Flame, ROMEX 12-2, Non Energized (Test No. 6)



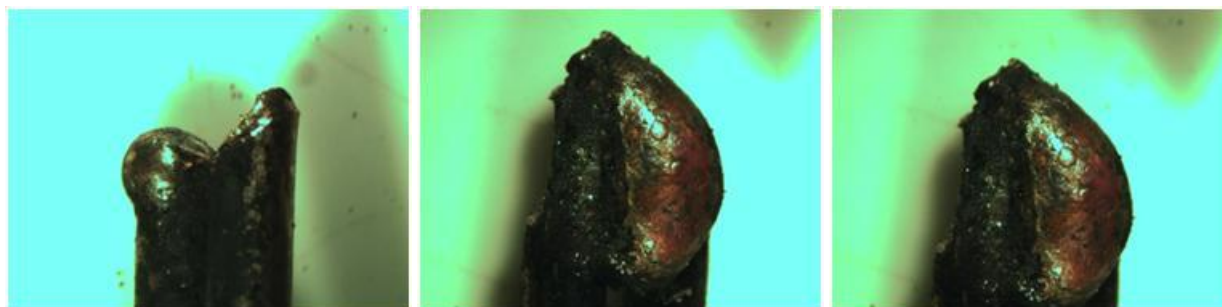


Figure A46: Direct Flame, ROMEX 12-2, Energized (Test No. 7)

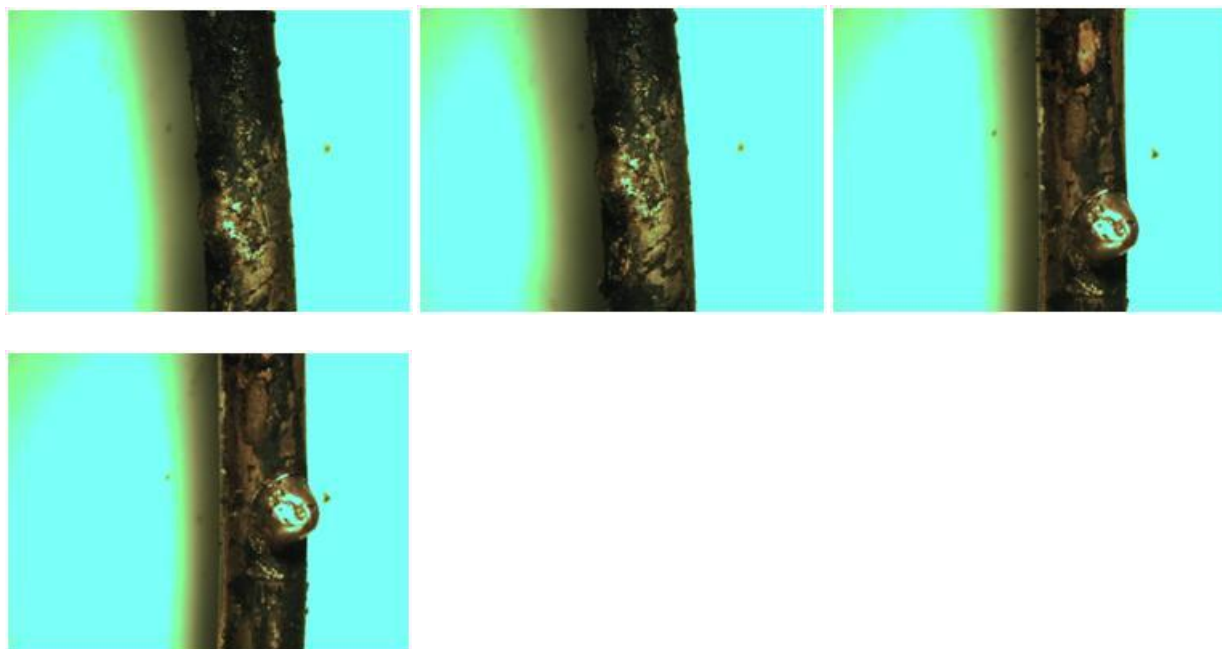
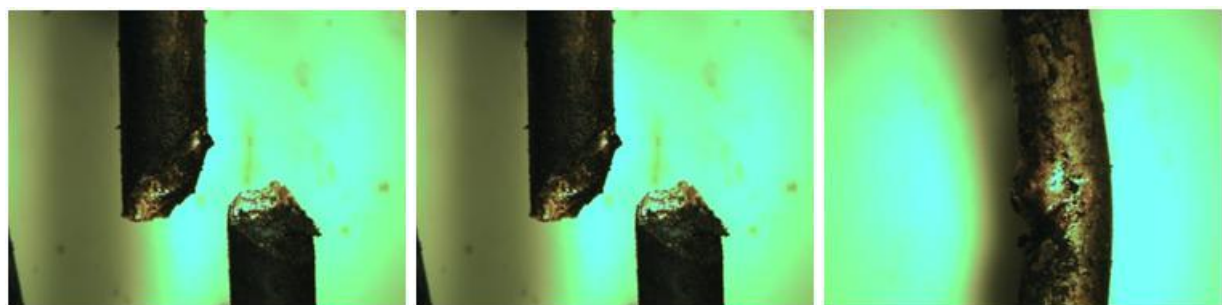


Figure A47: Direct Flame, ROMEX 12-2, Energized (Test No. 8)



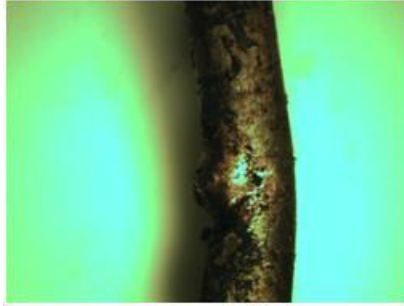


Figure A48: Direct Flame, ROMEX 12-2, Energized (Test No. 9)

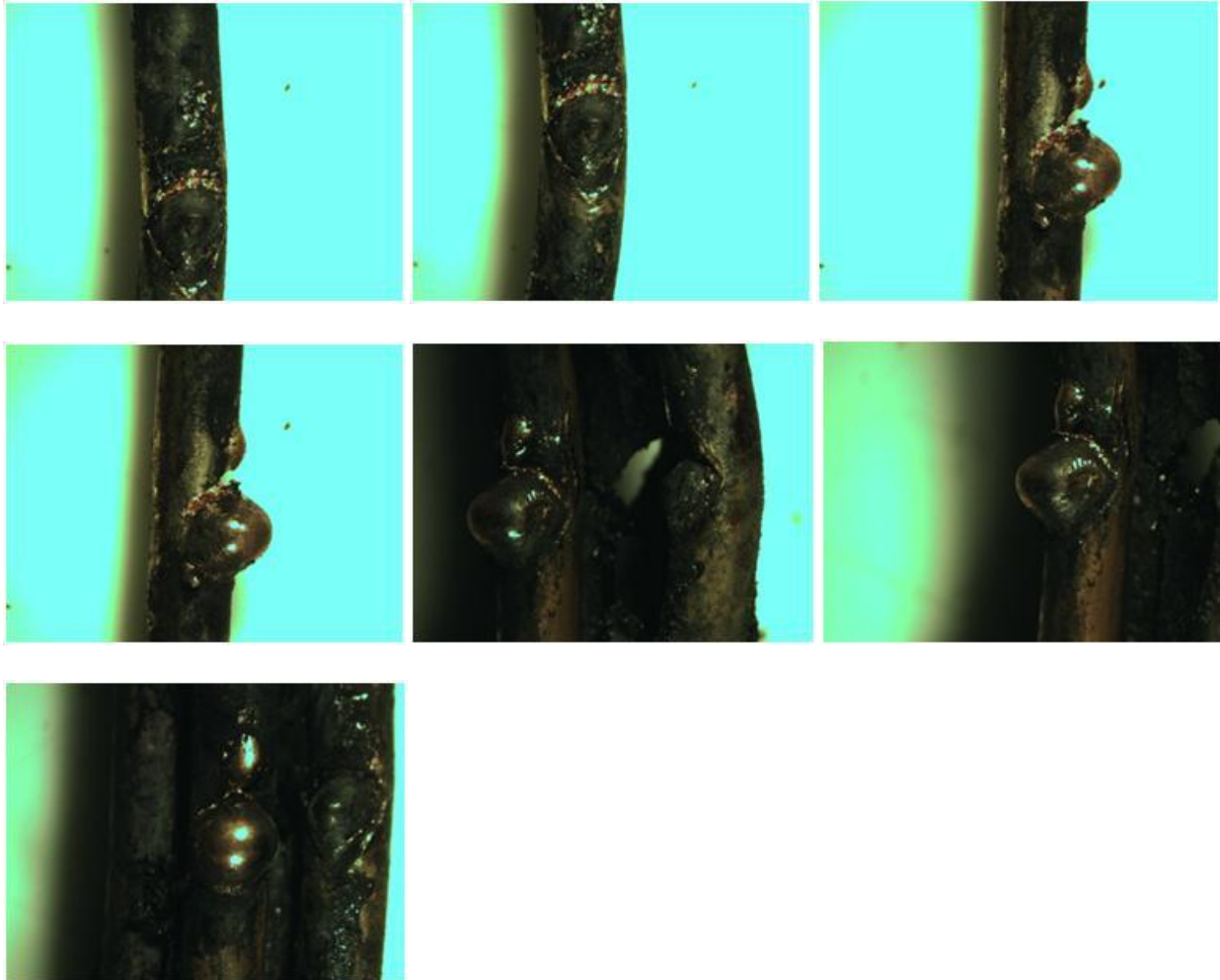
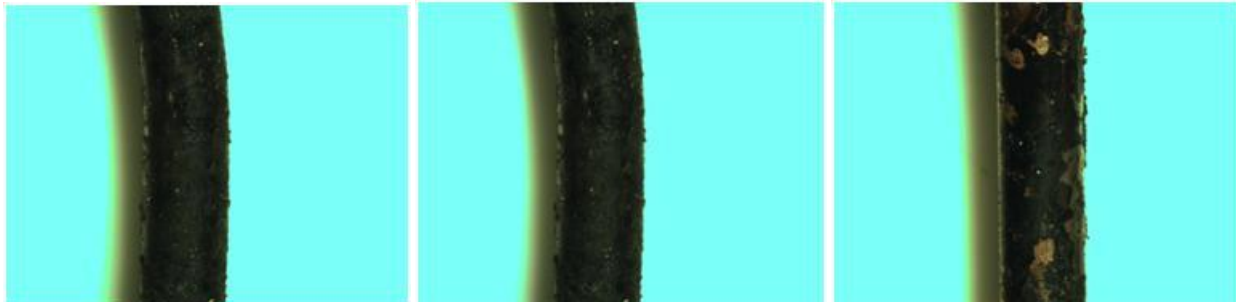


Figure A49: Direct Flame, ROMEX 12-2, Energized (Test No. 10)



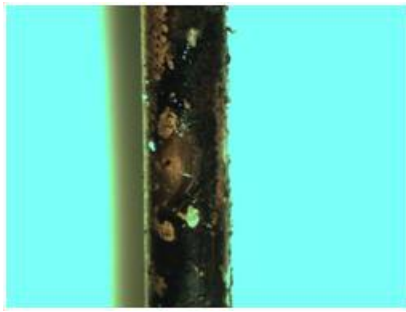


Figure A50: Direct Flame, ROMEX 12-2, Energized (Test No. 11)

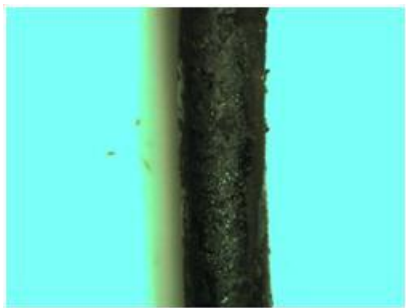
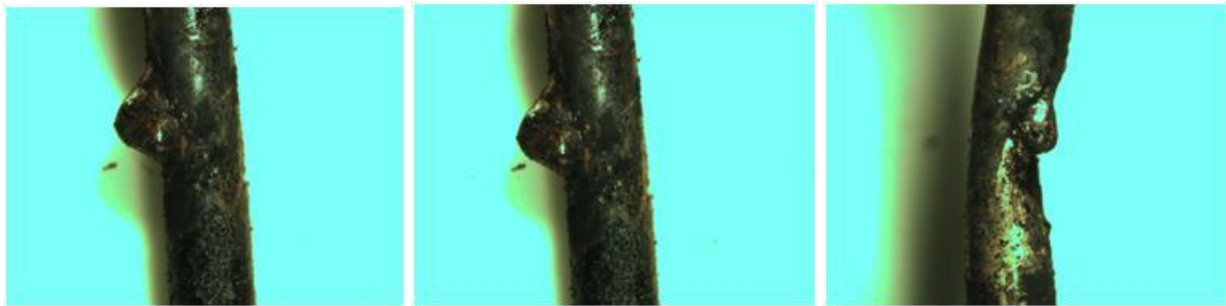


Figure A51: Direct Flame, ROMEX 12-2, Energized (Test No. 12)

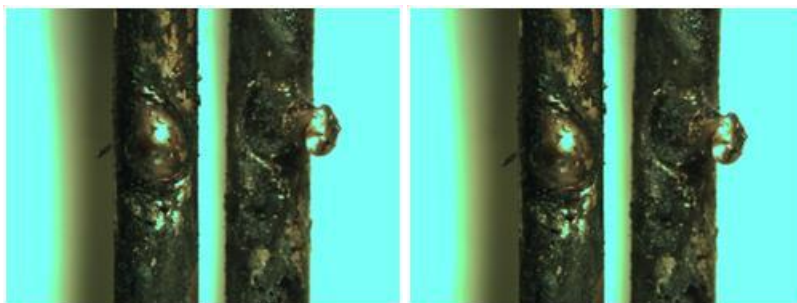


Figure A52: Direct Flame, ROMEX 12-2, Loaded (Test No. 13)

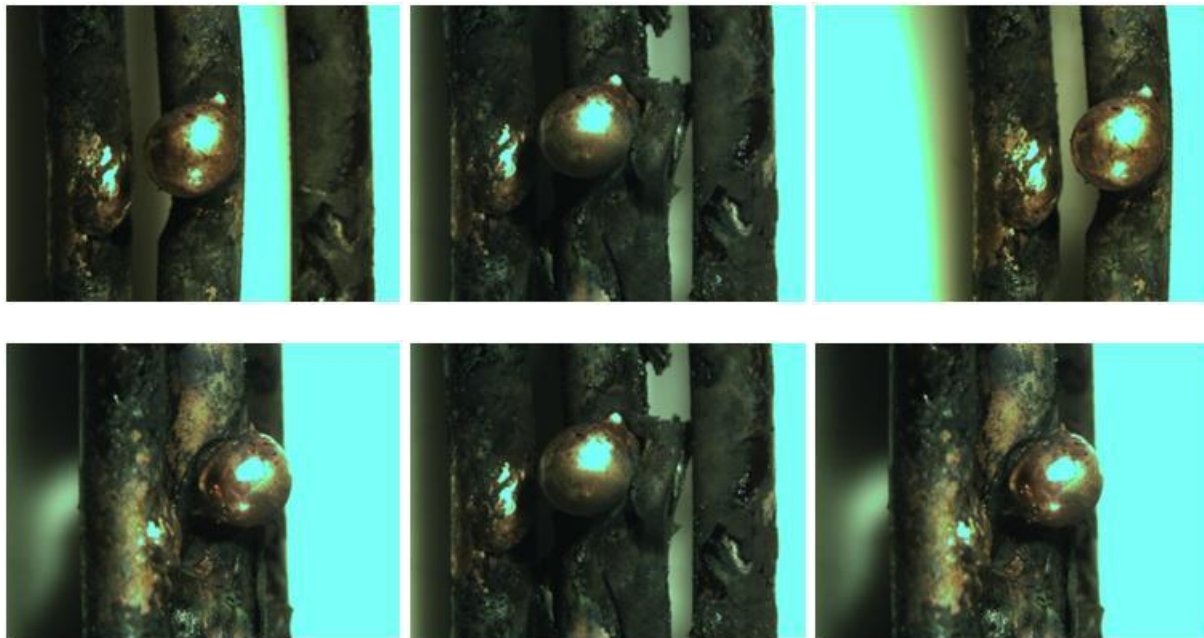


Figure A53: Direct Flame, ROMEX 12-2, Loaded (Test No. 14)

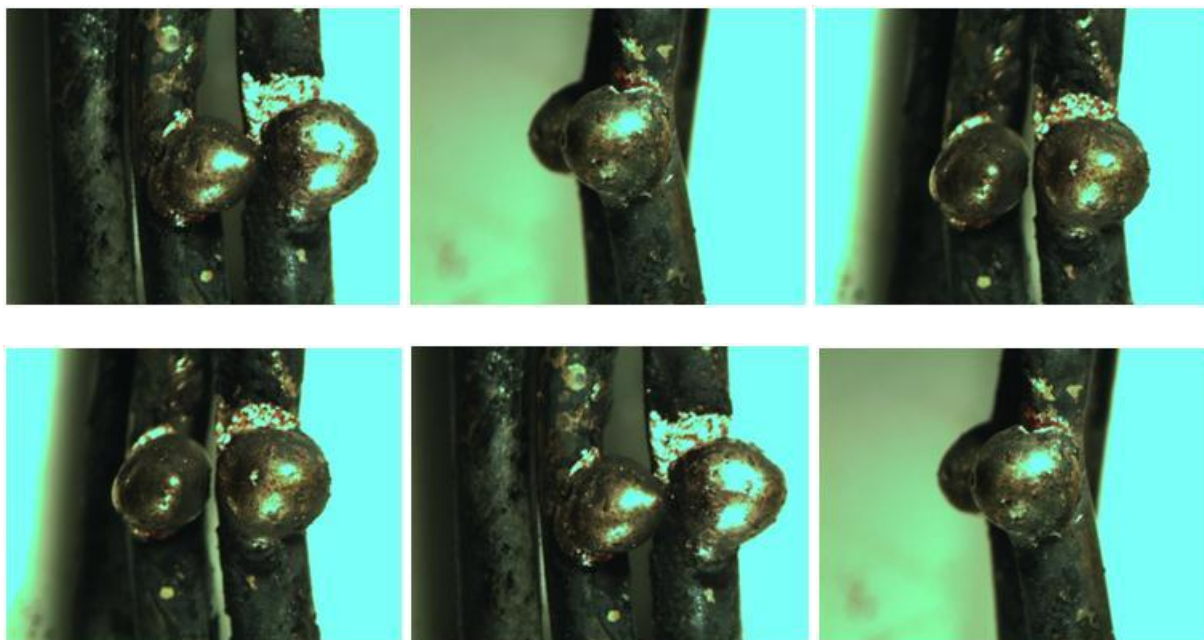


Figure A54: Direct Flame, ROMEX 12-2, Loaded (Test No. 15)

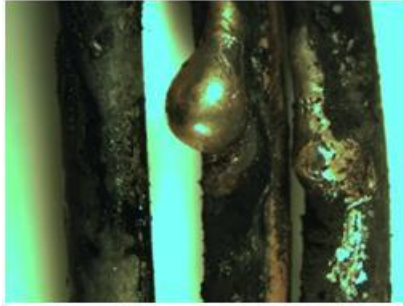


Figure A55: Direct Flame, ROMEX 12-2, Loaded (Test No. 16)

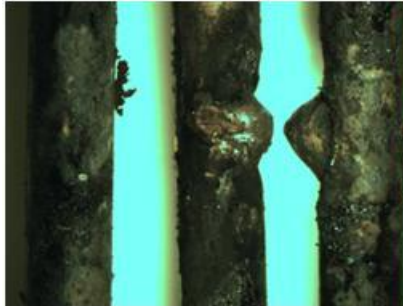


Figure A56: Direct Flame, ROMEX 12-2, Loaded (Test No. 17)

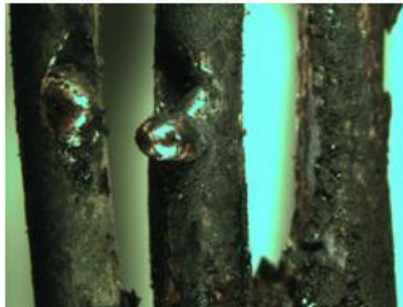


Figure A57: Direct Flame, ROMEX 12-2, Loaded (Test No. 18)

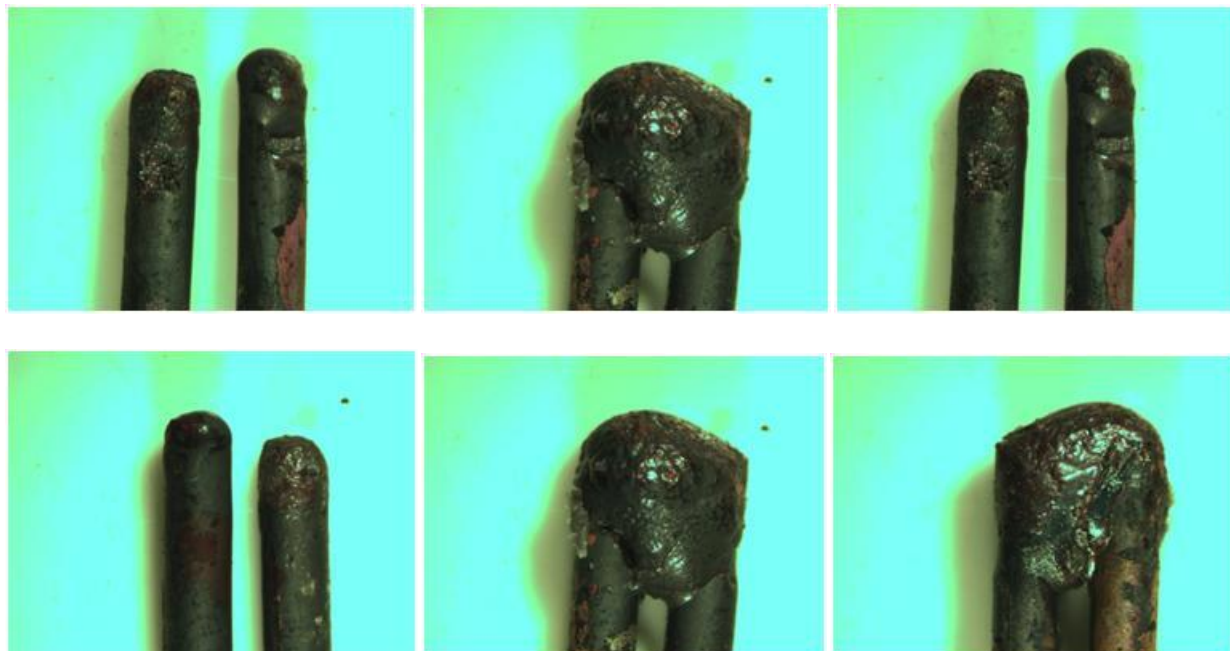
DIRECT FLAME TEST; 14-2 ROMEX WIRE



Figure A58: Direct Flame, ROMEX 14-2, Non Energized (Test No. 56)



Figure A59: Direct Flame, ROMEX 14-2, Non Energized (Test No. 57)



FigureA60: Direct Flame, ROMEX 14-2, Non Energized (Test No. 58)

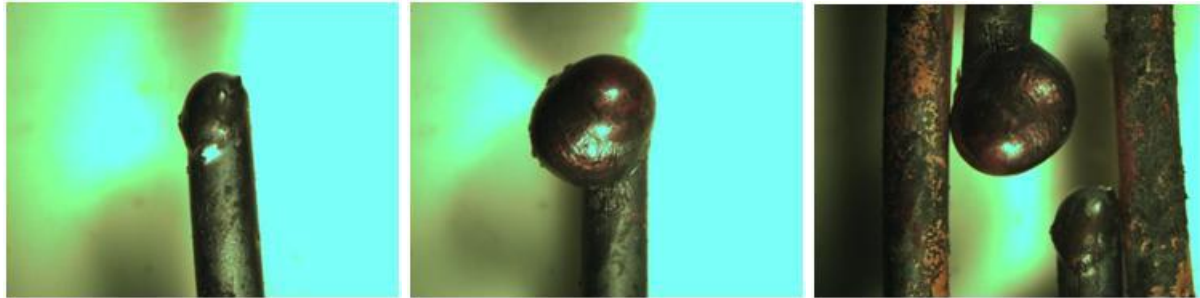


Figure A61: Direct Flame, ROMEX 14-2, Non Energized (Test No. 59)

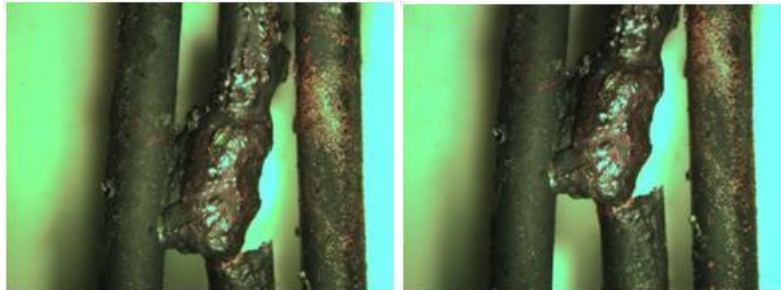


Figure A62: Direct Flame, ROMEX 14-2, Non Energized (Test No. 60)

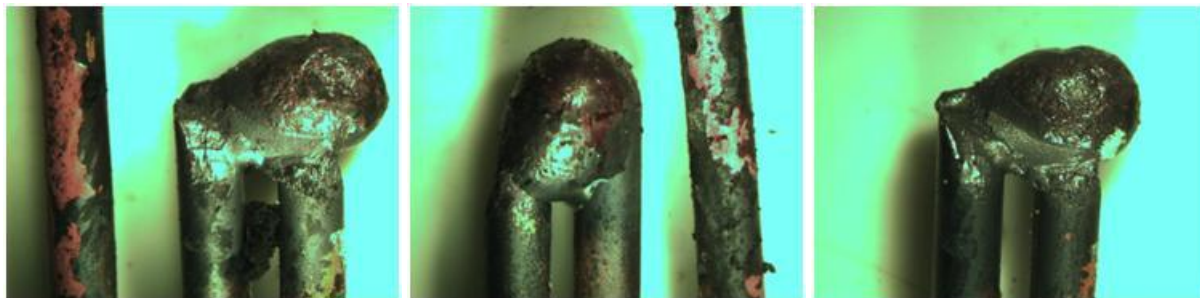


Figure A63: Direct Flame, ROMEX 14-2, Energized (Test No. 61)

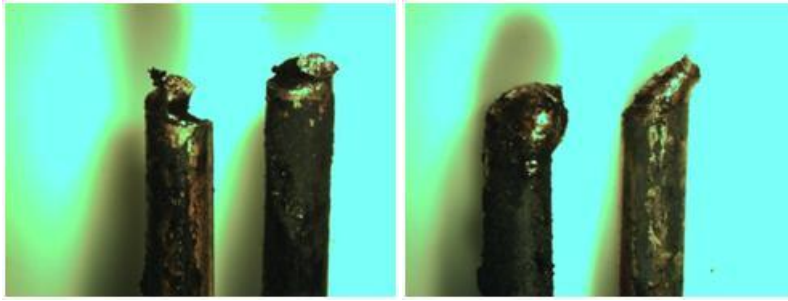


Figure A64: Direct Flame, ROMEX 14-2, Energized (Test No. 64)

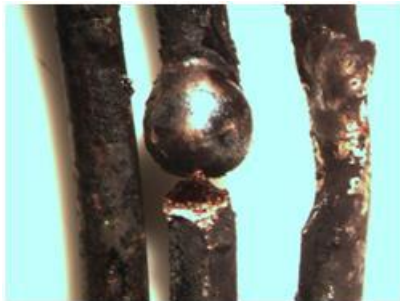


Figure A65: Direct Flame, ROMEX 14-2, Energized (Test No. 65)



Figure A66: Direct Flame, ROMEX 14-2, Energized (Test No. 66)

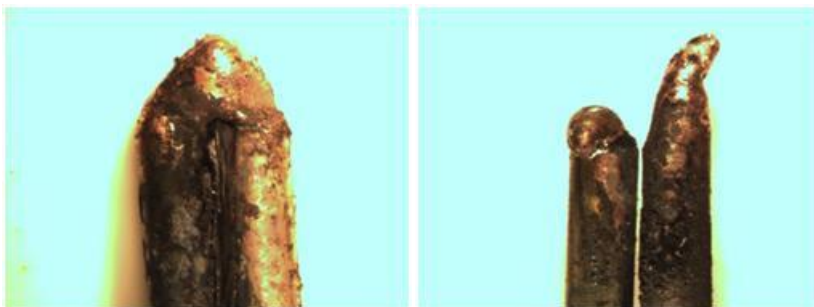


Figure A67: Direct Flame, ROMEX 14-2, Loaded (Test No. 67)

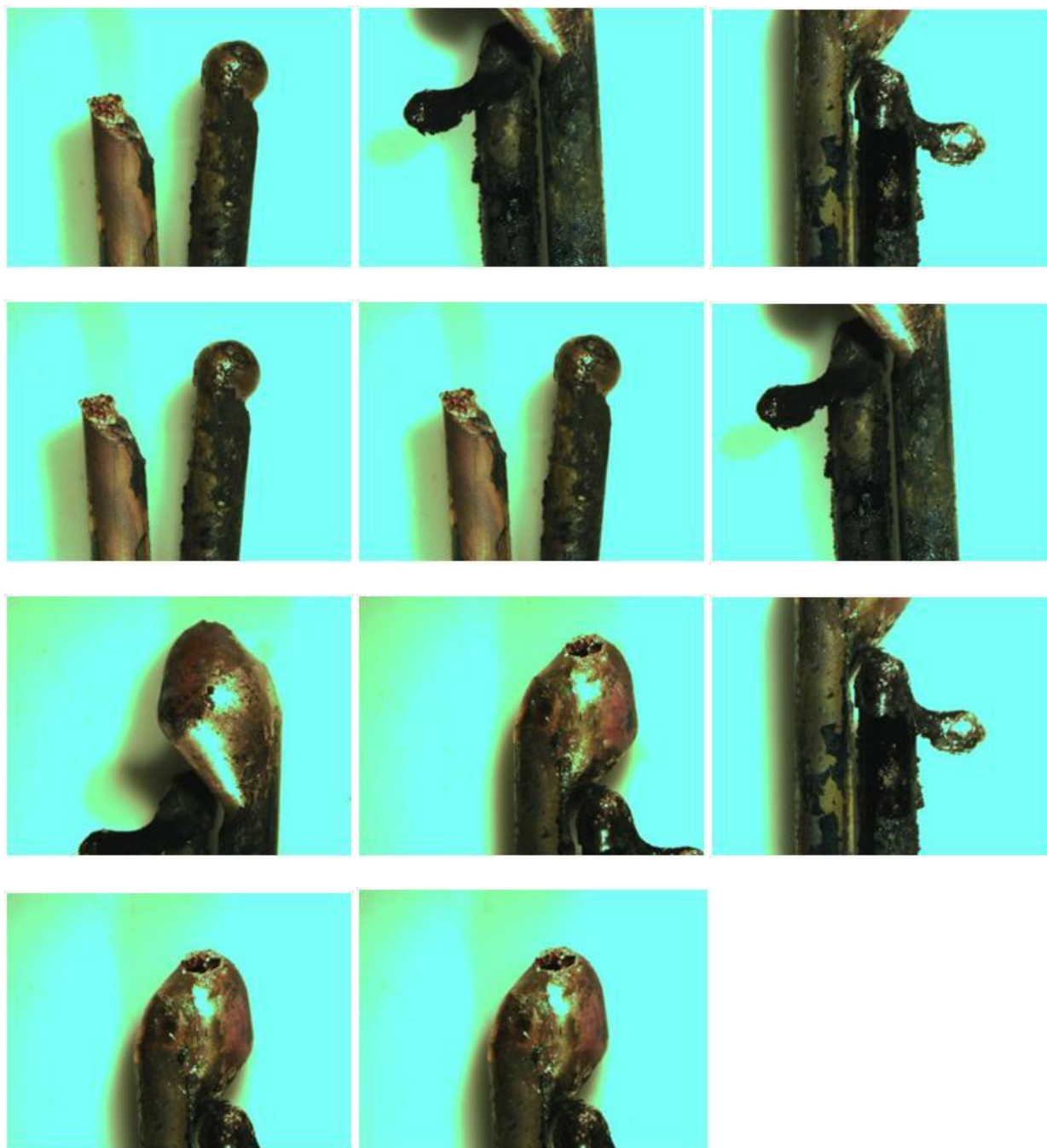


Figure A68: Direct Flame, ROMEX 14-2, Loaded (Test No. 68)

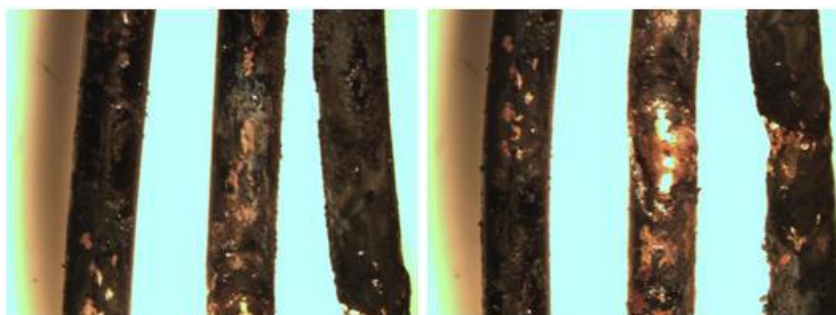


Figure A69: Direct Flame, ROMEX 14-2, Loaded (Test No. 69)

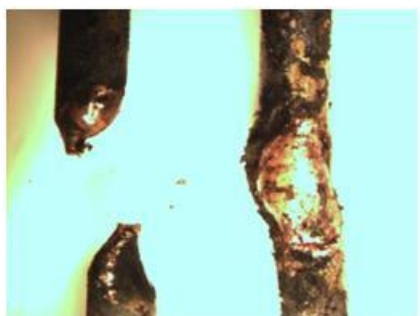


Figure A70: Direct Flame, ROMEX 14-2, Loaded (Test No. 70)

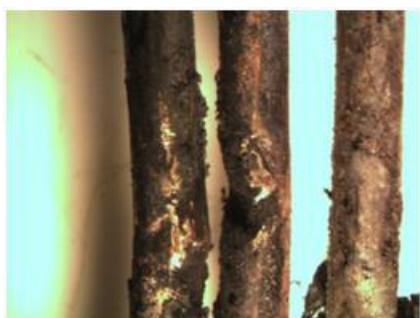


Figure A71: Direct Flame, ROMEX 14-2, Loaded (Test No. 71)





Figure A72: Direct Flame, ROMEX 14-2, Loaded (Test No. 72)

DIRECT FLAME TEST; 16-2 MULTISTRAND WIRE



Figure A73: Direct Flame, Multi-strand 16-2, Non Energized (Test No. 19)



Figure A74: Direct Flame, Multi-strand 16-2, Non Energized (Test No. 20)

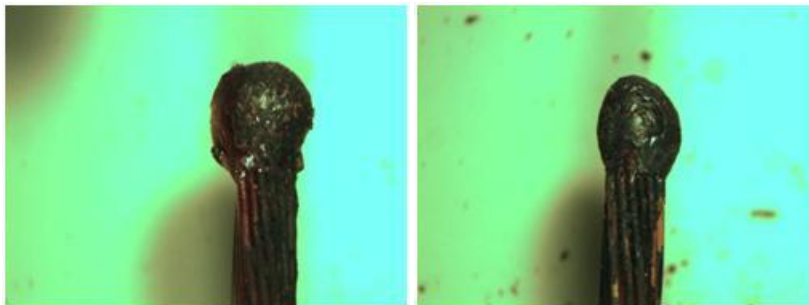
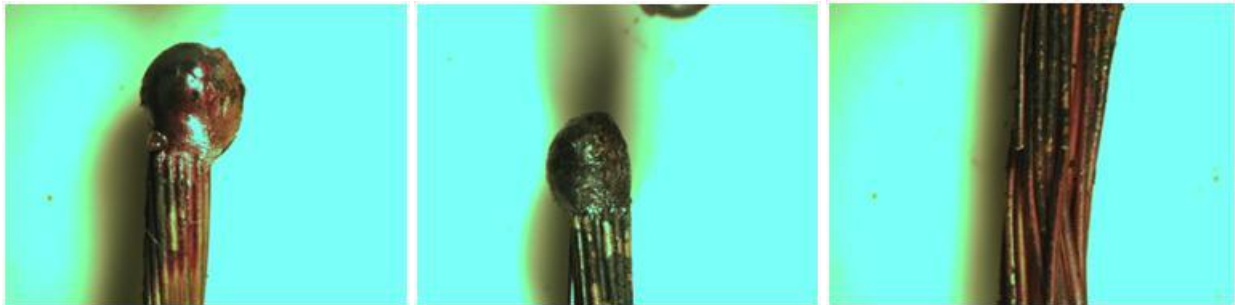


Figure A75: Direct Flame, Multi-strand 16-2, Non Energized (Test No. 21)

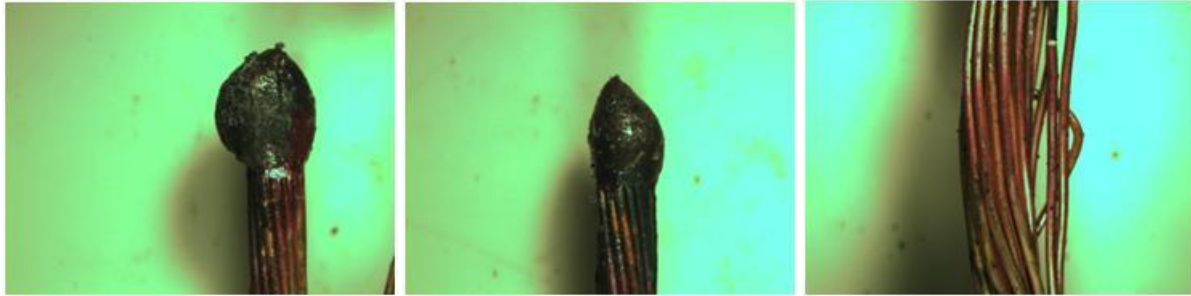


Figure A76: Direct Flame, Multi-strand 16-2, Non Energized (Test No. 22)



Figure A77: Direct Flame, Multi-strand 16-2, Non Energized (Test No. 23)



Figure A78: Direct Flame, Multi-strand 16-2, Non Energized (Test No. 24)

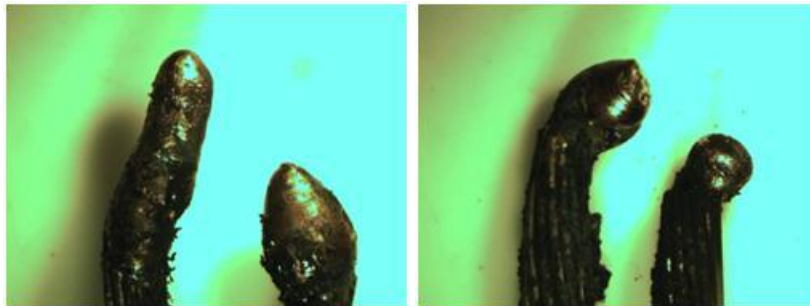


Figure A79: Direct Flame, Multi-strand 16-2, Energized (Test No. 25)





Figure A80: Direct Flame, Multi-strand 16-2, Energized (Test No. 26)

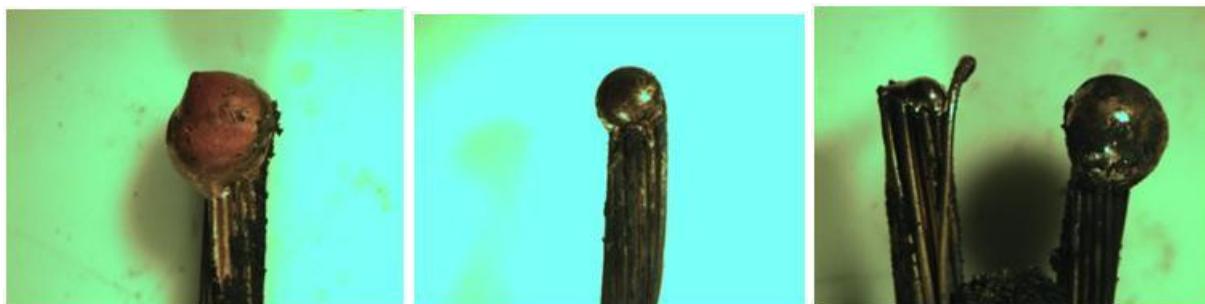


Figure A81: Direct Flame, Multi-strand 16-2, Energized (Test No. 27)

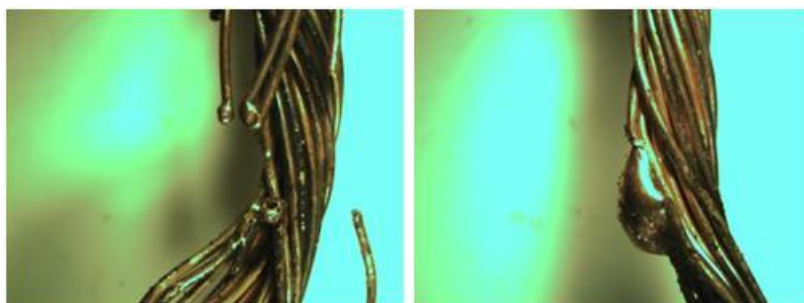


Figure A82: Direct Flame, Multi-strand 16-2, Energized (Test No. 29)



Figure A83: Direct Flame, Multi-strand 16-2, Energized (Test No. 30)

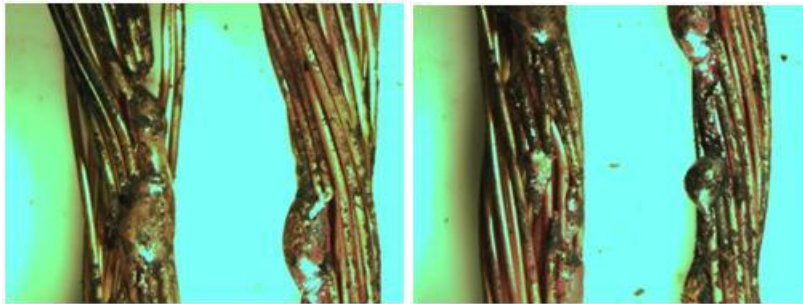


Figure A84: Direct Flame, Multi-strand 16-2, Loaded (Test No. 31)

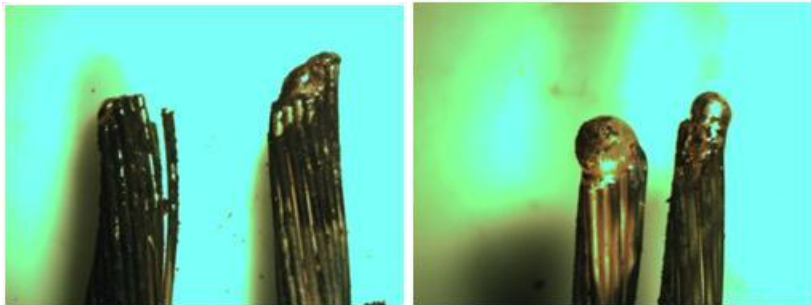


Figure A85: Direct Flame, Multi-strand 16-2, Loaded (Test No. 32)

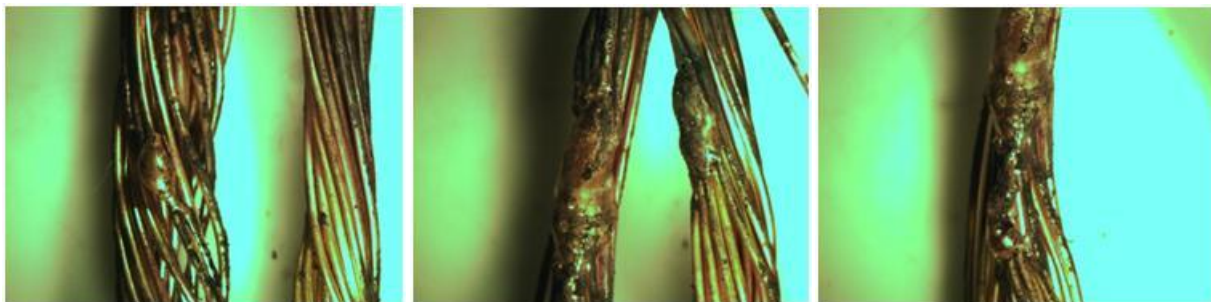


Figure A86: Direct Flame, Multi-strand 16-2, Loaded (Test No. 33)

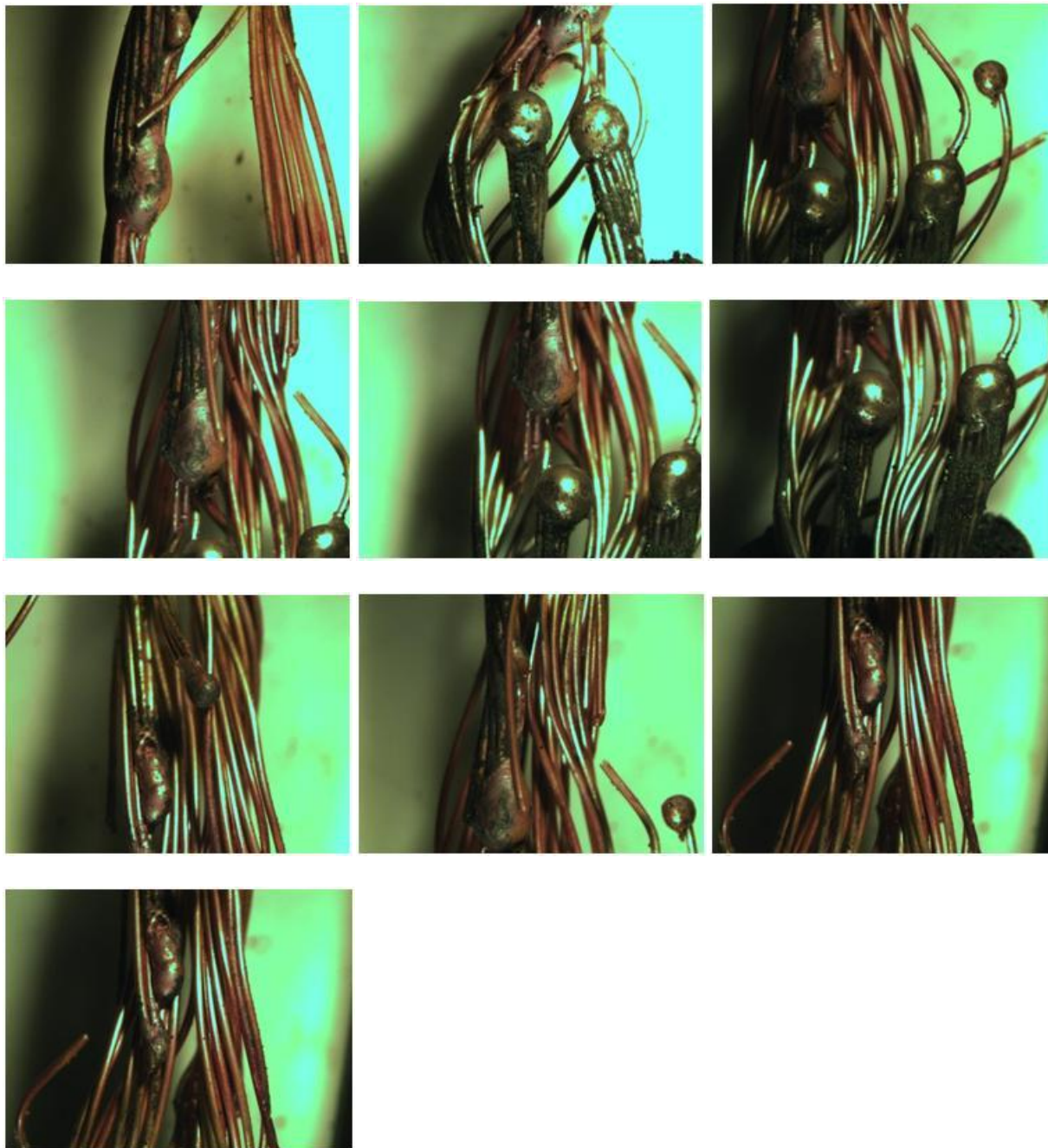


Figure A87: Direct Flame, Multi-strand 16-2, Loaded (Test No. 34)

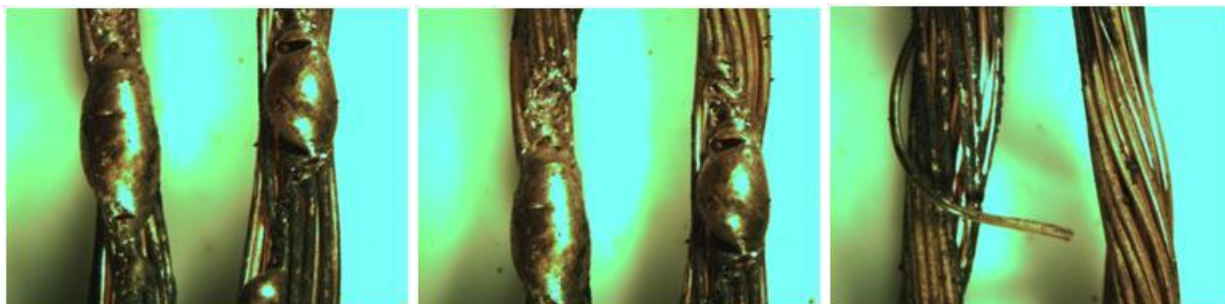


Figure A88: Direct Flame, Multi-strand 16-2, Loaded (Test No. 35)

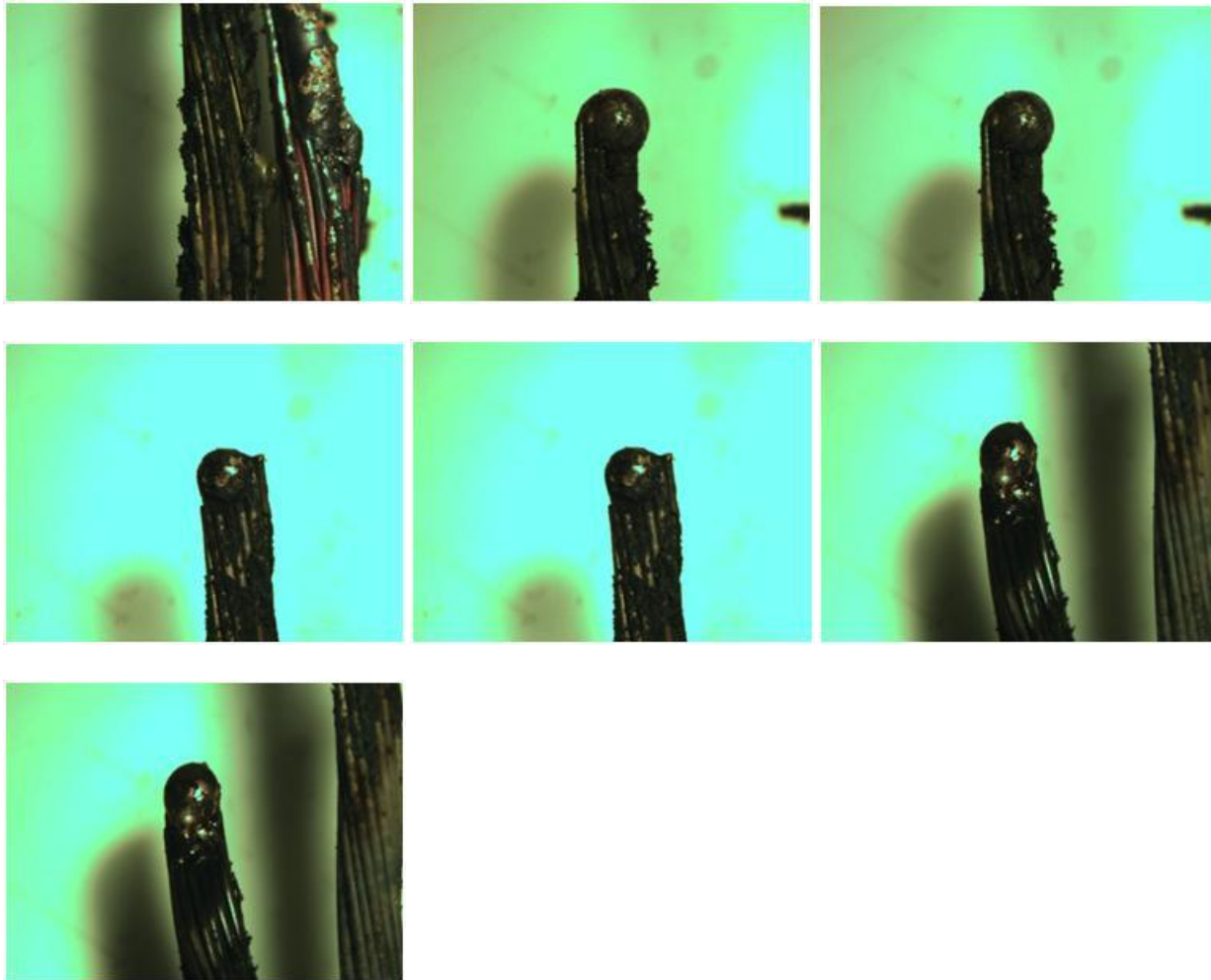


Figure A89: Direct Flame, Multi-strand 16-2, Loaded (Test No. 36)

DIRECT FLAME TEST; 18-2 MULTISTRAND WIRE



Figure A90: Direct Flame, Multi-strand 18-2, Non Energized (Test No. 37)

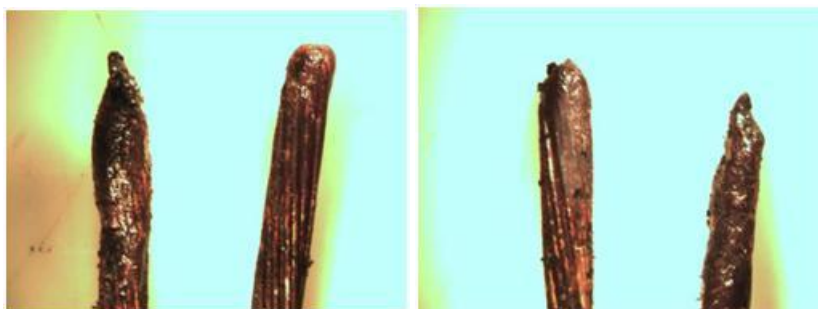


Figure A91: Direct Flame, Multi-strand 18-2, Non Energized (Test No. 38)

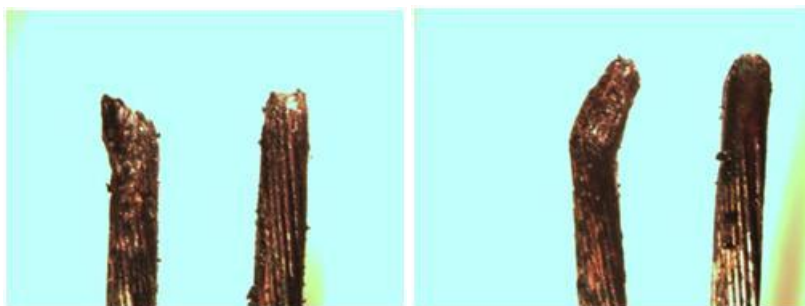
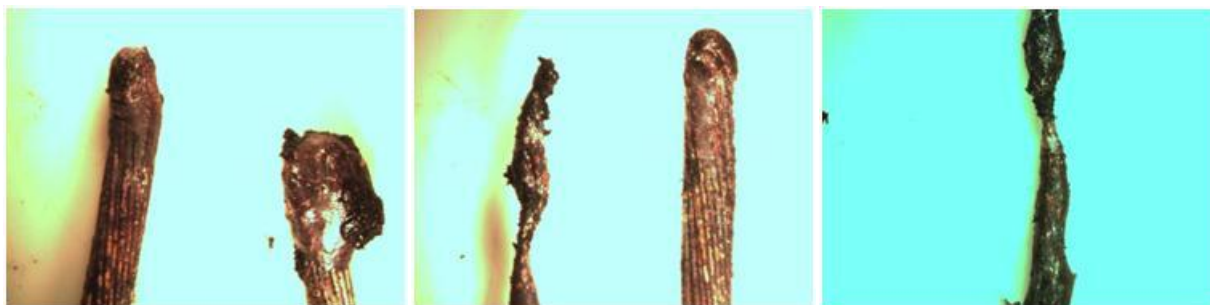


Figure A92: Direct Flame, Multi-strand 18-2, Non Energized (Test No. 39)



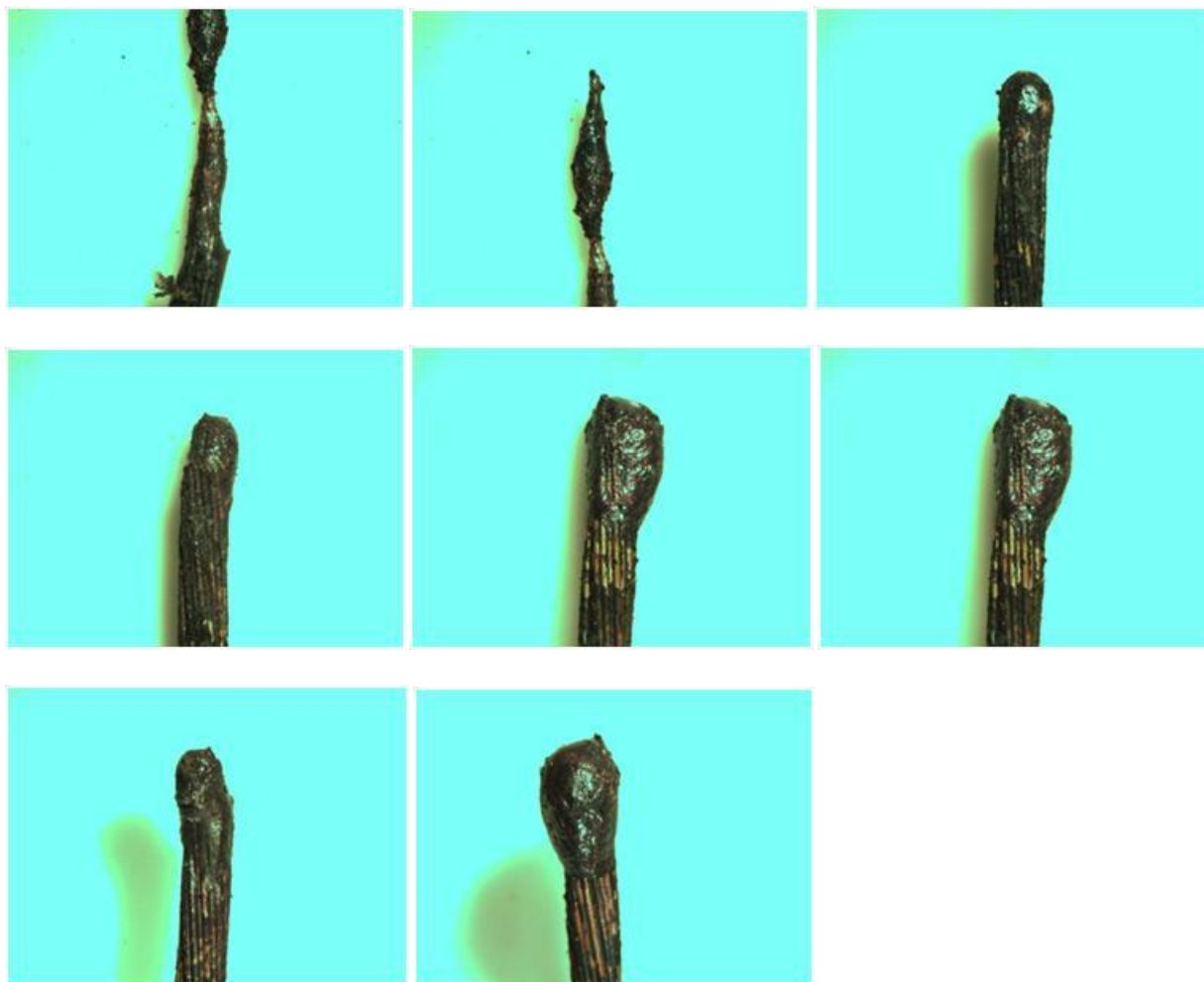


Figure A93: Direct Flame, Multi-strand 18-2, Non Energized (Test No. 40)

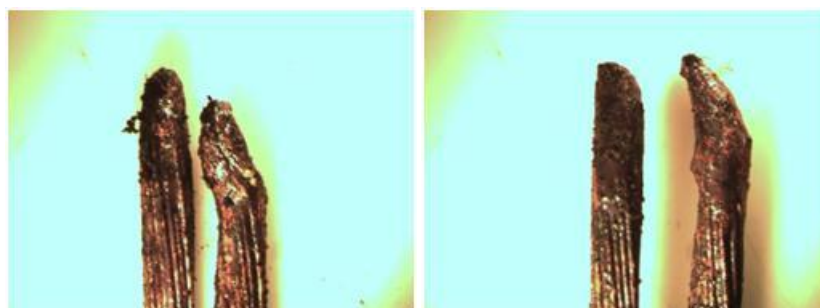


Figure A94: Direct Flame, Multi-strand 18-2, Non Energized (Test No. 41)

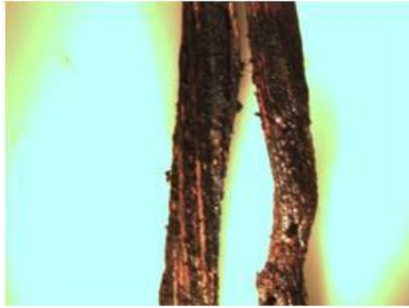


Figure A94: Direct Flame, Multi-strand 18-2, Non Energized (Test No. 42)

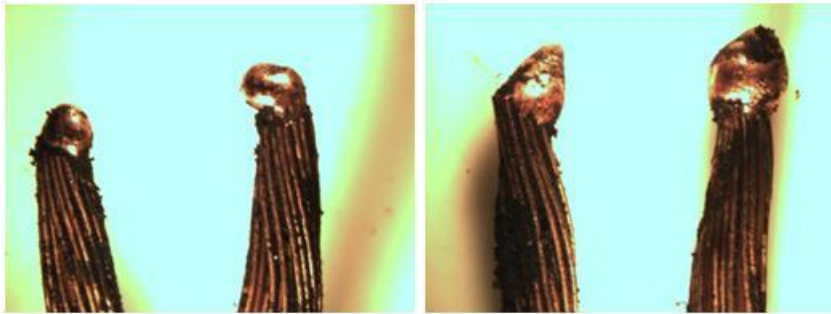


Figure A95: Direct Flame, Multi-strand 18-2, Energized (Test No. 43)

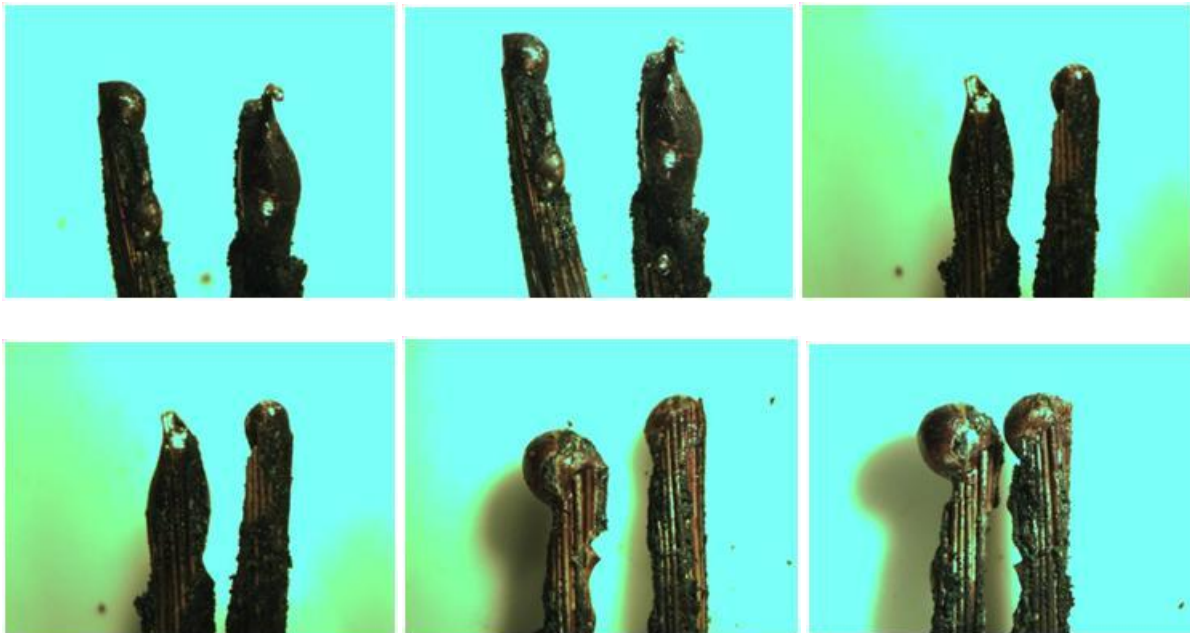


Figure A96: Direct Flame, Multi-strand 18-2, Energized (Test No. 44)



Figure A97: Direct Flame, Multi-strand 18-2, Energized (Test No. 46)

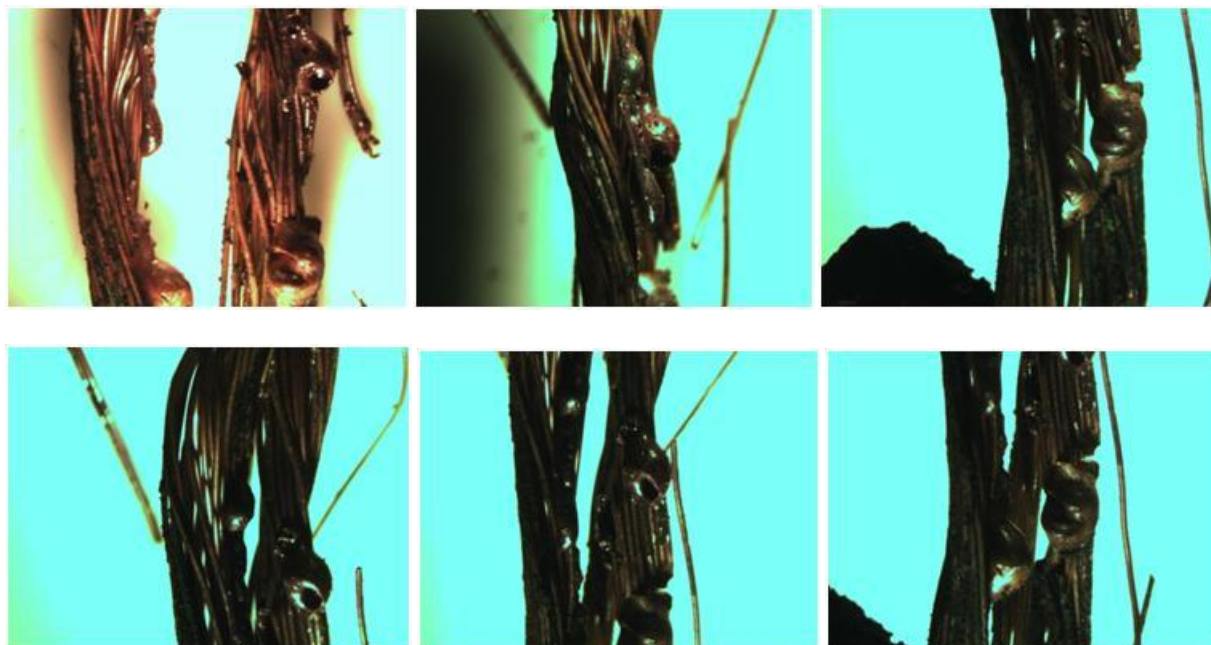


Figure A98: Direct Flame, Multi-strand 18-2, Energized (Test No. 47)

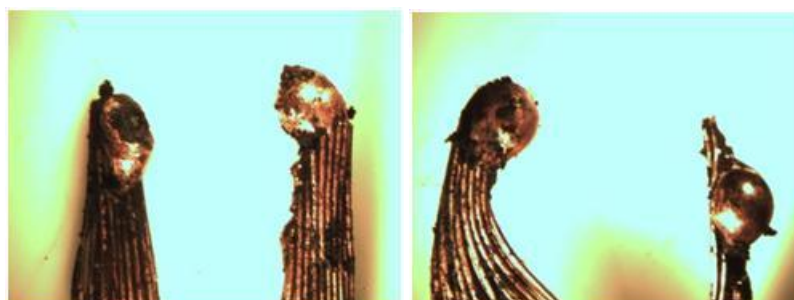


Figure A99: Direct Flame, Multi-strand 18-2, Energized (Test No. 48)

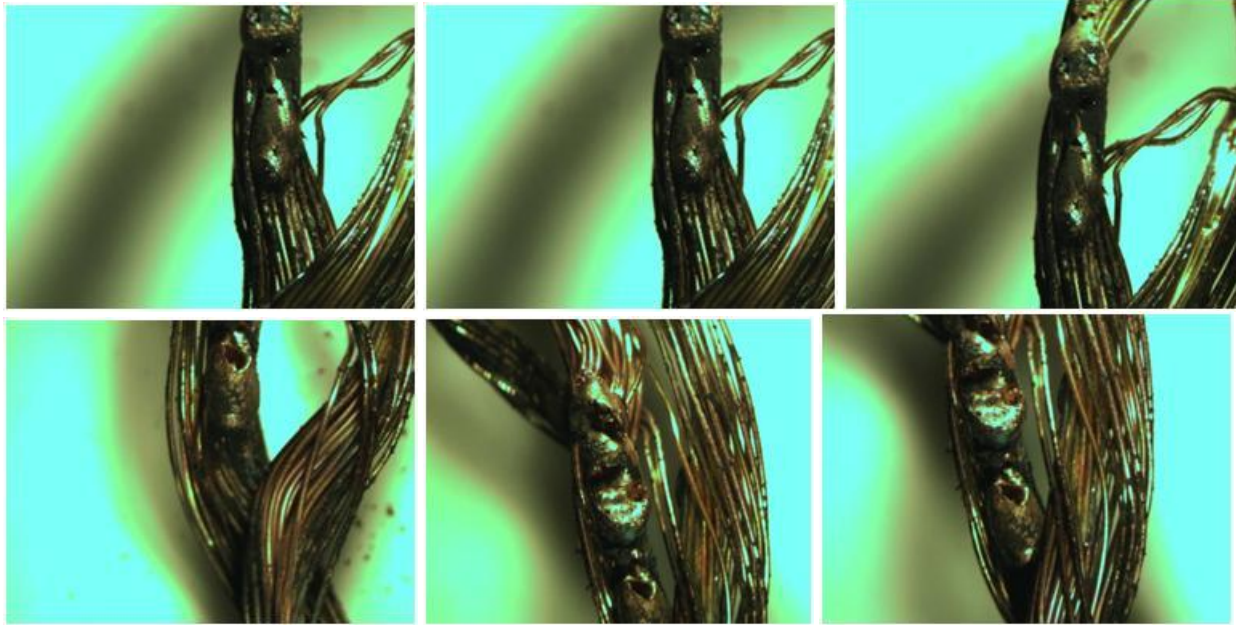


Figure A100: Direct Flame, Multi-strand 18-2, Loaded (Test No. 50)

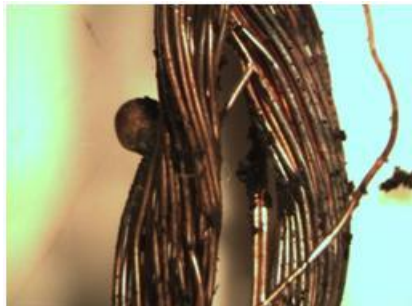


Figure A101: Direct Flame, Multi-strand 18-2, Loaded (Test No. 51)

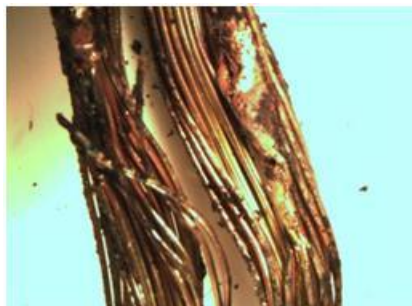


Figure A102: Direct Flame, Multi-strand 18-2, Loaded (Test No. 52)

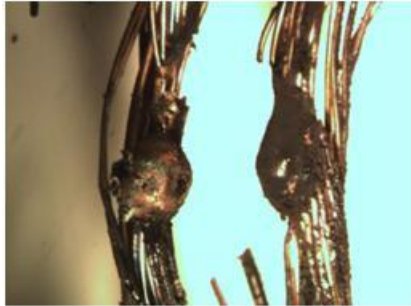


Figure A103: Direct Flame, Multi-strand 18-2, Loaded (Test No. 53)



Figure A104: Direct Flame, Multi-strand 18-2, Loaded (Test No. 54)

RADIATION TEST; 18-2 MULTISTRAND WIRE

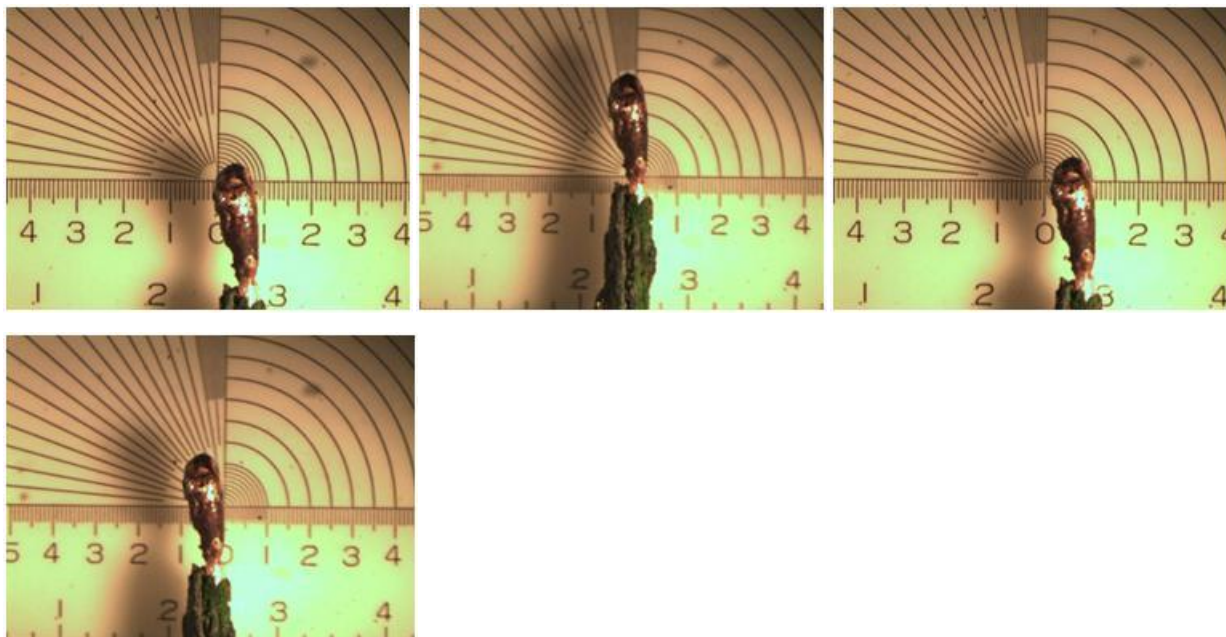


Figure A105: Radiation, Multi-strand 18-2, Energized (Test No. 1)

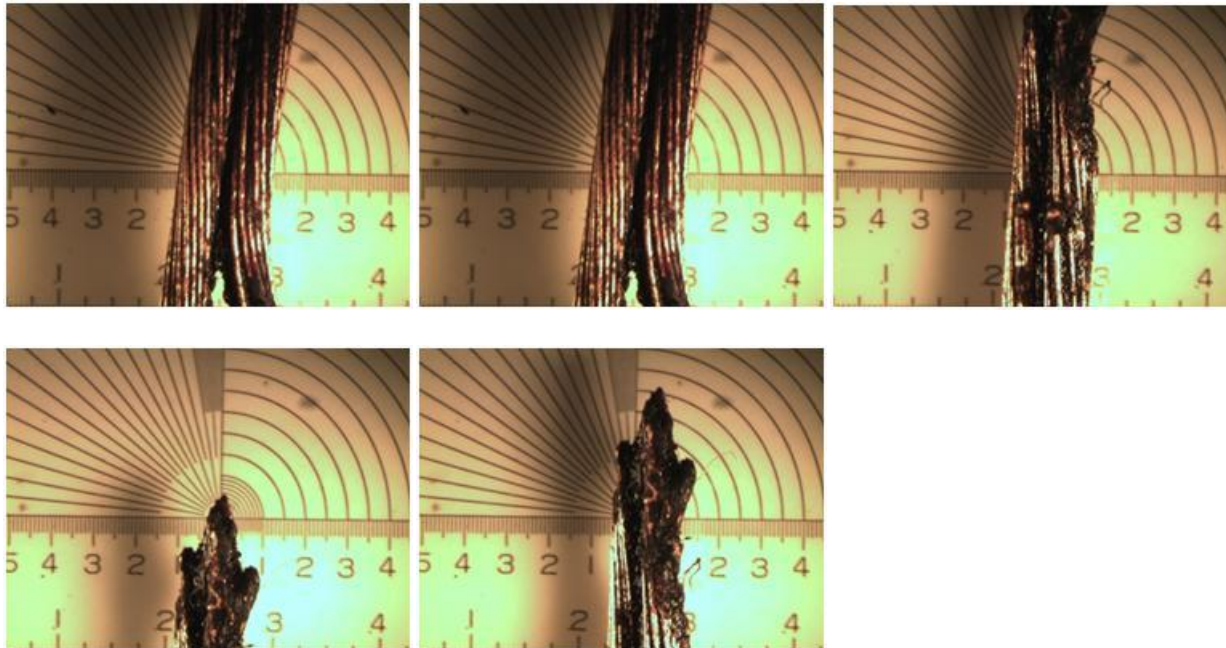


Figure A106: Radiation, Multi-strand 18-2, Energized (Test No. 2)

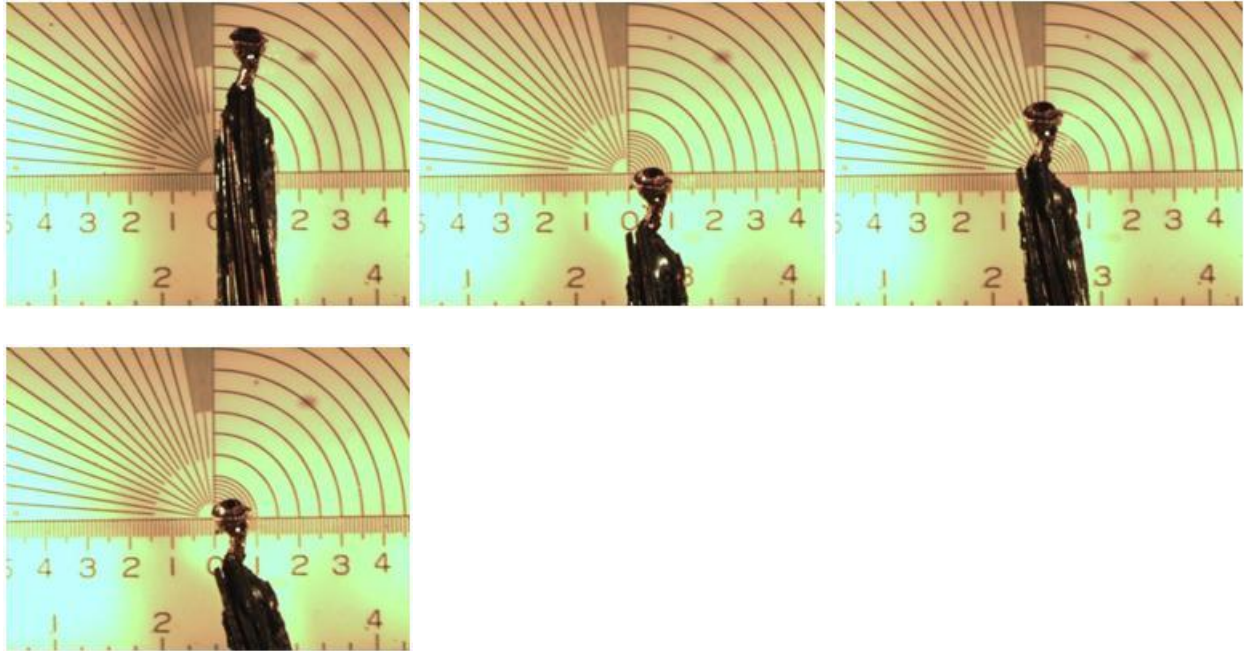


Figure A107: Radiation, Multi-strand 18-2, Energized (Test No. 3)

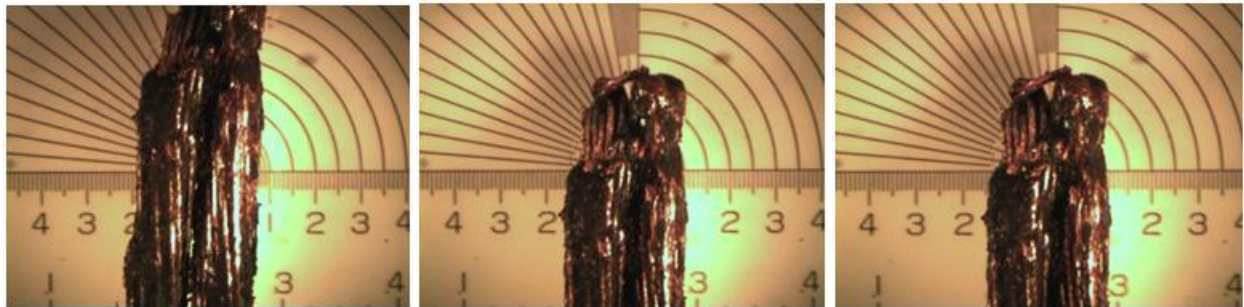
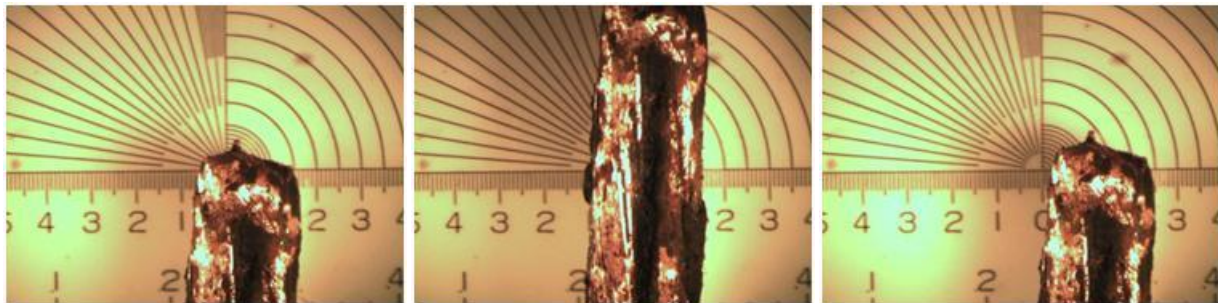


Figure A108: Radiation, Multi-strand 18-2, Non Energized (Test No. 1)



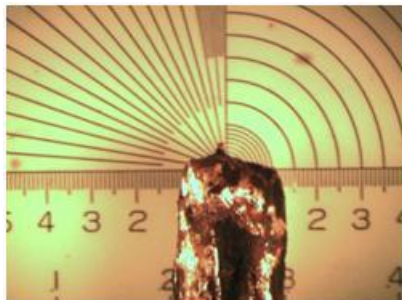


Figure A109: Radiation, Multi-strand 18-2, Non Energized (Test No. 2)

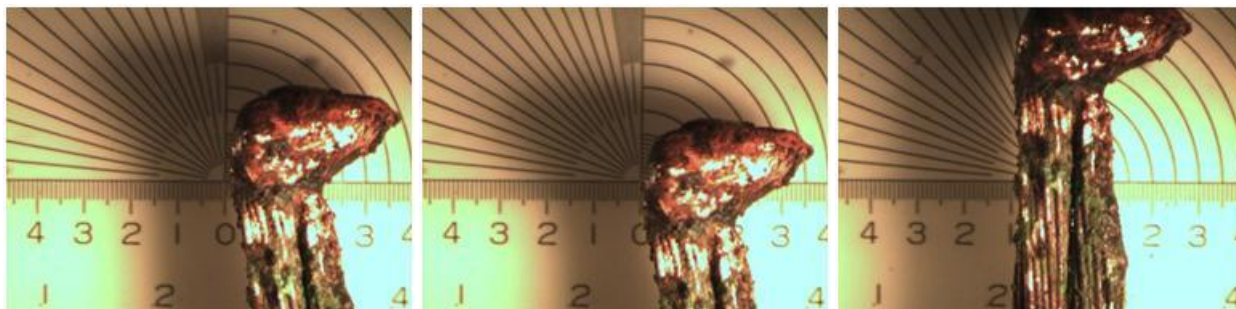


Figure A110: Radiation, Multi-strand 18-2, Non Energized (Test No. 3)

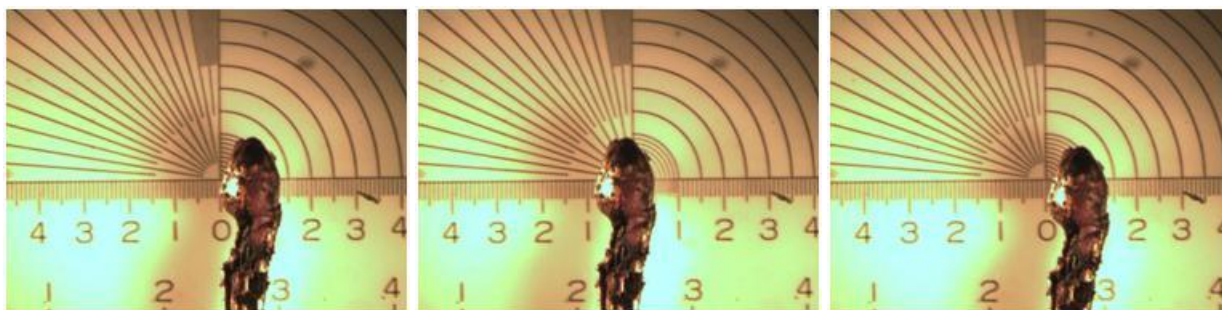
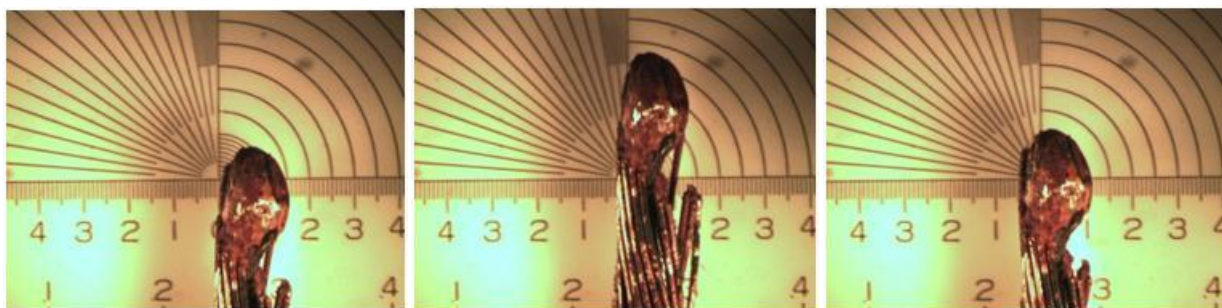


Figure A111: Radiation, Multi-strand 18-2, Loaded (Test No. 1)



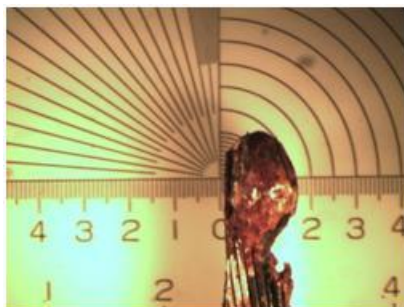


Figure A112: Radiation, Multi-strand 18-2, Loaded (Test No. 2)

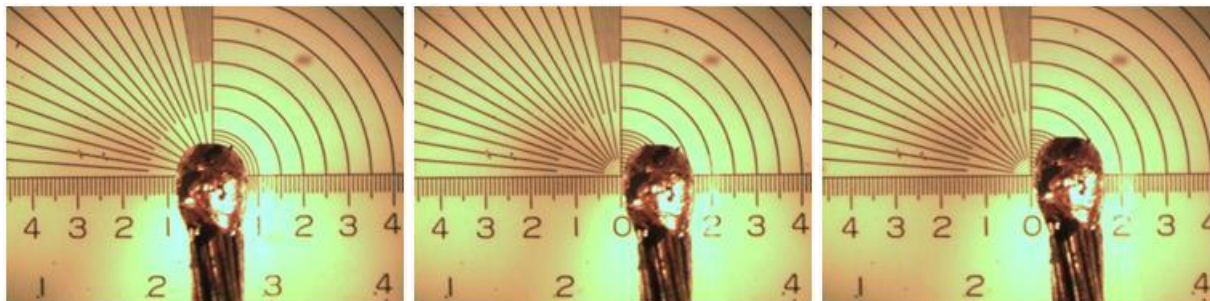


Figure A113: Radiation, Multi-strand 18-2, Loaded (Test No. 3)

RADIATION TEST; 16-2 MULTISTRAND WIRE

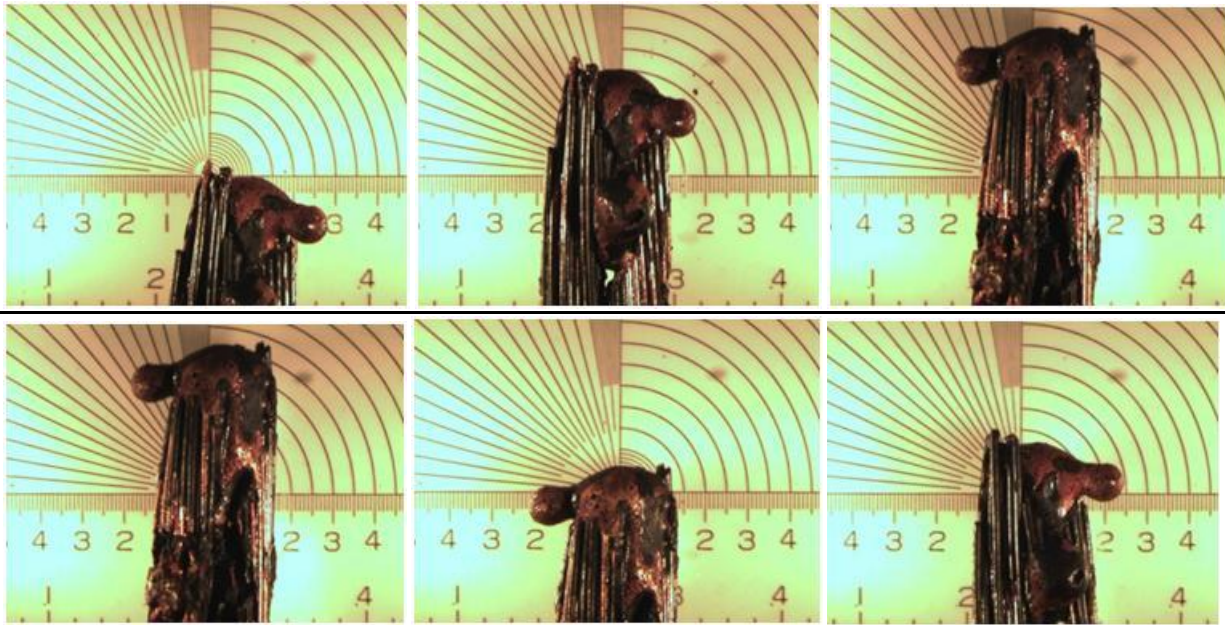


Figure A114: Radiation, Multi-strand 16-2, Energized (Test No. 1)

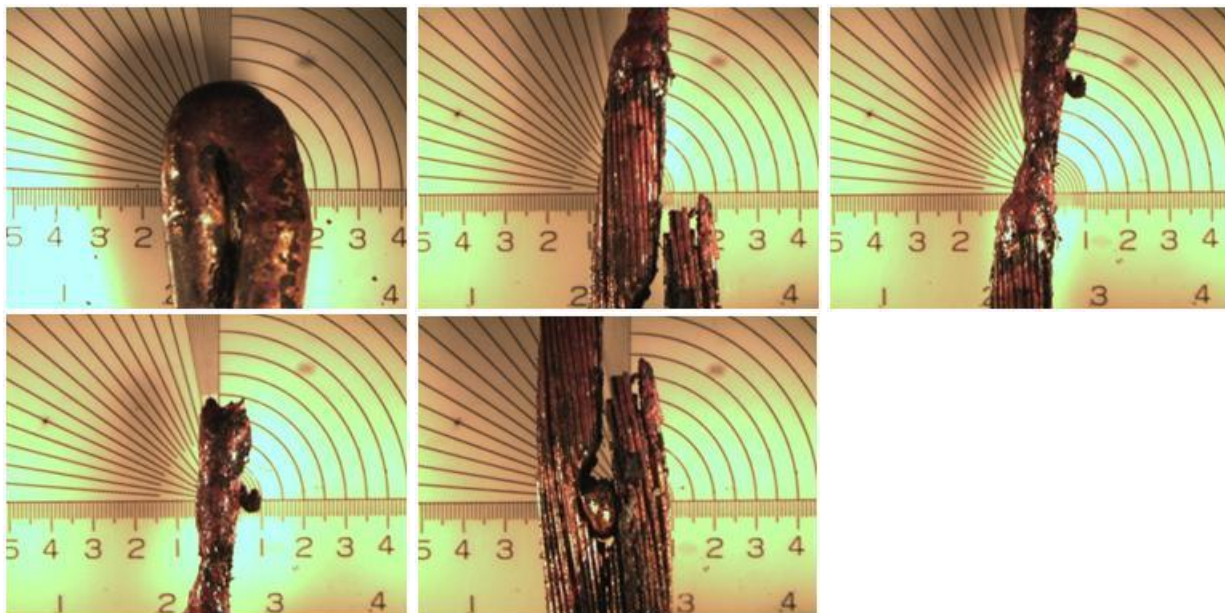


Figure A115: Radiation, Multi-strand 16-2, Energized (Test No. 2)

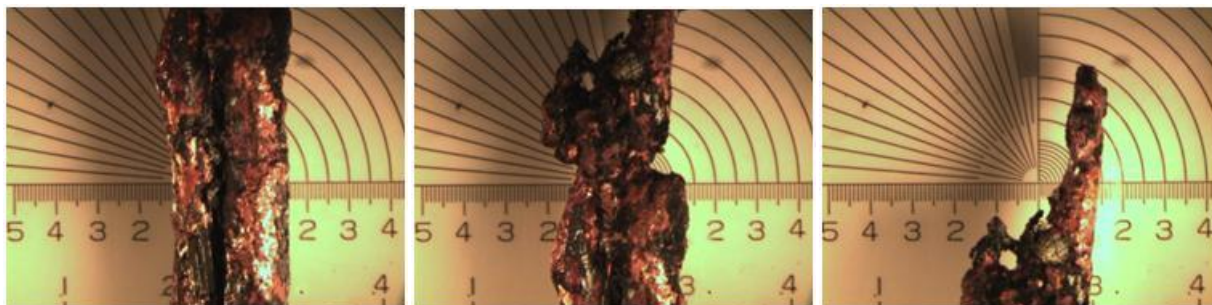


Figure A116: Radiation, Multi-strand 16-2, Energized (Test No. 3)

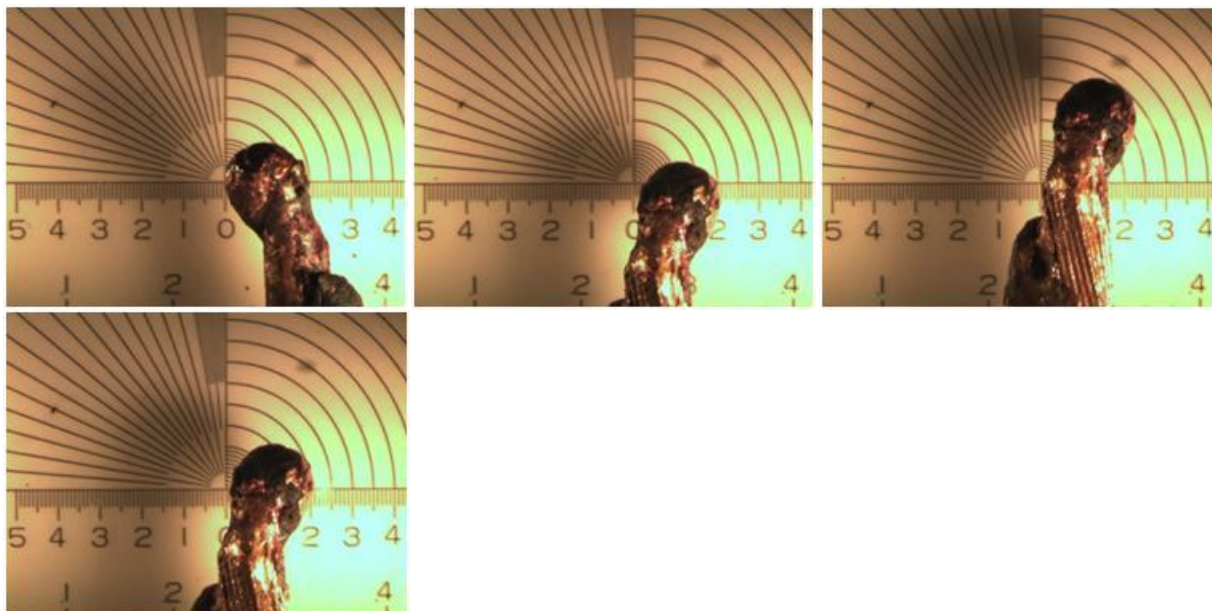


Figure A117: Radiation, Multi-strand 16-2, Non Energized (Test No. 1)

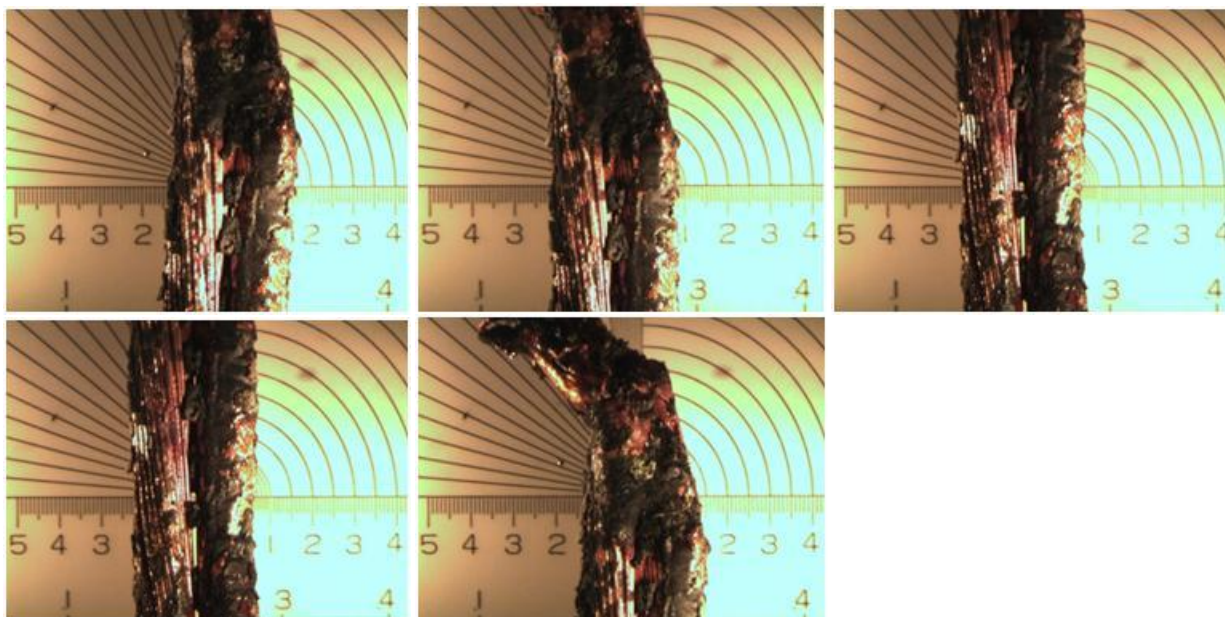


Figure A118: Radiation, Multi-strand 16-2, Non Energized (Test No. 2)

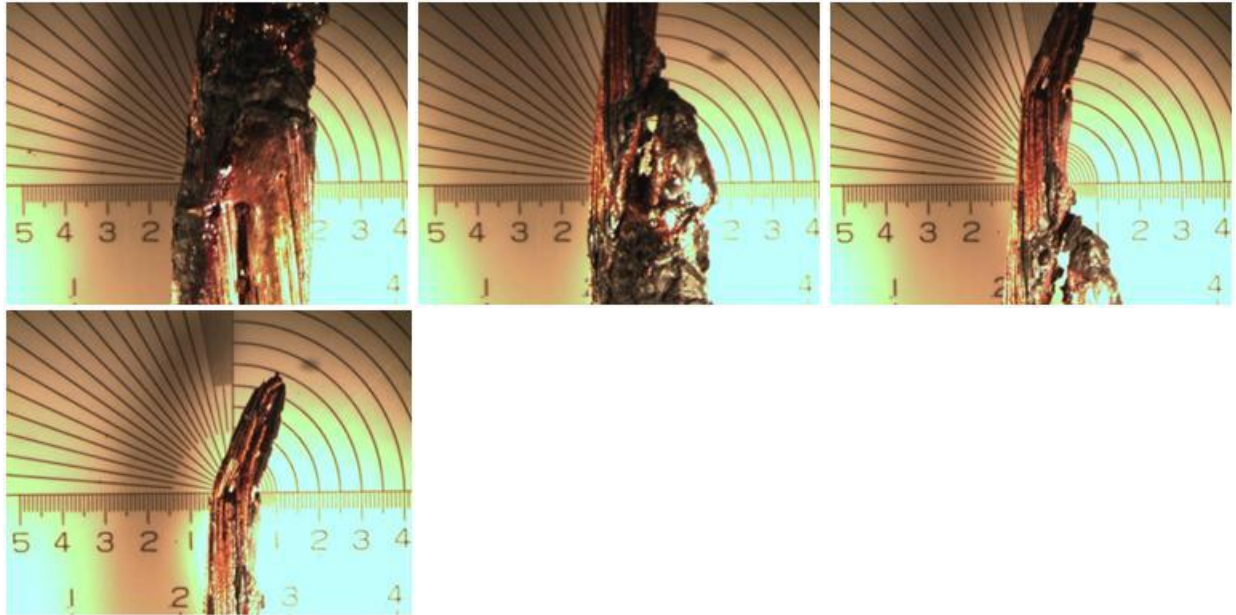


Figure A119: Radiation, Multi-strand 16-2, Non Energized (Test No. 3)

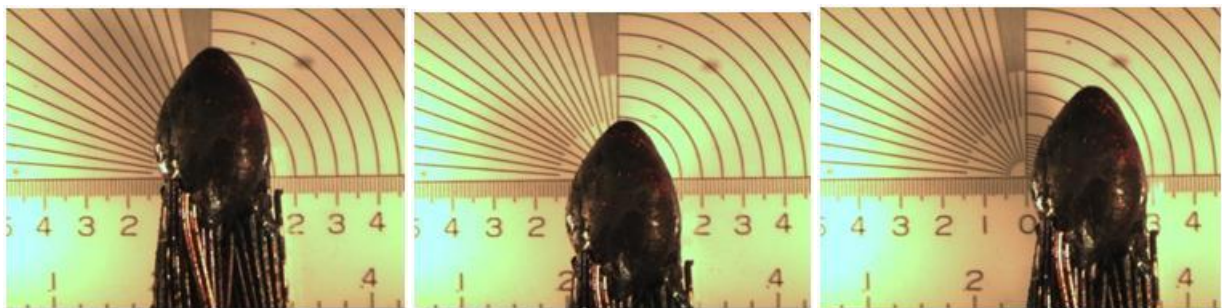


Figure A120: Radiation, Multi-strand 16-2, Loaded (Test No. 1)

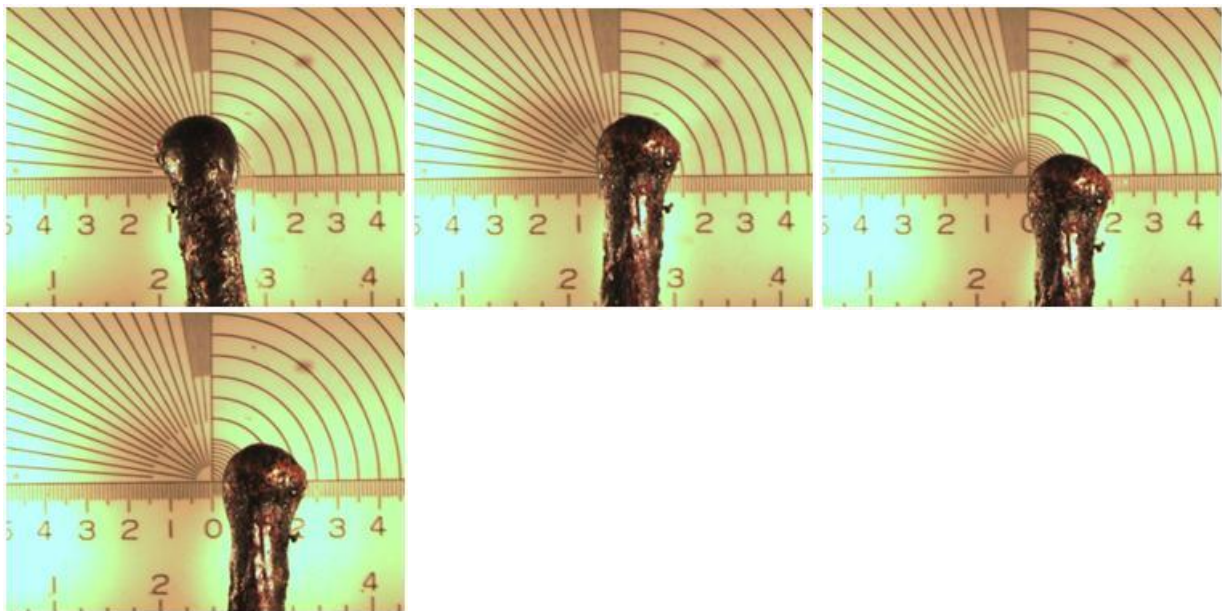


Figure A121: Radiation, Multi-strand 16-2, Loaded (Test No. 2)

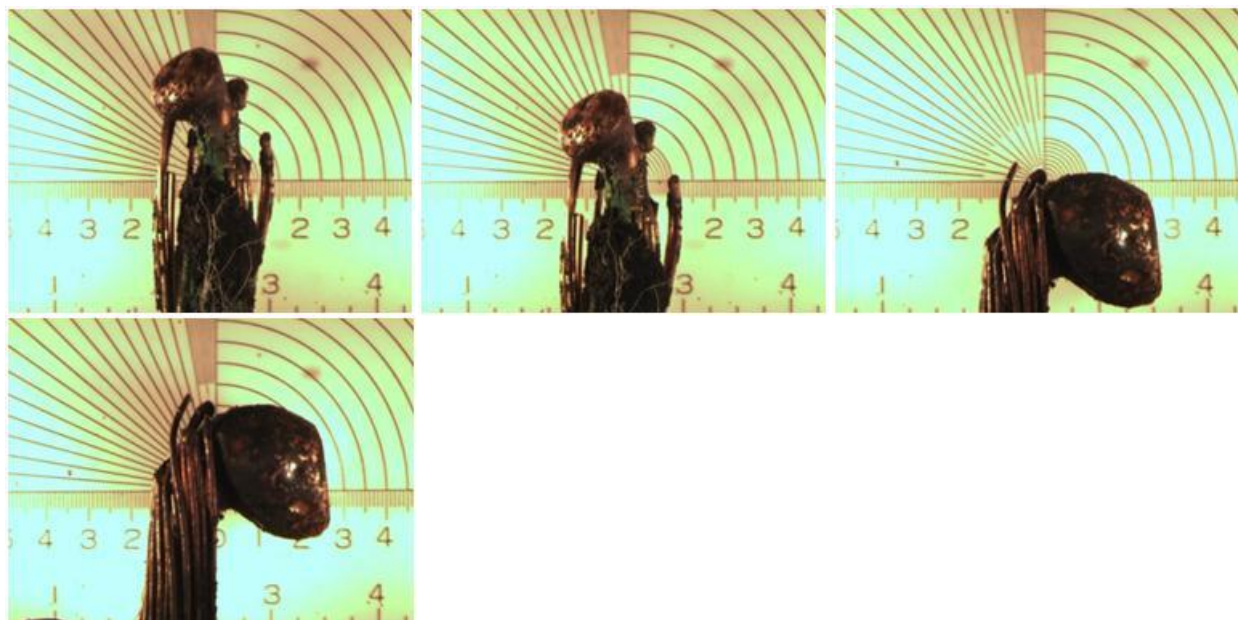


Figure A122: Radiation, Multi-strand 16-2, Loaded (Test No. 3)

RADIATION TEST; 14-2 ROMEX WIRE

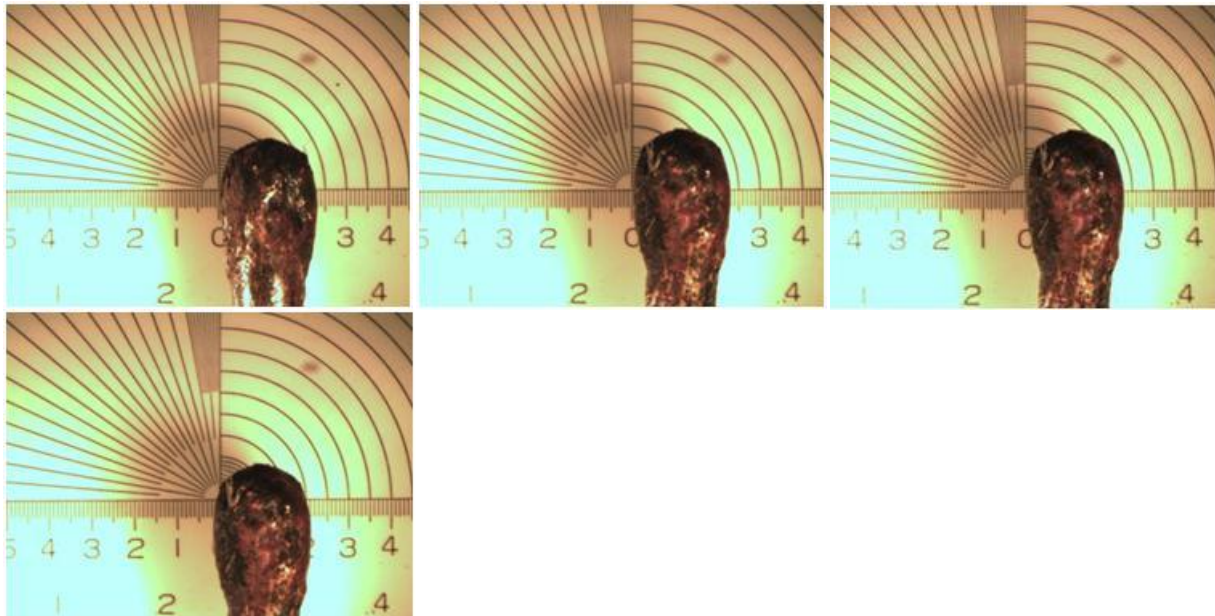


Figure A123: Radiation, Romex 14-2, Non Energized (Test No. 1)

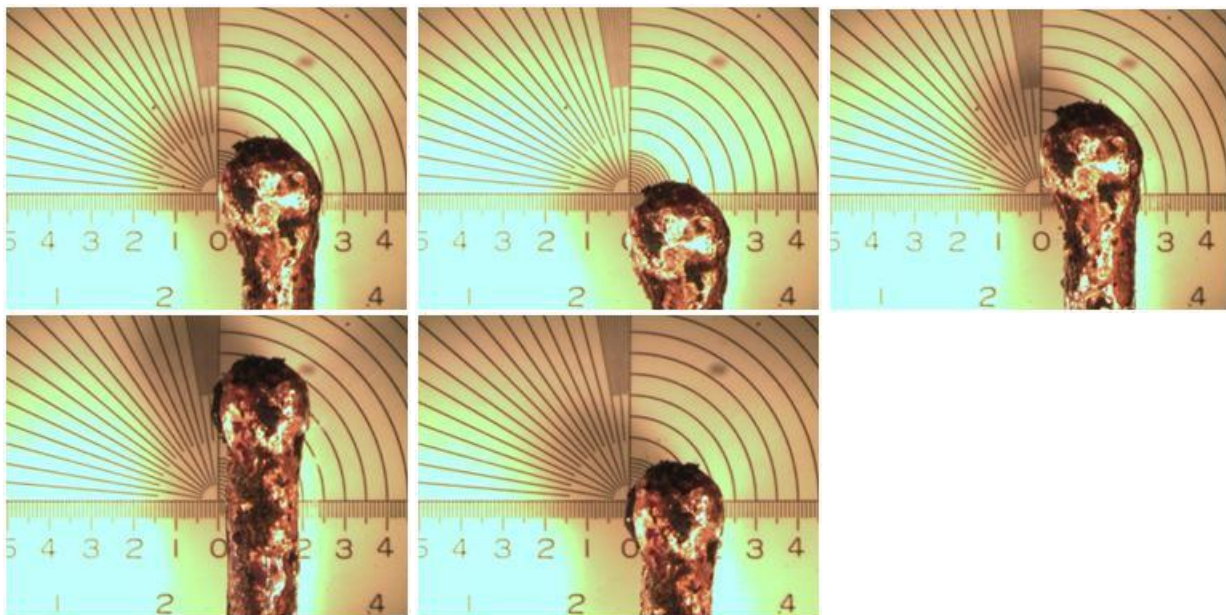


Figure A124: Radiation, Romex 14-2, Non Energized (Test No. 2)

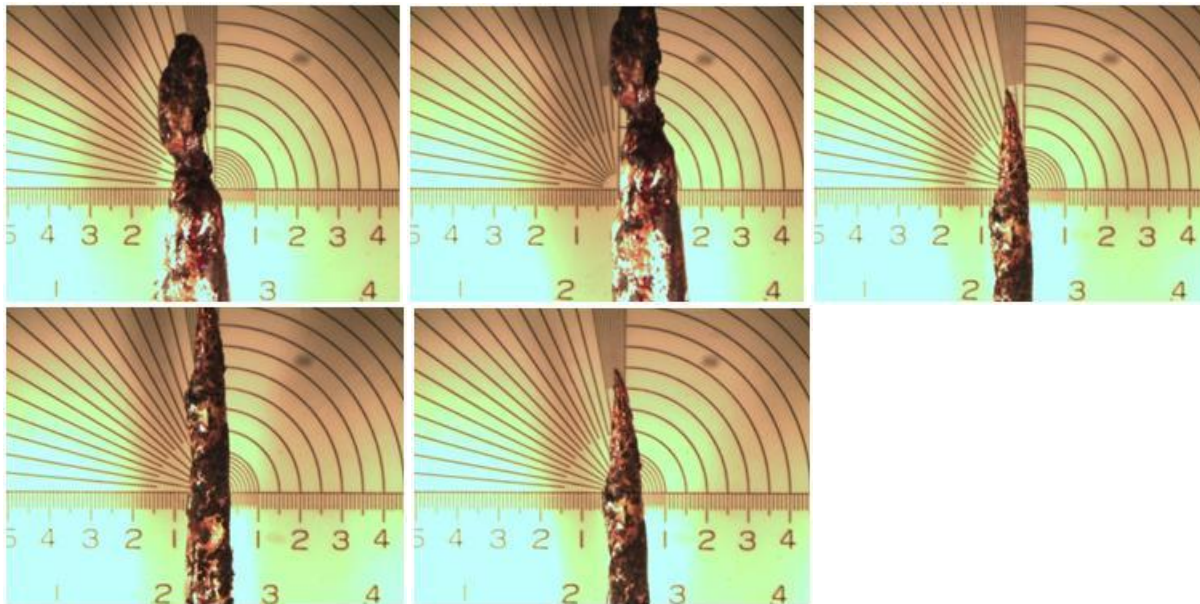


Figure A125: Radiation, Romex 14-2, Non Energized (Test No. 3)

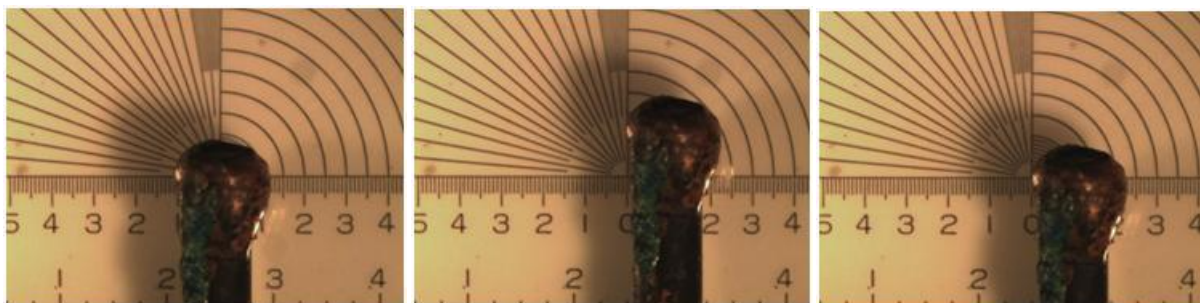


Figure A126: Radiation, Romex 14-2, Energized (Test No. 1)

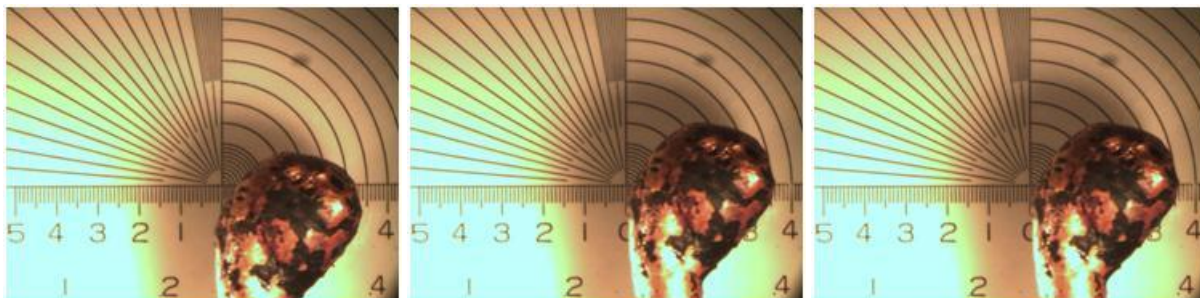


Figure A127: Radiation, Romex 14-2, Energized (Test No. 2)

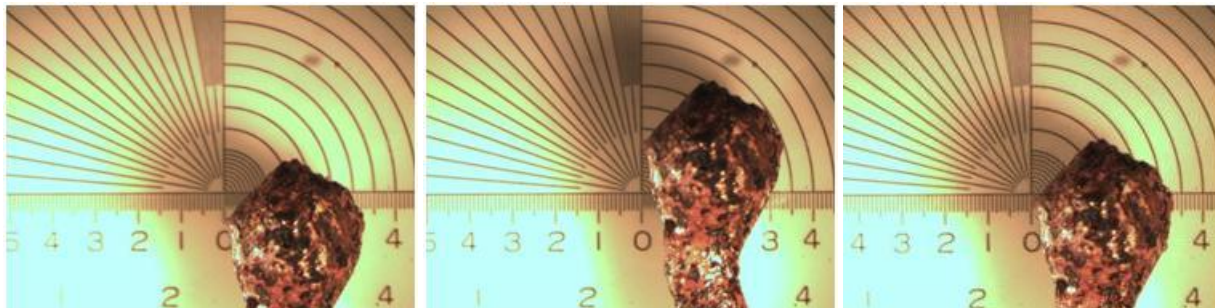


Figure A128: Radiation, Romex 14-2, Energized (Test No. 3)

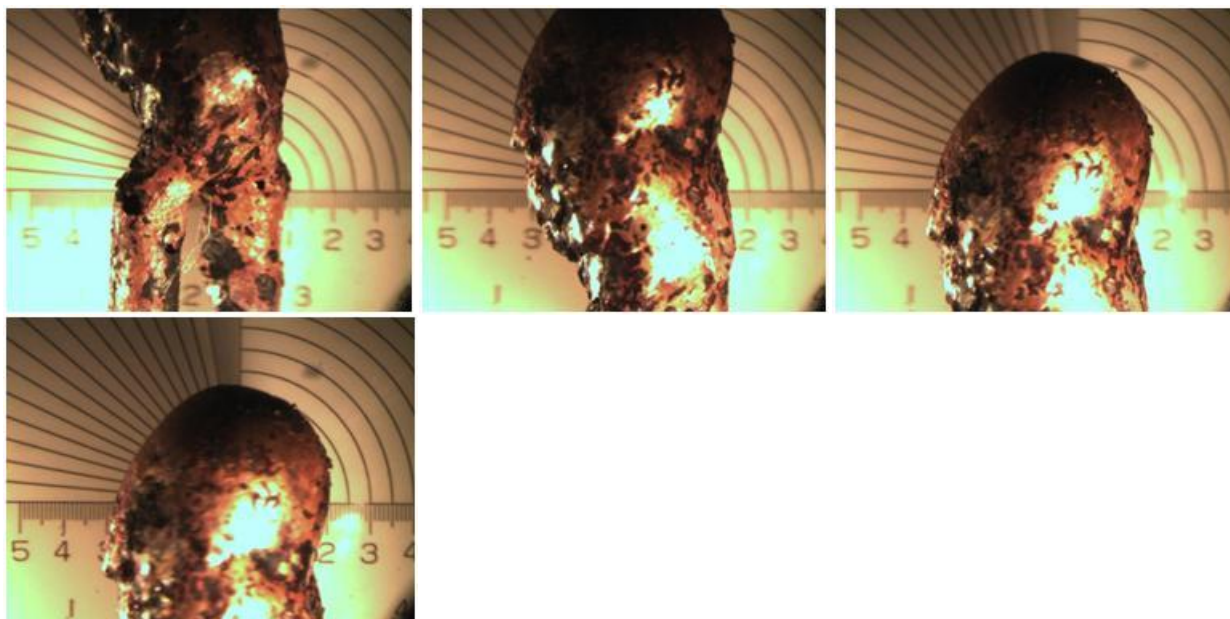


Figure A129: Radiation, Romex 14-2, Loaded (Test No. 1)

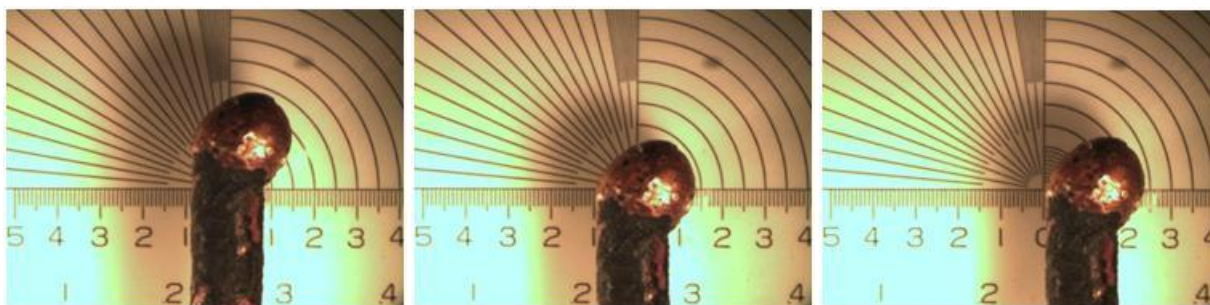


Figure A130: Radiation, Romex 14-2, Loaded (Test No. 2)

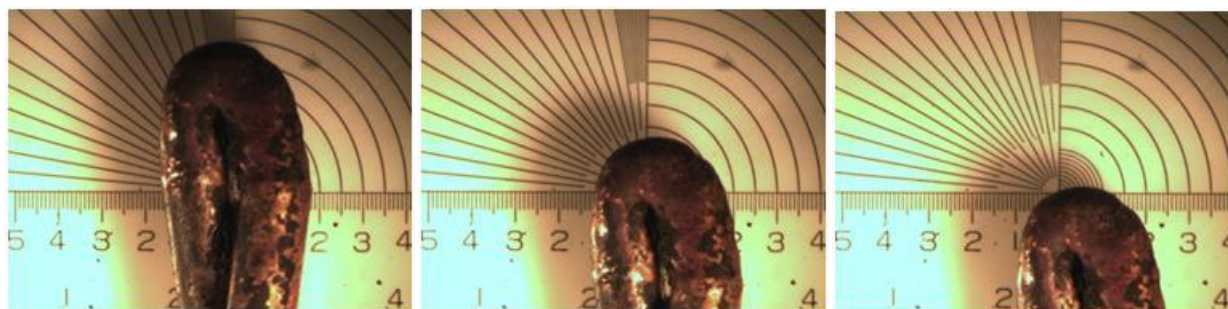


Figure A131: Radiation, Romex 14-2, Loaded (Test No. 3)

RADIATION TEST; 12-2 ROMEX WIRE

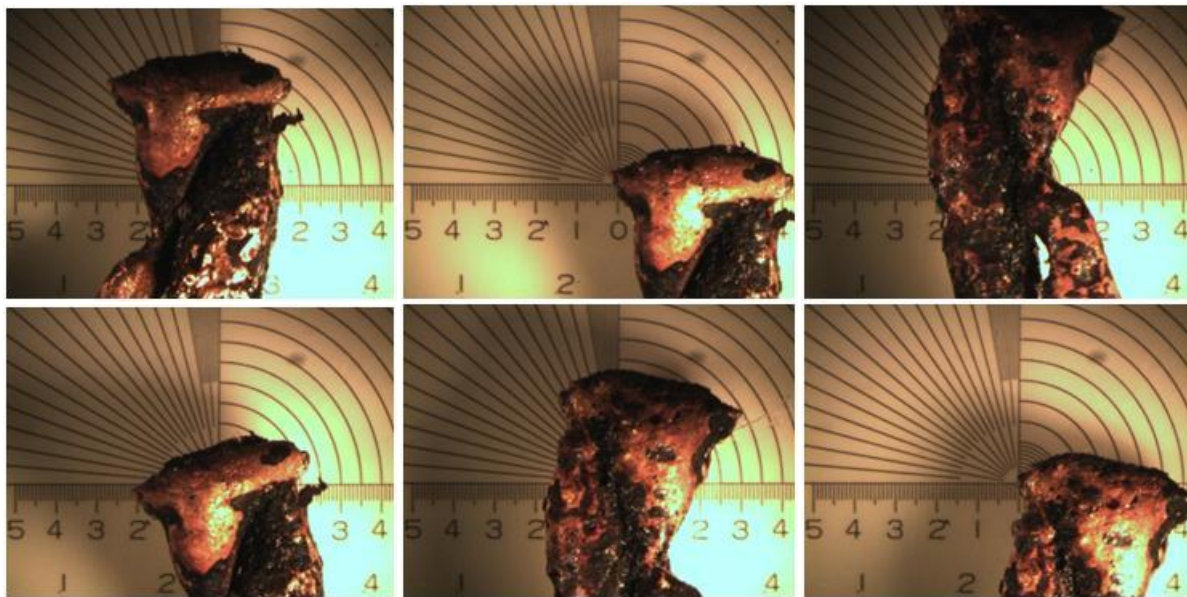
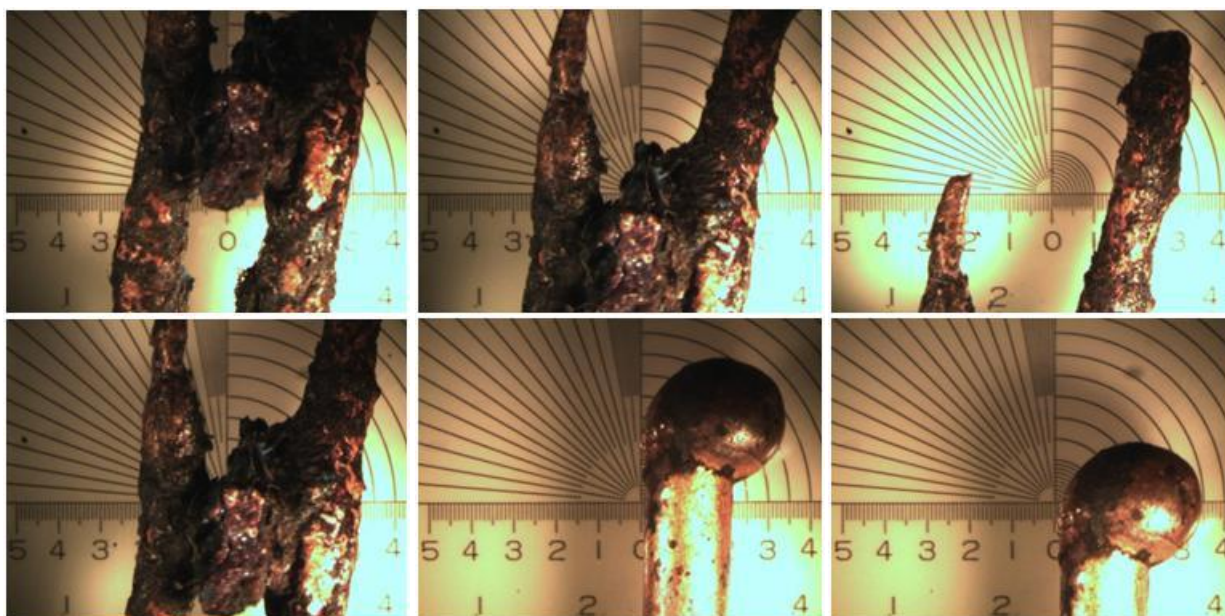


Figure A132: Radiation, Romex 12-2, Non Energized (Test No. 1)



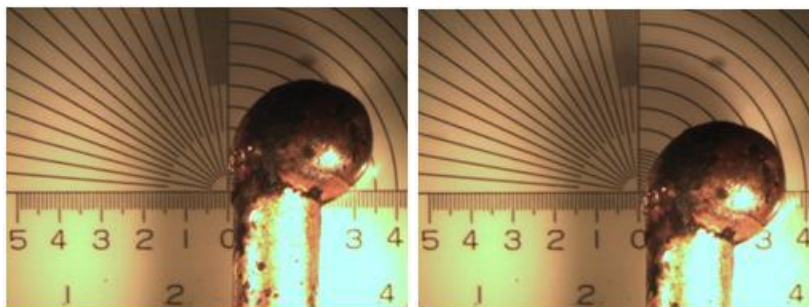


Figure A133: Radiation, Romex 12-2, Non Energized (Test No. 2)

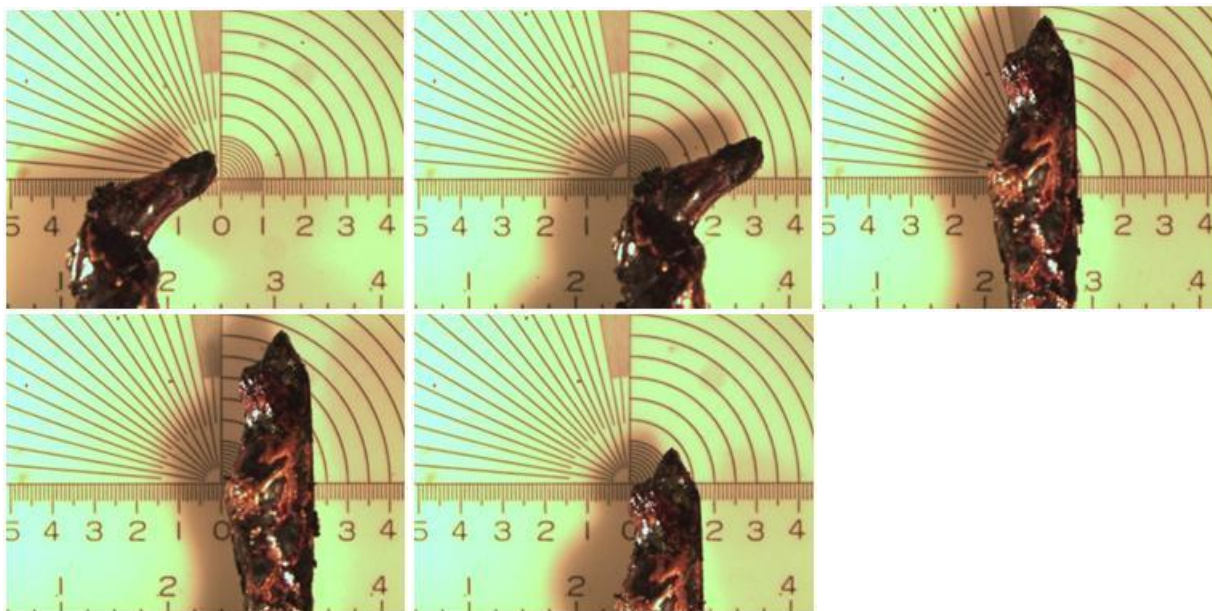


Figure A134: Radiation, Romex 12-2, Non Energized (Test No. 3)

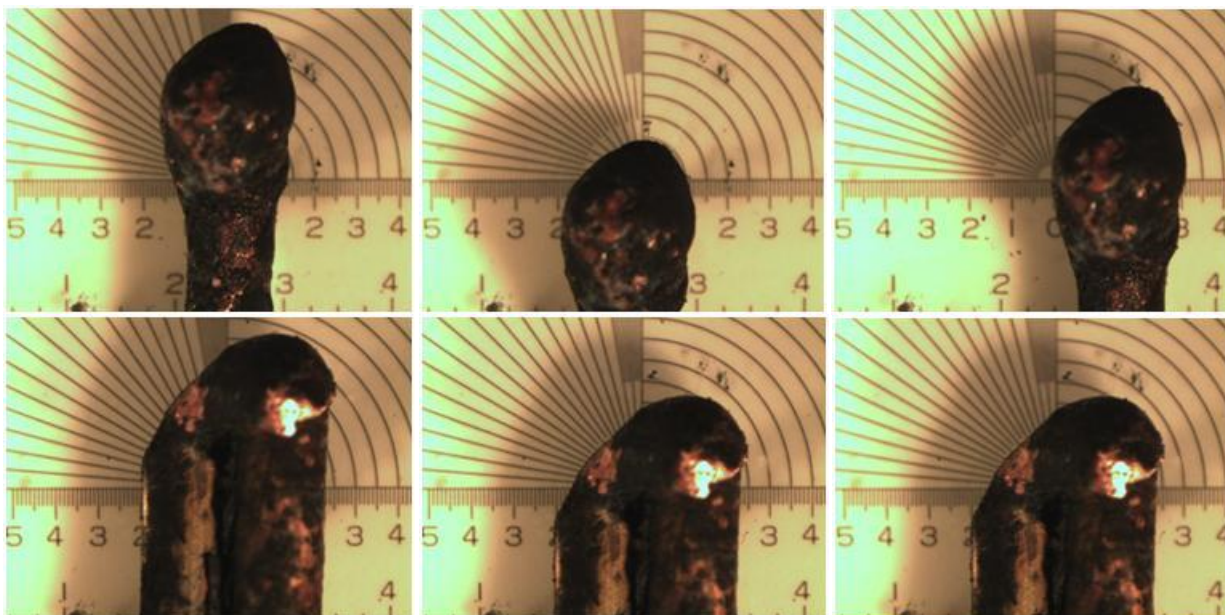


Figure A135: Radiation, Romex 12-2, Energized (Test No. 1)

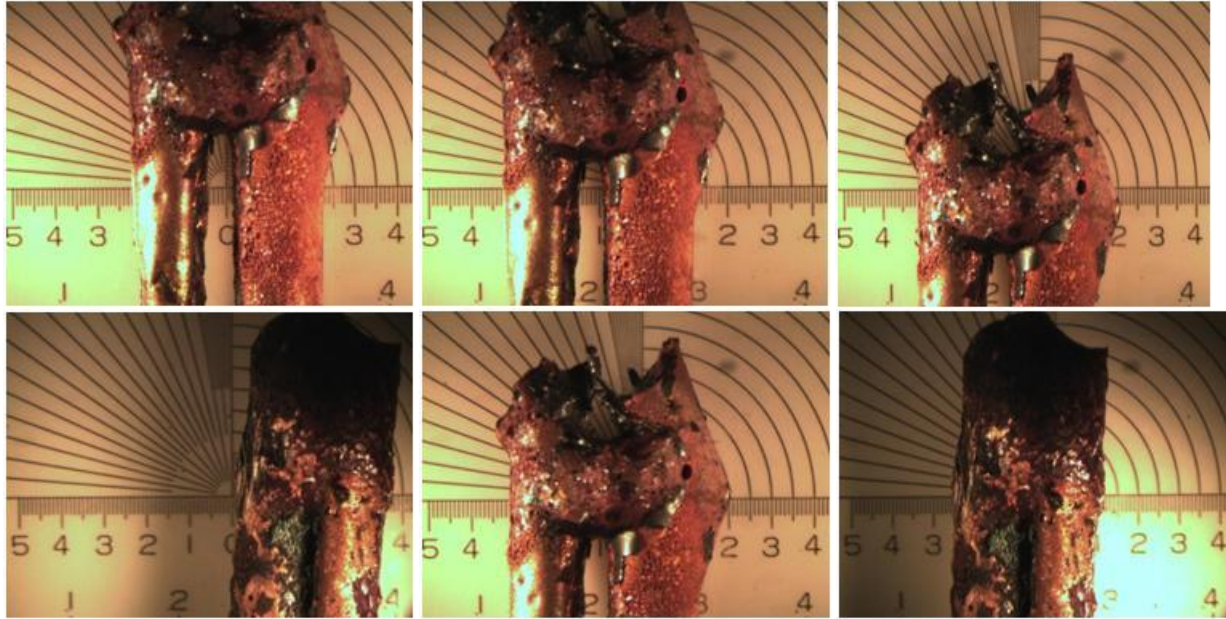
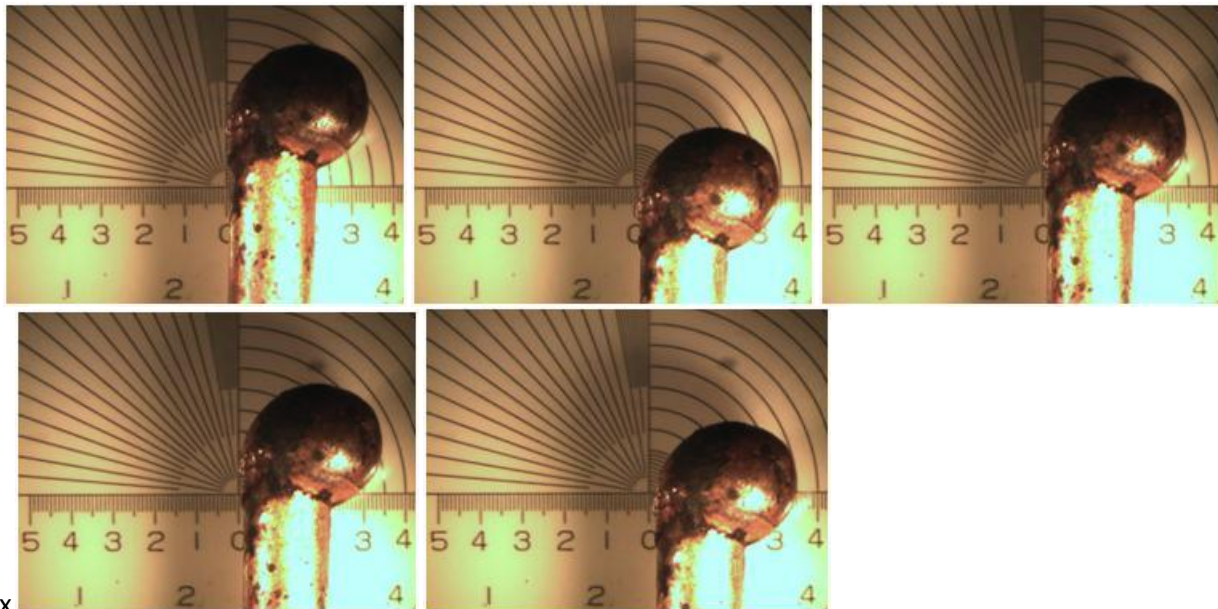
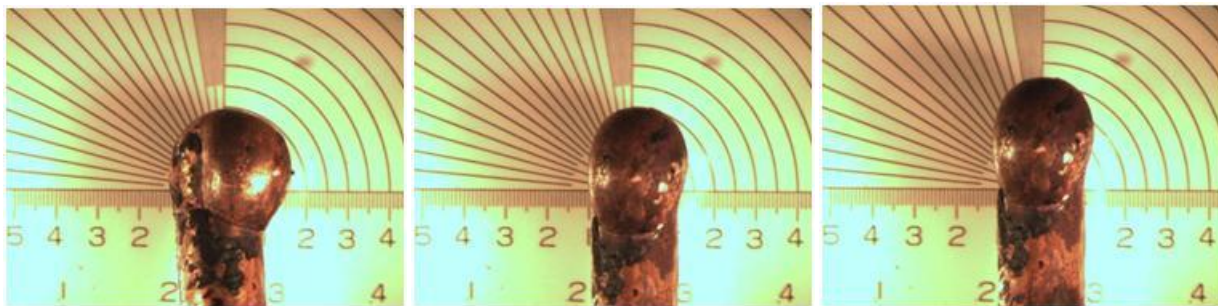


Figure A136: Radiation, Romex 12-2, Energized (Test No. 2)



x

Figure A137: Radiation, Romex 12-2, Energized (Test No. 3)



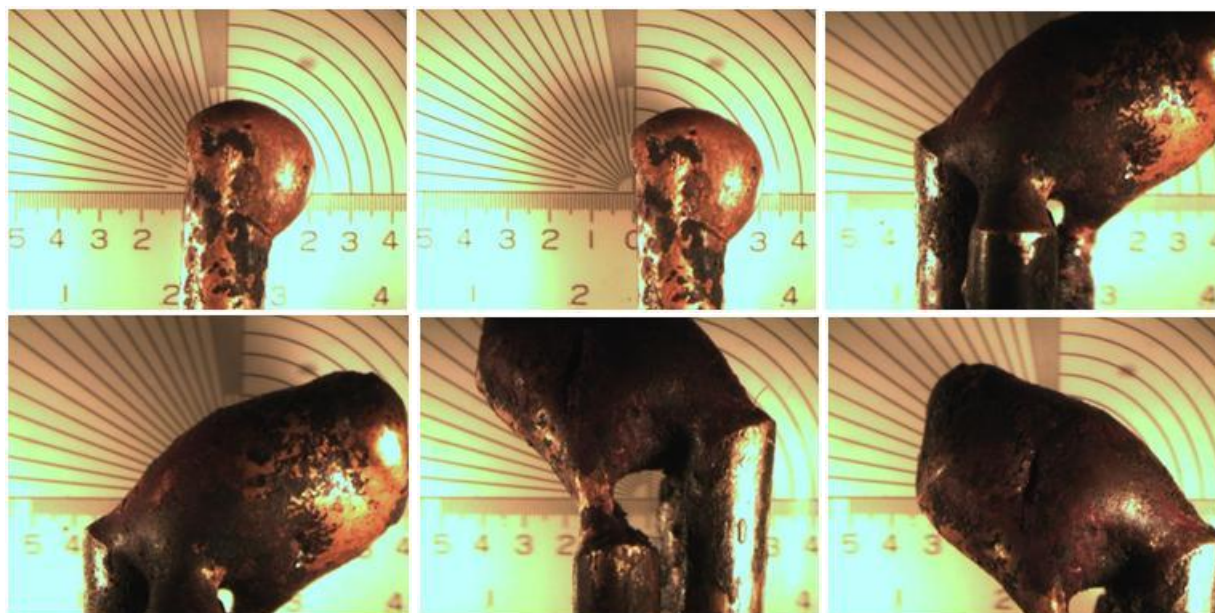


Figure A138: Radiation, Romex 12-2, Loaded (Test No. 1)

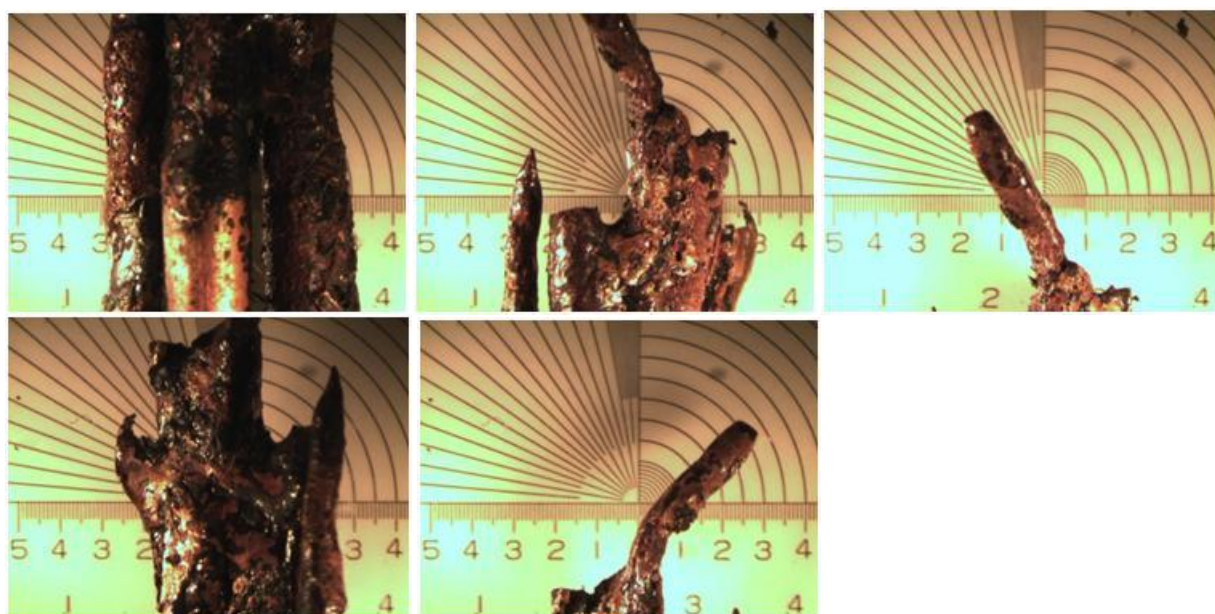
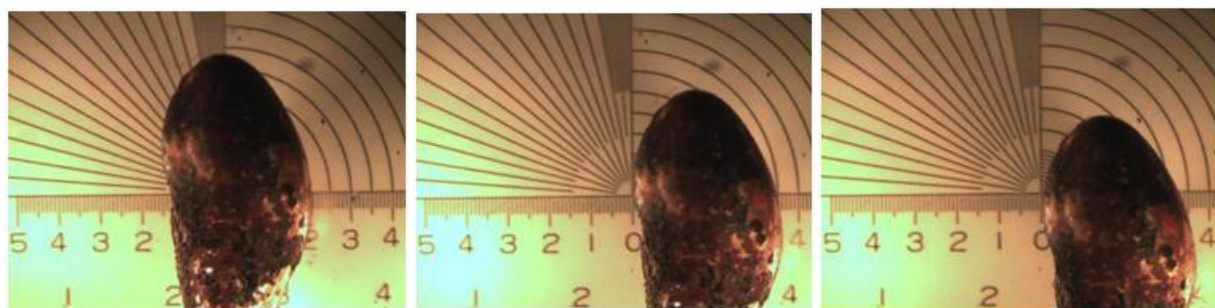


Figure A139: Radiation, Romex 12-2, Loaded (Test No. 2)



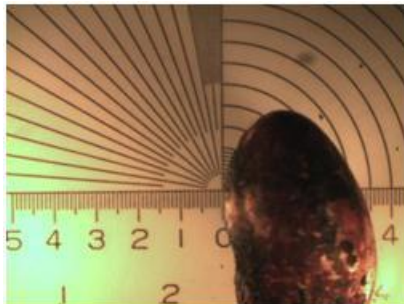


Figure A140: Radiation, Romex 12-2, Loaded (Test No. 3)

FULL SCALE COMPARTMENT TEST; 12-2 ROMEX WIRE

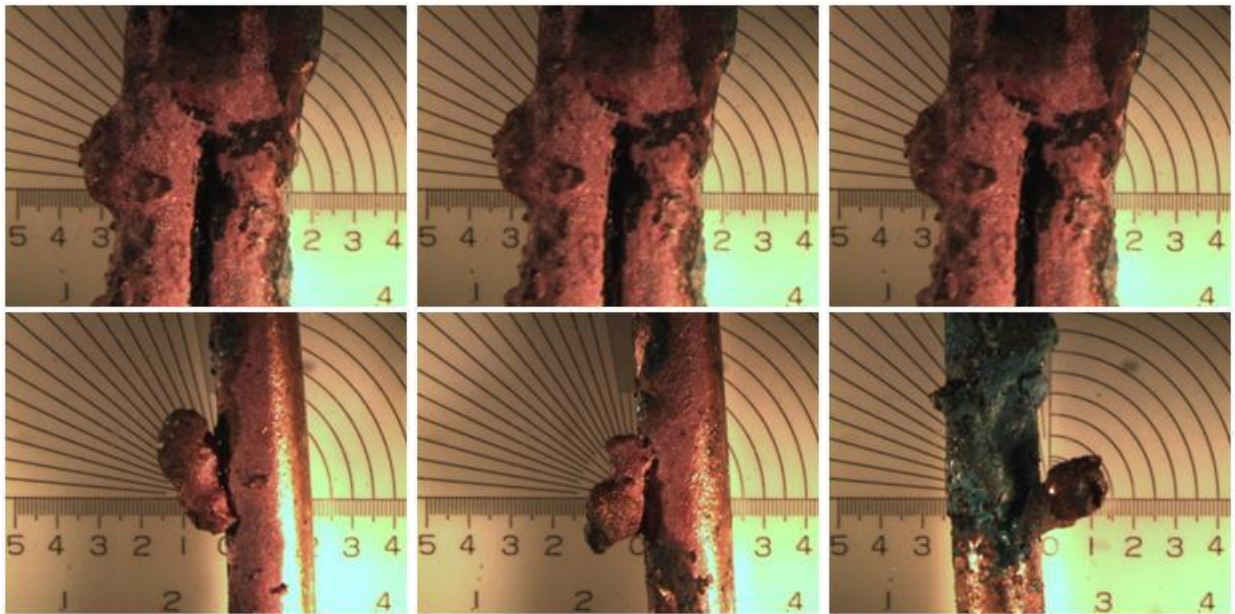
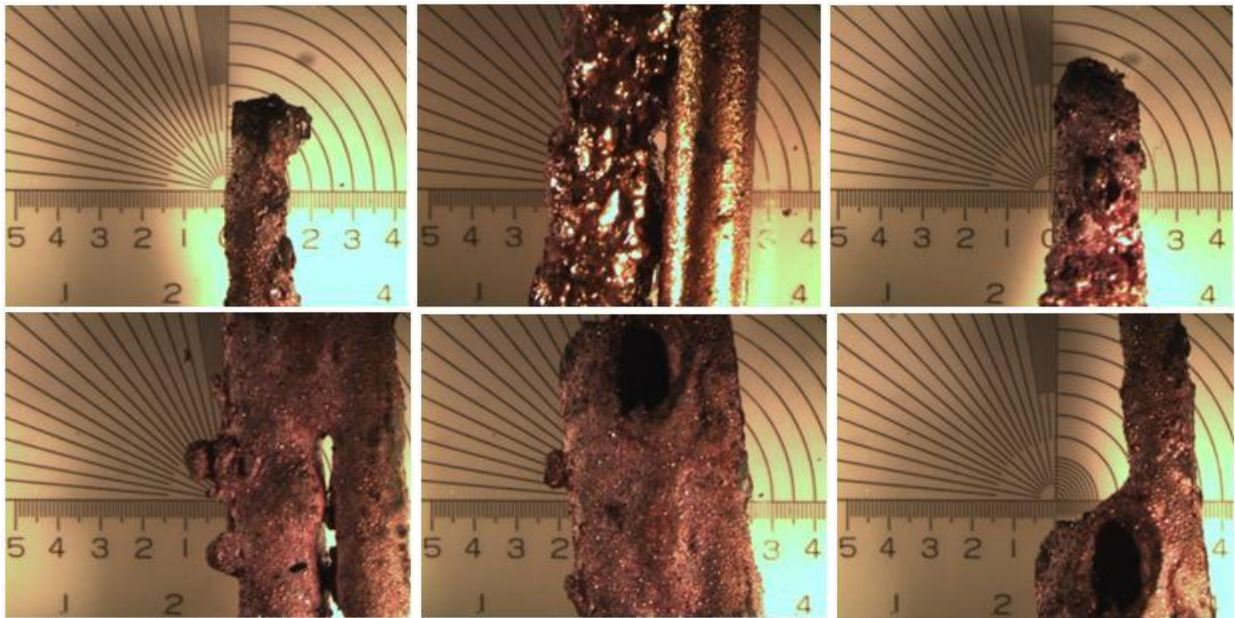


Figure A141: Full Scale, Romex 12-2, Energized (Room No. 6)



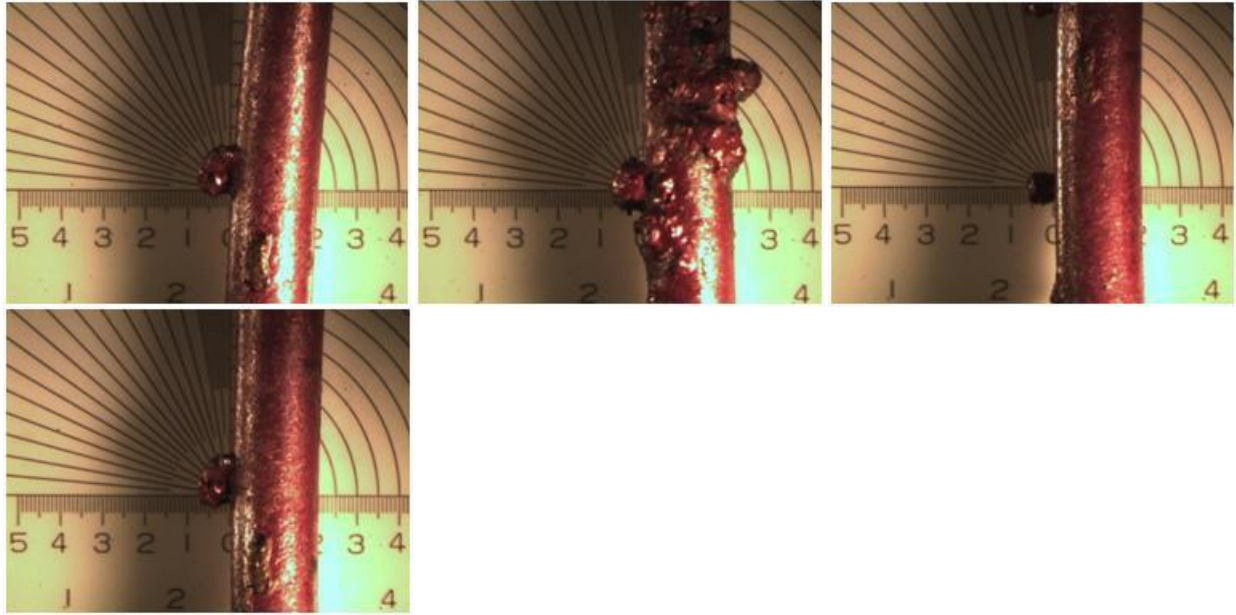


Figure A142: Full Scale, Romex 12-2, Loaded (Room No. 6)

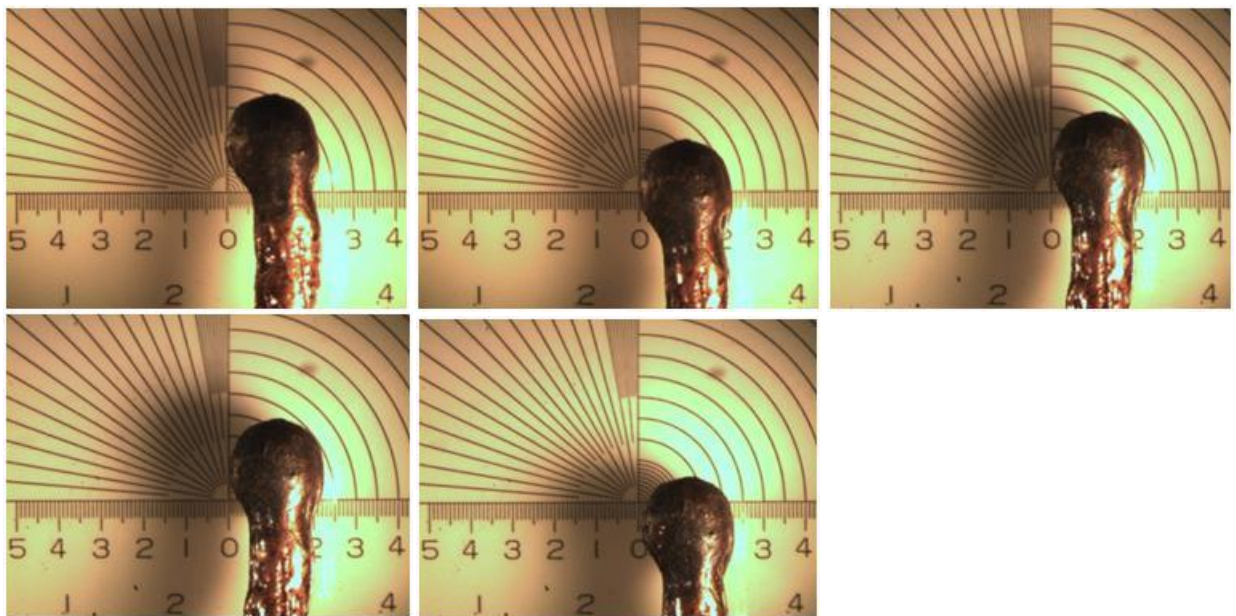


Figure A143: Full Scale, Romex 12-2, Loaded (Room No. 6)

FULL SCALE COMPARTMENT TEST; MULTISTRAND 16-2 WIRE

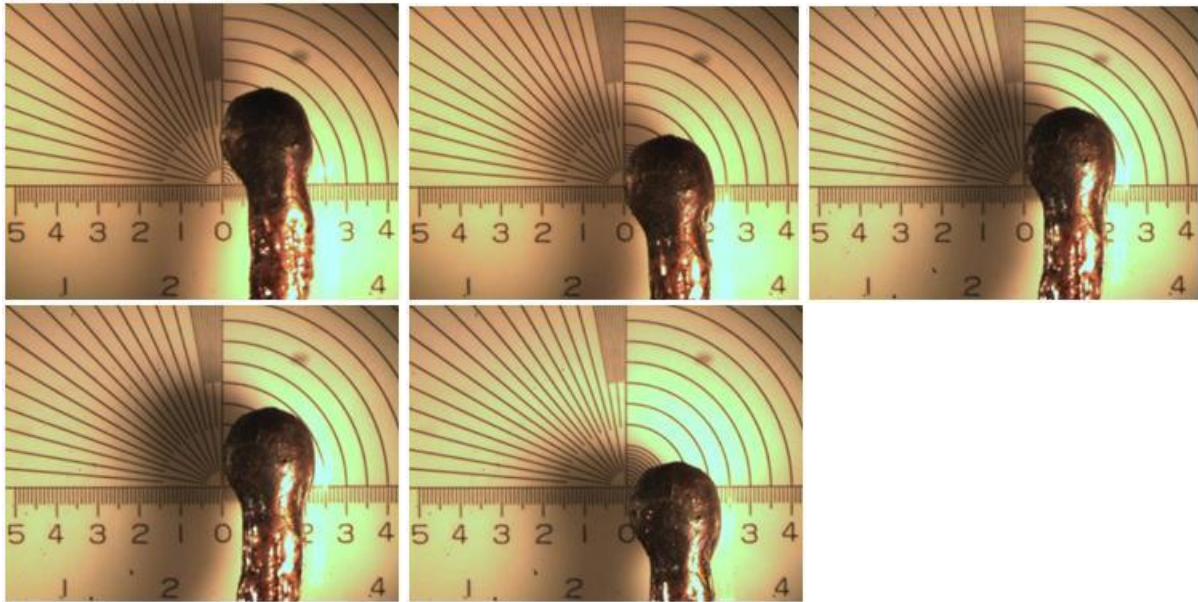


Figure A144: Full Scale, Multi-strand 16-2, Energized (Room No. 3)

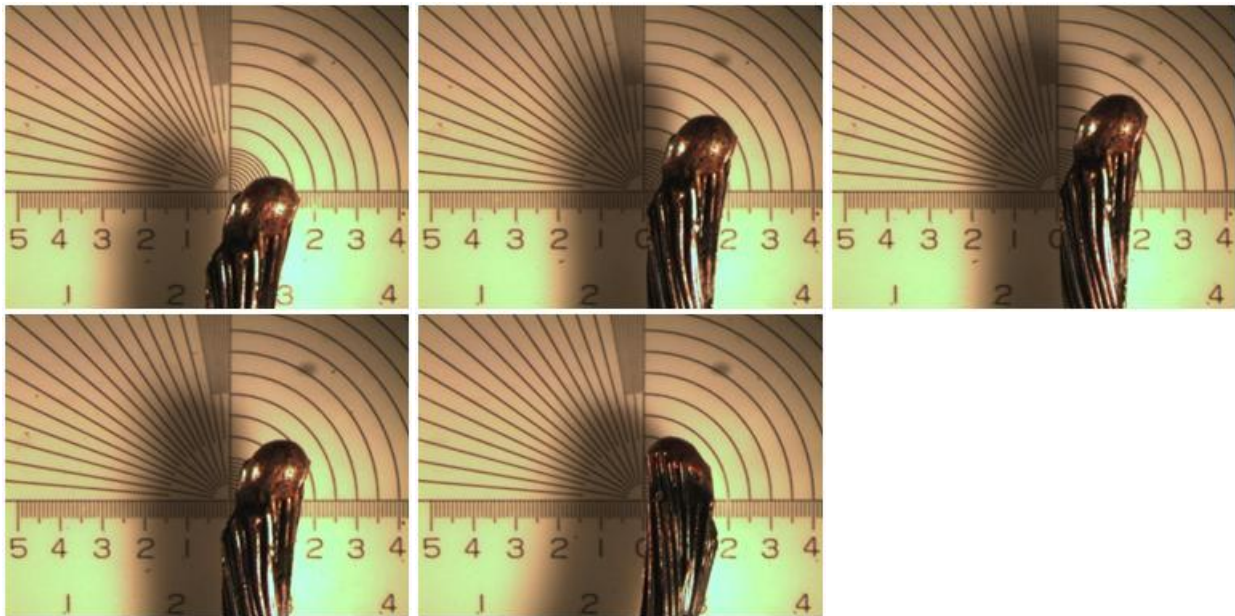


Figure A145: Full Scale, Multi-strand 16-2, Loaded (Room No. 3)

FULL SCALE COMPARTMENT TEST; MULTISTRAND 18-2 WIRE

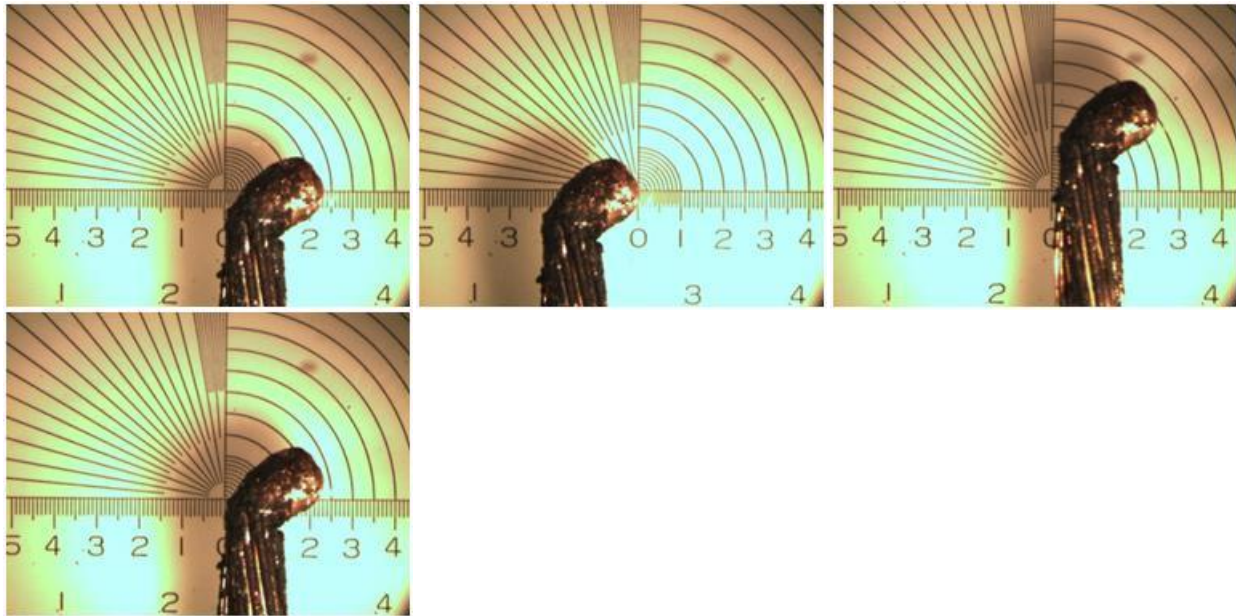


Figure A146: Full Scale, Multi-strand 18-2, Energized (Room No. 3)

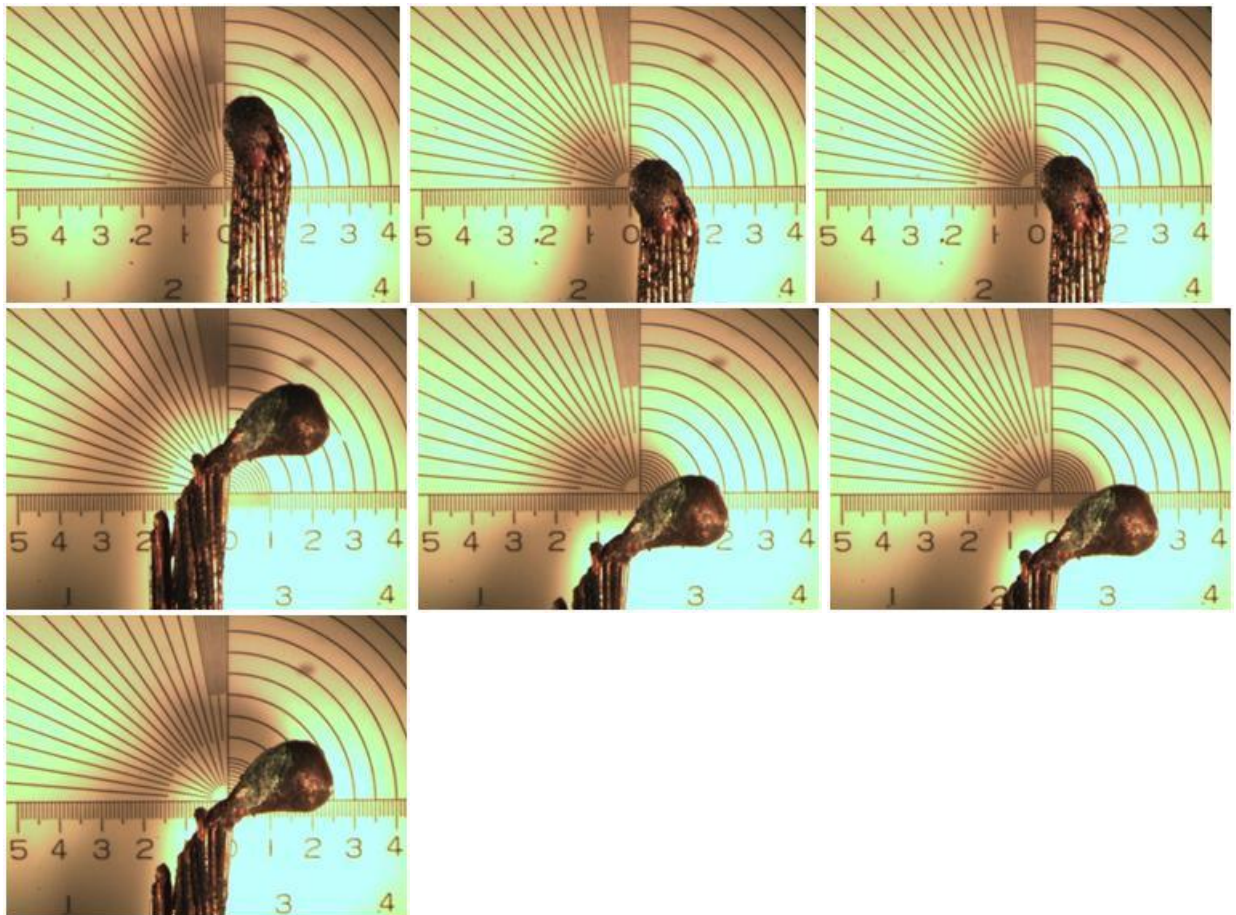


Figure A147: Full Scale, Multi-strand 18-2, Loaded (Room No. 5)

B1: Direct Flame Testing

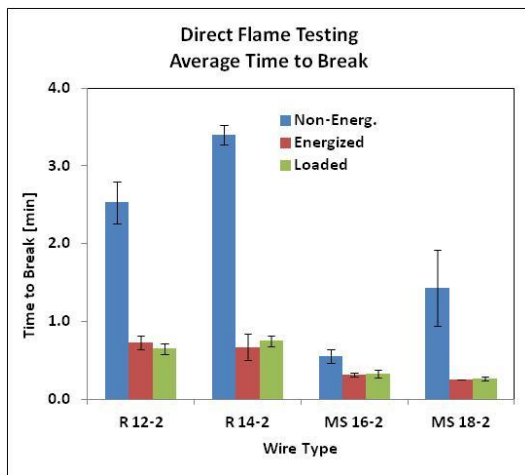


Figure B1.1: Average Time to Break (DF)

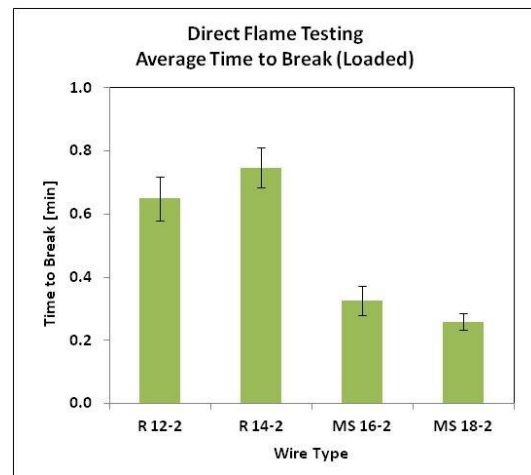


Figure B1.4: Average Time to Break Loaded (DF)

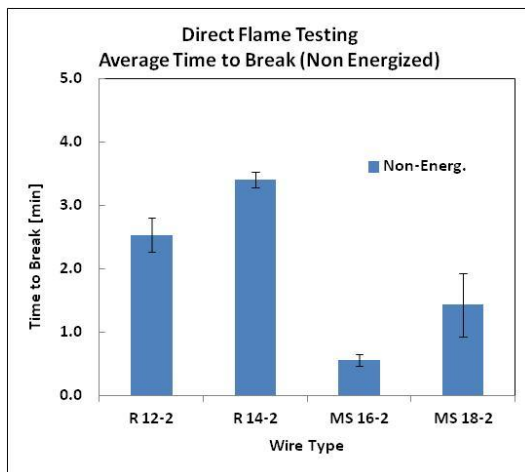


Figure B1.2: Average Time to Break Non-Energized (DF)

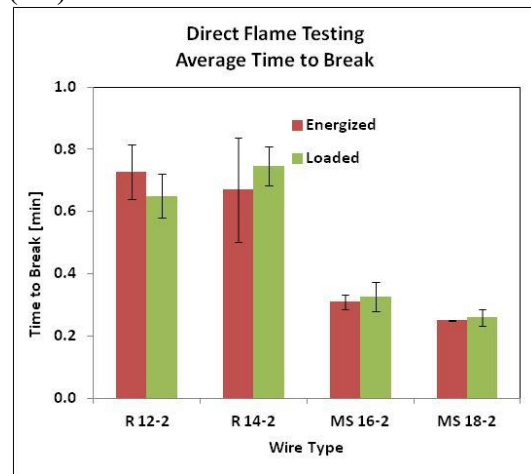


Figure B1.5: Average Time to Break Loaded vs Energized (DF)

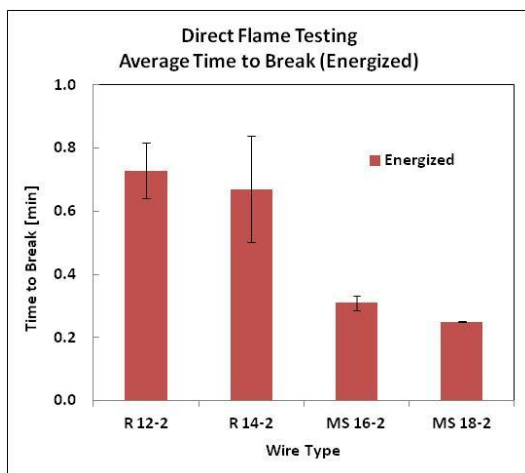


Figure B1.3: Average Time to Break Energized (DF)

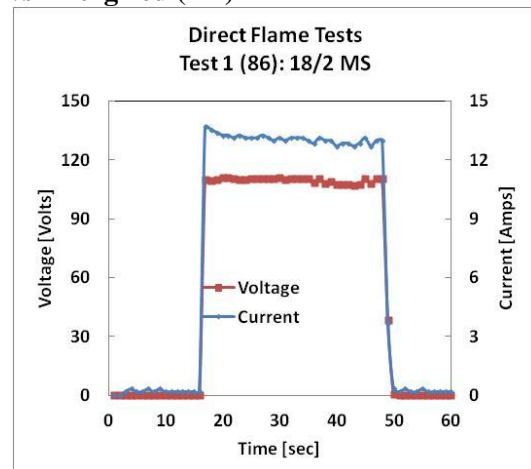


Figure B1.6: Test 1 (86): 18/2 MS (DF)

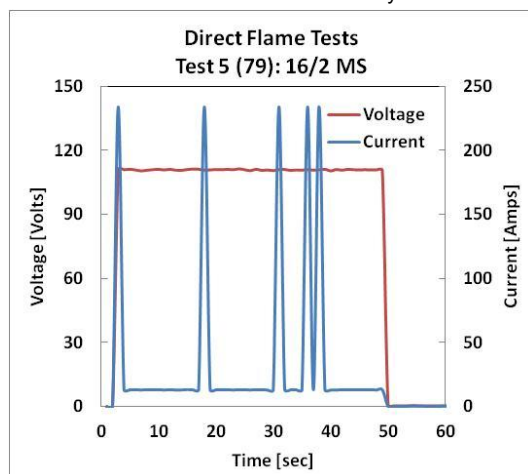


Figure B1.7: Test 5 (79): 16/2 MS (DF)

B2: Radiation Tunnel Testing

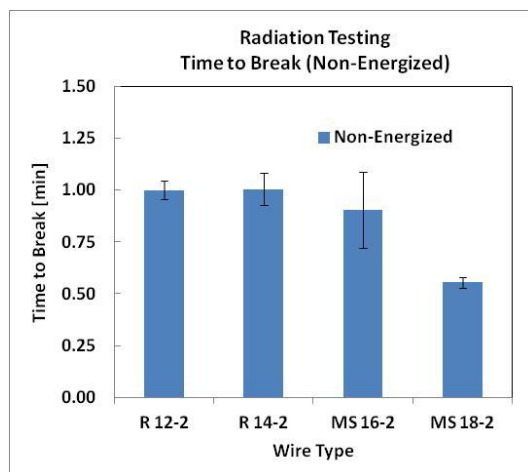


Figure B2.8: Time to Break Non Energized (R)

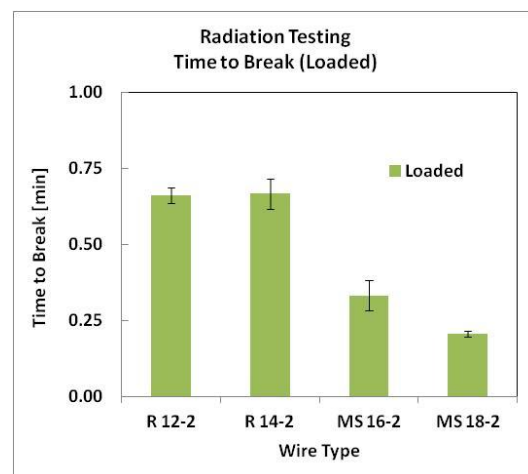


Figure B2.10: Time to Break Loaded (R)

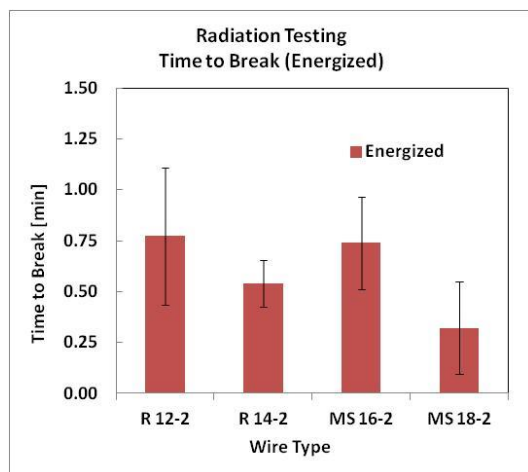


Figure B2.9: Time to Break Energized (R)

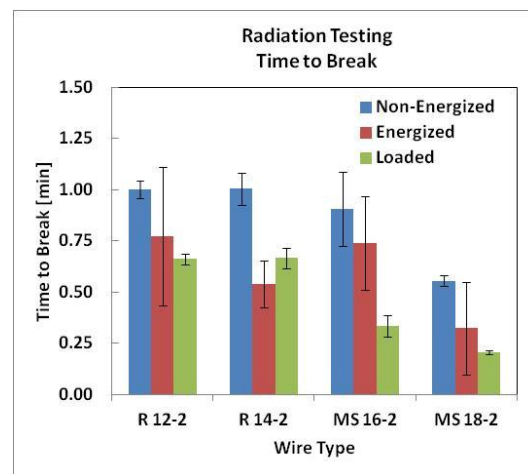


Figure B2.11: Time to Break Comparison (R)

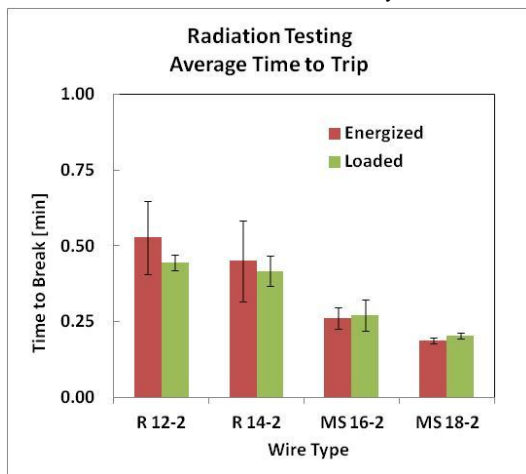


Figure B2.12: Average Time to Trip Loaded vs Energized (R)

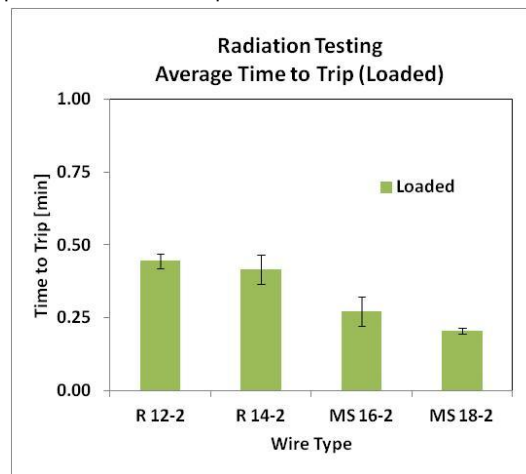


Figure B2.14: Average Time to Trip Loaded (R)

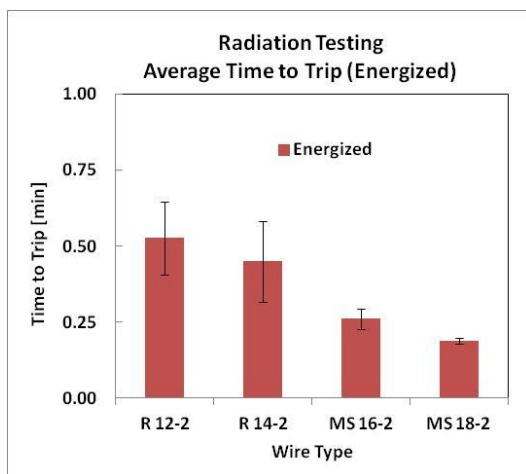


Figure B2.13: Average Time to Trip Energized (R)

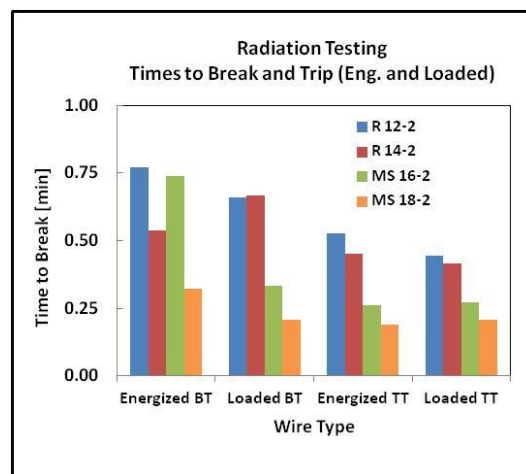


Figure B2.15: Times to Break and Trip Ener. and Loaded (R)

B3: Compartment Testing

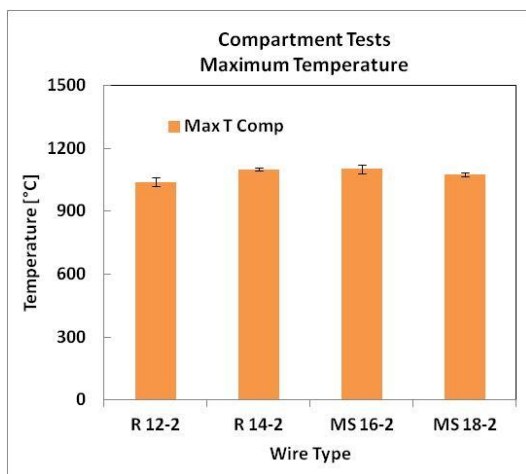


Figure B3.1: Maximum Temperature (C)

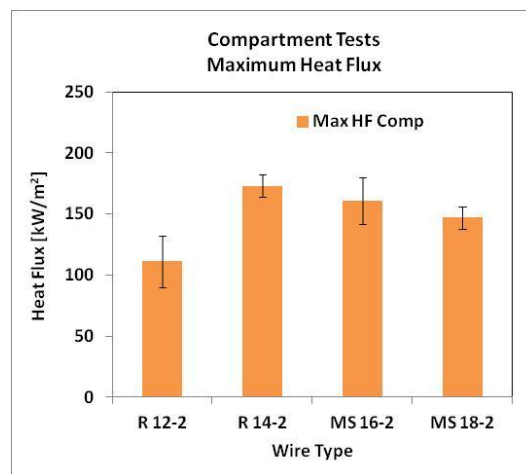


Figure B3.2: Maximum Heat Flux (C)

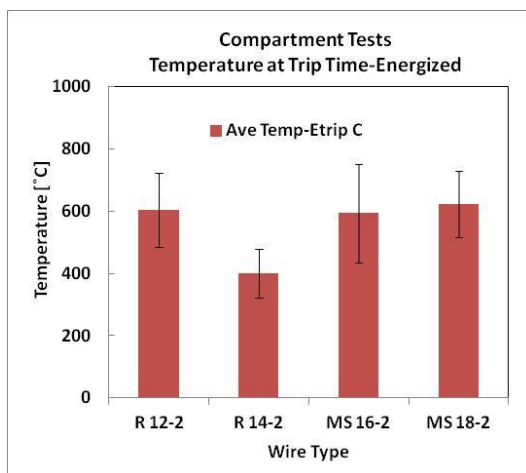


Figure B3.4: Temperature at the Trip Time Energized (C)

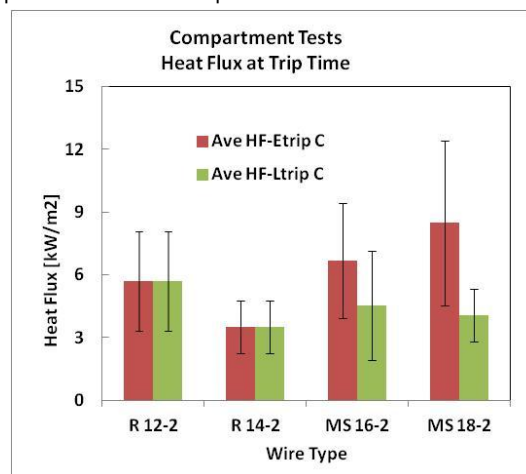


Figure B3.6: Heat Flux at Trip Time (C)

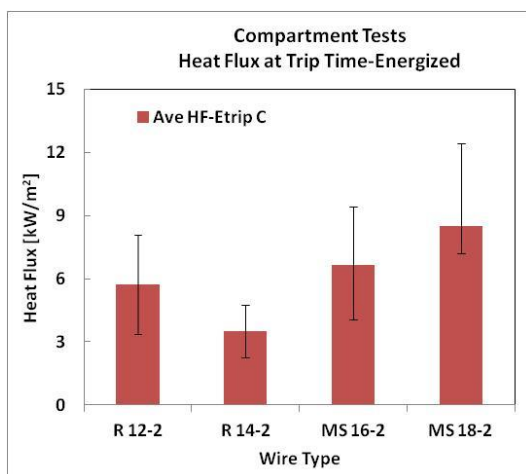


Figure B3.4: Heat Flux at Trip Time Energized (C)

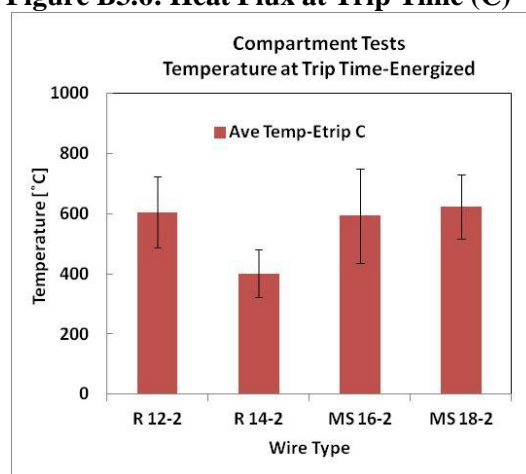


Figure B3.7: Temperature at Trip Time Energized (C)

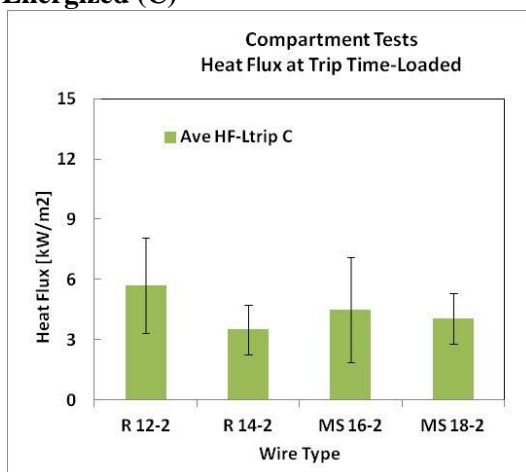


Figure B3.5: Heat Flux at Trip Time Loaded (C)

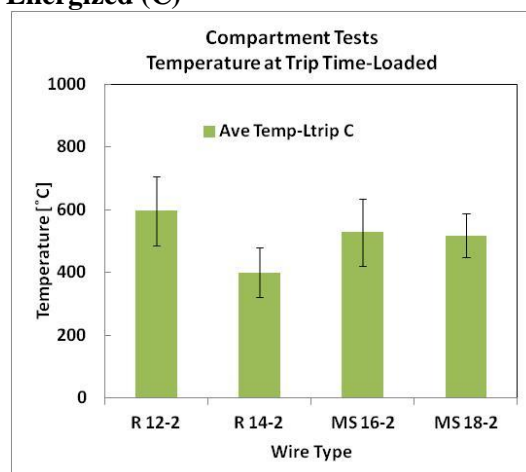


Figure 16: Temperature at Trip Time Loaded (C)

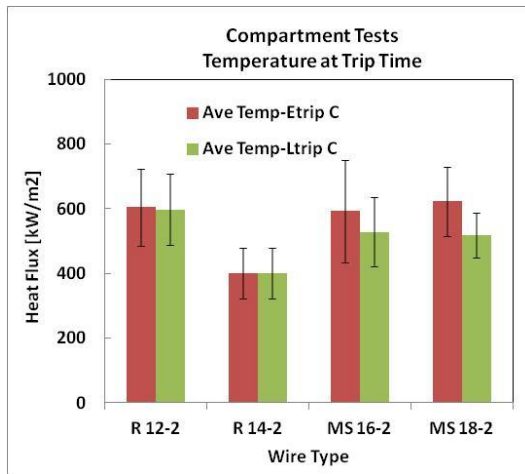


Figure B3.9: Avg Temperature at Trip Time Load/Ener (C)

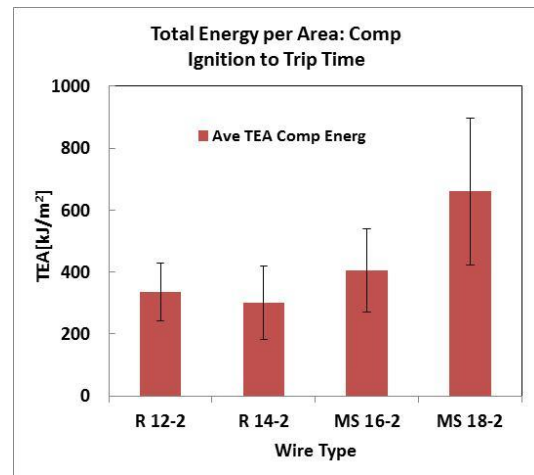


Figure B3.13: Total Energy per Area (C)

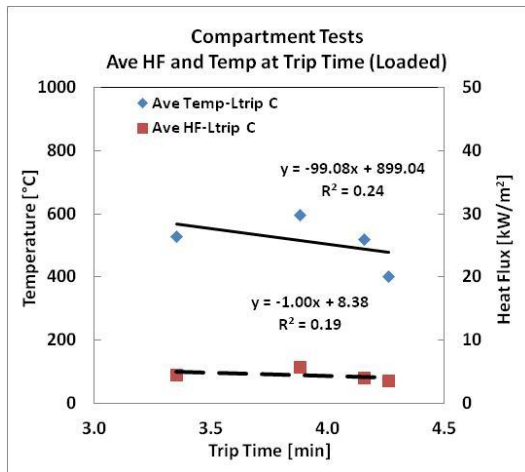


Figure B3.17: Avg HF and Temp at Trip Time Loaded (C)

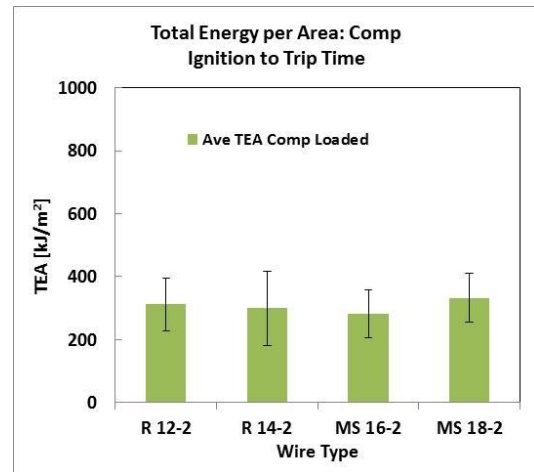


Figure B3.194: Total Energy per Area (C)

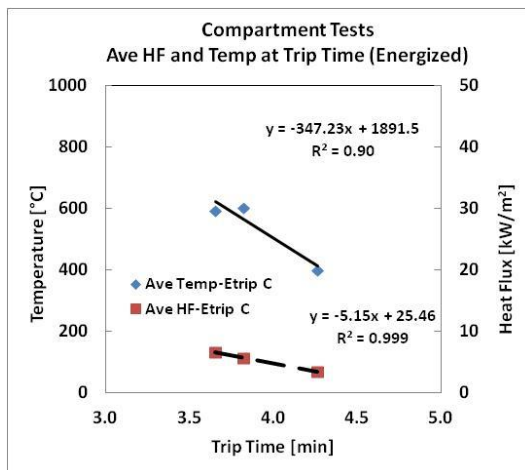


Figure B3.18: Avg HF and Temp at Trip Time Energized (C)

B4: Full Room Tests

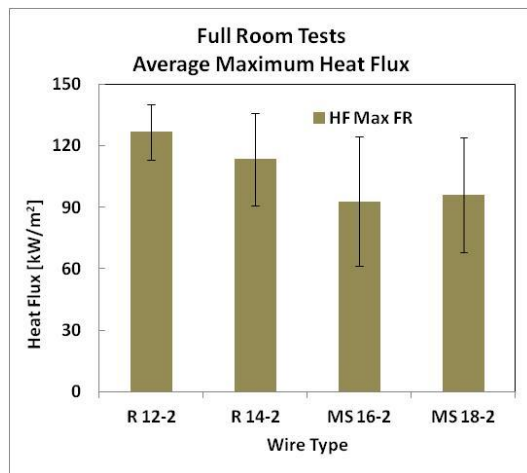


Figure B4.20: Average Maximum Heat Flux (FR)

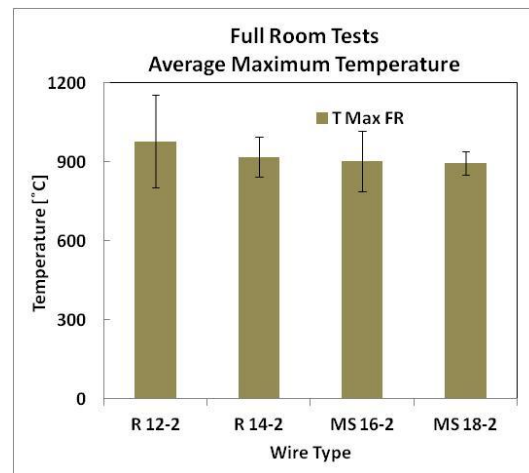


Figure B4.23: Average Maximum Temperature (FR)

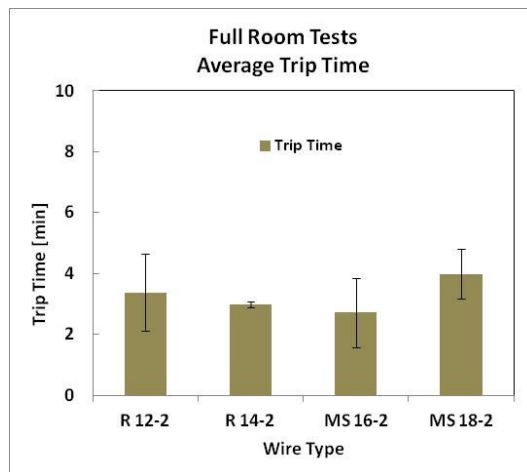


Figure B4.21: Average Trip Time (FR)

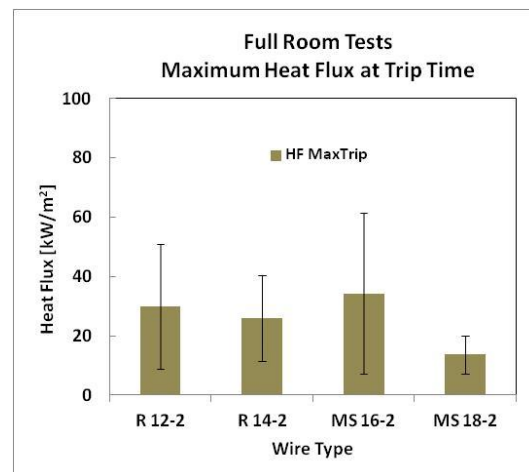


Figure B4.24: Maximum Heat Flux at Trip Time (FR)

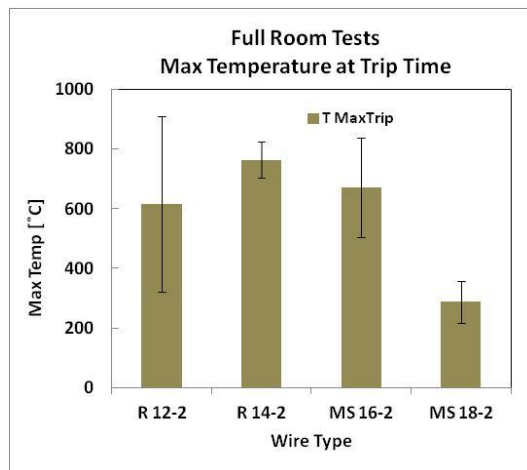


Figure B4.22: Maximum Temperature at Trip Time (FR)

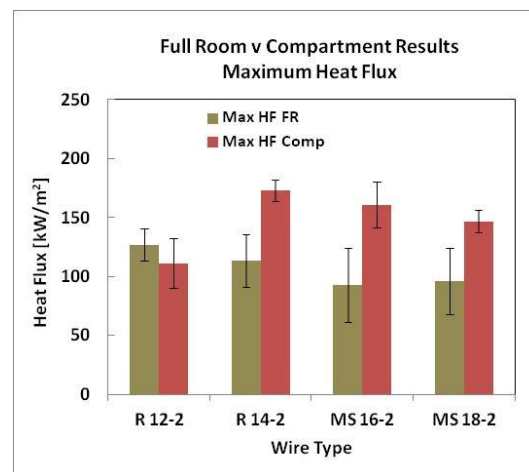


Figure B4.25: Average Maximum Heat Flux (FR)

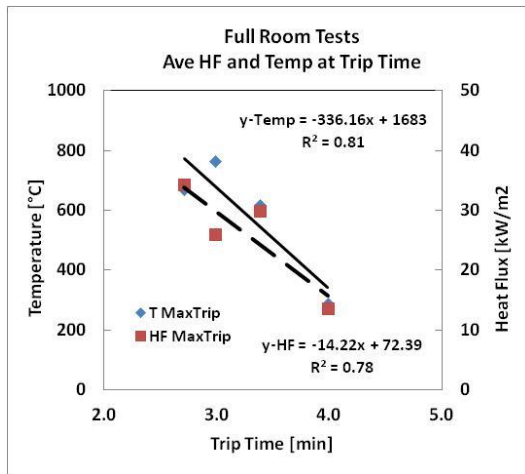


Figure B4.7: Avg HF and Temp at Trip Time Loaded (FR)

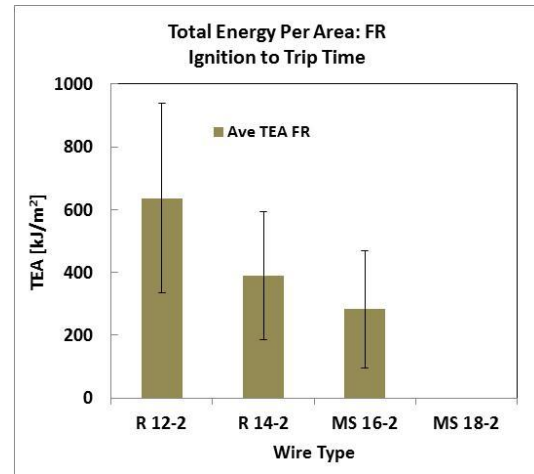


Figure 26: Total Energy per Area (FR)

B5: Full Room and Compartment Compare

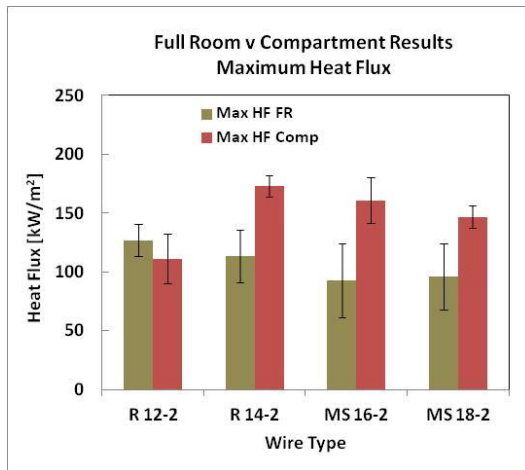


Figure B5.1: Average Maximum Heat Flux (FR)

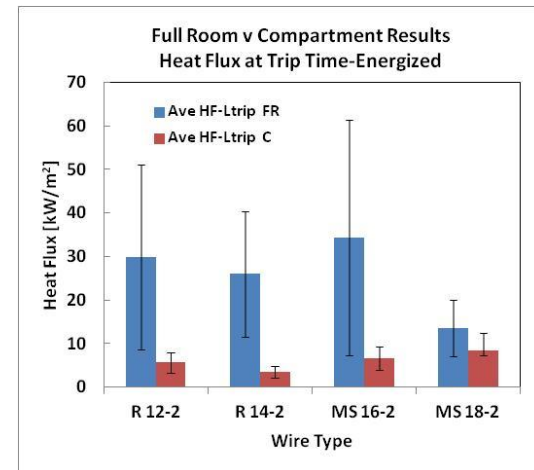
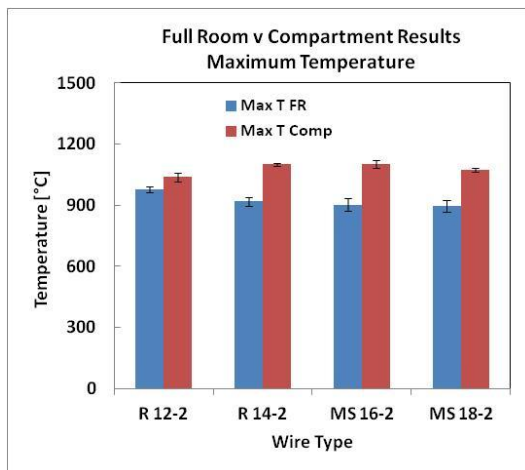


Figure B5.3: Heat Flux at Trip Time-Energized (FR vs C)



FigureB5.2: Maximum Temperature (FR vs C)

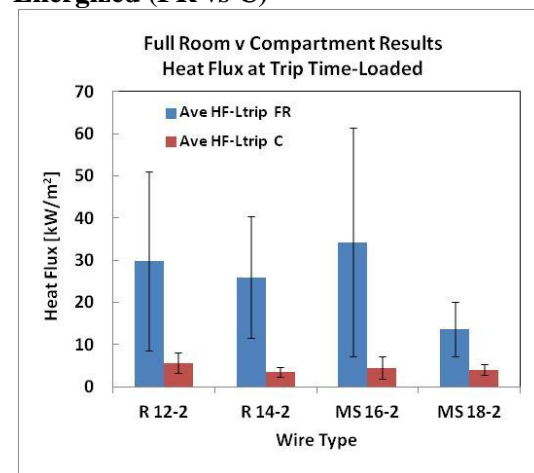


Figure B5.4: Heat Flux at Trip Time-Loaded (FR vs C)

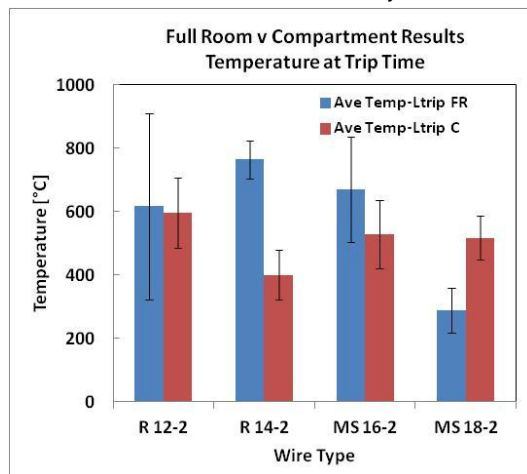


Figure B5.5: Temperature at Trip Time (FR vs C)

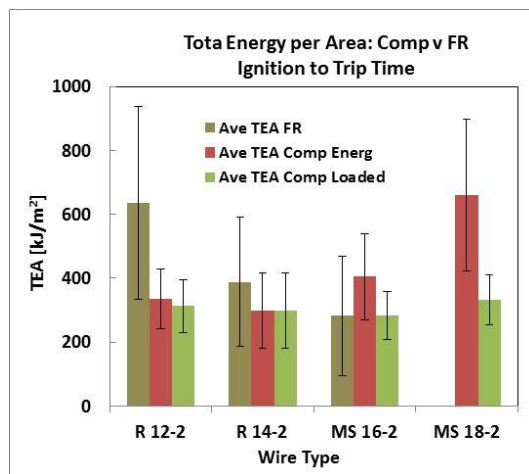
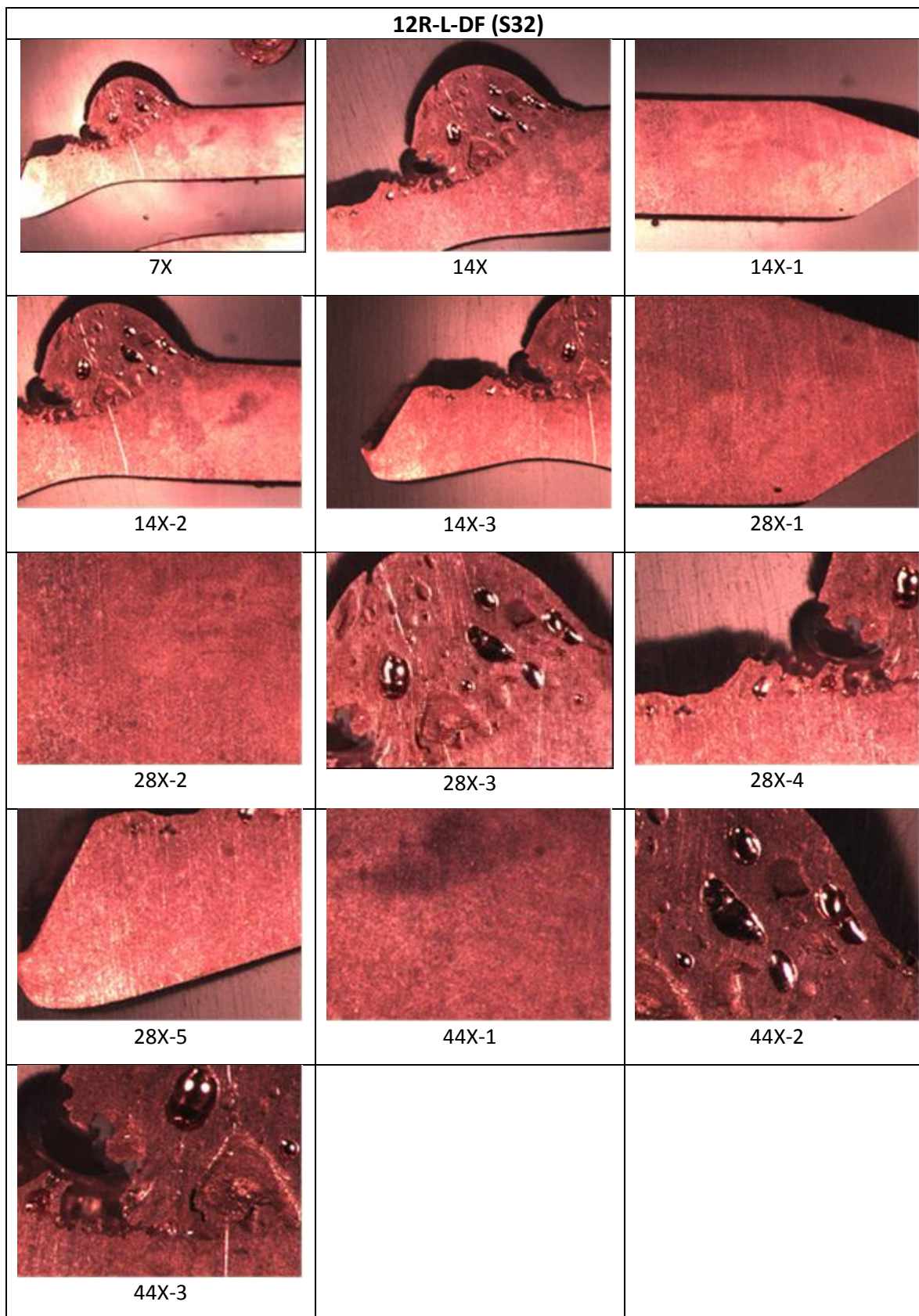
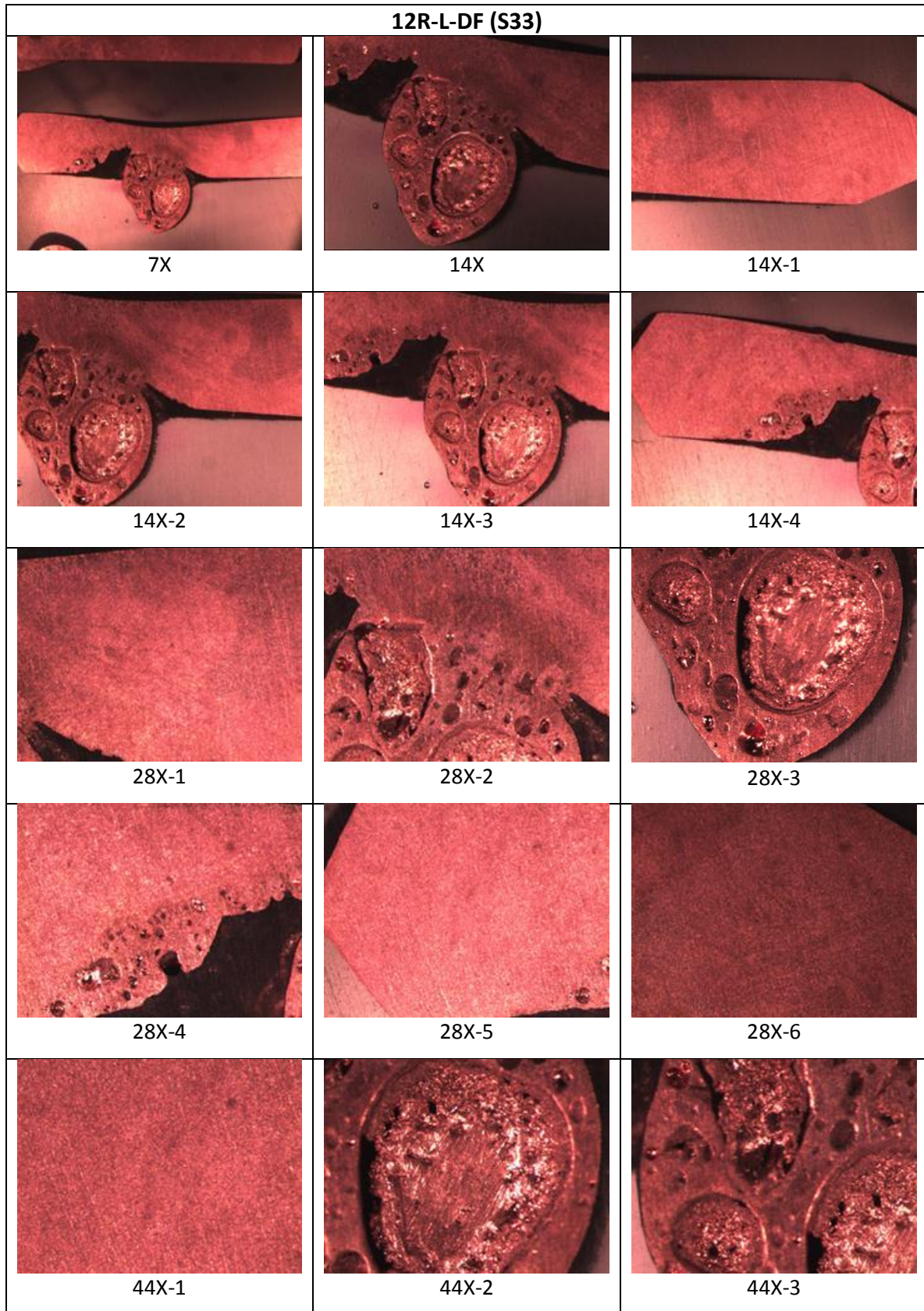
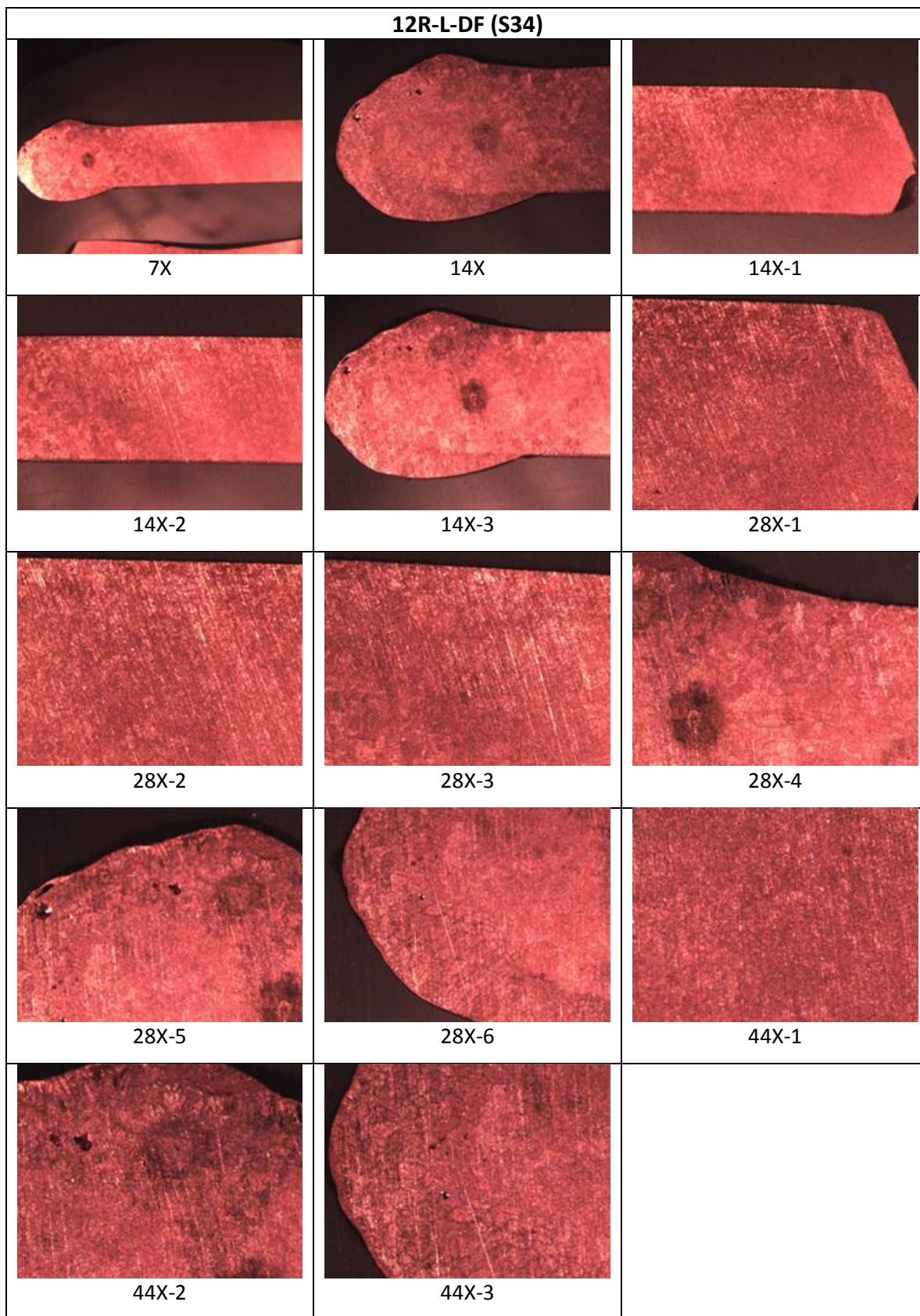


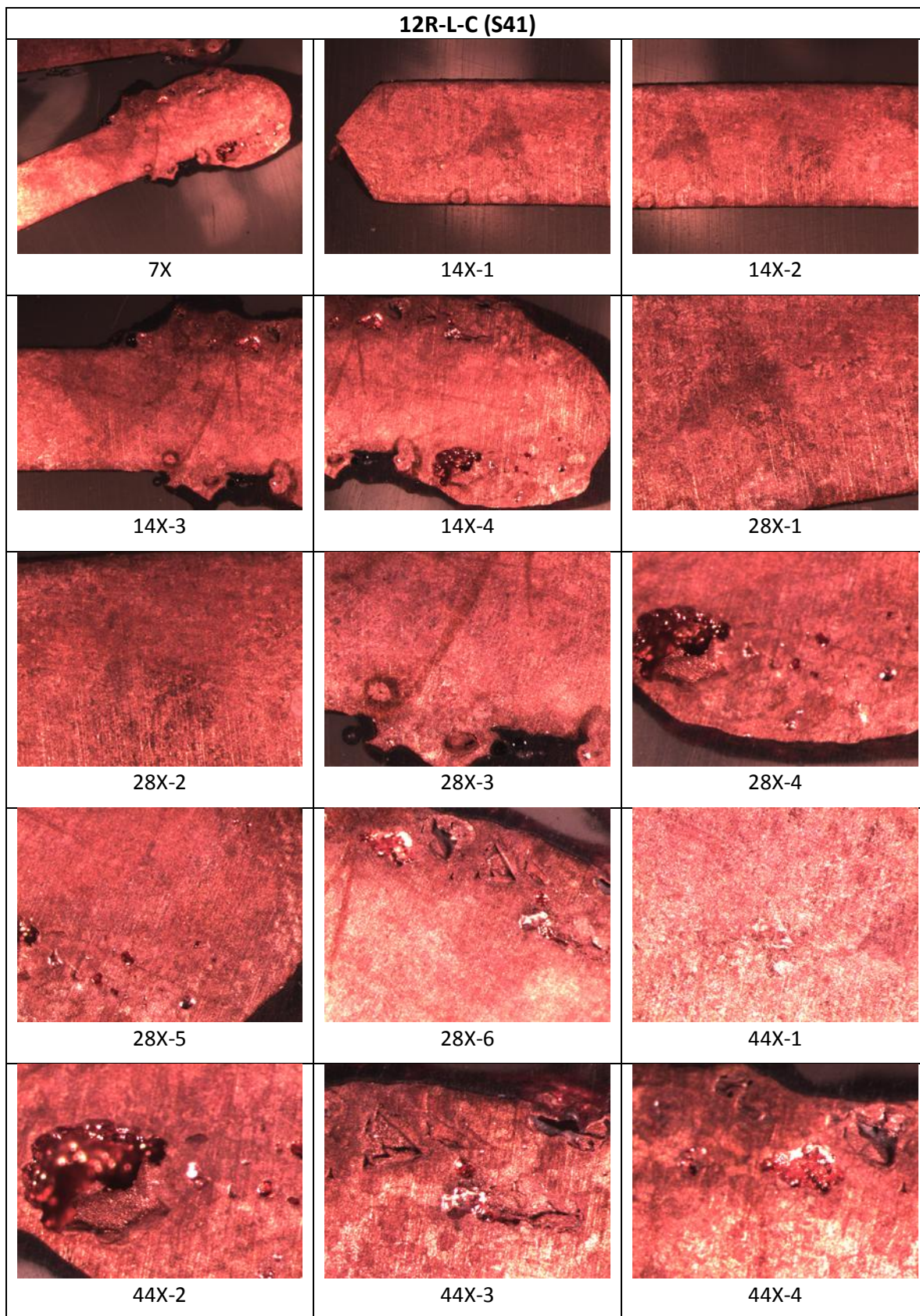
Figure B5.6: Total Energy per Area (FR v C)

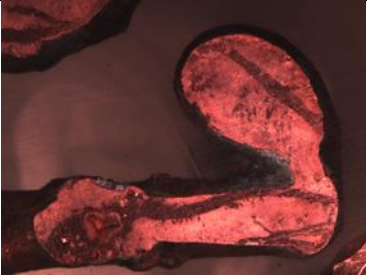
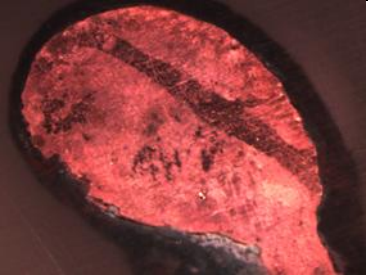


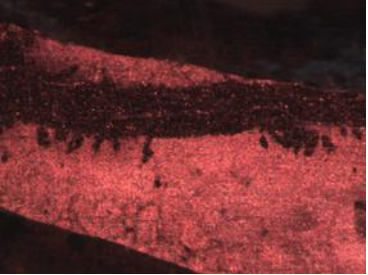
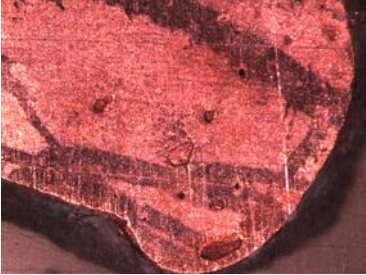

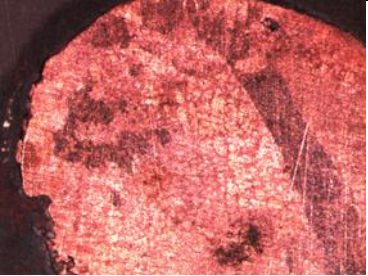
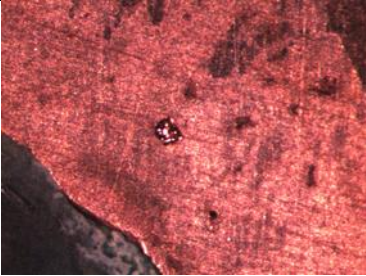

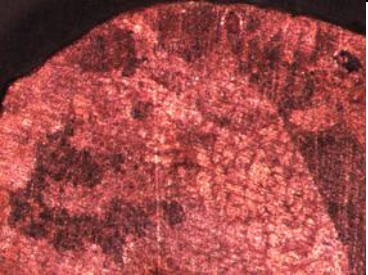
APPENDIX C

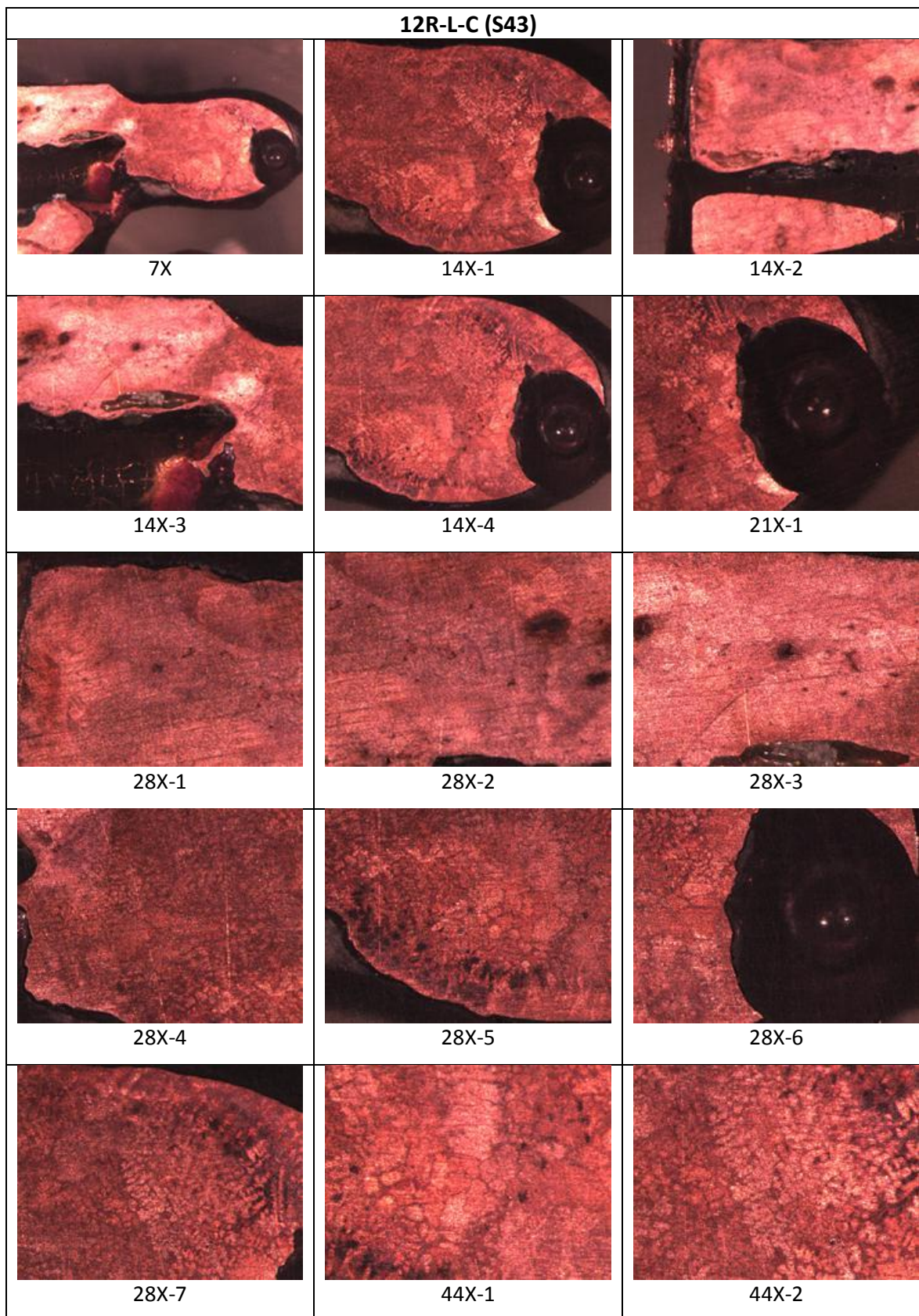


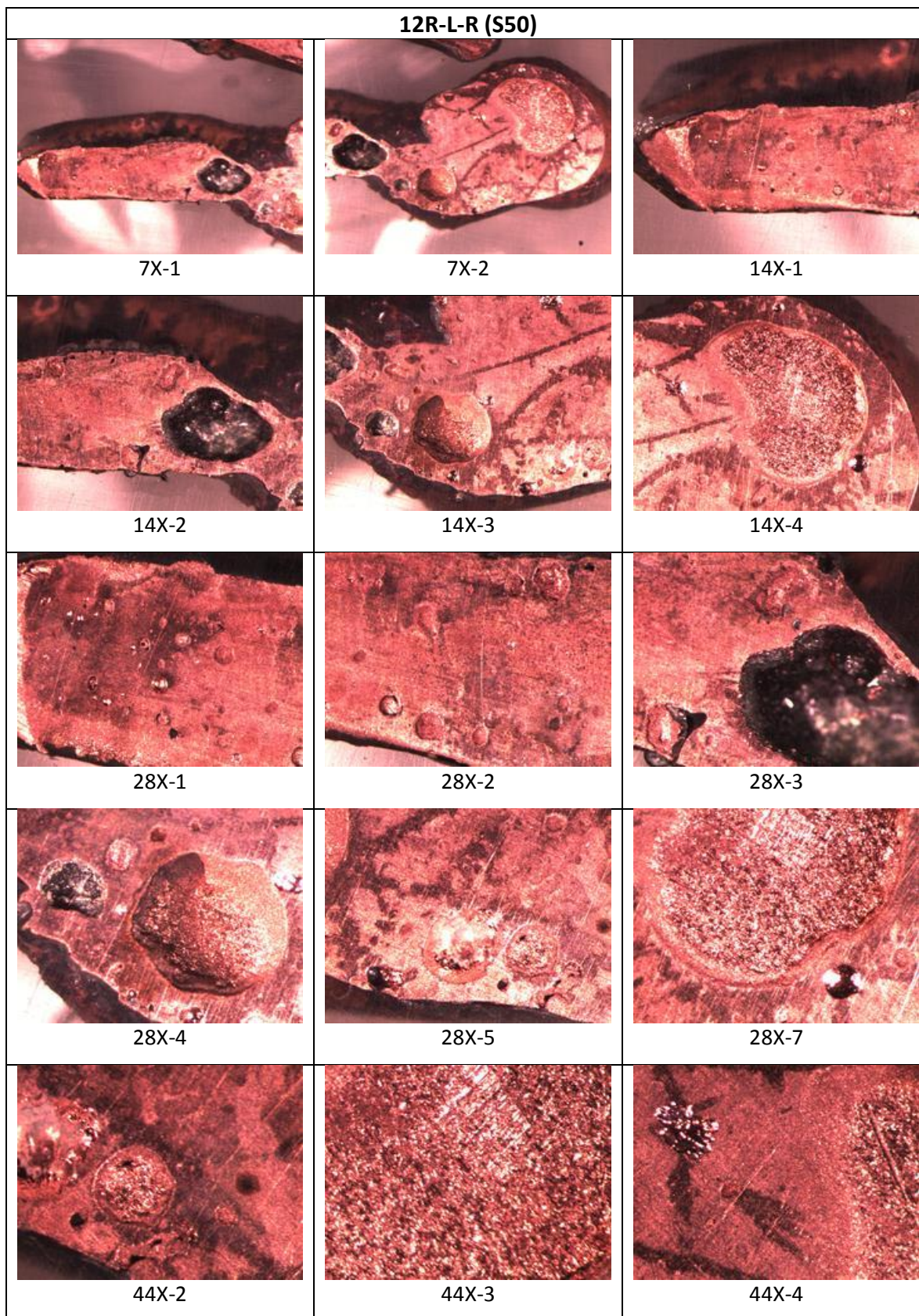


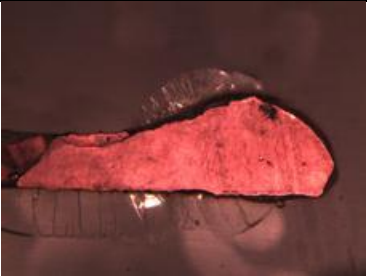
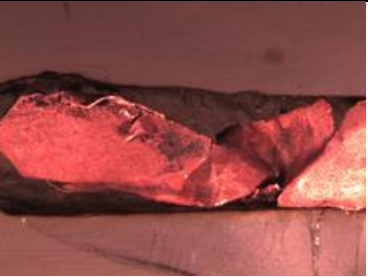
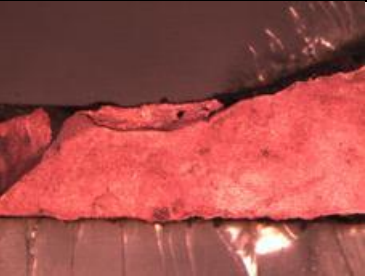
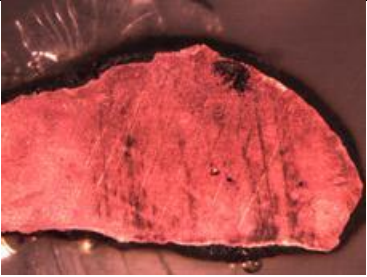
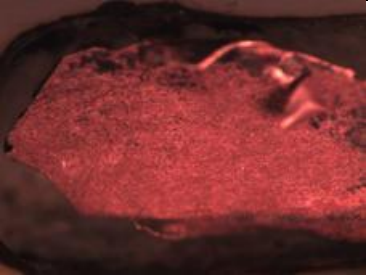
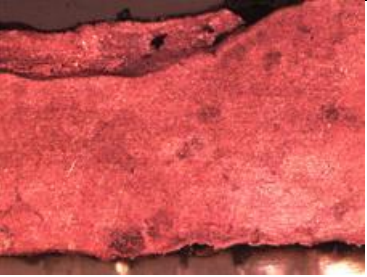
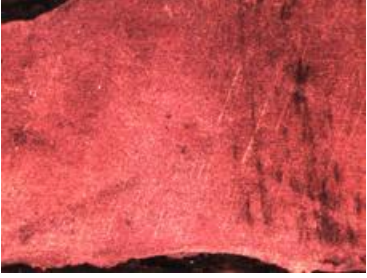
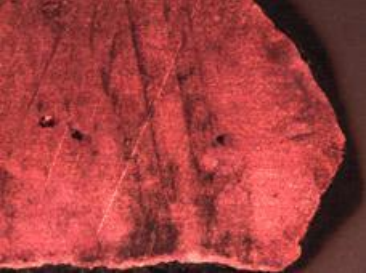
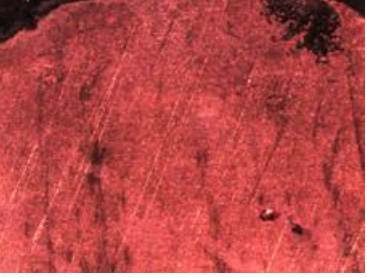

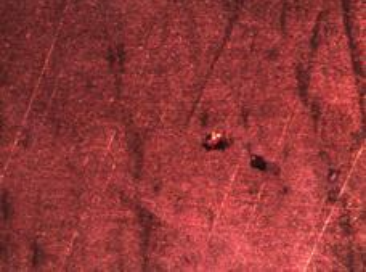


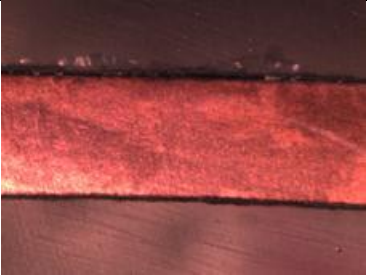


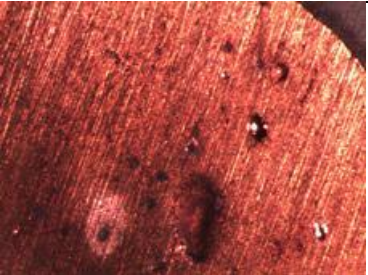


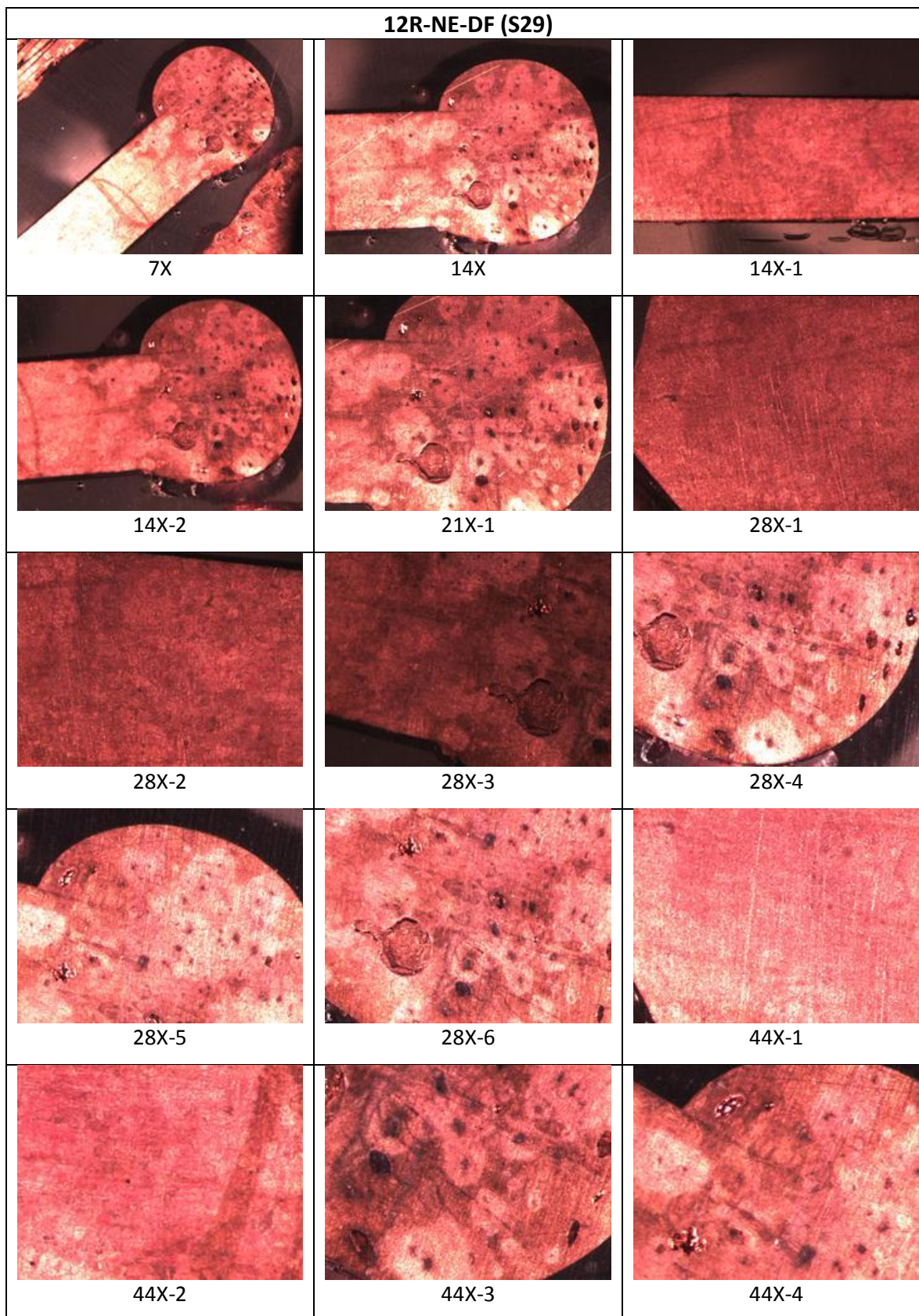
12R-L-C (S42)		
		
7X	14X-1	14X-2
		
28X-1	28X-2	28X-3
		
28X-4	28X-5	44X-1
		44X-1
44X-2	44X-3	


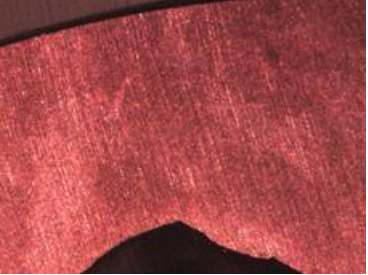


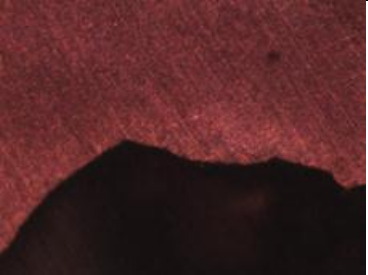


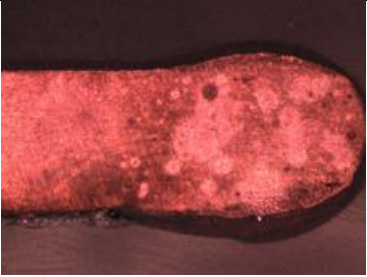
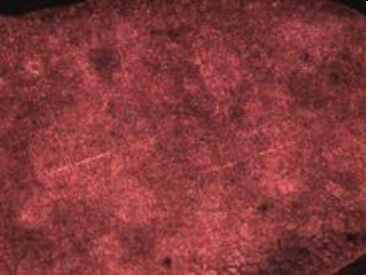
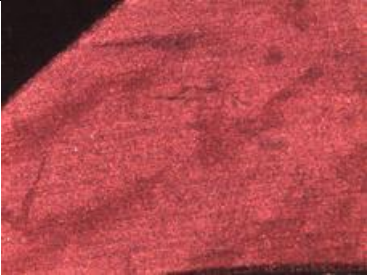


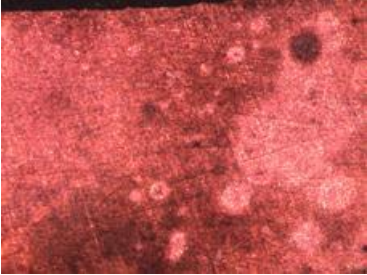
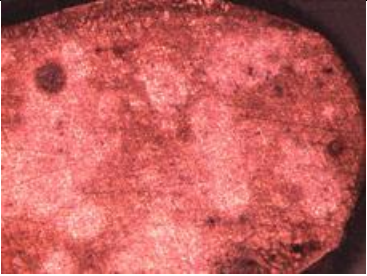
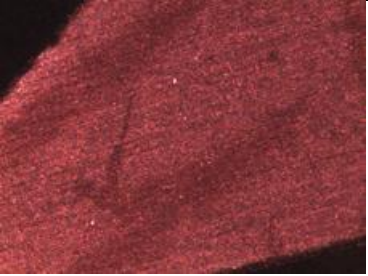
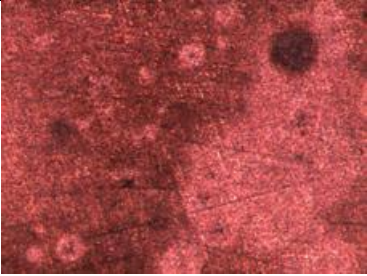
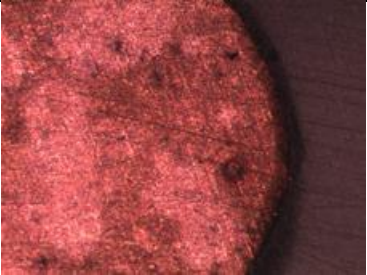


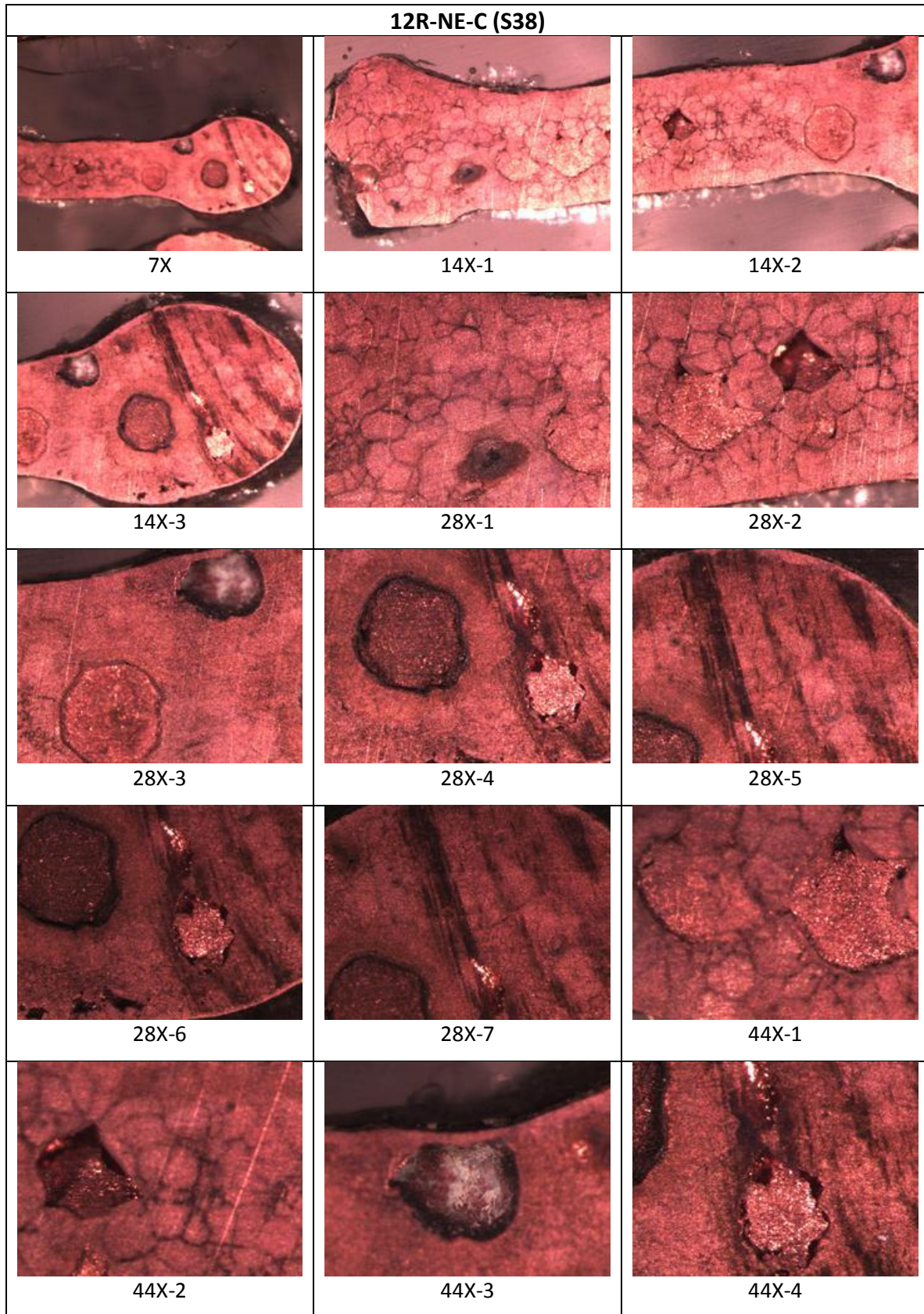
12R-L-R (S51)		
		
7X-1	14X-1	14X-2
		
14X-3	28X-1	28X-2
		
28X-3	28X-4	28X-5
		
44X-1	44X-2	

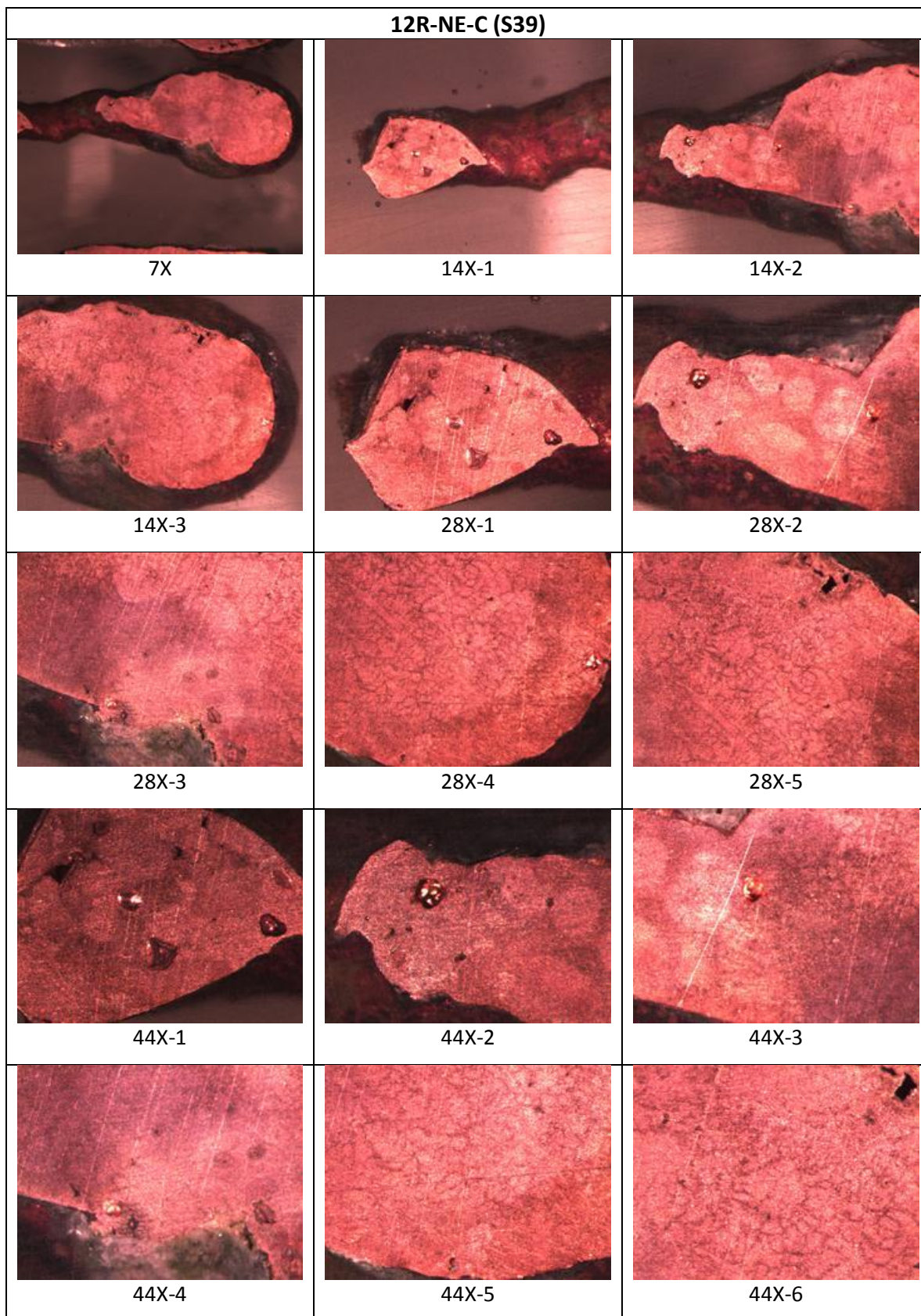
12R-L-R (S52)		
		
7X	14X	14X-1
		
14X-2	14X-3	28X-1
		
28X-2	28X-3	28X-4
		
44X-1	44X-2	44X-3

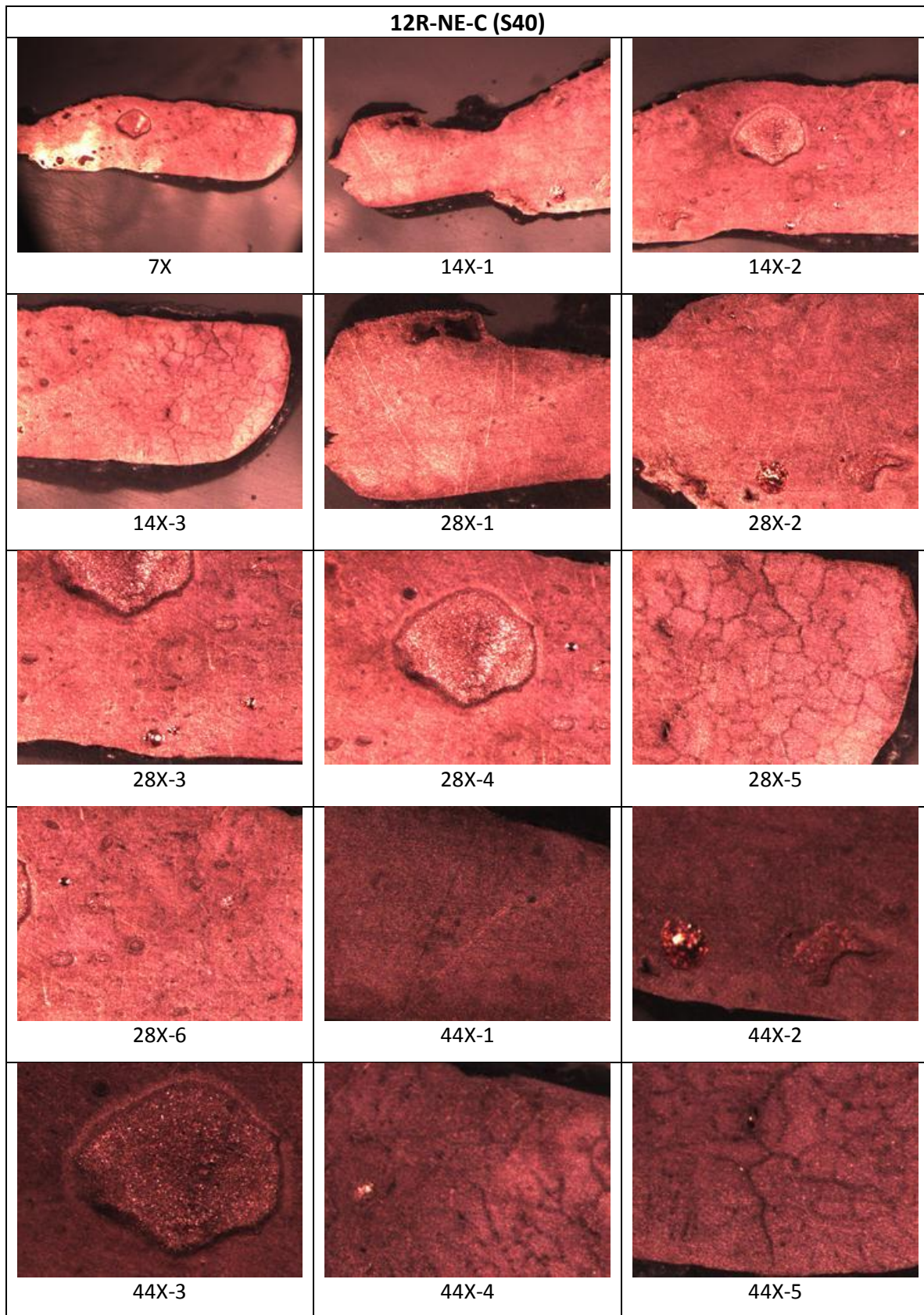


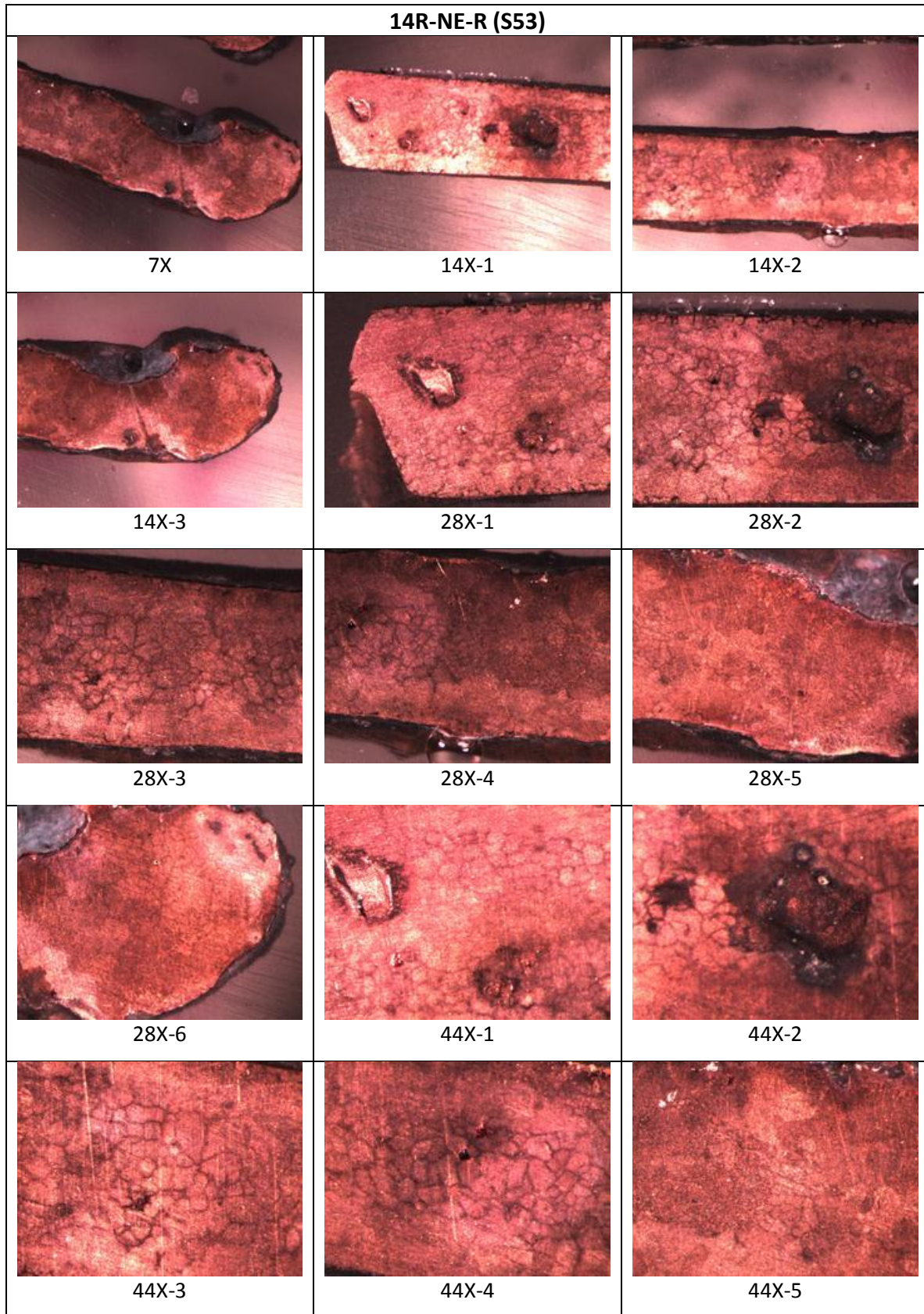
12R-NE-DF (S30) (BEAD wasn't cut Properly)		
		
14X	28X-1	28X-2
		
28X-3	28X-4	

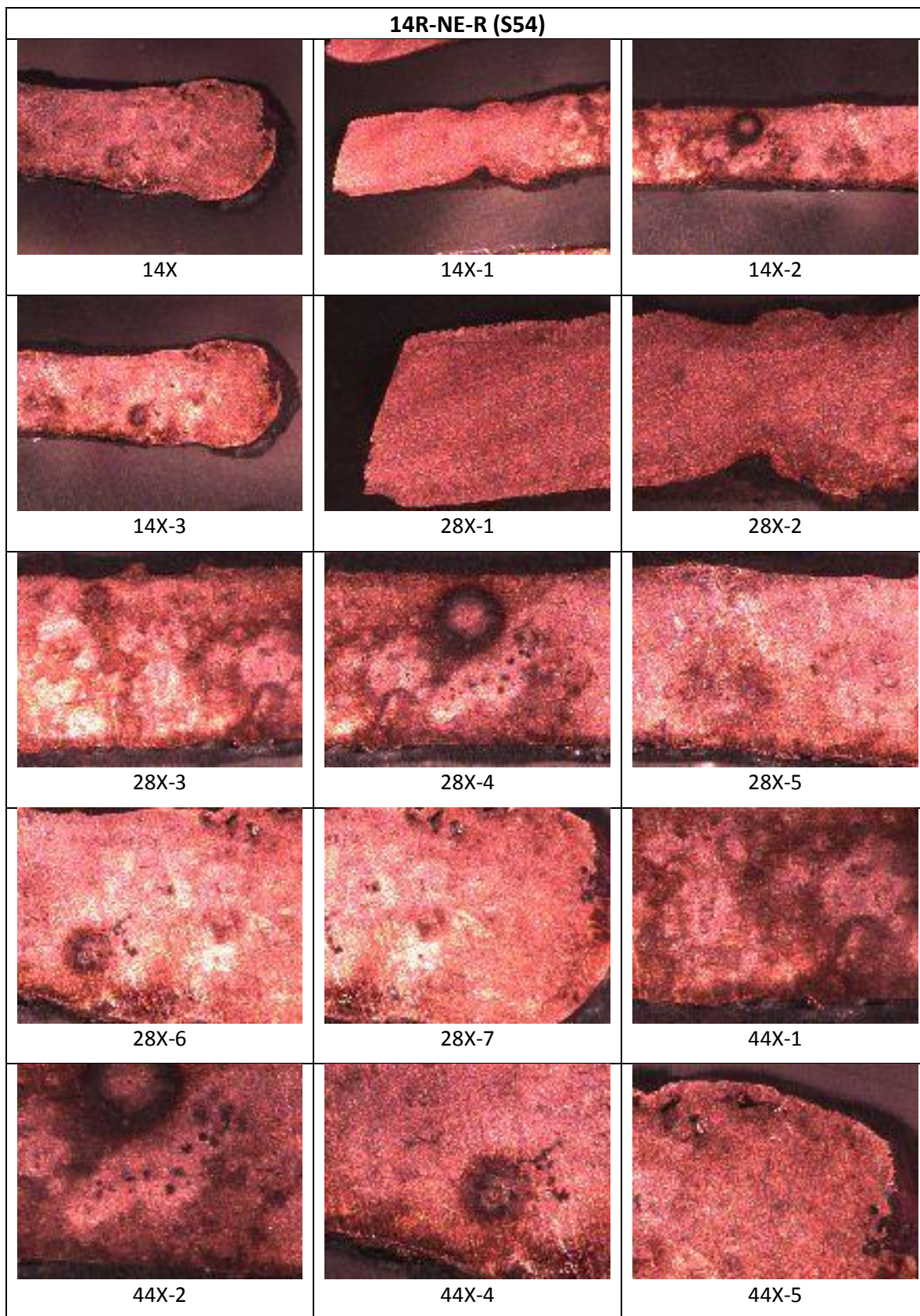
12R-NE-DF (S31)		
		
14X	28X	28X-1
		
28X-2	28X-3	28X-4
		
28X-5	44X-1	44X-2
		
44X-3		






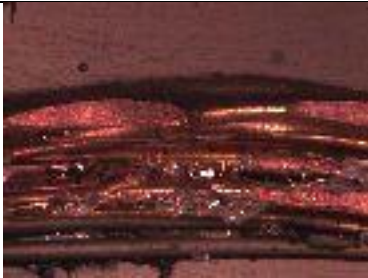







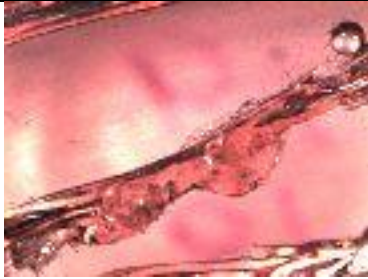
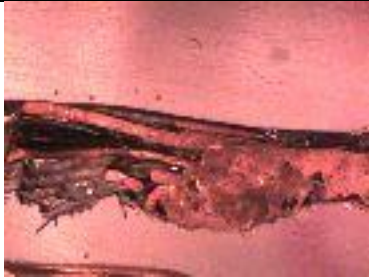
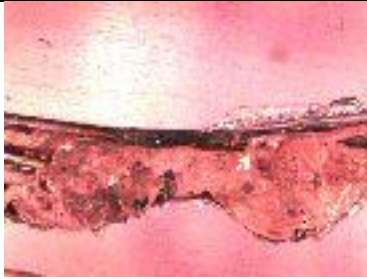

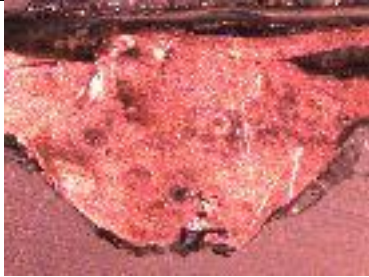



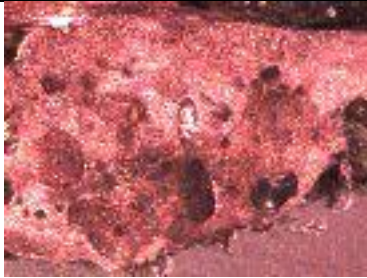
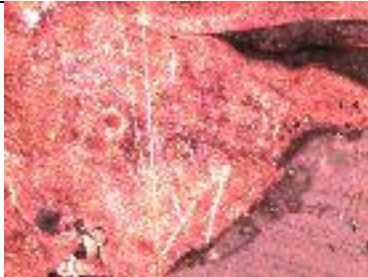


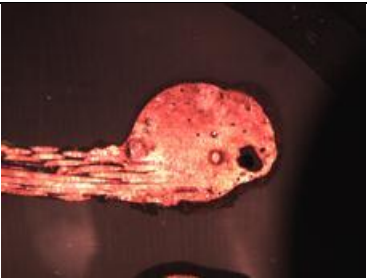

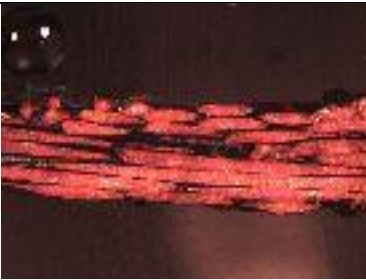



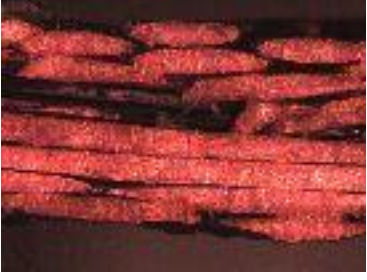
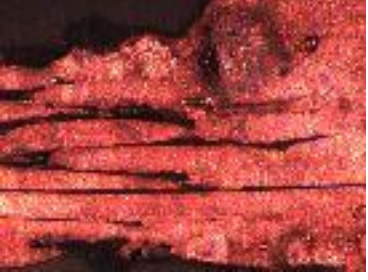
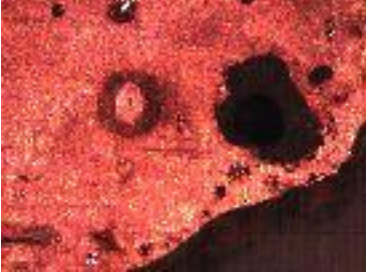


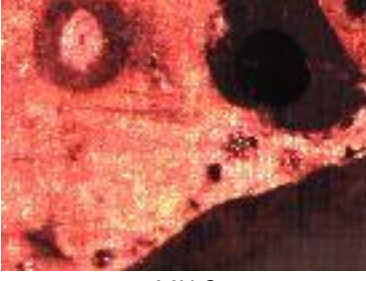
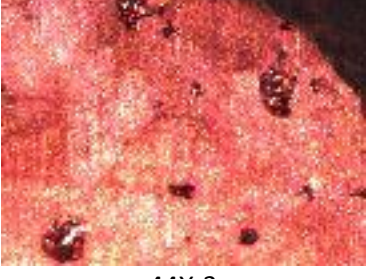


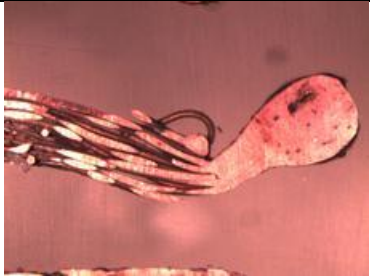












16MS-L-DF (S16)		
		
7X	14X-1	14X-2
		
14X-3	28X-1	28X-2
		
28X-3	28X-4	44X-1

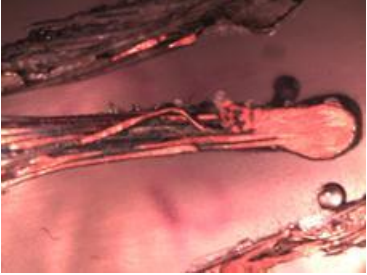

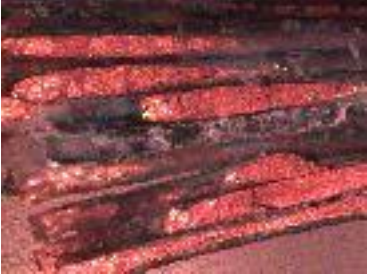




18MS-L-DF (S17)		
 7X	 14X-1	 28X-1
 28X-2	 44X-1	 44X-2

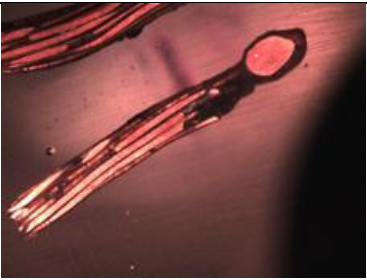
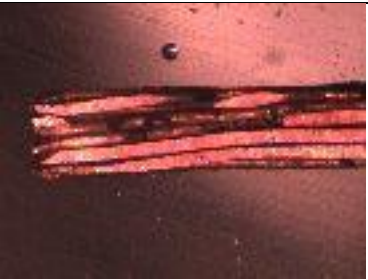
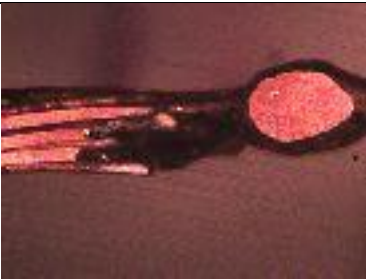

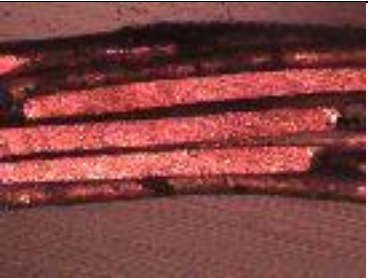
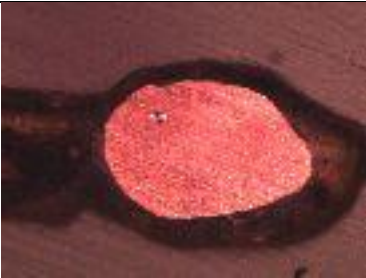
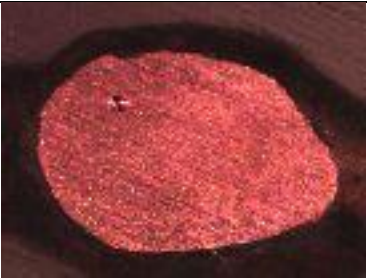
18MS-L-DF (S18)		
		
7X	14X-1	14X-2
		
14X-3	28X-1	28X-2
		
28X-3	44X-1	44X-2
		
44X-3		










18MS-L-C (S4)		
		
7X	14X-1	14X-2
		
14X-3	28X-1	28X-2
		
28X-3	28X-4	28X-5
		
28X-6	44X-1	44X-2
		
44X-3		

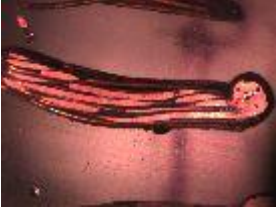
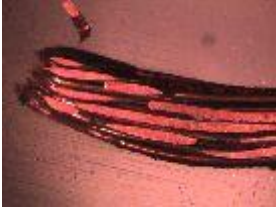




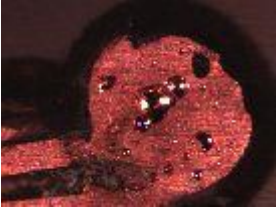
18MS-L-C (S5)		
		
7X	14X-1	14X-2
		
28X-1	28X-2	28X-3
		
44X-1	44X-2	44X-3
		
44X-4		

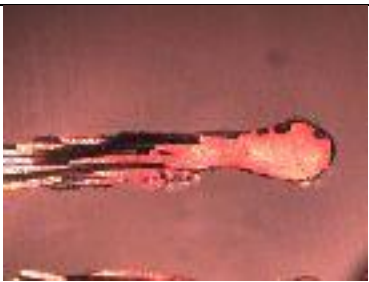
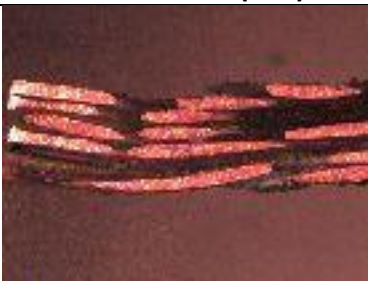







18MS-L-C (S6)		
		
14X	28X-1	28X-2
		
28X-3	28X-1	28X-2
		
28X-3		

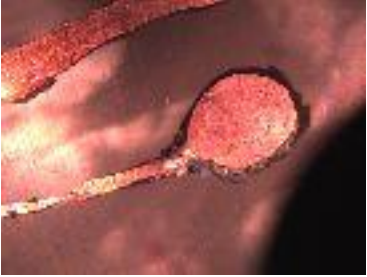



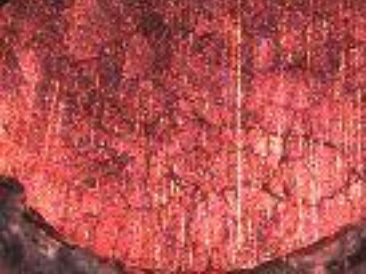

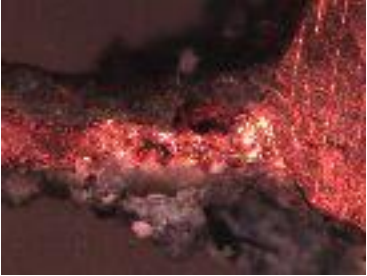
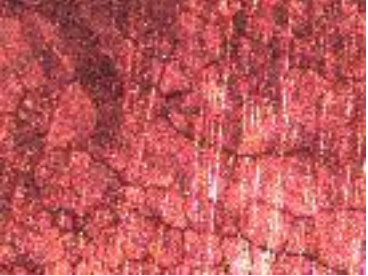
18MS-L-R (S19)		
		
7X	14X-1	28X-1
		
28X-2	28X-3	44X-1
		
44X-2		

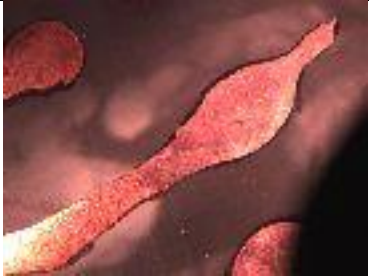









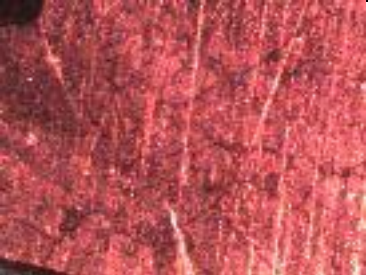


18MS-L-C (S21)		
		
7X	14X-1	14X-2
		
28X-1	28X-2	28X-3
		
44X-1		

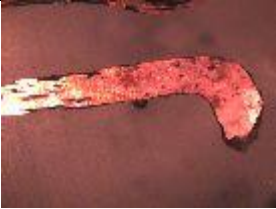






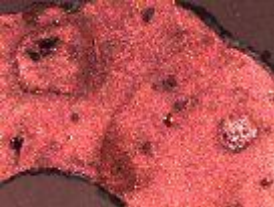
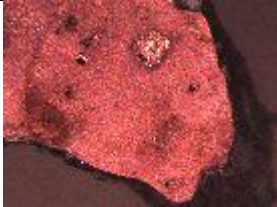



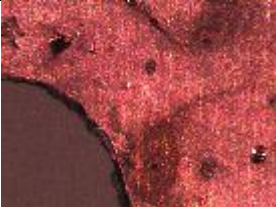


18MS-NE-DF (S13)		
 7X	 14X-1	 14X-2
 14X-3	 28X-1	 44X-1
 44X-2	 44X-3	 44X-4


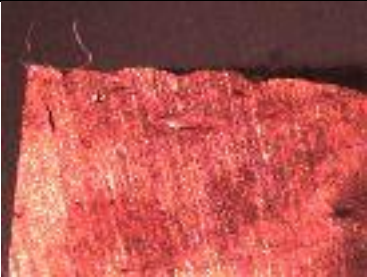



18MS-NE-DF (S14)		
 7X	 14X-1	 14X-2
 28X-1	 28X-2	 28X-3
 44X-1		

18MS-NE-DF (S15)		
		
7X	14X-1	14X-2
		
28X-1	28X-2	28X-3
		
44X-31	44X-2	44X-3

18MS-NE-C (S1)		
		
7X	14X-1	14X-2
		
14X-3	28X-1	28X-2
		
28X-3	28X-4	

18MS-NE-C (S2)		
		
7X	14X-1	14X-2
		
14X-3	14X-4	28X-1
		
28X-2	28X-3	28X-4
		
44X-1	44X-2	44X-3
		
44X-4		

18MS-NE-C (S3)		
 7X	 14X-1	 14X-2
 14X-3	 28X-1	 28X-2
 28X-3	 28X-4	 28X-5
 44X-1	 44X-2	 44X-3
 44X-4	 44X-5	 44X-6

16MS-NE-R (S25)		
		
14X	28X-1	28X-2
		
28X-3	28X-4	28X-5
		
44X-1	44X-2	